The role of gamma-ray in relation to the observed diffuse emission and the cosmic ray origin problem

Brian P. Houston

THE ROLE OF GAMMA-RAY SOURCES IN RELATION TO THE OBSERVED DIFFUSE EMISSION AND THE COSMIC RAY ORIGIN PROBLEM

by

Brian P. Houston, B.Sc.

A Thesis submitted to the University of Durham for the Degree of Doctor of Philosophy February, 1985.

Galilei : Und was wir heute finden, werden wir morgen von der Tafel streichen und erst wieder anschreiben, wenn wir es noch einmal gefunden haben.

Leben des Galilei, Bertolt Brecht (1955).

Hamm : J'aime les vieilles questions. (Avec élan). Ah les vieilles questions, les vieilles réponses, il n'y a que ça!

Fin de Partie, Samuel Beckett (1957)

Galileo : And what we find today, we will strike from the blackboard tomorrow and write down once more, when we have found it yet again.

Hamm : I love the old questions. (With fervour). Ah the old questions, the old answers, there's nothing like them!

ABSTRACT

Interpretation of the present gamma-ray data above 100 MeV is discussed in relation to cosmic ray interactions with the atomic and molecular hydrogen in the Galactic plane.

The SAS II gamma-ray data are analysed for supportive evidence on the 2CG candidate sources identified from the COS B observations. The strongest sources are confirmed. There is good evidence to suggest that many of the weaker sources are not truly discrete.

A Monte-Carlo analysis of the discrete source detection efficiencies suggests that many 2CG sources are unresolved giant molecular clouds, irradiated by the ambient cosmic ray flux. An attempt is made to define a genuine source catalogue. Taking account of the detection efficiencies the net source flux (from both resolved and unresolved sources) is estimated to be 11-23% of the Galactic plane emission.

Cosmic ray interactions with the Orion molecular cloud complex are investigated through an analysis of the gamma-ray emission above 100 MeV. There is no evidence for cosmic ray exclusion from the clouds. A new derivation of the CO/H_2 ratio is obtained.

$$N_{H_2} / \int T(^{12}CO)dv = (3.7 \pm 0.6) \times 10^{20} \text{ at } cm^{-2}(K\ kms^{-1})^{-1}.$$

Contributions to the extragalactic gamma-ray flux from radio galaxies and rich clusters are estimated.

The flux may be dominated by emission from these objects.

With the estimate of the discrete Galactic source flux and the $CO \rightarrow H_2$ ratio, the radial gamma-ray emissivity is compared to the HI, inferred H_2 and possible cosmic ray radial densities in the inner Galaxy. It is shown that a moderate cosmic ray gradient overestimates the gamma-ray flux, unless the metal abundance gradient reduces the inferred H_2 mass.

PREFACE

The work presented in this thesis was carried out between 1981 and 1984 while the author was a research student under the supervision of Professor A.W. Wolfendale, F.R.S., in the Physics Department of the University of Durham.

Part of the work was carried out in collaboration with Professor A.W. Wolfendale and Dr. E.C.M. Young, but the calculations reported represent the work of the author.

Some of the results in this thesis have been published, as follows:

Houston, B.P., and Wolfendale, A.W., 1982, Irish Astron. J., 15, 181.

Houston, B.P., and Wolfendale, A.W., 1983, Astron. Astrophys., 126, 22.

Houston, B.P., Wolfendale, A.W., and Young, E.C.M., 1984, J. Phys. G., 10, L147.

Houston, B.P., and Wolfendale, A.W., 1984, J. Phys. G., 10, 1587.

Bhat, C.L., Issa, M.R., Houston, B.P., Mayer, C.J., and Wolfendale, A.W., 1984, Nature (submitted).

Houston, B.P., and Wolfendale, A.W., 1984, J. Phys. G. (in the press).

CONTENTS

CHAPTER ONE

INTRODUCTION

1.1 Historical development

Since their discovery by Hess (1912), cosmic rays have continued to stimulate the interests of both experimental and theoretical physicists. There has been substantial progress in measuring cosmic ray energy spectra and important advances have been made in the field of elementary particle physics. Particle accelerators have now superceded cosmic ray studies as the primary source of data on high energy particle interactions. However, analyses of the highest energy cosmic ray initiated air showers are still the only means of constraining phenomenological theories above about 10^{14}eV. The low energy cosmic rays ($\lesssim$ 10 MeV) produced by the Sun do not concern us in this work. Answers to the fundamental questions concerning the origin and acceleration of the extra-solar cosmic rays still elude us. It is the purpose of this thesis to assess the relevance and limitations of current gamma-ray astronomical data to the cosmic ray origin problem.

Hess' experiments and those of subsequent workers demonstrated conclusively the existence of increasing residual ionization with height above the Earth's surface, thus excluding natural radioactive elements as the source. Millikan and Cameron (1926) concluded that the ionizing radiation must originate outside the Earth and he speculated on the existence of a universal flux of ultra-energetic gamma-

rays. Bothe and Kolhorster (1929) demonstrated this to be false with the conclusive evidence that the cosmic rays are charged particles.

Even at the highest energies we are unable at sea-level to detect the primary component of the cosmic ray flux. We must either place the detectors above the atmosphere or measure the secondary products of the electromagnetic cascade initiated by cosmic rays incident on the top of the atmosphere. High energy photons constitute one of the important products of these air showers.

The development of gamma-ray astronomy and its relationship to cosmic ray astrophysics is comparatively recent. Hayakawa (1952) and Hutchinson (1952) considered gamma-ray production by cosmic rays in the wider context of the interstellar medium. Their work stimulated further developments on the gamma-ray fluxes to be expected from cosmic ray interactions in the Galaxy; notably Morrison (1958), Felten and Morrison (1963). Gamma-ray astronomy was perceived as a means of shedding fresh light on the unresolved questions pertaining to cosmic rays.

Gamma-ray astronomy, still in its infancy, has so far been an inconclusive arbitrator. The poor quality of present gamma-ray data is an important factor in this respect. However, it is also important to recognise the constraints arising from the interrelation of cosmic ray and gamma-ray astrophysics with many other areas of astrophysical research.

1.2 Gamma-ray astronomy and the origin of cosmic rays

Before we consider gamma-ray astronomy as a probe of the cosmic ray origin question, it is useful to briefly outline the latter. The primary cosmic radiation has two distinct components, the nucleonic (protons, antiprotons and heavier nucleii) and the electronic (electrons and positrons). Measurements of the cosmic ray energy spectra show that protons constitute about 92% of the nucleonic flux above 1GeV/nucleon. In collisions with nucleons in the interstellar medium they produce π^0's which decay into gamma-ray photons. At the same energy the electron flux is a few percent of the nucleonic component. The electrons produce gamma-rays by bremsstrahlung, inverse Compton scattering off low energy starlight and microwave background photon fields and synchrotron radiation. Gamma-ray absorption in the interstellar medium is essentially negligible in the MeV to GeV energy range. However, pair production processes ($\gamma + \gamma \rightarrow e^+ + e^-$) become more important at higher energies. This mechanism must be considered whenever high energy gamma-rays traverse low energy photon fields. We do not consider here the mathematical formulation of gamma-ray production and propagation in an astrophysical context. This is treated extensively by many workers (e.g. Ginzburg and Syrovatsky, 1964; Stecker, 1975; Longair, 1981; and references therein).

There are in essence two views on the origin of the cosmic ray flux. The first contends that it is universal in origin, that is the cosmic rays pervade the entire

Universe with a uniform energy density. Cosmological processes must then be invoked to explain the production of the particles at a much earlier epoch. There are variants on this theme in which the cosmic rays are confined to lesser volumes; superclusters or perhaps clusters. These refinements have been postulated in the light of the enormous energy requirements for a truly universal origin ($\sim 4 \times 10^{73}$erg, corresponding to a few percent of the observed baryonic rest mass energy within one Hubble radius) However, energy requirements alone cannot rule out the possibility of a meta-Galactic origin for the particles.

The alternative explanation favours a Galactic origin for the particles, up to about 10^{18}eV above which origin in the local Virgo cluster seems likely. This model can be viewed as a further reduction in scale from the meta-Galactic theories. Its most important features are the relatively low energy requirements ($\sim 5 \times 10^{54}$erg for our Galaxy) and the prediction of a cosmic ray gradient within the Galaxy.

The inverse Compton reactions on the universal micro-wave background radiation effectively screen the Galaxy from electrons which diffuse out from other Galaxies. In this respect the observed cosmic ray electrons must be localized to our own Galaxy, that is they are Galactic in origin.

Gamma-ray astronomy holds out the best opportunity to investigate the large scale distribution of cosmic

rays within our own Galaxy and thereby discriminate between the Galactic and meta-Galactic origin theories. In Chapter 2 we review the gamma-ray spectrum from about 1 MeV to 10^{15}eV, excluding the medium energy range covering 50 - 1000 MeV. The latter is reviewed in Chapter 3 with the emphasis on previous analyses and their limitations. Two major areas of uncertainty are identified, the discrete gamma-ray source contribution and the mass of gas; particularly in the inner Galaxy. In Chapter 4 we re-analyse the SAS II data-base searching specifically for confirmation of the discrete sources claimed by COS B. A Monte-Carlo analysis is developed in Chapter 5 which allows us to place limits on the unresolved source flux from the Galactic plane. The important question of cosmic ray interactions with giant molecular clouds is addressed in Chapter 6 through an analysis of the gamma-ray flux from the Orion complex. In addition we derive a new calibration of the CO/H_2 ratio appropriate for typical molecular clouds. In Chapter 7 we briefly consider the extragalactic gamma-ray flux and the possible contributions from radio galaxies and rich clusters. Finally in Chapter 8 we re-analyse the large scale Galactic gamma-ray emissivity, taking account of the expected discrete source contribution and the new estimates of the molecular hydrogen distribution. Conclusions are drawn on the origin of the cosmic ray flux at these energies and an outline is given for future developments.

CHAPTER TWO

THE GAMMA-RAY SPECTRUM

2.1 Introduction

Gamma-ray emission has been detected from a variety of sources and regions primarily in our Galaxy, in the energy range 10^5 - 10^{16}eV. This is a wide energy range and it is not surprising that there is much diversity in the nature of the emission. Whereas the work described in this thesis is primarily concerned with gamma-rays in the medium energy ($E_\gamma \sim$ MeV to GeV), it is worthwhile to start with a summary of the gamma-ray emission at other energies.

It is evident that in the broad area of gamma-ray astronomy we are always observing the results of high energy processes, either diffuse (in the interstellar medium) or discrete in origin. These processes must involve high energy cosmic rays (as discussed in Chapter 1) and as such through gamma-ray astronomy we are obtaining information relevant to the origin and propagation of cosmic rays. Aside from the energy band often described as 'medium energy gamma-ray astronomy' (which will be reviewed in detail in the following chapter), there are three distinct phenomena, or areas of study: gamma-ray line astronomy, gamma-ray bursts and ultra high energy gamma-ray sources. Each branch is characterised by its own observational techniques and limitations. While it is beyond the scope of the present work to discuss the details of the detection systems employed

for gamma-ray astronomy we wish to consider briefly the present observational status of each of these branches, indicating the great potential each holds for unravelling some of the problems associated with the origin of cosmic rays.

2.2 Gamma-ray line astronomy

Gamma-ray line emission is expected when nuclei are excited above the ground state, for example, as a result of nuclear collisions. Emission also occurs during the radio-active decay of certain species. Cyclotron lines (both emission and absorption) are generated from electron transitions between Landau levels of atoms in strong magnetic fields. For magnetic field strengths believed typical for neutron stars ($\sim 10^{12}$G), the characteristic cyclotron transition energy is $\sim$ 50 keV. Also of considerable importance is the positron annihilation line at 511 keV, the positrons coming from nuclear interactions, or the β-decay of nucleosynthesis products.

Collisions between cosmic rays and the gas in the interstellar medium are also expected to generate a series of gamma-ray lines. Most of the lines are expected to arise from cosmic ray nucleons with energies in the range $\sim$ 1 - 100 MeV, which is a region where the energy spectrum of cosmic rays in interstellar space is not well defined, being subject to strong solar modulation effects. However, useful predictions have been made

from models based on an extrapolation of the nucleon spectrum from measurements above the modulation cut-off, and the likely density increase of both low energy cosmic rays and heavy elements towards the inner Galaxy. Ramaty and Lingenfelter (1981) consider the most important lines to be: 0.847 MeV (^{56}Fe), 4.438 MeV (^{12}C) and 6.129 MeV (^{16}O), none of which have been detected to date. This is a field where future improved observations will help constrain the MeV region of the cosmic ray spectrum, allow for a better understanding of the effects of solar modulation and enable the distribution of the low energy cosmic ray flux with position in the Galaxy to be studied.

The hot big bang model of the universe is generally accepted as a sufficient framework for the primordial synthesis of all the elements up to helium. The absence of zero metal stars in our Galaxy and the overall scarcity of low metal abundance stars is attributed to further element synthesis in pregalactic or supermassive stars. Additional element formation (especially Lithium, Beryllium and Boron) results from cosmic ray spallation of Carbon, Nitrogen and Oxygen in the interstellar medium. However, explosive nucleosynthesis, both in the late stages of massive star evolution and in supernovae, is essential for the production of all the heavy elements above carbon. It will be seen later (Section 5.4) that the continued recycling and enrichment of the interstellar medium

with heavy elements may have important consequences for the interpretation of medium energy gamma-ray emission from the inner Galaxy, through the effects of heavy elements on estimates of the mass of gas (primarily H_2). It is believed that many gamma-ray lines should be detectable as a consequence of the nucleosynthesis process, thereby providing firm evidence for the continuing evolution of the elemental composition of the Galaxy. The strongest lines are expected to be: 1.809 MeV ($^{26}Al \rightarrow {}^{26}Mg$), 1.332, 1.173, 0.059 MeV ($^{56}Fe \rightarrow {}^{60}Co \rightarrow {}^{60}Ni$) and 1.156, 0.078, 0.068 MeV ($^{44}Ti \rightarrow {}^{44}Sc \rightarrow {}^{44}Ca$). Additionally, the positron annihilation line (511 keV) should accompany these decays both in supernovae explosions and, later on, in the surrounding supernova remnants due to the diffusive escape of e^+.

Recently Matteson (1982) has claimed a detection of the 1.809 MeV $^{26}Al \rightarrow {}^{26}Mg$ line from the direction of the Galactic centre. If confirmed, this would be the first detection of a gamma-ray line from a product of explosive nucleosynthesis. Several workers have detected lines from the Crab nebula including one at around 400 - 410 keV (Leventhal et al., 1977; Yoshimori et al., 1979, Ayre et al., 1981) which could be interpreted as the 511 keV positron annihilation line redshifted in the strong gravitational field expected near the surface of a neutron star. Another line at about 73 keV has been detected from this object (Ling et al., 1979;

Ayre et al., 1981) with possible evidence for both time variability and pulsation (Strickman et al., 1982); and has been interpreted as due to cyclotron emission near the polar cap of the neutron star.

The positron annihilation line has definitely been detected from the direction of the Galactic centre (Leventhal et al., 1978, Riegler et al., 1981. The first detection was probably by Johnson and Haymes 1973). Taken together, the data imply significant time variability in the line flux and a positron annihilation rate $\sim 10^{43}$ s^{-1} for a typical average flux of 2×10^{-3} ph $cm^{-2}s^{-1}$. Several mechanisms have been suggested as plausible explanations of this line emission. Cosmic ray interactions in the interstellar medium at the Galactic Centre region could give rise to e^+e^- annihilation radiation. However, the observed flux would require a large enhancement in the cosmic ray density in that region which would conflict with the gamma-ray flux levels for $E_\gamma \geq 100$ MeV. Additionally if diffuse cosmic ray interactions were the source, the 511 keV would also be accompanied by observable emission lines at other energies, notably the 4.4 MeV line from ^{12}C and other MeV lines from Mg, Si and Fe. None of these has been detected. Additionally it is difficult to account for the time variability of the flux (at least a factor of 5 between 1974 and 1979, Riegler et al., 1981) in this model. Indeed, the variability implies a maximum source size $\lesssim 1$ light

year. Since the annihilation rate of $\sim 10^{43}$ s^{-1} is two orders larger than that expected from a pulsar $\sim$ 10^{41} s^{-1} (Sturrock and Baker, 1979), a massive rotating black hole, $\sim 10^{6} M_{\odot}$, has recently also been postulated as the source of the 511 keV line. In this model infalling matter would form an accretion disk. Ultraviolet radiation from the disk coupled with strong dynamo action of the rotating hole would initiate an electromagnetic cascade thereby providing the required $e^{+}e^{-}$ annihilation rate. Ramaty and Lingenfelter (1981) note that this model can provide the necessary $e^{+}e^{-}$ G.C. line flux while not being inconsistent with observations at infrared and hard X-ray wavelengths.

With increased sensitivity it will become possible to map out the distribution of positrons in the Galaxy from large scale surveys of the 511 keV line.

2.3 Gamma-ray bursts

Colgate (1968) first considered the possibility that detectable bursts of gamma-ray emission should accompany supernovae events. However, between 1967 and 1979, 111 burst events were detected and catalogued (Klebesadel et al., 1982), but none simultaneously with a known supernova event. Indeed only one burst (1979 March 5) has been sufficiently localized to allow a probable identification with the supernova remnant N49, situated in the Large Magellanic Cloud. It should be noted, however, that this identification would imply

a peak luminosity $\sim 10^{45}$ erg s^{-1} and it has been argued that this was either an atypical event or because of energy requirements for certain burst source models that the identification is a line of sight effect. The poor spatial determinations of many gamma-ray bursts are a consequence of the indirect methods of photon detection. Arrival directions are determined by triangulation, a technique dependent on accurate timing and long baselines between the detectors to achieve good resolution. The positional accuracies are being improved to arc minute accuracy, with the use of distant interplanetary satellites.

The observed energy range of bursts extends from several keV to a few MeV and the bursts generally last between 0.1s and 10s, with fluxes in the range 10^{-7} to 10^{-3} ergs cm^{-2}. From the analysis of the accumulated data three distinct features are apparent in burst spectra.

(i) Short, single peak bursts generally obey an exponential type spectral form:

$$dN/dE = N_o \exp(-E/kT)$$

with $kT \simeq 150$ keV (Cline et al., 1976). High resolution spectra of several of these bursts show evidence for both emission and absorption line features. The emission features are widely believed to be from free-free electron bremsstrahlung in an optically thin medium; however, synchrotron processes could also be considered if the absorption features are interpreted as cyclotron absorption.

(ii) There are only two cases of recurrent emission from burst sources, the 1979 March 5 event repeated three times while the 1979 March 24 event recurred twice. The recurrent bursts exhibited variations in luminosity by up to two orders of magnitude, which along with their recurrent nature has been taken as evidence to suggest that these two events may form a separate class of gamma-ray bursts.

(iii) High resolution temporal analysis has identified periodicity in two events : 1977 October 29 (4.2s) and 1979 March 5 (8s) which strongly favours pulse-related phenomena as the burst sources.

Hurley (1983) has reviewed the observational data on gamma-ray bursts and concluded that 'no self-consistent explanation of the observations has yet been found'. Lack of precise identification with other known objects coupled with lack of simultaneous detection in other regions of the electromagnetic spectrum has confounded attempts to understand these enigmatic events. If the bursts were extragalactic in origin their energy requirements (like the 1979 March 24 event) would be enormous. It is generally believed that they must represent a local Galactic phenomenon. Jennings (1982) has modelled the observed log N - log S distribution for the bursts and finds the best fit to the data to be a disk source geometry with a scale height greater than 300 pc. Many models

have been considered for gamma-ray bursts including flare stars, accreting objects such as white dwarfs, neutron stars and black holes, star quakes and evaporating black holes. Verter (1981) has extensively reviewed each of these candidate models and considers that the two models most widely favoured are neutron star accretion and neutron starquakes. The non unique identification of any gamma-ray burst with other unusual astrophysical objects is good evidence in itself that at least one class of objects must exhibit violent sporadic outbursts of activity over and above their normally quiescent states.

2.4 Ultra high energy gamma-ray sources

Extensive air showers have for many years been utilized to study the energy spectrum and to a lesser extent the composition of cosmic rays in the range 10^{14}eV to 10^{20}eV. It is only indirectly through the cascade of secondary particles and radiation initiated in the upper atmosphere that these highest energy cosmic rays can be detected. As a part of these cascade processes, Cherenkov radiation is also produced which propagates to ground level as a collimated pool of light of radius $\sim$ 100 - 200m. Its intensity and distribution can be used to estimate the initial energy of the primary event as well as provide directional information accurate to a few degrees ($\lesssim$ 2° - 3°). The application of this

technique to primary photons as opposed to cosmic ray particles is very difficult because of the low ratio of primary photons to particles ($\sim 10^{-6}$ at $\sim 10^{9}$eV). Nevertheless experiments have successfully detected gamma-ray showers above few 10^{11}eV. There are two distinguishing features of a gamma-ray initiated shower which help distinguish it from the more frequent cosmic ray showers, though it has not always been possible to utilize these features due to limited instrumental sensitivity. The higher energy gamma-ray showers are expected to be increasingly muon poor and to exhibit a smoother radial density of particles (mainly electrons at ground level) than those showers originating from cosmic ray particles. These effects are due to the gamma-ray shower being essentially an electromagnetic process, whereas the cosmic ray shower will also lose energy through nuclear interactions. However cosmic rays are charged particles and their interactions with the Galactic magnetic field acts to tangle their trajectories. This renders cosmic rays almost isotropic except at the highest energies, the anisotropy being $\sim$ 0.1% from 10^{12}eV to 10^{14}eV and rising to only $\sim$ 1% by 10^{17}eV. Any spatial anisotropy in arrival directions of showers is therefore clear evidence of uncharged particles or photons coming from a discrete source. Allowing for relativistic effects the nearest identified sources at these energies are too distant for the showers to have been generated by neutrons (scale length $\sim 0.6\ (^{E}/_{10^{14}})$pc), notwithstanding the problems associated with accelerating

uncharged particles. Similarly periodicity of the shower arrival time implies pulsation and a discrete source origin.

To date the results have been in many cases inconclusive or inconsistent due to low statistics, which may in part have been due to time variability of the emitting objects. Both the Crab and Vela pulsars have been considered as possible sources of ultra high energy gamma-ray emission. In the case of the Crab this is reinforced by its well defined periodicity at other wavelengths, its relatively young age and its comparative closeness. Measurements have been made covering the energy range $\sim 10^{11}$eV to few 10^{13}eV with many experiments only being able to give upper limits to the flux (e.g. Helmken et al., 1973; Grindlay et al., 1976; Erikson et al., 1976; Bhat et al., 1980a). Nevertheless several positive detections have been made and the most recent observations point to short ($\sim$ 15 min) periods of pulsed emission (Dowthwaite et al., 1983). The situation with the Vela pulsar is similar with the evidence suggesting strong time variability of the signal (Grindlay et al., 1975; Bhat et al., 1980a).

The gamma-ray spectra for both these pulsars have been measured by the SAS II and COS B experiments (Section 3.7). The exponents of the COS B power law differential spectra are -1.9 and -2.2 for the Crab and Vela respectively. These spectra can be extrapolated from the medium energy satellite measurements to those at 10^{11} - 10^{13}eV. In

the case of the Crab pulsar the data suggests that the extrapolated spectrum must steepen slightly above ~ 10 GeV. However, for Vela the situation is markedly different. Based on the extrapolated spectrum, the predicted fluxes above 10^{11}eV are about three orders of magnitude larger than the observed upper limits. Clearly the Vela energy spectrum must steepen significantly above the present medium energy observations. It is interesting to speculate whether the required steepening of the Vela spectrum is related to its greater age in comparison to the Crab (Vela $\sim 10^4 - 10^5$ years, Crab 930 years).

The most consistent source of ultra high energy gamma-rays yet detected is the binary object Cygnus X-3 which has been monitored continuously by various groups since the radio outburst in 1972 (e.g. Vladimirsky et al., 1973; Galper et al., 1977; Dowthwaite et al., 1983). Phase analysis of the air shower arrival times have confirmed the 4.8hr. periodicity of this source which has been well established at other wavelengths. Through comparison of these accumulated data sets two interesting conclusions have been obtained. The gamma-ray flux ($\gtrsim 10^{12}$eV) varies with time, showing an overall decreasing trend since the first observations, a feature which is also apparent for radio and X-ray observations over the same period. This in itself is most interesting but it may also be related to the apparently conflicting observations of this object above 100 MeV (Section 3.6). Secondly the

absolute phase of the peak emission changes with epoch and although the statistics are limited in some cases there is also evidence favouring a double peak structure.

Recently Cyg X-3 pulsed emission has also been detected at higher energies (10^{14} - 10^{16}eV) by groups using the extensive air shower and Cherenkov techniques (Samorski and Stamm 1983a; Lloyd-Evans et al., 1983). These measurements are highly significant when it is remembered that space is essentially transparent to gamma-ray photons except above $\sim 10^{14}$eV, the threshold for e^+e^- pair production from photon-photon collisions involving the microwave background radiation field (Section 1 .2). The most recent distance determination of Cyg X-3 is based on measurements made during the 1982 radio outburst and place the object at a minimum distance of 11.6 kpc from the sun (Dickey 1983). The gamma-ray flux above 10^{14}eV must therefore suffer quite severe attenuation over the intervening path due to the presence of the isotropic microwave background photon field. Taking the attenuation into account the corrected fluxes are plotted in Figure 2.1, a general summary of the gamma-ray measurements of Cyg X-3. It should be noted that the corrections have been derived assuming the distance to be 11.6 kpc. and the microwave background temperature to be 2.7K both of which are matters of some contention, especially as the absorption coefficient for this process varies as T_{ph}^3. Assuming all these observations to be

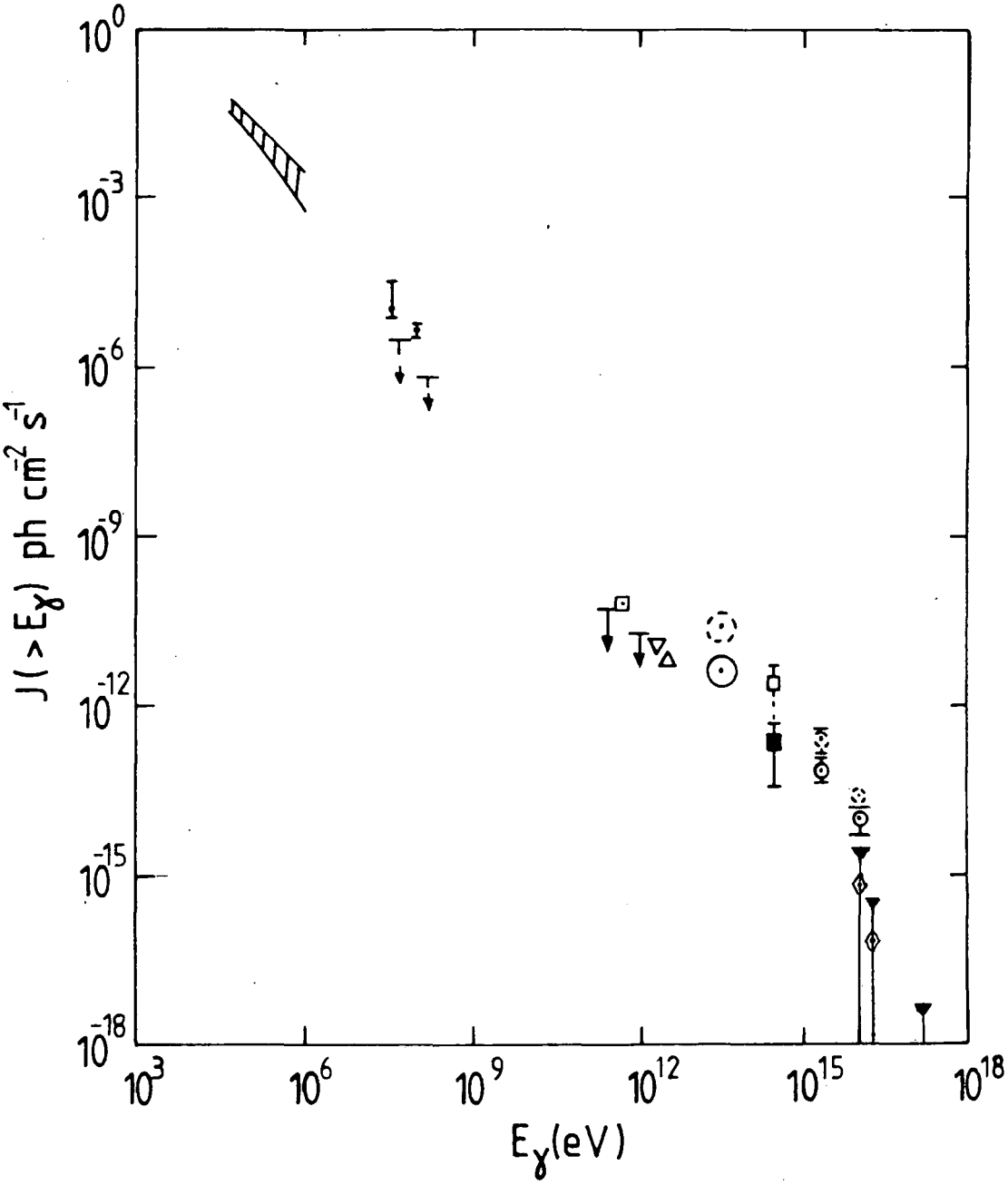

Figure 2.1 The integral spectrum for Cygnus X-3.
Meegan et al. (1979), Lamb et al. (1977), SAS II, Hermsen (1983), COS B, Weekes et al. (1977), Danaher et al. (1981), Mukanov et al. (1979), Lamb et al. (1982), Samorski and Stamm (1983a), Morello et al. (1983), Bhat et al. (1984d), Lloyd-Evans et al. (1983)
The broken points are the observations corrected for attenuation as described in the text. It should be noted that these observations span a period of almost 10 years. Many of the features in the spectral shape may be due to time variability, a well established phenomenon at other

correct it is apparent from Figure 2.1 that the spectral shape in the region above $\sim 10^{14}$eV exhibits unusual structure and that the emission cannot be described by a single power law extending over all energy ranges. Further observations are needed here to confirm the nature of the spectral features and to bridge the gap between a few GeV and 100 GeV.

Samorski and Stamm (1983b) have also found tentative evidence for up to five more ultra high energy gamma-ray sources, while the Adelaide group (Protheroe et al., 1984a) have reported the detection of a pulsed signal ($\gtrsim 10^{15}$eV) from Vela X-1. It is increasingly apparent that the evidence for the existence of ultra high energy gamma-ray sources is very strong indeed. There are several important implications arising from the production of gamma-rays up to $\sim 10^{16}$eV in Galactic sources which will be briefly discussed.

Anisotropies in the arrival direction of cosmic ray showers have long been studied for clues as to the possible origin of these energetic particles. Although many early results in this field were inconsistent there is now a generally accepted view that between 10^{12} and 10^{14}eV the cosmic rays appear remarkably isotropic (anisotropy $\sim 0.1\%$ and the phase of the first harmonic of the arrival directions remaining constant). However, Wdowczyk and Wolfendale (1983, 1984) have studied the accumulated data on air shower arrival directions at these energies. They have found evidence for an excess of air showers (10^{14} - 10^{16}eV)

from the Galactic plane and preferentially from the inner Galaxy. In the light of the Cyg X-3 and other observations at these energies they consider it likely that ultra high energy gamma-ray sources contribute significantly (perhaps as much as 0.1%) to the primary cosmic radiation. They find the observations consistent with the rapid variations in phase and anisotropy. Furthermore, they conclude that the gamma-ray flux from such objects must fall rapidly above about 3×10^{16}eV (as air shower measurements suggest) to be consistent with the observed anisotropy of the highest energy air showers. Finally, they note the possible consequences for cosmic ray energy requirements on the basis of Cyg X-3 observations. Assuming isotropic emission the minimum gamma-ray luminosity for this object is $\sim 10^{37} - 10^{38}$erg s^{-1} above 10^{15}eV. It seems plausible to expect 10^{15}eV protons to be emitted with at least the same efficiency. The total estimated energy in cosmic rays in the Galaxy is $\sim 3 \times 10^{40}$ erg s^{-1} above $\sim 10^{9}$eV and the implication is clear that a small population of Cyg X-3 type objects could provide most if not all, of the observed cosmic ray flux at least up to $\sim 10^{16}$eV.

Ultra high energy gamma-ray ($\sim 10^{15}$eV) interactions with photons of the microwave background will produce e^+e^- pairs each with energy $\sim 10^{14}$eV which can then synchrotron radiate to give X-rays of energy few keV up to few MeV. In applying these considerations to a possible Galactic population of Cyg X-3 type sources there are many

uncertainties, not least in the time variability of the gamma-ray output but also in the spatial variations of the Galactic magnetic field and uncertainty in the total number of such sources. Nevertheless, Rana et al. (1984) have addressed this problem and have found that there should be a significant contribution to the hard X-ray flux above $\sim$ 100 keV at high Galactic latitudes, even if there is just one Cyg X-3 type source in the Galaxy.

Finally, mention should also be made of the gamma-ray flux (0.4×10^{-10}ph cm^{-2}s^{-1} above 3×10^{11}eV) detected by Grindlay et al. (1975) from the nearby radio galaxy Centaurus A (distance $\sim$ 6.3 Mpc), but unconfirmed by other groups. Interestingly Protheroe et al. (1984b) claim to have detected emission from this object above $\sim 10^{15}$eV. If these observations are confirmed it will be difficult to reconcile them with the severe attenuation expected from photon-photon collisions on the intervening microwave background radiation. Nevertheless it would appear that even for this first extragalactic ultra high energy gamma-ray source, time variability is an important characteristic of the emission.

It is clear from the brief review presented in this chapter that the various branches of gamma-ray astronomy all show good evidence for time variability of the source emission and especially in the case of ultra high energy emission strongly imply that a Galactic origin for most cosmic rays (at least up to $\sim 10^{16}$eV) is not unreasonable.

CHAPTER THREE

MEDIUM ENERGY GAMMA-RAY ASTRONOMY

3.1 Introduction

In the region of the gamma-ray spectrum from a few tens of MeV to several hundred MeV the signal from the Galaxy and beyond is masked from ground based observations by the presence of secondary photons, generated by cosmic ray particles in the earth's atmosphere. Thus satellite borne spark chamber detectors are generally used for observations in this energy range. However, at the lower end of the range high altitude balloons have also made useful contributions to our knowledge of the spectrum. Spark chambers have poor angular resolution, often characterised by a cone of half-angle σ_θ containing 68% of the reconstituted arrival directions of incident photons. Typically $\sigma_\theta \simeq$ 8° - 10° at 30 MeV and improving to about 1° - 2° above several hundred MeV. Coupled with this lack of definition is the intrinsically low flux, adding uncertainty to the data interpretation.

The first detection of non-atmospheric gamma-rays above 100 MeV was made by scintillators aboard Explorer XI (Kraushaar et al., 1965). Using a spark chamber, OSO III in 1967 was able to detect a finite flux from the Galactic plane above 50 MeV. The angular resolution was very poor (Gaussian, full width half maximum = 24°), however analysis of the data showed an enhancement from the region of the Galactic centre and some evidence from high latitude observations for an isotropic component

of possible extragalactic origin (Kraushaar et al., 1972).

Since then our knowledge of the gamma-ray sky has been significantly improved through analysis of the data collected by NASA's SAS II satellite and ESA's COS B. SAS II, launched five years after OSO III, was able to survey more than half the sky before an instrumentation failure terminated the mission after only six months. This database produced the first detailed picture of the Galaxy in gamma-rays. In addition, it provided the first observations of gamma-ray pulsars and confirmed the existence of an apparently isotropic component of the emission at high Galactic latitudes.

In terms of instrumental performance, COS B was in many ways similar to SAS II. Whereas SAS II covered the energy ranges 35-100 MeV, 100-1000 MeV, COS B energy resolution extended over 50-150 MeV, 150-300 MeV and 300-5000 MeV. Angular resolution was similar in both cases (about 3.6^{o} - 3.8^{o} degrees above 100 MeV). However, COS B suffered from a large and uncertain instrumental background which was essentially negligible in SAS II. This tended to restrict COS B usefulness to regions close to the Galactic plane. The background problem is further discussed in Section 4.3 in relation to the detection of discrete sources. The longer lifetime of COS B (1975 - 1982) enabled it to significantly improve the counting statistics along the Galactic

plane, with an estimated 100,000 useful events obtained in comparison to 13,500 for SAS II and only 621 for OSO III. Analysis of the COS B data is still continuing, although many results have already been obtained.

COS B was able to confirm many of the SAS II results but the major scientific importance of COS B rests with the claim to have detected 25 discrete gamma-ray sources, 22 of which lie within 10° of the Galactic plane. The existence of these sources, their consequences for gamma-ray astronomy and its role in interpreting Galactic cosmic ray dynamics has proved to be the most enduring and as yet unresolved issue within the subject.

While the questions relating to gamma-ray sources are central to the work of this thesis, it is appropriate here to review the preceeding work on medium energy gamma-ray astronomy, giving perspective to the arguments we shall develop in subsequent chapters.

3.2 General features of the Galactic gamma-ray emission

The data from SAS II and COS B have been used in conjunction with measuremnts of HI, H_2 (via CO), galaxy counts and radio synchrotron emission to elucidate the relationship between cosmic rays and the constituents of the interstellar medium. These studies have been carried out on a variety of scales ranging from small scale structures and the local interstellar medium (such as nearby molecular clouds) through to comparison with large scale Galactic structure as traced by the

spiral arm features.

Interpretation of the data over such a wide range of scale lengths is necessarily dependent on our knowledge of additional inter-related factors. Our understanding of the composition of the interstellar medium decreases as we move further away from the local stellar environment. Specifically, the mass of molecular hydrogen plays a major role in limiting the precision of large scale Galactic studies. Analyses and conclusions drawn must consider the problems of deriving the column density of H_2, N_{H_2}, from CO measurements and the possible effects of the Galactic metallicity gradient upon the conversion. Similarly the contribution to the gamma-ray emission from inverse Compton processes depends on our inferred knowledge of the photon distributions in the Galaxy. While these problems can, to some extent, be tackled independently of the gamma-ray measurements, the role of discrete gamma-ray sources poses severe uncertainties for any large scale analysis of the gamma-ray data, particularly in the inner Galaxy.

Generally we find the uncertainties in the conclusions drawn from the data increase with the scale over which we perform the analysis. However, progress has been made and while many uncertainties still remain, it is clear that gamma-ray astronomy can benefit from observations in other regions of the electromagnetic spectrum. Indeed, in some cases the knowledge gained

from gamma-ray observations can be used to constrain the interpretation of related astronomical phenomena.

3.3 Gamma-ray correlations with Galactic tracers

The data collected by the SAS II experiment have been extensively analysed by the NASA group (e.g. Fichtel et al., 1975; 1978a; Kniffen et al., 1977; Hartman et al., 1979). These workers presented the variation of the gamma-ray flux with Galactic longitude and latitude. The improved resolution and statistical accuracy over that achieved by OSO III enabled several features to be identified. Figure 3.1 is an intensity contour map of the Galactic plane derived from the tabulated SAS II data, published by Fichtel et al. (1978b). An enhanced region along the Galactic plane is visible extending from $l \simeq 335°$ to $l \simeq 40°$ without showing a narrow peak at the Galactic centre. The longitudinal and latitudinal distributions have been shown to correlate well with Galactic structure, in particular the spiral arm patterns. Good correlations also exist between the gamma-ray observations and measurements of gas column density N_{HI} and with radio synchrotron data. These studies permitted the identification of gamma-ray emission from the local concentration of clouds known as Gould's belt.

The COS B data enabled a more detailed analysis of the Galactic gamma-ray flux to be made. Mayer-Hasselwander et al. (1980, 1982) have presented these

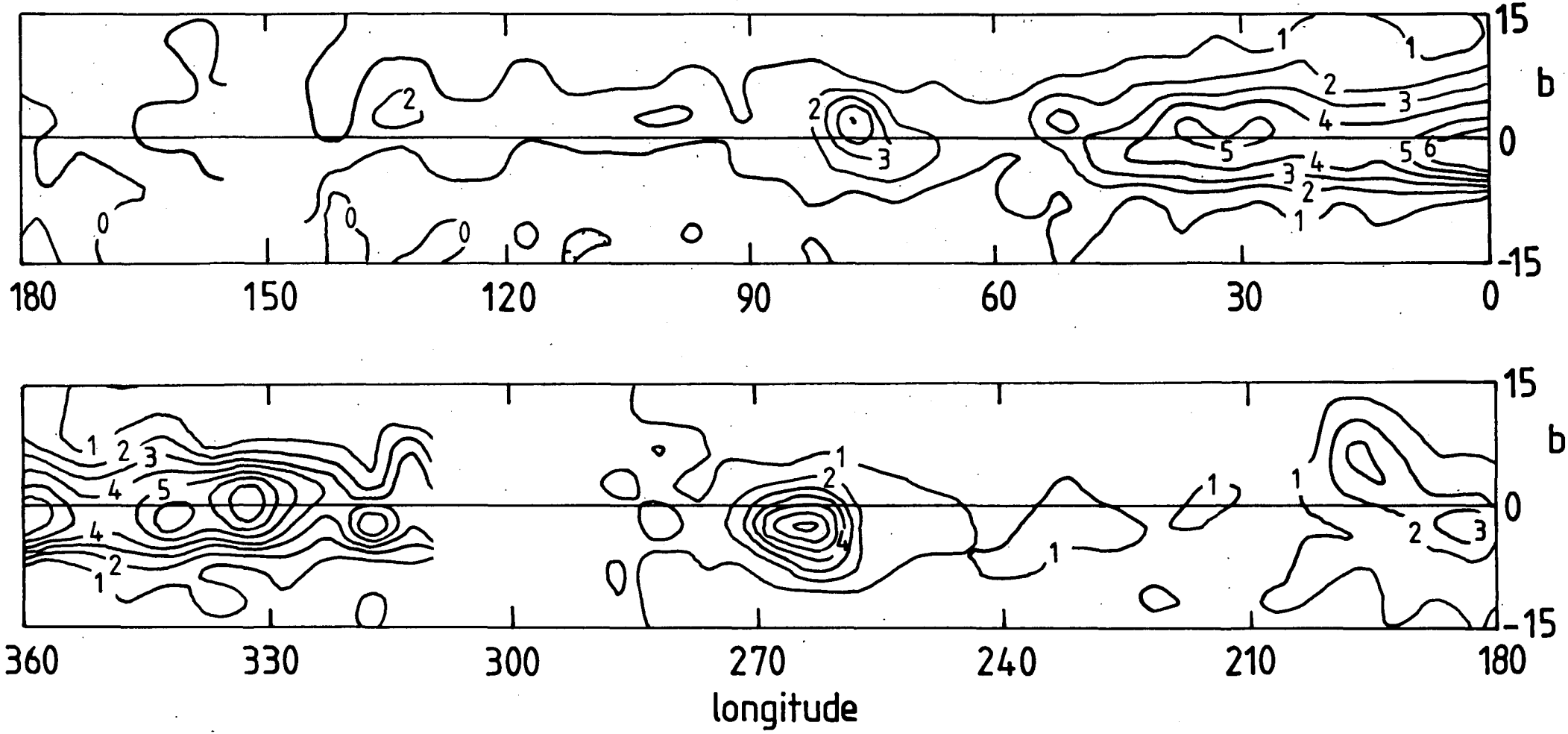

Figure 3.1 Gamma-ray intensity contours ($E_\gamma > 100$ MeV) derived from the SAS II data. The contour levels are i x 10^{-4} ph $cm^{-2}sr^{-1}s^{-1}$. Two longitude ranges totalling $\Delta l = 30^o$ are excluded as the data are inadequate.

data and confirmed both the large and small scale relationships between features of Galactic structure and the gamma-ray observations.

Haslam et al. (1981) made a detailed spatial comparison between the COS B data and radio continuum emission at 408 MHz. These workers were able to show that both data sets exhibited a strong similarity. They considered it good evidence that cosmic rays, gas and magnetic fields in the Galaxy are dynamically coupled, at least along the Galactic plane, and strongly suggestive of a diffuse origin for the bulk of the observed gamma-rays.

Many workers have used the gamma-ray data to investigate the Galactic distribution of cosmic rays, by comparing the observed fluxes with those expected from cosmic ray interactions with the gas and photons of the interstellar medium (e.g. Bignami et al., 1975; Fichtel et al., 1976, Kniffen et al., 1977; Lebrun et al., 1983, Fichtel and Kniffen 1984). Other workers (e.g. Puget and Stecker, 1974; Strong and Worrall, 1976; Caraveo and Paul, 1979, Issa et al., 1981 ; Li et al., 1982) unfolded the gamma-ray data to a radial emissivity distribution. Comparison with radial gas distributions then in principle allowed the cosmic ray radial density to be determined. The unfolding procedure is limited in that it requires assumptions on radial symmetry and scale heights, thus losing much of the small scale

variations.

Initially there was modest evidence from both the unfolding and direct approaches for the existence of a cosmic ray enhancement (by a factor $\simeq$ 4-10) towards the Galactic centre. However, these arguments were subject to the limitations imposed by uncertainties in the mass of gas in the inner Galaxy. Additionally, it was possible that an unresolved population of discrete gamma-ray sources could mimic the longitudinal variation of the gamma-ray flux while being consistent with a uniform cosmic ray intensity throughout the Galaxy.

In an attempt to overcome both these difficulties Dodds et al. (1975) considered only the outer Galaxy where the contribution from discrete sources could reasonably be expected to be small.

Similarly the uncertainties in the gas distribution were believed to be negligible, the gas being primarily atomic hydrogen. These workers concluded that a reduced cosmic ray density relative to the local value could explain the observed gamma-ray fluxes. Such a reduction in the cosmic ray density outside the solar circle could only reasonably be accommodated within a Galactic origin model for these particles.

Interestingly, Bloemen et al. (1984a,b) have repeated this analysis with COS B data and improved measurements of HI and CO in the outer Galaxy. Using results from three energy bands they concluded that the data are

consistent with a gradient (and hence Galactic origin) for cosmic ray electrons and a uniform distribution of cosmic ray protons. There remain uncertainties in the gas distribution in the outer Galaxy and in the relative contributions from electron and proton gamma-ray processes to the observed COS B signal. Further work is required before the latter conclusion can be confirmed.

Instead of analysing the data in the Galactic plane many workers have recently considered intermediate latitudes ($|b| \simeq 10° - 20°$) as a restrictive probe of the local interstellar medium. Thus the probable contributions of H_2 and discrete sources are restricted, adding weight to the conclusions.

Issa et al. (1981) analysed the SAS II and HI data and found evidence for a local cosmic ray gradient, extending over Galacto-centric radii $\sim$ 8-12 kpc. A similar analysis using both COS B and SAS II data and galaxy counts as a total gas tracer made by Bhat et al. (1984a) has supported the existence of a local cosmic ray gradient.

Galaxy counts can be used as an indirect tracer of gas (Section 6.3) and the extensive available sky coverage has prompted several workers to combine them with gamma-ray data. This technique is generally limited to regions away from the Galactic plane, saturation effects making it less reliable at small Galactic latitudes.

Lebrun and Paul (1983) analysed the SAS II data in this manner, comparing the observed fluxes with those predicted from cosmic ray interactions with gas as derived from galaxy counts. The correlations between gamma-rays and galaxy counts were shown to be better than between gamma-rays and HI, thus inferring the presence of additional non-atomic gas, presumably H_2. Strong et al. (1982) and Lebrun et al. (1982) analysed the COS B data ($|b|$: 11° - 19°) with similar conclusions to those obtained by Lebrun and Paul. They were also able to use the gamma-rays, galaxy counts and HI to map out on a scale of a few degrees the local distribution of molecular gas at these latitudes. Recent CO observations by Lebrun and Huang (1984) have confirmed the general nature of this H_2 distribution in the Sagitarius region. Although their measurements of N_{H_2} are less than inferred by Strong et al. (1982) ($\sim$ a factor of 2) part of the difference is likely due to uncertainties in the gas-to-dust and CO-to-H_2 ratios. Nevertheless the essential technique is correct, illustrating how gamma-rays can provide a useful indicator for other astronomical measurements.

3.4 Spectral shape of the diffuse Galactic emission

Both COS B and SAS II provided limited energy resolution of the observed gamma-ray spectrum. After allowing for the energy response of the detectors it was possible to derive the spectral shape of the incident

flux. These data are plotted in Figure 3.2 along with the theoretical predictions made by Fichtel and Kniffen (1984) based on current best estimates of the gas and photon distributions within the Galaxy. Additional low energy data come from balloon experiments. From their detailed analysis of the longitude and latitude distributions of the observed intensities they concluded that there was reasonable agreement with their models based on contributions to the intensity from cosmic ray nucleon-nucleon collisions, bremsstrahlung and inverse Compton emission. They also noted the areas of potential uncertainty : point source contributions (especially below 100 MeV), the shape of the interstellar electron spectrum below about 1 GeV and the absolute mass of H_2 determined from CO. Bertsch and Kniffen(1983) concluded from their balloon measurements (10 - 80 MeV) that the spectral shape observed by SAS II and COS B appears to continue down to at least 10 MeV. Studies of the spectral shape can be used to constrain the interstellar electron spectrum below 1 GeV where direct measurements are not obtainable (e.g. Strong and Wolfendale, 1981, Lebrun et al. 1982, 1983).

Mayer-Hasselwander et al. (1982) noted that the spectral shape of the COS B data ($|b| < 10°$) did not vary significantly with longitude and was in close agreement with that determined by Lebrun et al. (1982)

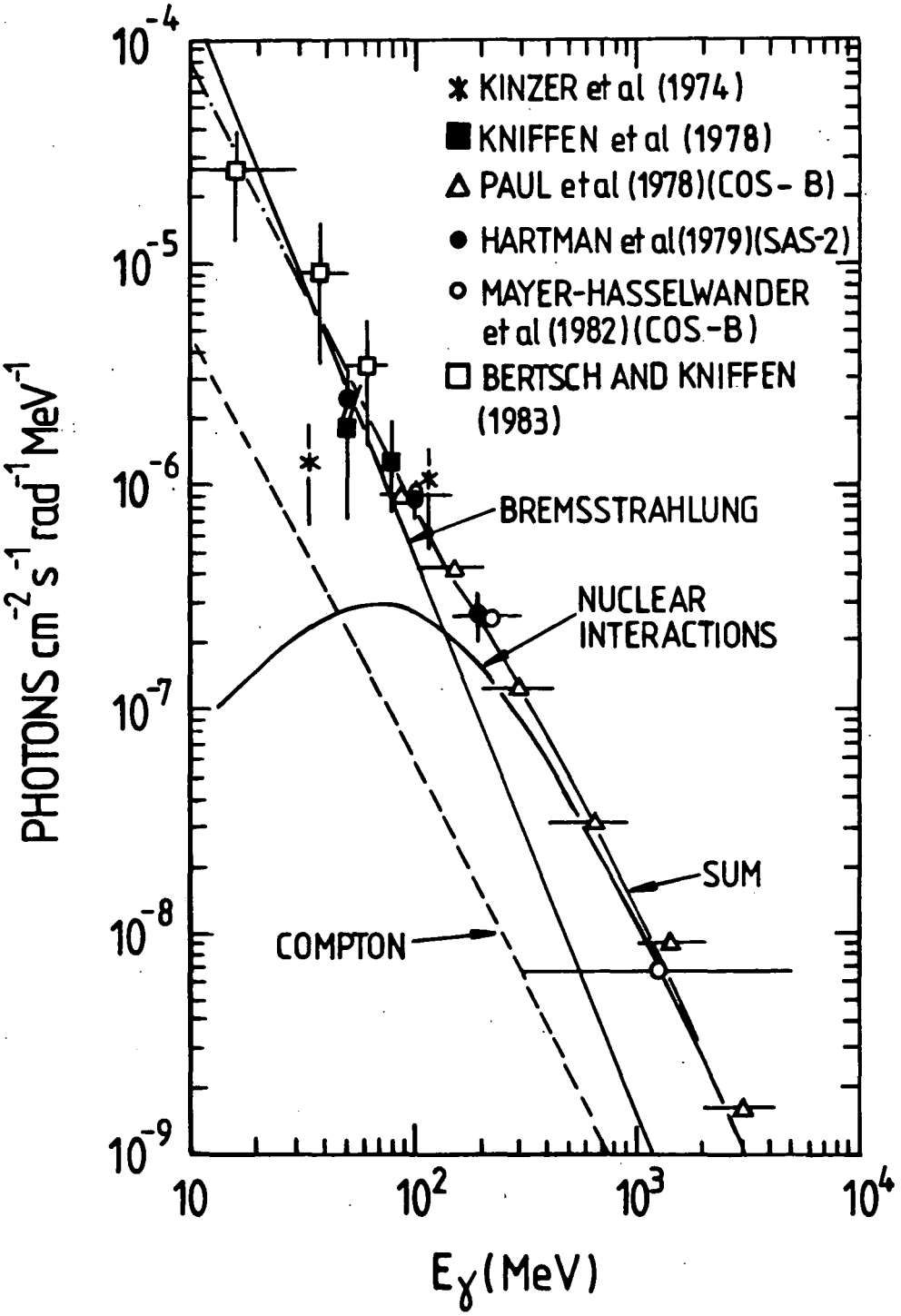

Figure 3.2 Observations of the Galactic gamma-ray spectrum compared with the calculated model of Kniffen and Fichtel (1984) for a region near the Galactic centre.

from the local interstellar medium. As an approximation the gamma-ray data (> 100 MeV) can be described by a single power law ($N(E) \sim E^{-\gamma}$) of index $\gamma \sim 2.0$.

3.5 Gamma-ray emission from molecular clouds

Several workers have analysed the expected gamma-ray fluxes from local molecular clouds ($\lesssim 2$ kpc). The Orion molecular clouds have been detected in both the SAS II data base (Wolfendale, 1981) and that of COS B (Caraveo et al., 1980). Issa and Wolfendale (1981a) have analysed the gamma-ray fluxes from the directions of 13 nearby molecular clouds. They were able to show that the flux from most clouds required cosmic ray intensities within a factor of 2 of the local value. The remainder, requiring cosmic ray intensities in excess of the ambient local value, were considered as possible cases of cosmic ray enhancement within the clouds. The Orion complex is the best resolved both in gamma-rays and in CO measurements. Recent work has focused on these clouds to calibrate the local $CO \rightarrow H_2$ conversion (Bloemen et al., 1984c, Houston and Wolfendale, 1984b). These clouds are treated in more depth in the present work (Chapter 6) where an investigation is made of the degree of penetration of the dense molecular gas by the ambient cosmic ray flux.

Black and Fazio (1973) first considered molecular clouds as possible gamma-ray 'sources' because of their high column density relative to the general interstellar

medium and the poor angular resolution of gamma-ray detectors. These objects would not be genuine discrete gamma-ray sources, but rather unresolved regions of enhanced emission. Interestingly one of the sources originally claimed by COS B (2CG 353 + 16) is now acknowledged to be consistent with cosmic ray irradiation of the extensive molecular complex ρ Ophiuci. The earlier claims for its discrete nature were based on a subset of the complete COS B data base.

Li and Wolfendale (1981, 1982) and Arnaud et al. (1982) used Monte-Carlo techniques to analyse the extent to which molecular complexes irradiated by cosmic rays could be mistaken for discrete sources when observed by a typical gamma-ray detector. From their analyses they concluded that many of the weaker sources claimed by COS B could be explained as unresolved giant molecular clouds. The implications of these studies for the COS B sources are most important, particularly in relation to the discrete source contribution to the observed emission. This is pivotal to the present work and the role of these pseudo sources is developed in Chapters 4 and 5.

3.6 Discrete gamma-ray sources

The angular resolution and statistics collected by OSO III were insufficient to permit the identification of any discrete gamma-ray sources. The data collected

by SAS II and COS B enabled spatial and temporal (pulsed emission) identification of discrete sources to be made. Two distinct classes of gamma-ray sources exist at present. Those identified with known objects observed at other wavelengths, and hence genuinely discrete, and the majority detected by COS B which remain unidentified.

The SAS II group was able to detect pulsed emission from the Crab (Kniffen et al., 1974) and Vela pulsars (Thompson et al., 1975) and from Cygnus X-3 (Lamb et al., 1977). They also observed pulsed emission from an unknown source situated towards the Galactic anti-centre. COS B confirmed the detections of the Crab and Vela pulsars. Initially the source in the anti-centre (now known as Geminga or 2CG 195 + 5) was confirmed by both spatial and temporal analyses. Detection by COS B of the pulsed emission was later retracted, though it now appears that the initial COS B and SAS II results were essentially correct (Bignami et al., 1984).

COS B was unable to detect the characteristic 4.8 hr. period pulsed emission from Cygnus X-3 (Swannenburg et al., 1981). This non-detection by COS B does not invalidate the observations made by SAS II. As pointed out previously (Section 2.4) repeated observations of this object have shown strong long term temporal variability in radio, X-ray and ultra-high energy gamm-ray fluxes, with the flux $\gtrsim 10^{12}$eV passing through

a minimum during the period of the COS B observations. It is not inconsistent to expect the flux > 100 MeV to also exhibit variability. The COS B data can be regarded as strongly suggesting that Cygnus X-3 is in fact a time variable medium energy gamma-ray source. One further source (2CG 356 + 00) detected by COS B in 1 out of 5 observation periods is also considered to be time variable.

From comparison of the SAS II and COS B data there is no evidence for long term temporal variation of the fluxes from Crab, Vela and Geminga, within the statistical limits of the observations.

Further analysis of the SAS II data for gamma-ray pulsars was unable to produce any positive results (Thompson et al., 1983). Similar results have been found by COS B (Buccheri et al., 1983) though further work is continuing.

Through a statistical analysis of the spatial distribution of the COS B data a complete catalogue of gamma-ray sources has been derived (Hermsen, 1980; Swannenburg et al., 1981). The 2CG catalogue comprises 25 sources (including the now resolved ρ Ophicui molecular cloud). One source is identified with the quasar 3C273 (Bignami et al., 1981) and our own analysis of the SAS II data produced similar fluxes, Table 3.1. Another high latitude source (2CG 010 - 31) has only

been observed once and remains unidentified.

Of the remaining 22 sources ($|b| < 10°$) only the Crab and Vela have been positively identified. Geminga is most probably identified with the periodic X-ray source detected by Bignami et al. (1983, 1984) using data from the EINSTEIN and EXOSAT satellites. The X-ray source has been detected as a faint optical source ($m_V \sim 21$) (Caraveo et al., 1984). Searches for pulsed radio emission have as yet proved unsuccessful.

The relatively large error circles (typical radii being 1° - 1.5° for the weaker sources) on the remaining low latitude 2CG sources preclude identifications on purely positional coincidences. X-ray and radio pulsar searches of the error circles are continuing for objects with unusual characteristics. No conclusive identifications have yet been made and are unlikely to be made until refined gamma-ray data become available.

3.7 The nature of the gamma-ray sources

The 20 unidentified 2CG sources are termed Galactic because of their narrow latitude distribution ($\langle b \rangle \simeq 1.5°$). Several models have been proposed for these objects. Lamb (1978) suggested they may be young supernova remnants while Montmerle (1979) considered the combination of a supernova remnant with a nearby OB association (SNOB). These are extended source models relying on cosmic ray interactions with components of the interstellar

medium. In this respect unresolved molecular clouds (Section 3.5) have also been suggested for several of the 2CG sources.

Free radio pulsars and accreting neutron stars in binary systems are the favoured models for genuine discrete sources, in light of the identifications of the Crab and Vela pulsars and the observations of Geminga. Bignami and Hermsen (1983) have summarized the present data on the 2CG sources, observations at other wavelengths and the details of the various theoretical models under consideration.

The spectral characteristics of the Crab, Vela and Geminga sources are similar. The COS B data can be well described by power law spectra with indices ($N(E) \sim E^{-\gamma}$) γ = 2.2, 1.9, 1.8 respectively. For the quasar 3C273 (2CG 289 + 64) γ = 2.6 and the remaining unidentified sources are consistent with $\langle\gamma\rangle$ = 2.0.

Both the Crab and Vela exhibit double pulsed structure at gamma-ray energies > 50 MeV with reduced interpulse emission. The Crab gamma-ray light curve exhibits strong similarities with the light curves at radio, optical and X-ray energies. For Vela the light curves differ at radio, optical and gamma-ray energies, though interestingly the phase separation of the double gamma-ray peaks in Vela is similar to that for Crab.

Early speculation on the nature of the gamma-ray sources considered them as a new class of astrophysical

objects. While this possibility cannot as yet be completely rejected it does appear most unlikely. The present 2CG source catalogue is not considered complete in the sense of only containing genuine discrete sources. Rather the present work favours a mixture of discrete sources (probably pulsars or neutron stars) and unresolved regions of enhanced emission (the cosmic ray irradiated giant molecular clouds).

3.8 Extragalactic gamma-ray emission

Analysis of the SAS II data (Fichtel et al., 1978b) confirmed the tentative results from OSO III on the existence of a diffuse extragalactic component to the gamma-ray flux. Correlation of the gamma-ray data with HI and radio synchrotron emission indicated a residual component to the gamma-ray flux towards the North Galactic pole. This has since been confirmed in studies using galaxy counts as total gas tracers (Thompson and Fichtel, 1982; also Section 7.2). The residual flux has a relatively steep differential spectral index ($\simeq$ 2.8) compared with the low latitude Galactic component ($\simeq$ 2.0). COS B has been unable to confirm these measurements because of its large instrumental background which made it unsuitable for observations at high Galactic latitudes (i.e. low flux regions).

The sparse nature of the data on the extragalactic gamma-ray component has given rise to extensive theoretical speculation on its origin. Indeed there is the possibility that it is not truly extragalactic but results from

inverse Compton interactions of cosmic rays diffusing out of our Galaxy (Worrall and Strong, 1977; Worrall, 1977). Although the statistics are poor the high latitude ($|b| \geqslant 30°$) SAS II data are relatively isotropic on scales greater than the angular resolution. In terms of a simple halo model for the additional high latitude flux the isotropy requires a halo radius $\gtrsim$ 50 kpc. This in turn necessitates much greater diffusion of the cosmic ray particles (primarily electrons) than is conventionally assumed in the Galactic plane. Recent analysis of the SAS II and 408 MHz synchrotron data (Riley and Wolfendale, 1984) has suggested a modest contribution to the Galactic flux from an extended inverse Compton component. Thus it is likely that a small fraction of the extragalactic flux should be associated with our own Galaxy. However, there are compelling reasons to believe that a truly extragalactic component must also be present.

Our Galaxy can itself be thought of as a single gamma-ray source and it is to be expected therefore that other normal galaxies should contribute to an extragalactic flux. Analysis of the SAS II data from the region of the Large Magellanic Cloud (LMC) supports this contention. For this object we estimate F_γ (> 100 MeV) $(1.5 \pm 1.4) \times 10^{-6}$ ph $cm^{-2}s^{-1}$, not inconsistent with a simple model assuming gamma-ray luminosity scales as the galactic mass. The Small Magellanic Cloud (SMC)

and M31 have not been detected at these energies, but their fluxes are expected to lie just below the current threshold.

From the SAS II data we can derive the upper limit to the flux above 100 MeV from M31. We find F_γ $(>100$ MeV$) \lesssim 0.3 \times 10^{-6}$ ph $cm^{-2}s^{-1}$ (Table 3.1) and assuming the spectral shape is similar to our own Galaxy $(N(E) \sim E^{-2})$ then F_γ $(> 10^{12}$eV$) \lesssim 0.3 \times 10^{-10}$ ph $cm^{-2}s^{-1}$. Dowthwaite et al. (1984) have detected a flux above 10^{12}eV from M31 using the atmospheric Cherenkov technique. They find F_γ $(> 10^{12}\text{eV}) = 2.2 \pm 0.7 \times 10^{-10}$ph $cm^{-2}s^{-1}$, an order of magnitude above the upper limit expected from the SAS II data. These measurements strongly suggest the spectrum is flatter than E^{-2} or has an additional component at ultra-high gamma-ray energies.

Turning to active galaxies, Cen A has been detected both at X-ray energies (10 keV - MeV; Dean and Ramsden 1981 and references therein) and also at ultra-high gamma-ray energies (Section 2.4). Similarly the flux from the Seyfert galaxy NGC 4151 has been measured from keV up to MeV energies (see Dean and Ramsden, 1981). There is some evidence from the SAS II data and we have estimated the fluxes from these objects, Table 3.1. In Chapter 7 we explore further the role of discrete sources (specifically radio galaxies and galaxy clusters) as a component of the extragalactic flux.

	SAS II		COS B
Object	F_γ(35–100 MeV)	F_γ(>100 MeV)	F_γ(>100 MeV)
LMC	3.4	1.5 ± 1.4	
M31	0.5	0.3	0.8
Cen A	2.3 ± 1.6	1.5	1.2
NGC4151	0.4 ± 0.3	0.6 ± 0.4	0.9
3C273	0.4 ± 0.3	0.6 ± 0.4	0.6 ± 0.4

Table 3.1 All fluxes are in units of 10^{-6}ph $cm^{-2}s^{-1}$. The SAS II values are derived by us from the tabulated data of Fichtel et al. (1978b). The COS B values are from Pollock et al. (1981) assuming $N(E) \sim E^{-2}$. The SAS II upper limits are 1 σ , those from COS B are maximum likelihood estimates.

The low angular resolution of present gamma-ray detectors renders it impossible to resolve potential extragalactic sources such as galaxies or clusters. However, the possibility remains that the extragalactic flux may be predominantly diffuse in nature. It is useful to compare present measurements with those extending down to several hundred keV, as shown in Figure 3.3.

Two models have been proposed to explain a genuinely diffuse extragalactic gamma-ray flux. Ginzburg (1968) and Stecker (1969) have considered the interactions of cosmic rays in the early universe. In this model gamma-rays are produced at high redshifts and the characteristic π° peak at $E_{\gamma} \simeq 67$ MeV (Section 1.2) is displaced to lower energies during the cosmic expansion. These workers noted that the gamma-ray spectrum and the bump evident at a few MeV (Figure 3.3) would be consistent with the redshifted production spectrum after allowing for distortions by cosmological effects.

A similar cosmological explanation has been suggested by Stecker (1983), Stecker and Wolfendale (1984) and draws its inspiration from the baryon symmetric cosmology developed by Omnes (1969). Here the universe is partitioned into matter-antimatter regions, at least on the scale of galaxy clusters. The formation of these cells in the early universe would have given rise to matter-antimatter annihilations ($p\bar{p}$) producing gamma-

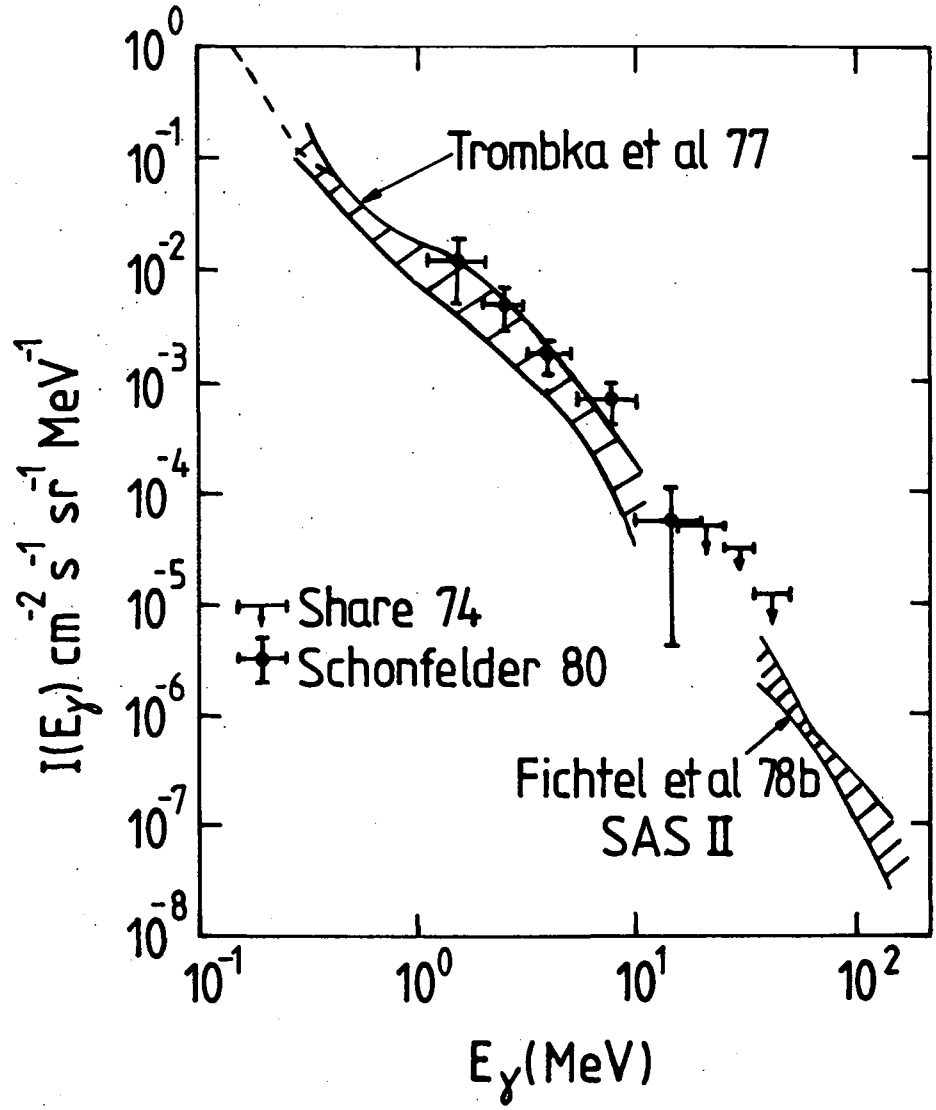

Figure 3.3 The observed diffuse gamma-ray spectrum, presumed to be extragalactic in origin. The bump around a few MeV is apparent when compared with the extrapolation from lower energies.

rays from π^0 decays. The spectrum from these early epochs would then be redshifted to produce that observed today.

An additional prediction of the latter model is the existence of antimatter in the cosmic ray flux. Buffington et al. (1981) have detected an antiproton flux, $F_{\bar{p}} = (1.7 \pm 0.5) \times 10^{-4}$ $\bar{p}$ $m^{-2}sr^{-1}s^{-1}$ MeV^{-1} between 130-320 MeV. This is in excess ($\sim$ a factor of few 10^2) of that expected from Galactic production in spallation products of protons and heavier nucleii with the interstellar medium. Galactic black holes have been suggested as sources of the additional antiprotons (Kiraly et al., 1981; Protheroe, 1983). However Stecker and Wolfendale also consider that the excess might be consistent with the extragalactic gamma-ray flux and matter-antimatter cosmology. A conclusive test of these ideas must await the positive detection of antinuclei ($Z > 1$) in the cosmic radiation and the resolution of the gamma-ray flux into filaments delineating the matter-antimatter boundaries.

Said et al. (1982) have compared the SAS II extragalactic flux above 100 MeV with that expected for several Universal cosmic ray origin models involving combinations of cosmic ray density and estimates of gas in galaxy clusters and the intergalactic medium at the present epoch. They conclude that the measured extragalactic gamma-ray flux indicates that at least

90% of cosmic ray protons in the energy range 1-10 GeV are Galactic in origin.

CHAPTER FOUR

SAS II - THE EVIDENCE FOR DISCRETE SOURCES

4.1 Angular resolution of the gamma-ray data

Both SAS II and COS B employed spark chambers for detection of incident gamma-rays. The incoming photons produced electron positron pairs which were deflected through the spark chamber stack and an energy calorimeter. The latter provided an estimate of the gamma-ray energy while reconstruction of the spark chamber tracks allowed the incident direction to be derived. The angular resolution of these detectors was limited by the uncertainty in reconstructing the characteristic forked track of the electron positron pair.

Preflight calibration using tagged gamma-ray beams has shown that the angular response of both SAS II and COS B is well described by a point spread function of the form

$$f(\theta) = N \exp-(\theta / \theta_o)^{2c} \qquad 4.1$$

where N is an appropriate normalization factor. The parameters θ_o, c are energy dependent and were determined experimentally. Hermsen described in detail the calibration of the COS B instrument while Fichtel et al. (1975) gave similar information for SAS II. We adopt $\theta_o = 5.0°$, $c = 0.8$ and $\theta_o = 1.52°$, $c = 0.5$ for SAS II E_γ : 35-100 MeV and $E_\gamma > 100$ MeV respectively. For COS B the relevant parameters are $\theta_o = 1.4°$, $c = 0.5$ ($E_\gamma > 100$ MeV). Above 100 MeV the SAS II width is larger because of the relative data bin sizes ($\Delta l \times \Delta b = 2.5° \times 0.8°$ for SAS II

0.5° x 0.5° for COS B). The two width parameters are related by assuming an equivalent circular area of radius $\theta_{eq} = 0.58°$ for the SAS II bins and adding this in quadrature to the COS B parameter.

The angular resolution can be defined by a cone of half angle σ_θ, containing 68% of the arrival directions of photons from a point source. In terms of the point spread function $f(\theta)$ this can be expressed as

$$0.68 = \int_0^{\sigma_\theta} 2\pi\theta f(\theta)d\theta \Big/ \int_0^{\infty} 2\pi\theta f(\theta)d\theta \qquad 4.2$$

Substitution of the appropriate values for θ_o, c yield σ_θ (SAS II, E_γ : 35-100 MeV) $\simeq 6.1°$, σ_θ (SAS II, $E_\gamma > 100$ MeV) $\simeq 3.8°$ and σ_θ (COS B, $E_\gamma > 100$ MeV) $\simeq 3.6°$. Angular resolutions of a few degrees clearly restrict the ability to identify point sources, their fluxes being smeared out over the underlying background structure.

4.2 The cross-correlation technique

To improve the detectability of point sources the COS B group employed a cross-correlation technique, described in detail by Hermsen (1980). The method involved cross-correlating the raw gamma-ray data with a matrix representing the appropriate point spread function. Structure in the raw data consistent with the point spread function produces a maximum signal whereas wider and narrower structures are suppressed. Assuming the observed counts in any bin are sufficiently large ($\gtrsim 10$) they can be regarded as following a Gaussian distribution. Figure 4.1 illustrates the idealized case of a point source superimposed on a

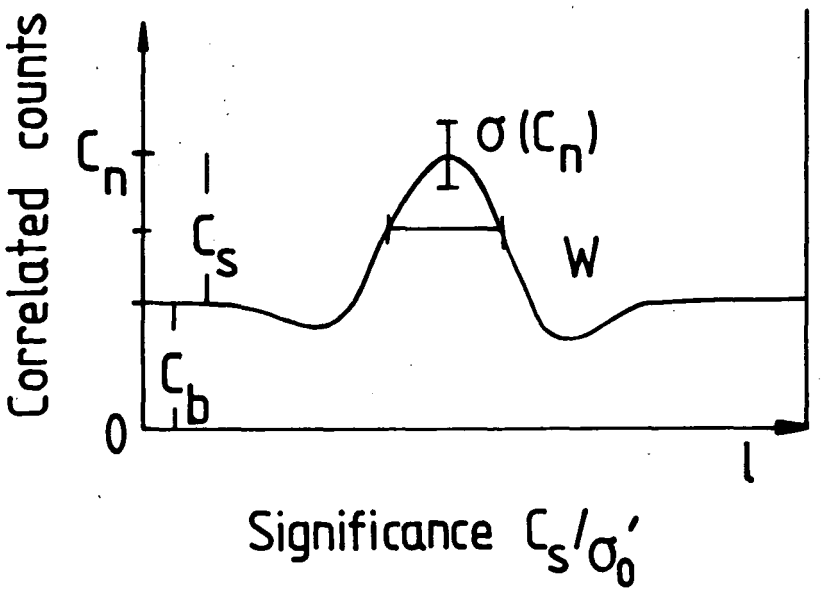

Figure 4.1 Idealized profile of the correlated count versus longitude for a peak of height C_s superimposed on a background of height C_b. W is the width parameter described in the text (Section 4.2).

$$C_s/\sigma_0' = C_s / \sqrt{(\sigma^2(Cn) - \gamma C_s)\ (1 + C_s/[\Sigma N - C_s])}$$

γ is a parameter dependent on the point spread function (Hermsen, 1980). ΣN measures the number of photons in a 10^o x 10^o area centred on the particular bin.

smooth background. The significance of the excess correlated count can be calculated and is related to the Gaussian probability that the excess in a given bin is due to an upward statistical fluctuation. The expression derived by Hermsen for the significance

$$C_s/\sigma_o' = C_s \Big/ \sqrt{(\sigma^2(C_n) - \gamma C_s)(1 + C_s/\sum N - C_s)} \quad 4.3$$

allows for the contribution to the excess count which could be due to a local enhancement of the underlying background at that point.

The 2CG catalogue (Hermsen 1980, Swannenburg et al. 1981) was compiled using the cross-correlation technique with two criteria applied for the identification of a peak as a discrete source.

(i) A minimum significance level $C_s/\sigma_o' \geq 4.75$ was required. This corresponds to a Gaussian probability $P \leq 10^{-6}$ per bin of the excess being statistical. For the Galactic plane data (1 : 0° - 360°, $|b| < 10°$) there are 28,800 COS B data bins. Thus the probability of one spurious source being included in the 2CG catalogue is about 2.9%.

(ii) The measured width W (Figure 4.1) of the correlation function should be consistent with the point spread function. From our own analysis of the published correlation profiles (Hermsen, 1980) we estimate $3.5° < W < 6.0°$ as appropriate for the 2CG sources. The spread in allowed width reflects both the statistical nature of the data and the effect of underlying background structure in contributing to the excess signal.

In principle a source catalogue derived from these criteria should be genuine, that is contain no spurious sources. However, the cross-correlation analysis makes the assumption that the background is smoothly varying and thus produces a zero correlation signal. In the gamma-ray data this is not the case, the background being highly structured over scales comparable with the point spread function. As described earlier (Section 3.5) other workers have shown that this effectively reduces the significance of excesses because upward fluctuations of the background structure can satisfy the above criteria (i.e. appear source like). We shall return to this in Section 4.3.

Given the importance of gamma-ray sources to interpretation of the data it is clear that there is a need to re-examine the significance of those sources already detected, that is the 2CG catalogue. We endeavour to address this problem from two distinct standpoints. In this chapter we use the earlier SAS II data and employ the cross-correlation technique to assess the evidence for or against the 2CG sources. In the second approach (following chapter) statistical methods are used to estimate the number of spurious sources attributable to confusion effects. By combining with the number of genuine sources we determine the best estimate of the Galactic gamma-ray flux coming from genuine discrete sources.

4.3 Cross-correlation analysis of SAS II

The complete SAS II data were published by Fichtel

et al. (1978b). The data consist of binned counts ($\Delta l \times \Delta b = 2.5° \times 0.8°$) and sensitivity factors for two energy ranges E_γ : 35-100 MeV, $E_\gamma > 100$ MeV. The total numbers of photons recorded in these respective energy bands were 6415 and 6085, collected over a period of 7 months. The satellite failed prematurely having only surveyed about two-thirds of the sky.

The 2CG catalogue was based on data accumulated by COS B over about 5 years, ammounting to about 50,000 photons $|b| < 10°$, $E_\gamma > 100$ MeV. The corresponding number for SAS II was 4172. The ratio $\simeq$ 12 : 1 indicates the overall statistical precision of the two data sets. However in any search for point sources the important parameter is the effective number of counts above the background. For SAS II the instrumental background was effectively zero ($I_\gamma \lesssim 10^{-6}$ ph $cm^{-2}sr^{-1}s^{-1}$) whereas for COS B the background was large and uncertain. It has been estimated (Mayer-Hasselwander et al. 1980) that up to 25% of the COS B photons detected from the Galactic plane were due to instrumental effects. Thus the actual effective count ratio was about 7 : 1. This is confirmed by considering the mean count per source flux unit (1 flux unit = 10^{-6} ph $cm^{-2}s^{-1}$, henceforth used throughout this chapter). For COS B the number is about 80 (Hermsen, private communication). Our analysis of the SAS II data indicates the corresponding value to be about 13, a ratio $\simeq$ 6 : 1. It is therefore considered worthwhile to

analyse the SAS II data for point sources.

Using the appropriate point spread function a cross-correlated count map of the SAS II data is produced. The analysis is restricted to $E_\gamma > 100$ MeV, $|b| < 9.6°$. The lower energy data E_γ : 35-100 MeV were initially subjected to the analysis procedure but because of the low angular resolution ($\sigma_\theta \simeq 6.1°$) no useful information was obtained. Two regions totalling $\Delta l = 30°$ are not analysed due to insufficient statistics (less than 10 photons per $\Delta l = 10°$).

Following the criteria employed for the 2CG catalogue (Section 4.2) a similar selection procedure is used to identify SAS II candidate sources. We adopt a significance level $C_s/\sigma_o' \geqslant 4.28$ corresponding to 3×10^{-2} expected spurious sources in the range analysed (3168 bins). This is comparable to the COS B significance and expected spurious source number. A reduced significance level $C_s/\sigma_o' \geqslant 3.4$ is also employed, corresponding to 1 spurious source over the region analysed. The latter significance cut produces a useful candidate source list for SAS II although it is not directly comparable with the 2CG catalogue. Following the 2CG analysis the width parameter W is required to satisfy $3.5° < W < 6.0°$. This range is compatible with the values measured for the three most significant source peaks (Vela, Crab, 2CG 078) in the SAS II data.

The binning of the SAS II data, coupled with the low statistics make estimation of the correlated background

C_b (Figure 4.1) uncertain. For the present analysis the mean background is derived using a 5-point weighted mean applied to each longitude profile. This background level is further smoothed in several regions, on a subjective basis, to remove statistical spikes. The difference introduced by this additional smoothing is always small and negligible in comparison to the errors on the total count.

Each correlated count longitude profile is analysed for candidate sources. The positions of peaks are measured at the maximum of the significance, after interpolating between the discrete longitude points. The widths W at half maximum source count are also measured from these profiles. By combining the gamma-ray count and sensitivity data binned fluxes are calculated for $E_\gamma > 100$ MeV. A cross-correlated flux map is produced following the procedure for the correlated count. At the positions of the correlated count maxima the corresponding source fluxes are measured.

4.4 Results of SAS II analysis

A total of 30 peaks are identified with ${}^{C}s/\sigma_o' \geqslant 2.0$ and the correct width, regardless of the measured flux. This is the minimum significance level for which a candidate source peak could be identified. At the lower significance levels (${}^{C}s/\sigma_o' \lesssim 2.5$) the confusion between potential sources is increasingly serious. It is clearly not possible to identify two peaks in adjacent bins and there is an area surrounding each observed peak in which another genuine peak could remain unobserved. By checking the positional distribution of all the detected excesses

we estimated the number of dead bins n_D to cover an area $l \times b = 4° \times 8°$. The significance $'s/\sigma_o'$ is directly related to the Gaussian probability $\mathbb{P}$ of the excess being a statistical fluctuation. A good estimate of the number of undetected peaks surrounding each observed excess is $n_D \mathbb{P}$. The total number of expected peaks above that significance level can be expressed as

$$n_T (< \mathbb{P}) = N_o (< \mathbb{P}) \left[1 + n_D \mathbb{P} \right] \qquad 4.4$$

where $N_o(< \mathbb{P})$ is the number of observed peaks above that significance level.

The Log N - Log S distribution of the 30 observed peaks is derived after scaling linearly to allow for the loss due to incomplete sky coverage ($\Delta l = 30°$ not analysed). This corrected distribution is compared with that of the 2CG catalogue ($|b| < 10°$) in Figure 4.2. The expected Gaussian distribution for 3456 independent SAS II bins is also shown. The observed SAS II distribution can be further corrected using 4.4, the broken line in Figure 4.2. It is seen that this improves the fit of the observed distribution to that expected from statistical fluctuations. This is encouraging as at the low significances considered statistical fluctuations should dominate over any inherent structure within the data. In addition the corrected distribution falls below expectation at the lowest significances because the data bins are not truly independent due to angular resolution effects. The expectation line can therefore only be considered as an upper limit.

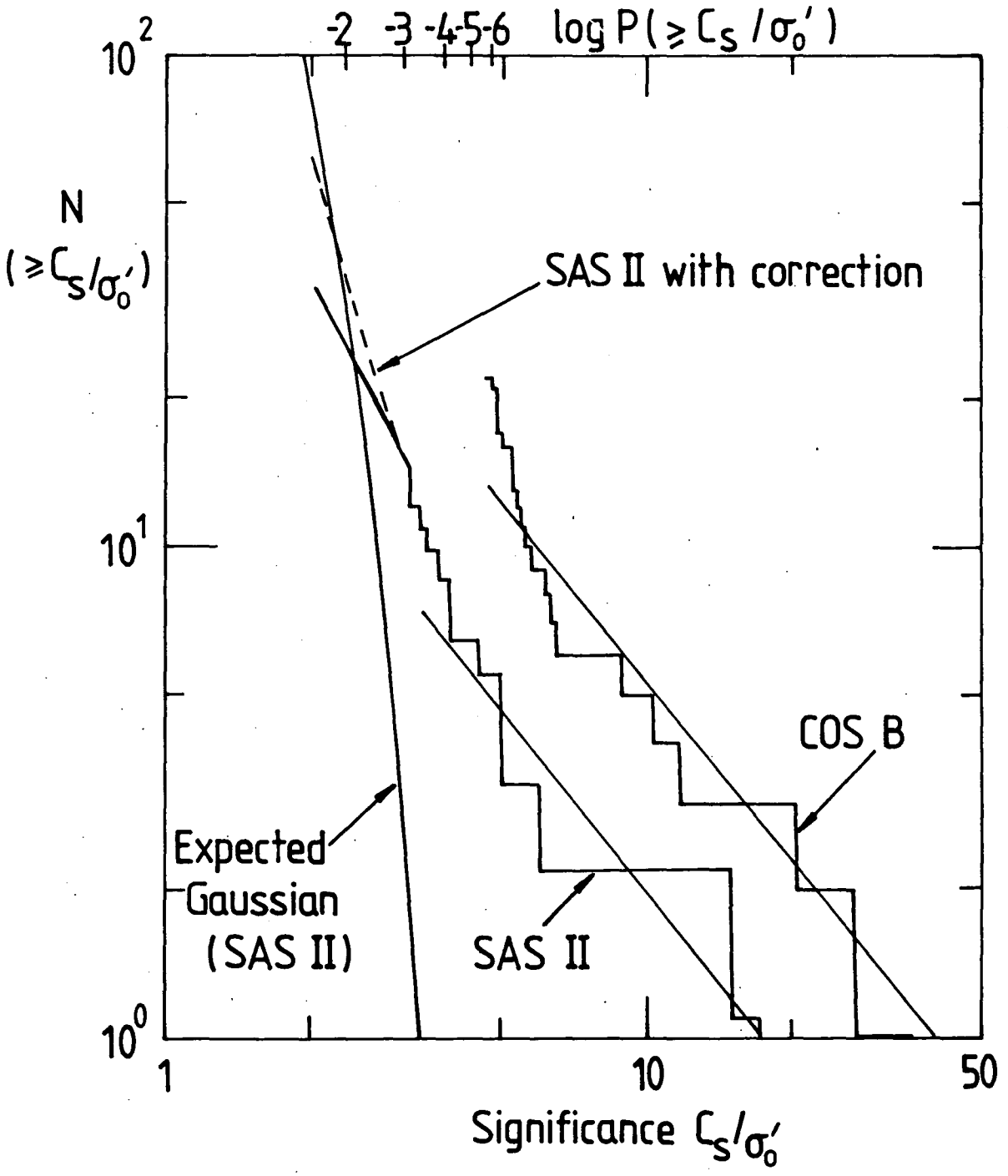

Figure 4.2 Integral distribution of significance for the COS B and SAS II candidate sources.

It is useful to consider the relative displacement of the SAS II and COS B lines as measured from their high significance tails. From Figure 4.2 this shift is estimated to be about 2.3. For a given flux the significance is approximately a measure of the square root of the number of detected source counts. Therefore $2.3^2 = 5.3$ is to a first approximation the effective count ratio. This parameter is lower than the total count ratio (10 : 1) and is closer to the previous estimates (7 : 1, 6 : 1, Section 4.2).

4.5 Derivation of SAS II discrete source catalogue

We now proceed to restrict our attention to those peaks which satisfy the criteria of Section 4.2 for identification as candidate sources. Selecting only those peaks with $^{C}s/\sigma_o' \geqslant 4.28$ gives the top candidate sources listed in Table 4.1. Identification is made with a 2CG source if the SAS II peak is within 3.8^{o} of this position (1 σ width of the point spread function). Reducing the significance level to $^{C}s/\sigma_o' \geqslant 3.4$ gives a further 5 candidate sources. We expect this list (Table 4.1) to be complete in that it should contain only one spurious source. For those 2CG sources not listed in Table 4.1 a further search of the data is carried out to identify the maximum SAS II peaks within 3.8° of the COS B positions. These results are listed in Table 4.2. By combining the data in Tables 4.1 and 4.2 we obtain information on 22 2CG sources. This information from the SAS II experiment is used to group the 2CG sources according to their degree of

TABLE 4.1

SAS II candidate source catalogue for $E_\gamma > 100$ MeV with significance, measured as C_s/σ_o', greater than 3.4. Flux F_γ,m measured in flux units at the position of maximum significance. F_γ,s: flux measured at 2CG position. F_γ, COS B denotes the actual flux measured by the COS B workers and given in the 2CG catalogue.

2CG	l^o	b^o	Significance	F_γ,m	F_γ,s	F_γ COS B
359-00	0.0	-1.2	4.5	2.3±0.5	2.2	1.8
078+01	78.2	1.2	6.0	3.2±1.2	2.9	2.5
	125.3	-0.4	5.0	3.8±1.3		
184-05	185.3	-3.6	15.1	3.6±0.8	2.0	3.7
195+04	196.0	5.2	5.0	4.9±1.3	3.8	4.8
263-02	264.1	-2.8	17.1	10.7±1.5	9.0	13.2
	25.0	8.4	3.5	1.4±0.6		
	105.0	1.2	3.7	2.1±0.9		
	114.9	-4.4	3.4	1.7±0.7		
	312.0	7.6	3.7	2.9±1.4		
311-01	314.8	-0.4	3.9	5.6±2.0	0.0	2.1

TABLE 4.2

Data on SAS II peaks ($E_\gamma > 100$ MeV) within 3.8° of those 2CG sources not identified in Table 1. Significance measured as 'C_s/σ_o'. W indicates that the profile had the correct width. Flux $F_{\gamma,m}$ measured in flux units at the point of maximum significance. $F_{\gamma,COS\ B}$ is the flux measured by the COS B workers. Blank line indicates no peak found. None of the significances is above our lower limit for acceptance (3.4) but it will be seen that the actual values found are not too far away (> 2.0). There is thus some support for nine more 2CG sources and rather more support for the seven which have correct W-values. *(Note 2CG 356±00 'may be variable' and 2CG 284-00 and 288-00 'may be extended').

2CG	l^o	b^o	Significance	Width	$F_{\gamma,m}$	$F_{\gamma,COS\ B}$
006-00	8.0	-0.4	2.5		1.9±0.9	2.4
013+00					($\lesssim$ 0.7)	1.0
036+01	35.3	0.4	3.9	W	2.0±1.0	1.9
054+01	54.4	1.2	2.3	W	1.9±1.1	1.3
065+00					($\lesssim$ 1.3)	1.2
075+00	74.5	-1.2	2.5	W	2.4±1.3	1.3
095+04					($\lesssim$ 1.5)	1.1
121+04	118.1	6.0	3.1	W	1.8±0.9	1.0
135+01	135.0	2.0	3.2	W	2.7±1.7	1.0
218-00	216.7	-2.0	2.4		1.5±0.8	1.0
235-01	235.0	-0.4	1.7		1.1±0.5	1.0
284-00	283.0	-2.0	2.1	W	2.2±1.2	2.7
288-00					($\lesssim$ 2)	1.6*
333+01	334.0	0.4	2.3	W	3.9±1.7	3.8
342-02	343.0	-1.2	1.5	W	1.9±1.3	2.0
356+00					($\lesssim$ 2)	2.6*

confirmation.

Five 2CG sources are strongly confirmed, in that the corresponding SAS II peaks satisfied the strict significance and width criteria. A comparison of the fluxes from Table 4.1 is made in Figure 4.3. Allowing for the possibility of temporal variability between the SAS II and COS B observations the best SAS II estimate is presumably between the two SAS II flux estimates; that at maximum significance and that at the 2CG position. The ratio of the average COS B fluxes to the average for SAS II is 1.31 and 0.91 for the upper and lower SAS II estimates respectively. The mean = 1.1 and is very close to unity. We consider these 5 excesses as significant, that is genuine gamma-ray sources. The consistency of the flux estimate also suggests that long term variability is much less than the statistical precision of these measurements.

SAS II gives a reduced level of support for 12 further 2CG sources, the latter set in Table 4.1 and those in Table 4.2. These peaks are detected in SAS II. However their significances lay below the strict level and in 3 cases the widths are inconsistent with that expected for a point source. In that these peaks are detectable in the SAS II data does offer some confirmation to the COS B observations. It is interesting to compare the fluxes for these sources as measured by both experiments, shown in Figure 4.4. The agreement is reasonable when it is remembered that the SAS II values are the peak values and the best estimate (as in Figure 4.3) is likely to

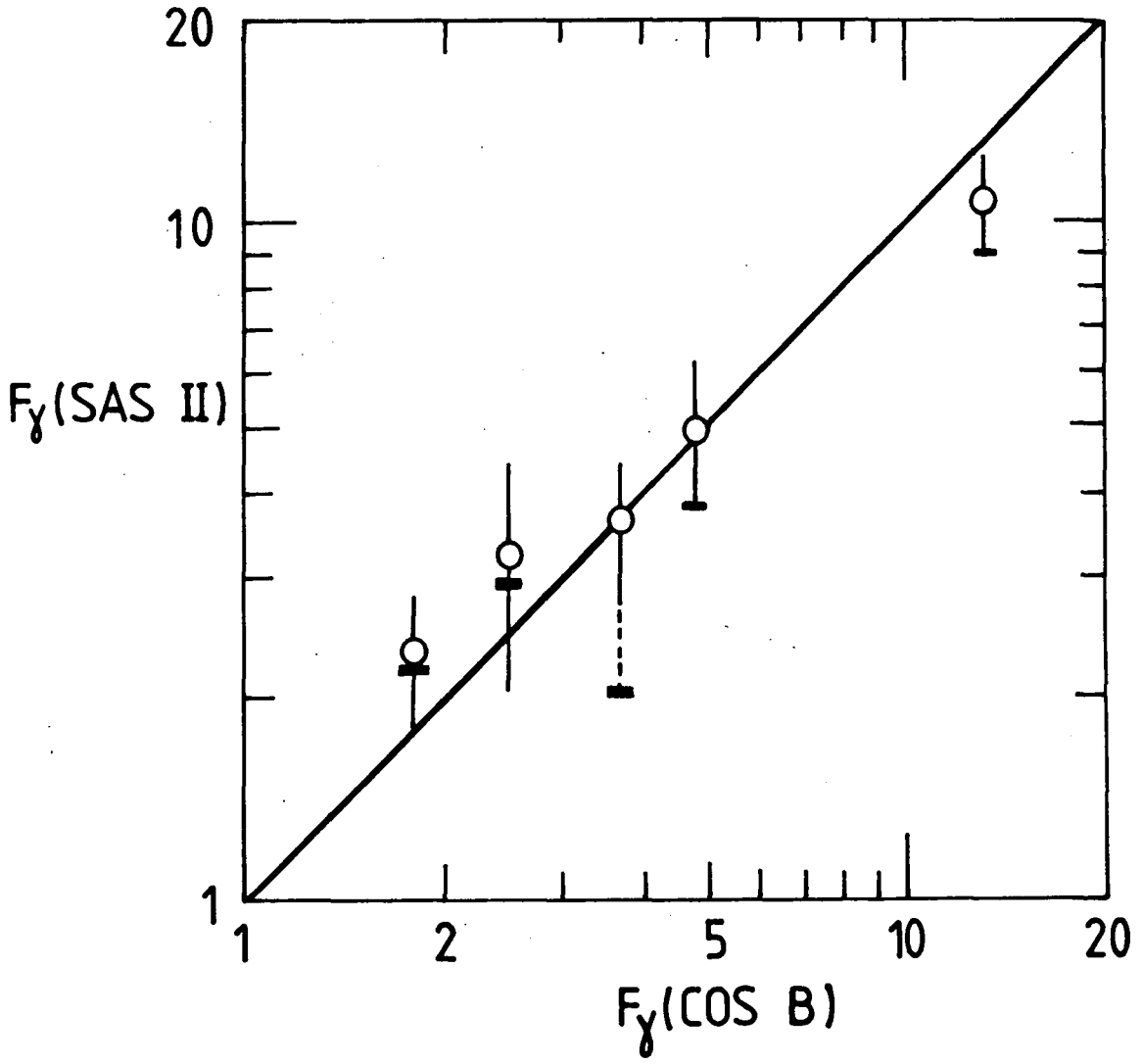

Figure 4.3 Comparison of the fluxes recorded for the 5 strongest 2CG candidate sources in Table 4.1. Two estimates are made for SAS II : open circles corresponding to the peak value for the source (which is often not coincident with the COS B position) and horizontal bars corresponding to the SAS II flux at the COS B peak position.

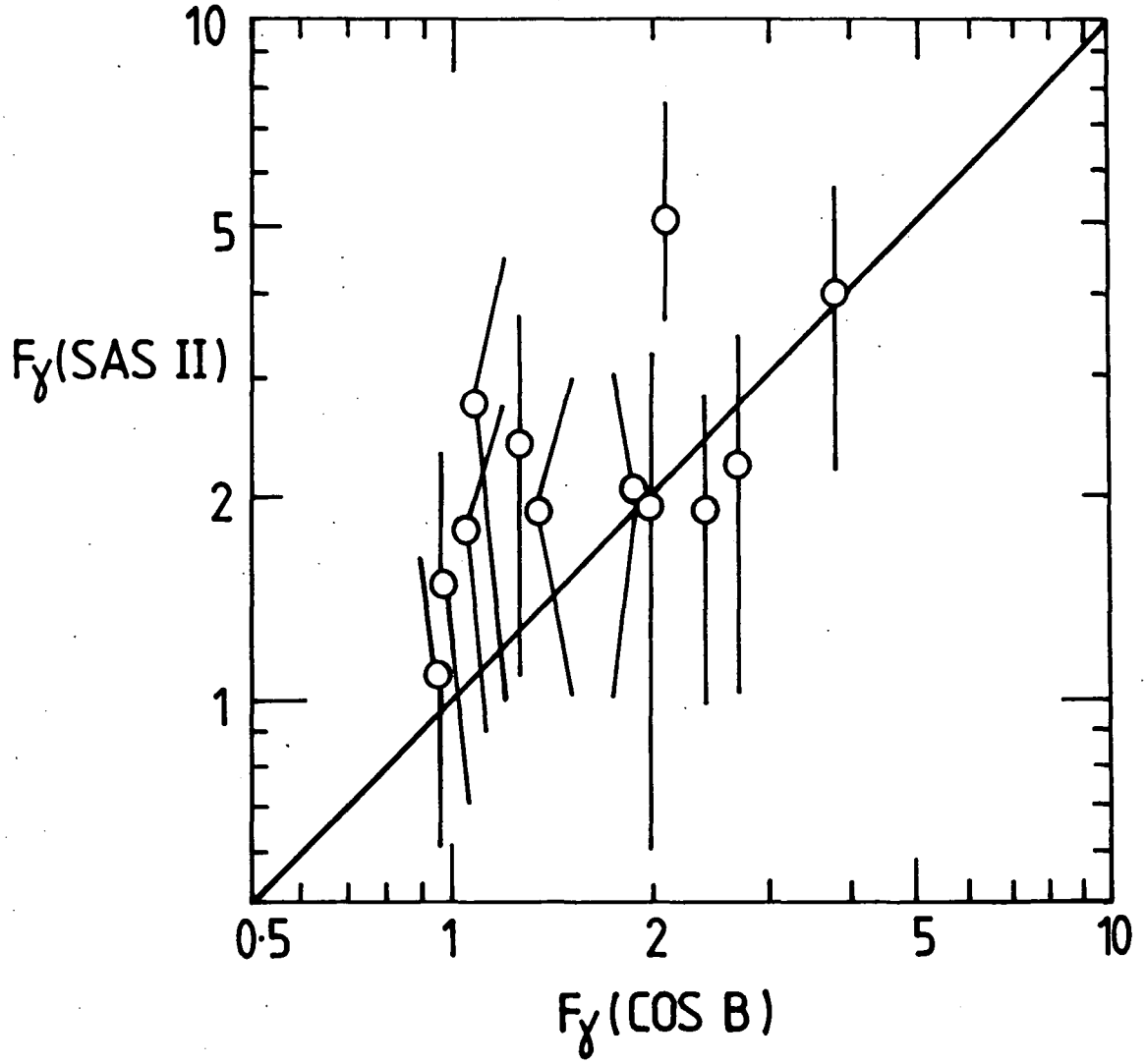

Figure 4.4 Comparison of the fluxes recorded for the same sources by SAS II and COS B, where the significance limit of the SAS II source is poorer than that for COS B.

be about 10% below this level.

There remains 5 2CG sources for which the SAS II data are unable to offer confirmation in the sense of peaks being observable above the background. Nevertheless at these positions we estimate the upper limit to the SAS II fluxes (Table 4.2). Most of these sources have low fluxes as measured by COS B ($F_\gamma < 2.6$ flux units) suggesting that some will be undetectable by SAS II. Two of the strongest of these sources are atypical. The data collected by COS B suggested that 2CG 284/288 probably constitute an extended region of enhanced emission associated with the Carina spiral arm. The region around 2CG 356 was observed 5 times yet this source was only detected in 1 observing period. Clearly if this object exhibits strong temporal variability it is likely that its non-detection by SAS II may be attributed to a quiescent state at that epoch. It is worth recalling that this source is close to the Galactic centre a region which is known to exhibit temporal variability at lower energies, the 511 keV electron positron annihilation line (Section 2.2). Further observations of this region are needed before firm conclusions can be drawn on the possible gamma-ray sources present and the nature of their emission processes at different energies. Solely on the basis of the SAS II analysis it is not possible to rule out the existence of the 3 remaining sources 2CG 013, 065 and 095 which have F_γ, COS B = 1.0, 1.2 and 1.1 flux units respectively.

Inspection of Table 4.1 shows that 5 sources are visible in the SAS II analysis with significance $^{C}s/\sigma_{o}' \geq$ 3.4. As this significance level corresponds to 1 spurious source being detected there is seen to be an observed overabundance. Adoption of the stricter significance (corresponding to 10^{-2} spurious sources) still results in 1 candidate source (l,b : 125.3°, -0.4°) being visible in the SAS II data set yet remaining undetected by COS B. A check of the published COS B contour maps (Mayer-Hasselwander et al., 1982) reveals no evidence for point-like excesses at the positions of the 5 unidentified SAS II candidate sources. While this search cannot be considered conclusive it is most unlikely that these 5 excesses are genuine in the sense of being point objects with $F_{\gamma} > 1$ flux unit. It is more probable that they are upward statistical fluctuations of the underlying background, reflecting a true overabundance on the expected spurious source rate.

We consider the sources common to both the 2CG analysis and the present work, regardless of their significance but satisfying the width criterion. There are 22 2CG sources and 14 counterparts visible in SAS II. The Log N - Log S distribution for these two sets is given in Figure 4.5 along with that for the SAS II sources satisfying the strict significance requirement ($^{C}s/\sigma_{o}' \geq 4.28$). Both SAS II distributions are scaled to allow for incomplete sky coverage. Above about 2.5 flux units the agreement among the distributions is good. It is seen that the

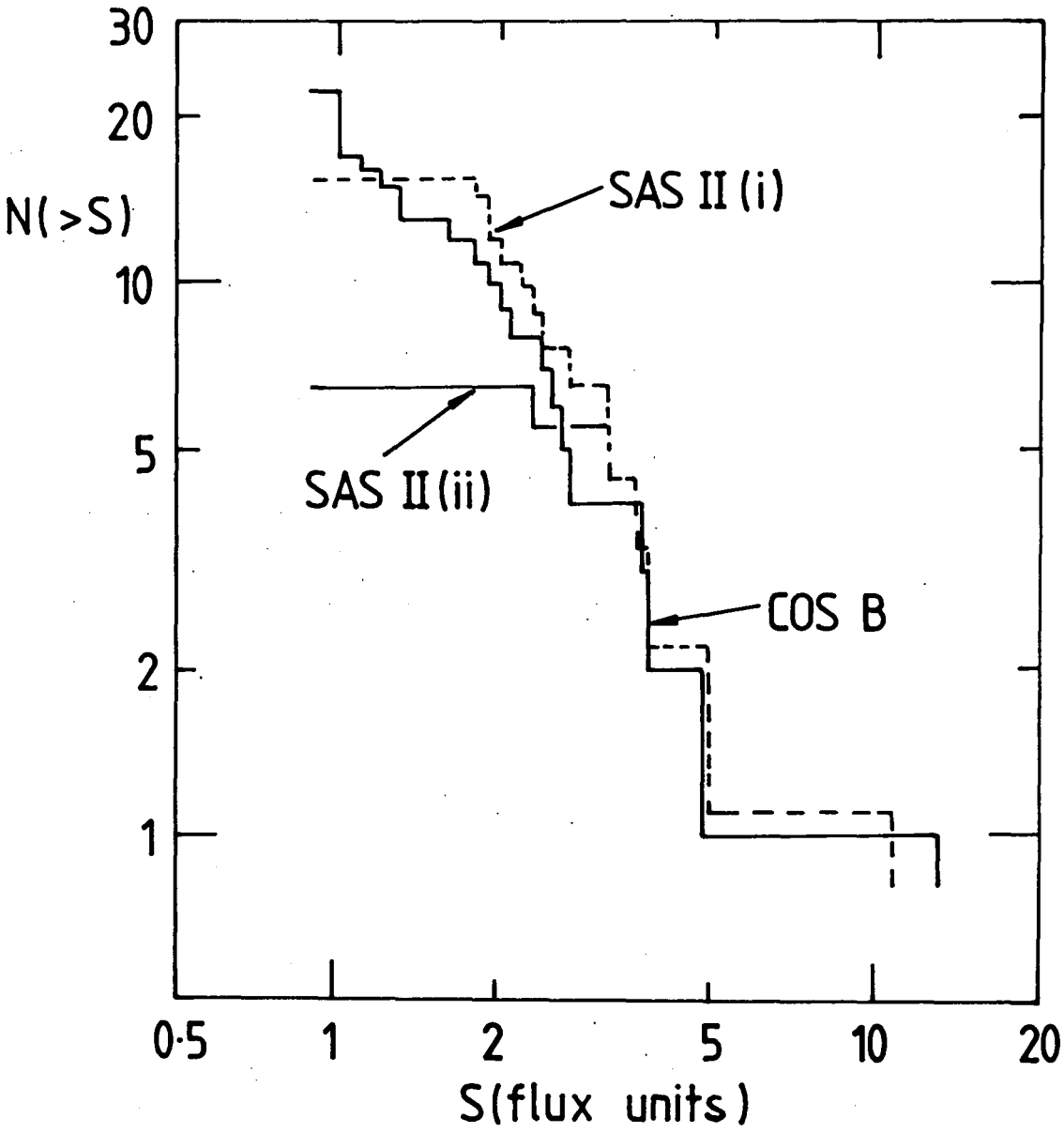

Figure 4.5 Log N - Log S distributions for the COS B and SAS II catalogues. SAS II (i) : sources seen in both experiments, down to $C_s/\sigma_o' \simeq 1.5$ for SAS II. SAS II (ii) : sources seen in SAS II with $C_s/\sigma_o' > 4.28$.

high significance limit results in the loss of the weaker 2CG sources. Adopting the lower flux limit for SAS II sources at 2.5 flux units we can compare with that for COS B, 1.0 flux units. Again the effective count ratio is seen to be about $2.5^2 \simeq 6.3:1$ in confirmation of previous estimates. The fluxes measured by SAS II are slightly larger than the corresponding COS B values. This may be due to differences in absolute zero level between the two experiments (primarily the large and uncertain COS B instrumental background). However, part of the effect can be attributed to the method of analysis in which the SAS II fluxes are always measured at the maximum peak nearest the 2CG positions and thereby biasing our measurements to an overestimate of the COS B value by about 10% (Figure 4.3).

4.6 The nature of sources detected by the cross-correlation technique.

It is pertinent at this stage to briefly discuss the nature of the sources detected by COS B and of those candidate sources from our own analysis. There is good evidence suggesting an overabundance of spurious sources, assuming of course, the 2CG catalogue forms a complete sample down to 1 flux unit. The SAS II spurious sources have a wide flux range (1.4 - 3.8 flux units) and given the better exposure of COS B it is unlikely that poor statistics can explain their non-detection by COS B. The good consistency in measured fluxes for the 5 strongly confirmed 2CG sources suggest that time variability is

not a property of genuine sources and this explanation of the SAS II unidentified candidate sources must also be considered most unlikely. Li and Wolfendale (1982) found evidence from their Monte-Carlo analysis of COS B ($E_\gamma > 100$ MeV) for the overabundance of spurious sources. This effect does appear to be real and both analyses strongly suggest the gamma-ray data more structured than expected statistically. That is they contain fluctuations of the structured background which mimic the appearance of genuine point sources.

We conclude that cross-correlation is a powerful technique for source analysis. However the complexity of the gamma-ray data suggest that three distinct features are likely to be involved:

(i) Genuine discrete sources such as Crab, Vela and Geminga.

(ii) Giant molecular cloud complexes irradiated either by the ambient cosmic ray flux or by internal cosmic ray sources and appearing point like because of the limited angular resolution. These are regions of diffuse emission which contribute to the structured nature of the observed background emission. Their role as pseudo gamma-ray sources is considered by other workers and is more fully discussed in Section 3.5.

(iii) Spurious peaks which due to the comparatively low statistics and uneven background appear as random upward fluctuations.

With improved resolution and statistics the objects in

categories (ii) and (iii) would be more tightly defined. The case of 2CG 353/ ρ Oph (Section 3.5) is of relevance in this context.

CHAPTER FIVE

A MONTE-CARLO ANALYSIS OF THE GALACTIC GAMMA-RAY SOURCE CONTRIBUTION

5.1 General comments

The early work on radio source counts has parallels with the present situation regarding gamma-ray sources. Radio source observations were originally expected to help reveal the geometrical nature of the universe through measurement of the Log N - Log S distribution at very low flux levels. However, interpretation of the data was inconclusive because of source confusion at low flux levels and the likelihood that evolutionary effects in the sources would distort the counts at high redshifts. Murdoch et al. (1973) discussed the effects of noise and confusion on the radio source identifications, which they showed had a significant effect on the observations even at the 5 sigma level. They concluded that at weaker flux levels the source count was progressively enhanced because of upward statistical fluctuations in the number of sources at even fainter flux levels. The statistical noise effectively degraded the source count in a particular flux bin, led to an overestimate of the true flux of weaker sources, and the effect on the integral count was cumulative below that flux level. For the case of purely Gaussian noise the effect of the error distribution on the true flux and differential count can be calculated analytically. However, for confusion limited surveys this problem is best treated by a Monte-Carlo method.

The present observational status of gamma-ray sources

is similar, in that confusion is also important at the weakest flux levels, as borne out by the previous chapter and the results of other workers (Section 3.5). Whereas for radio sources the confusiuon is due to the cumulative effect of weaker sources, it is generally believed that gamma-ray sources are observed against a background predominantly diffuse in origin. For gamma-ray sources, confusion is due both to proximity with other weak sources and to the difficulty of detection when viewed against a highly structured background. It is clear that the low angular resolution of present detectors plays a significant role in these processes. We can adopt the methods used to correct the radio source counts. Given an adequate model of the gamma-ray background, Monte-Carlo methods can be employed to study confusion in relation to gamma-ray sources.

5.2 The Monte-Carlo background model

Previous analyses and interpretation of the gamma-ray data have been extensively discussed in chapter 3. The observed emission is predominately Galactic in origin and it is clear that, in principle at least, most of the emission can be explained in terms of cosmic ray interactions with the gas of the interstellar medium. As a model of the diffuse gamma-ray emission we therefore adopt the distribution of total gas and cosmic rays throughout the Galaxy. The expected gamma-ray intensity along a given line of sight (l ,b) can be expressed as

$$I_\gamma(l,b) = \left(q/4\pi\right)\int n(l,b,r)\left[I_{cr}(l,b,r)/I_o\right] dr \quad 5.1$$

where $q/4\pi$ is the local gamma-ray emissivity, n the gas density ($HI + 2H_2$), and I_{cr}/I_o the ratio of the cosmic ray intensity to the local value. Atomic hydrogen is sufficiently well mapped to enable an accurate distribution to be obtained, within the limitations imposed by the choice of rotation curve and the effects of random cloud motions. The situation with CO is similar. However the inferred molecular hydrogen distribution is conditional on the conversion parameter ($CO \rightarrow H_2$) and its variation throughout the Galaxy. There is only modest information available on the large-scale Galactic distribution of cosmic rays. Indeed most of the evidence favouring a local gradient ($\lesssim$ 2-3 kpc) is dependent on knowing the gas distribution (Section 3.3). Further towards the inner Galaxy our knowledge of the cosmic ray intensity is proportionately reduced due to both the greater uncertainty in the mass of gas (primarily H_2) and to the unknown contribution of discrete gamma-ray sources to the observed gamma-ray emission. Although the arguments concerning Galactic cosmic ray gradients, gamma-ray sources and the total mass of gas are to a large extent interrelated, the current best estimates (Section 3.3) indicate that the cosmic ray intensity in the inner Galaxy is unlikely to be greater than that locally by a factor of more than about 3-5. As a simplifying approximation we assume the cosmic ray intensity ($\gtrsim$ 1 GeV) to be uniform throughout the entire Galaxy and equal to the local value, 5.1 then reduces to

$$I_\gamma(l,b) = (q/4\pi)N(HI + 2H_2) \qquad 5.2$$

We use this as the basis for our model of the diffuse gamma-ray emission, implicitly assuming that discrete sources (pulsars, unusual objects) make only a small contribution to the gamma-ray background. This latter assumption is of crucial importance when we come to interpret the present data on discrete gamma-ray sources and we shall return to this later (Section 5.13).

5.3 The HI and CO data

The Weaver and Williams (1973) survey of 21 cm atomic hydrogen emission covers the region 1 : 10° - 249°, $|b| < 10°$. These data give velocity profiles sampled every 0.25° in latitude, 0.5° in longitude and were obtained with the Hat Creek Observatory 85-foot telescope (half power beam width = 35'.5). Column densities are obtained by assuming that the gas has a spin temperature T = 125K, to correct for optical depth effects. Close to the Galactic plane, especially in the inner Galaxy, the observed temperature profiles are often optically thick. This is partly due to the large mass of gas towards the Galactic centre but is also affected by velocity crowding of the Doppler shifted profiles in this region. By assuming an infinite spin temperature (i.e. optically thin) the reduction in the column density for the optically thick case is found to be generally $\lesssim$ 20%. The column density N_{HI} is related to the observed temperature profile by:

$$N_{HI} = 1.823 \times 10^{18} \int T \, dv \quad \text{atoms cm}^{-2} \qquad 5.3$$

Turning to the large scale distribution of molecular hydrogen, its magnitude is not well known. Its presence can be observed directly as emission from transitions between vibrational states. However, this technique is limited to local regions ($\lesssim$ 2 kpc) because of saturation effects at greater distances. The large scale distribution must be inferred indirectly from observations of other molecular species, principally CO. It is conventional to believe that H_2 is substantially confined to dense regions - the so-called molecular clouds. Inside these regions the H_2 is shielded from photo-dissociation by an external shell of HI and HII. The internal chemistry of molecular clouds has only recently become the subject of intense study, partly because of the complexity and profusion of the possible chemical reactions. Nevertheless millimetre and submillimetre observations of these regions have confirmed the existence of many complex molecular species. CO is the most abundant of these species and as such is an ideal tracer of the large scale distribution of molecular clouds because it is rotationally excited through collisions with other molecules (principally H_2). The most abundant isotope, ^{12}CO, decays ($J = 1 \rightarrow 0$) emitting a characteristic wavelength; $\lambda = 2.6$ mm $\nu_o = 115.3$ GHz.

^{13}CO (λ = 2.7mm ν_o = 110.2GHz) has been detected from the more intense sources. Other isotopes (e.g. $^{12}C^{18}O$) and higher transitions (J = 2 $\rightarrow$ 1) have also been detected but are less useful in that these observations are limited to a few sources of intense molecular emission.

The Columbia group have carried out a survey of ^{12}CO (J = 1 $\rightarrow$ 0) covering l : 10° - 100°, b: -5° to + 10° and l : 100° - 180°, b: -3° to + 5° (Cohen et al. 1980; Dame, 1984). These data were obtained using their 4m telescope, with a resolution (half power beam width) = 0.125°.

It is commonly assumed that the ^{12}CO line is optically thick, the rotational levels being thermalized within the cloud. In this case the observed antenna temperature uniquely measures the gas kinetic temperature of the source. This has been confirmed for those clouds in which higher order CO transitions have been observed. For these lines similar gas kinetic temperatures are inferred, supporting the reliability of CO as a thermometer. For sources not in local thermodynamic equilibrium (non-LTE) calculations of gas kinetic temperature and column density rely on a radiative transfer model.

It has been shown (e.g. Solomon et al. 1979, Cohen et al. 1980) that for the LTE approximation the molecular hydrogen column density N_{H_2} can be expressed as

$$N_{H_2} = X \int T(^{12}CO)dv \qquad 5.4$$

We follow Arnaud et al. (1982) in adopting X = 2.3 x 10^{20} mol. cm^{-2} (K kms^{-1})$^{-1}$, a value which is by no means

unique. Sanders et al. (1984a) have extensively discussed the arguments surrounding the calibration of X . They note that a wide range of X: $(1.0 - 7.2) \times 10^{20}$ has been adopted by various workers in the past and this in part has led to inconsistency among the different estimates of the total mass of H_2 in the Galactic plane.

5.4 The CO→H_2 calibration, the metallicity gradient

The preferred method of calibrating X has relied on measurements of visual extinction towards local dark clouds (e.g. Dickman, 1978) to give column densities. These are compared with column densities inferred from CO observations. While this method in principle, gives an accurate calibration for an individual cloud, the evidence suggests that X varies from cloud to cloud (Bhat et al. 1984c). These workers find X = $(1.25 - 1.5) \times 10^{20}$ mol. cm^{-2} $(K\ kms^{-1})^{-1}$. Many of the local clouds used to calibrate X have relatively low mass ($\sim 10^{2-3} M_\odot$). Giant molecular clouds are believed to be more massive ($\sim 10^{5-6} M_\odot$), probably have higher temperatures and different chemical composition; reflecting the increased activity (turbulence, star formation, supernovae ...) in the inner Galaxy. While it is by no means certain that a locally determined X is applicable to the giant molecular clouds we follow previous workers in implicitly assuming this to be the case. That is, the nearby clouds constitute a reliable sample of those deeper into the inner Galaxy.

Alternative calibration methods have also been employed. The SAS II and COS B data have been compared to the large-scale distribution of HI and CO in the first and second quadrants to estimate X , assuming a uniform cosmic ray distribution throughout the Galaxy. Issa and Wolfendale (1981a) and Lebrun et al. (1983) found $X = 1.2 \times 10^{20}$ mol. cm^{-2} $(K\ kms^{-1})^{-1}$ and $(1.0 - 3.0) \times 10^{20}$ mol. cm^{-2} $(K\ kms^{-1})^{-1}$ respectively, though these analyses are limited by the asusmptions made about the cosmic ray distribution and the role of discrete gamma-ray sources. Nevertheless they are in reasonable agreement with the preferred values obtained locally. In the following chapter we examine the Orion molecular clouds in a further attempt to estimate X appropriate for local massive clouds. From this analysis we find $X = 1.85 \times 10^{20}$ mol. cm^{-2} $(K\ kms^{-1})^{-1}$.

Apart from the uncertainty surrounding the mean value of X, an important additional factor must be considered; the metallicity gradient. This gradient can be characterised by the ratio of Carbon to Hydrogen ($[C]/[H]$) and is observed to decrease with increasing Galactocentric radius (Pagel and Edmunds, 1981). The variation is due to the increased rate of processing of the interstellar medium towards the inner Galaxy (gas →stars →supernovae →gas). The ratio $[CO]/[H]$ in molecular clouds is in consequence likely to increase with decreasing Galactocentric radius and several workers (e.g. Blitz and Shu 1980, Li et al., 1982, Bhat et al.

1984b) have pointed out the implications for the mass of H_2 inferred from CO. If the metallicity gradient is expressed as the abundance ratio $M = [C]/[H]$ then N_{H_2} could be reduced by a factor $M^{-1} \int T(CO)dv$ or perhaps as much as $M^{-2} \int T(CO)dv$. The latter reflects the gradient of $[O]$ / $[H]$ as similar to $[C]$ / $[H]$ and both affect $[CO]$ / $[H]$. While the existence of the metallicity gradient is not in dispute there is no agreement as to whether it affects the estimates of H_2, and if it does, to what extent.

5.5 Simulation of the diffuse gamma-ray background

For the present analysis we assume the metallicity to have no effect on N_{H_2} and calculate column densities direct from the observed ^{12}CO line intensities using 5.4. Predictions of the expected gamma-ray intensity follows from 5.2 where we assume the local emissivity $q/4\pi(>100\ MeV) = 2.2 \times 10^{-26}$ ph $at^{-1}sr^{-1}s^{-1}$ as derived by Issa et al. (1981). This value is not unique (see the summary in Tables A1, A2), nevertheless it is chosen to enable direct comparison with previous work on Monte-Carlo analysis of pseudo-sources (Li and Wolfendale, 1982). The evidence discussed previously (Section 3.3) suggests a modest Galactic cosmic ray gradient. The resulting overproduction of gamma-rays in the inner Galaxy would be countered (in an approximate manner) if we were to adopt the metallicity correction to reduce H_2 in our model. It is interesting that these effects act to reduce the probable error in the present model.

After binning ($\Delta l \times \Delta b = 0.5° \times 0.5°$), and converting to flux, an expected count map is derived. By considering the 2CG source fluxes and observed counts (Hermsen 1980) we estimate the count rate for a typical source as $N_s = 80$ counts/flux unit (1 flux unit = 10^{-6}ph $cm^{-2}s^{-1}$, henceforth used throughout). This is confirmed by Hermsen (private communication). We also adopt $N_s = 40$ counts/flux unit as a suitable lower bound on this parameter. The count map data are then convolved to the COS B resolution ($E_\gamma > 100$ MeV) using the appropriate point spread function (Section 4.1).

Figure 5.1 is a contour map of the expected gamma-ray count map. These data form the basis for the Monte-Carlo background. The structure is confined to within a few degrees of the Galactic plane and is dominant in the inner Galaxy. This is a reflection of the highly structured nature of the H_2(CO) distribution which is predominantly clumped into giant clouds, whereas the HI is rather smoothly distributed throughout the inter-stellar medium. After allowing for Poisson fluctuations (before convolution to the COS B resolution), representing the statistics of counting, a typical count map is shown in Figure 5.2. The small scale structure is now more apparent, and it is this noise which limits the detection of genuine discrete sources.

As an interim check 10 Poisson samples of the back-ground are generated and searched for spurious sources using the cross-correlation method. That is, we look

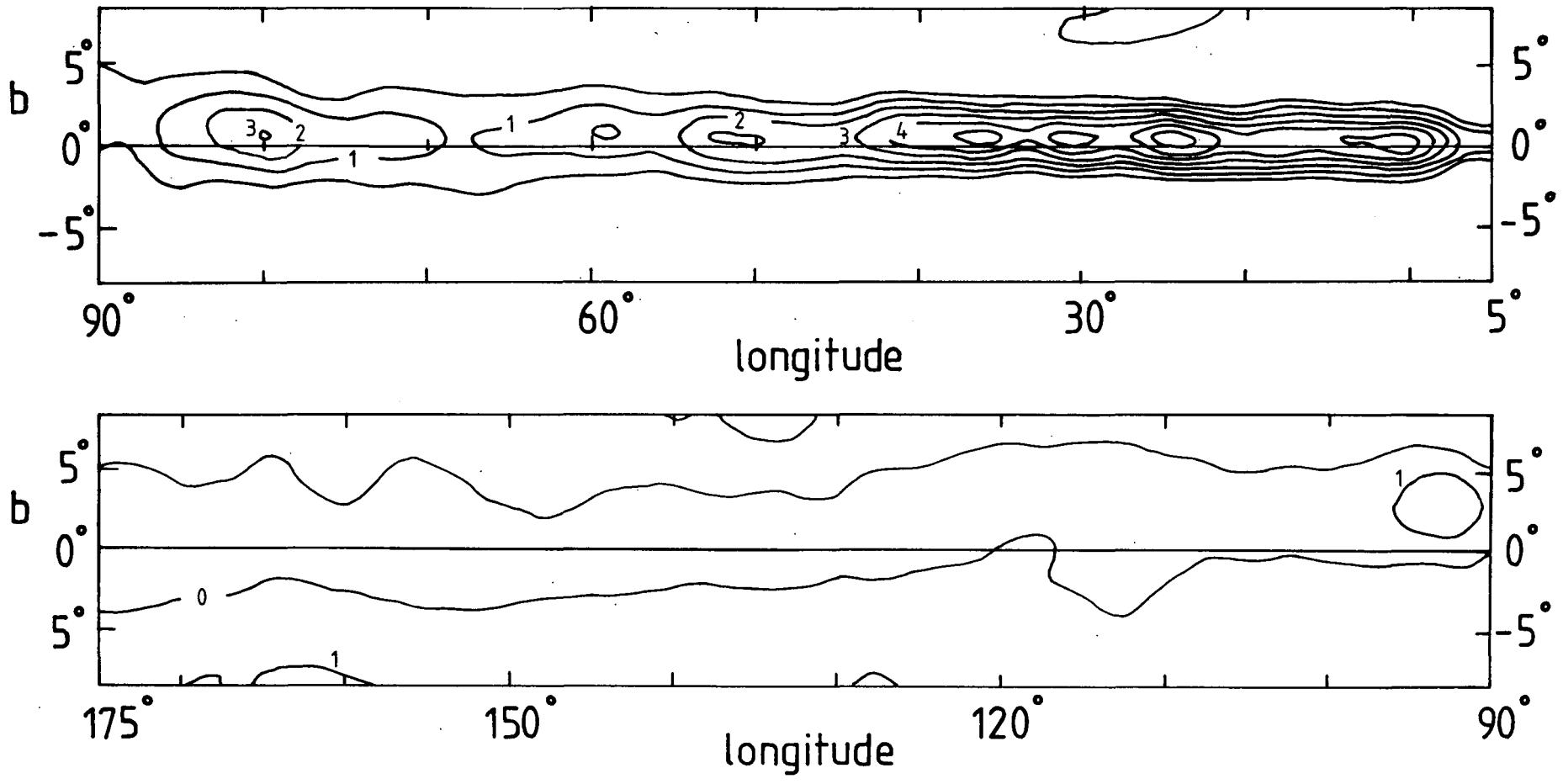

FIGURE 5.1 Cross-correlated flux expected from the background. Contours are F_γ (>100 MeV) = n x 0.5 x 10^{-6}ph cm^{-2} s^{-1} with a bin size $\Delta l \times \Delta b$ = 0.5° x 0.5°

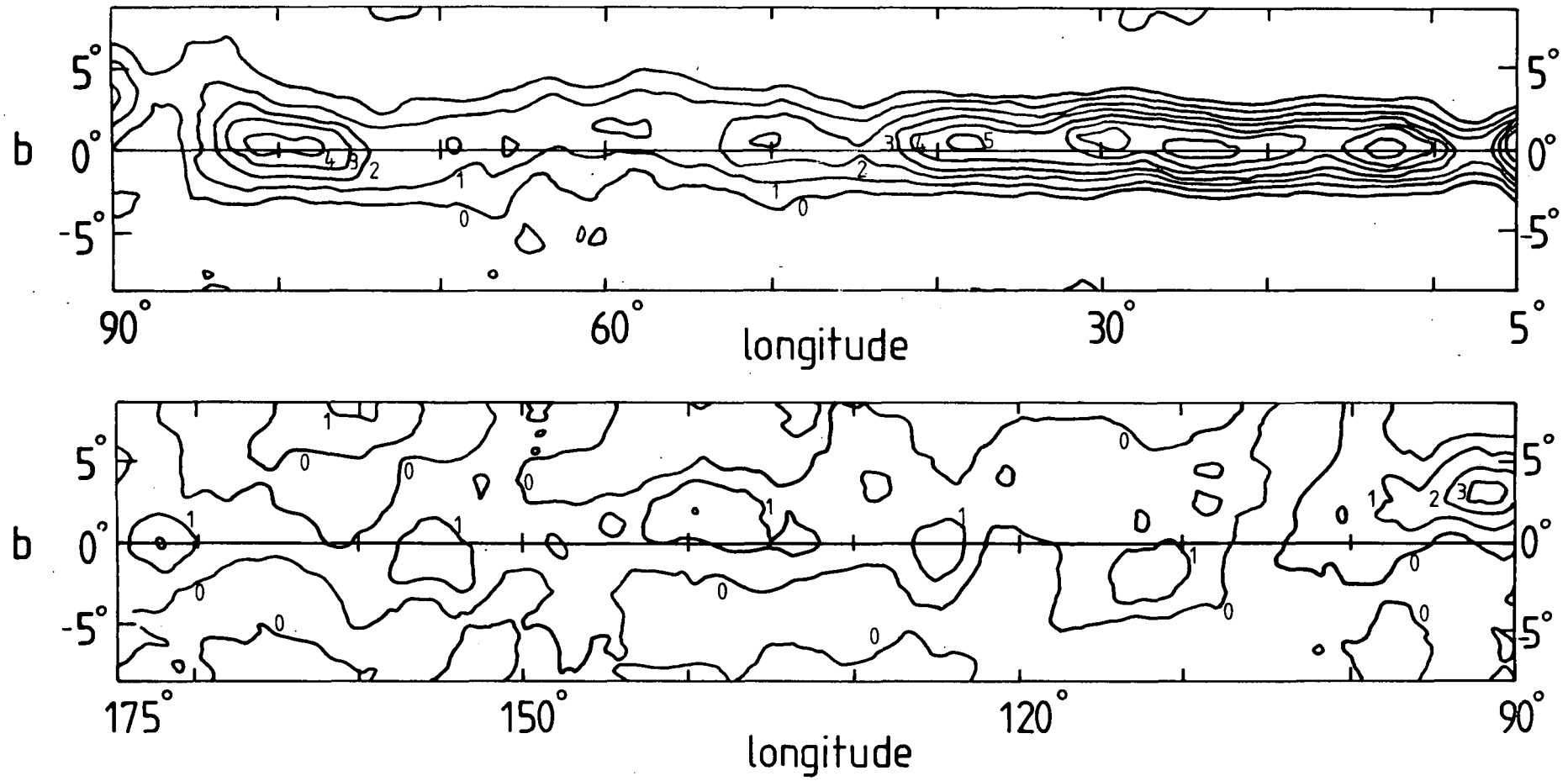

FIGURE 5.2 Cross-correlated flux of a typical Monte-Carlo background sample. Contours are $F_\gamma(>100\ \text{MeV}) = n \times 0.5 \times 10^{-6}\text{ph cm}^{-2}\text{s}^{-1}$ (negative fluxes omitted) with a bin size $\Delta l \times \Delta b = 0.5° \times 0.5°$.

for peaks satisfying the COS B significance and width criteria (Section 4.2). The frequency of occurrence of these upward statistical fluctuations are found to be in close agreement with the more extensive earlier work by Li and Wolfendale (1982), lending weight to the correctness of the present analysis.

5.6 Monte-Carlo simulation of discrete sources

We proceed to simulate the count distribution for a genuine point source. For a given source flux the point spread function distribution of the count is superimposed on the expected background count map. The combined data are then subjected to Poisson fluctuations. Each sample is analysed for the expected sources using the cross-correlation method. In addition to the COS B criteria, already discussed for source identification (Section 4.2), a further selection criterion is also imposed. For positive identification of the simulated source we require the observed peak to lie within 3.6° (the angular resolution of the data, $E_\gamma > 100$ MeV) of the original position.

Four sources are randomly superimposed on a background data set, widely separated ($l > 20°$, $|b| < 2°$) to avoid possible confusion between two or more sources. Different combinations of position and source strength are used to give a wide coverage in longitude for the detection efficiency of each simulated source flux. We simulate flux levels F_γ = 0.5, 0.8, 1.0, 1.3, 2.0 and 4.0 flux units, each configuration being treated for both N_s = 80

and N_s = 40 counts/flux unit. While the lowest observed 2CG source flux was 1.0 flux units ($|b| < 10°$), this was not due to any selection procedure on source flux. Therefore it is considered appropriate to simulate sources weaker than this observational limit in addition to those comparable to the stronger 2CG sources (c.f. F_γ , Crab = 3.7 flux units). It is expected that confusion should be negligible for the strongest sources, while at the weakest flux levels ($F_\gamma \lesssim 1.0$ flux units) confusion is expected to dominate the detection efficiencies. At the intermediate flux levels ($F_\gamma \gtrsim 1.0$ flux units), typical of the weakest 2CG sources, confusion with upward fluctuations of the background structure will also be important. It is these 2CG sources which have previously been considered as consistent with fluctuations of the underlying background structure (Li and Wolfendale, 1982, Arnaud et al., 1982).

5.7 Discrete source detection efficiencies

By using the Monte-Carlo samples we determine the detection probabilities for each true source strength as a function of Galactic longitude. The data from each source sample are combined, and the detection probabilities are plotted in Figures 5.3 and 5.4 for N_s = 80, 40 respectively. The overall trend as indicated by the solid line is apparent, indicating detection efficiency increasing with both Galactic longitude and true (i.e. expected) source flux. This is as expected in view of the reduced background structure evident

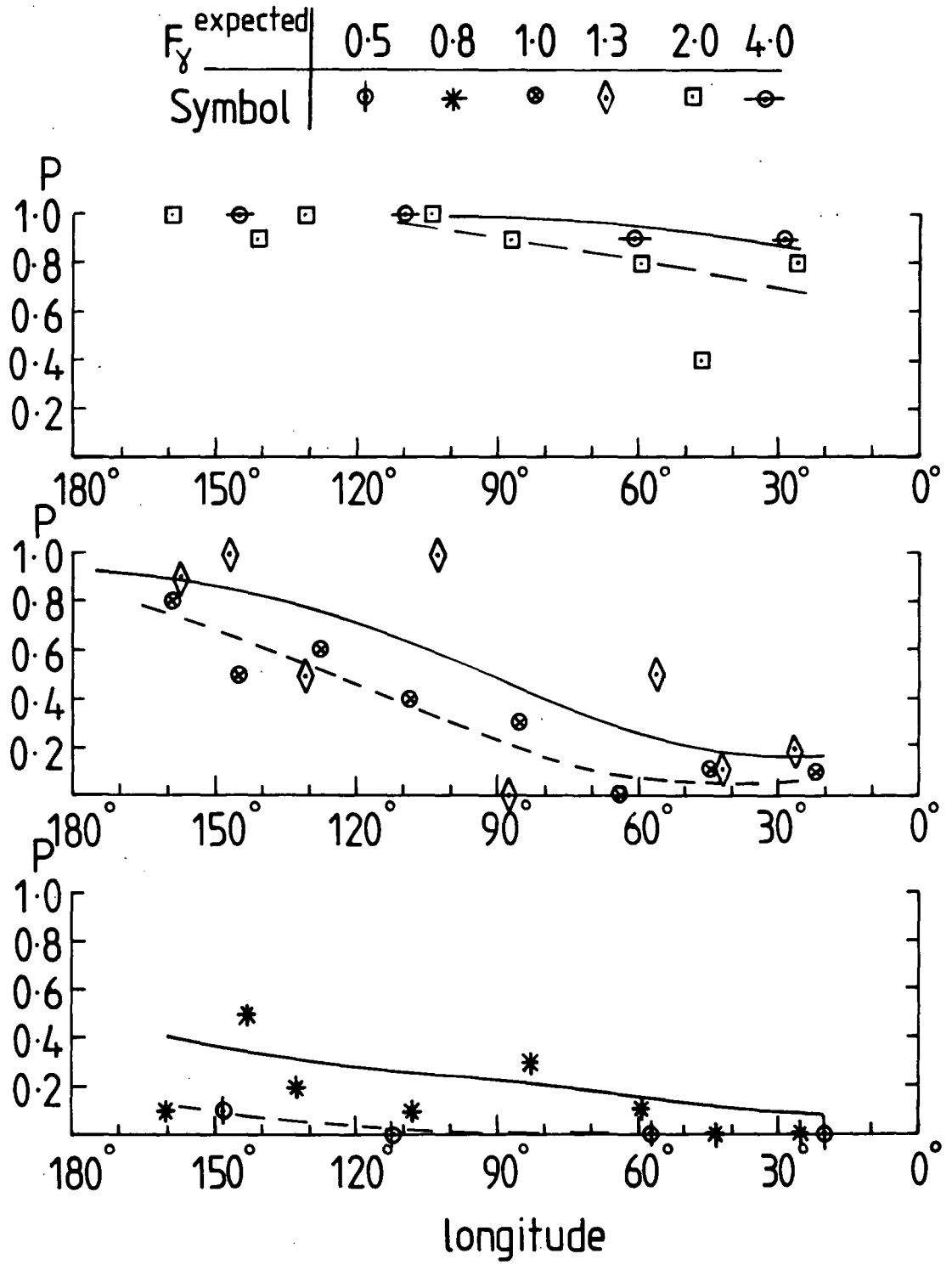

Figure 5.3 The longitude variation of the source detection probability as a function of expected flux, each point being based on 10 Monte-Carlo samples. The calculations are for N_s = 80 counts/flux unit. Curves are drawn as a visual aid, illustrating the overall trend.

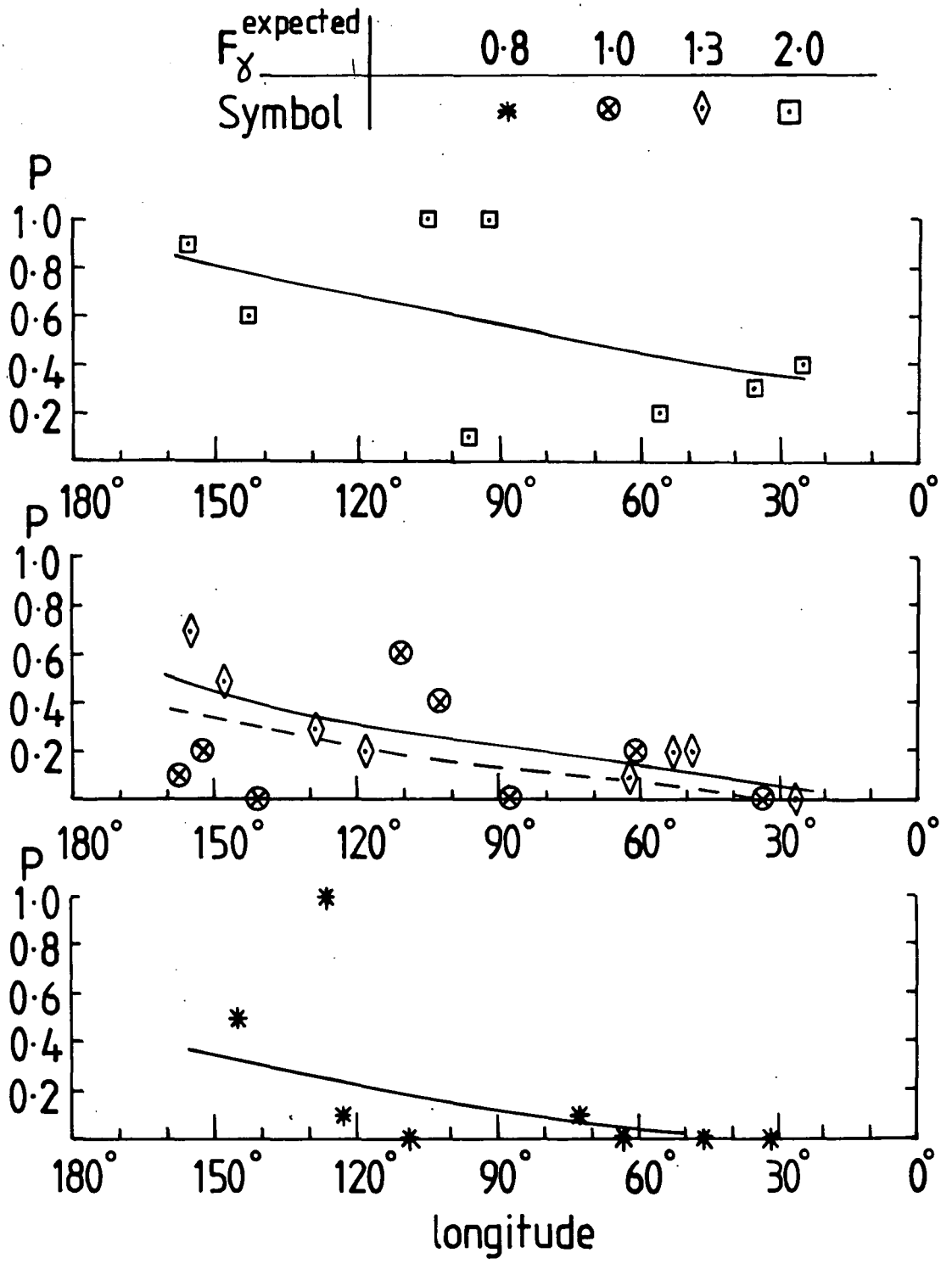

Figure 5.4 The longitude variaiton of the source detection probability as for Figure 5.3 but with N_s = 40 counts/flux unit.

in the outer Galaxy (Figure 5.2), leading to less confusion.

However, several anomalous points are apparent, exhibiting reduced probability at some positions, while for others the reverse is true. Part of this is probably due to statistical fluctuations. However, the data at these positions are further analysed. Close to these positions ($\lesssim 2°$) small scale structure is apparent in the initial background count. In those cases where the background peak is close to the superimposed source the combined counts after fluctuation effectively enhance the true source flux, thereby increasing the detection probability. An initial peak offset from the superimposed source broadens the observed source profile reducing the probability of the source satisfying the width selection criterion. An analysis of the observed source fluxes as a function of the expected flux and Galactic longitude (Figures 5.5 and 5.6) confirms this behaviour. Detected sources (i.e. those satisfying the selection criteria) are found on average to have their true flux enhanced. Interestingly those sources for which F_γ, expected = 0.5, 0.8 flux units are only detectable whenever F_γ, observed $\geq$ 1.0 flux units and no sources are detected with F_γ, observed $<$ 1.0 flux units. This seems to account for the lower flux limit of 1.0 flux units evident in the 2CG catalogue ($|b| < 10°$).

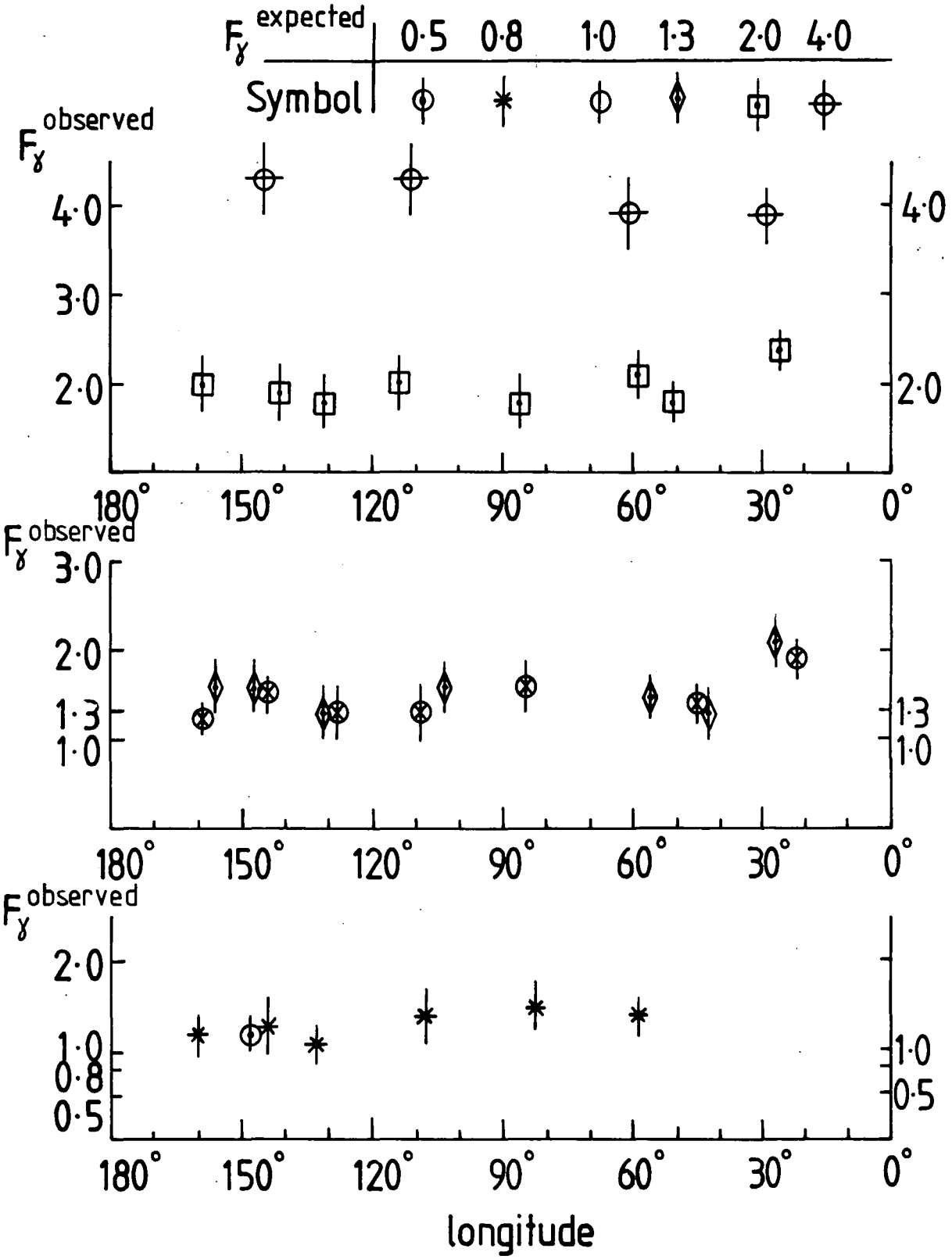

Figure 5.5 The longitude variation of the observed source flux as a function of expected flux for N_s = 80 counts/flux unit. Error bars are $\pm 1\sigma$.

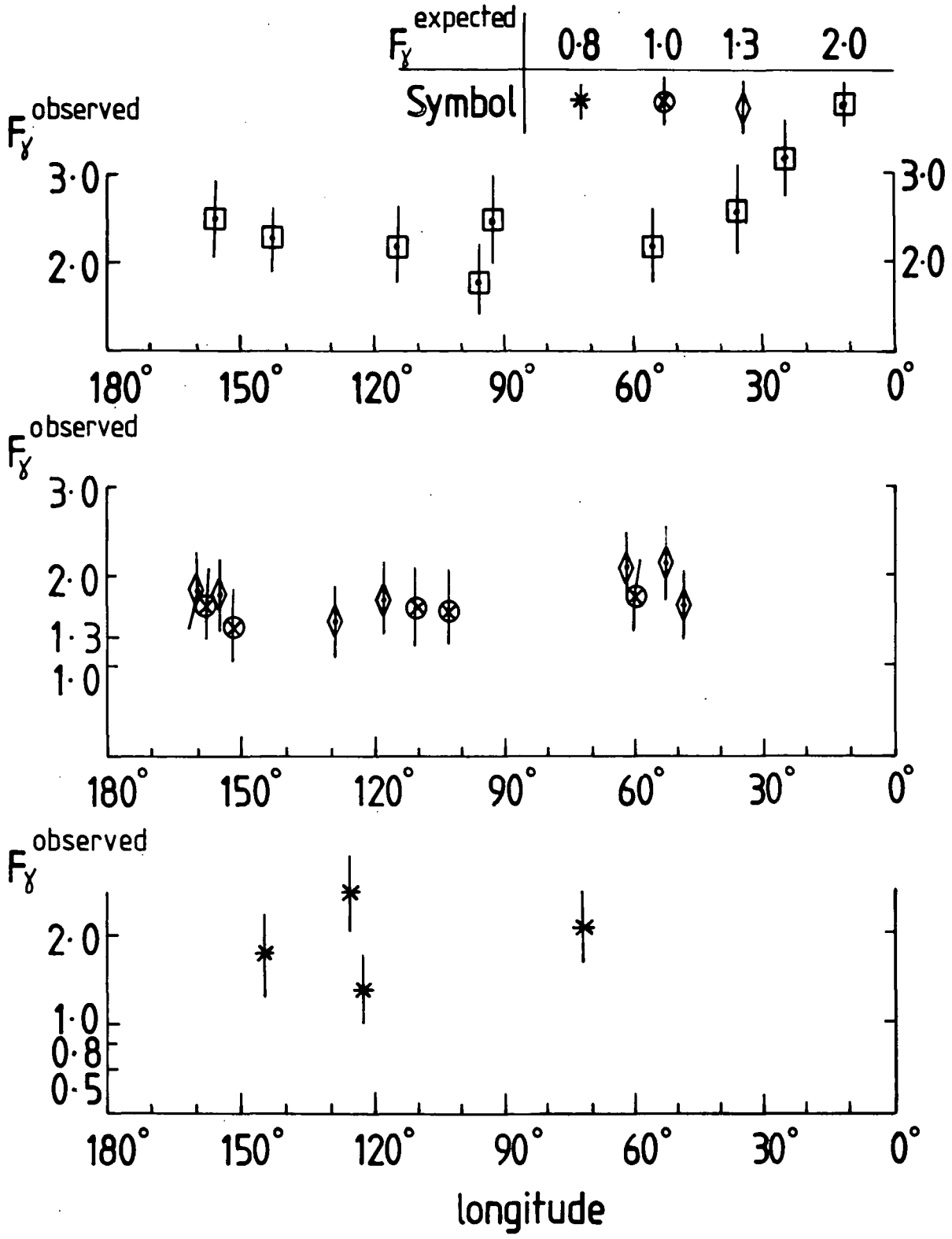

Figure 5.6 The longitude variation of the expected source flux as for Figure 5.5 but with N_s = 40 counts/flux unit.

5.8 Application of detection efficiencies to the Log N - Log S distribution

The results of the Monte-Carlo simulations complement the conclusions of the SAS II analysis (Chapter 4). Specifically we find that the probability of source detection is altered by confusion and that the observed flux is likely to be higher than the true value. The combined effect on the true log N - log S distribution is important at low flux levels where confusion is shown to be significant. The Monte-Carlo analysis gives us information on the relative numbers of sources which will remain undetected in a typical observation of the parent population. We seek to combine these data with the observed 2CG source distribution to correct for losses, and thereby obtain the true distribution.

We begin by assuming that the 2CG catalogue is genuine and complete down to 1.0 flux units, giving 22 sources with $|b| < 10°$. The source detection efficiencies (Figures 5.3 and 5.4) are observed to vary continuously with longitude, and ideally these correction factors should be applied similarly. However, the limited statistics of the observed sample necessitate the use of mean corrections applied over large regions of the sky. The sources are considered in two specific regions, the inner Galaxy ($270° < l < 90°$) and the outer Galaxy ($90° < l < 270°$).

The average detection efficiencies for these longitudes are derived directly from Figures 5.3 and 5.4 and are plotted in Figure 5.7 as a function of true source flux

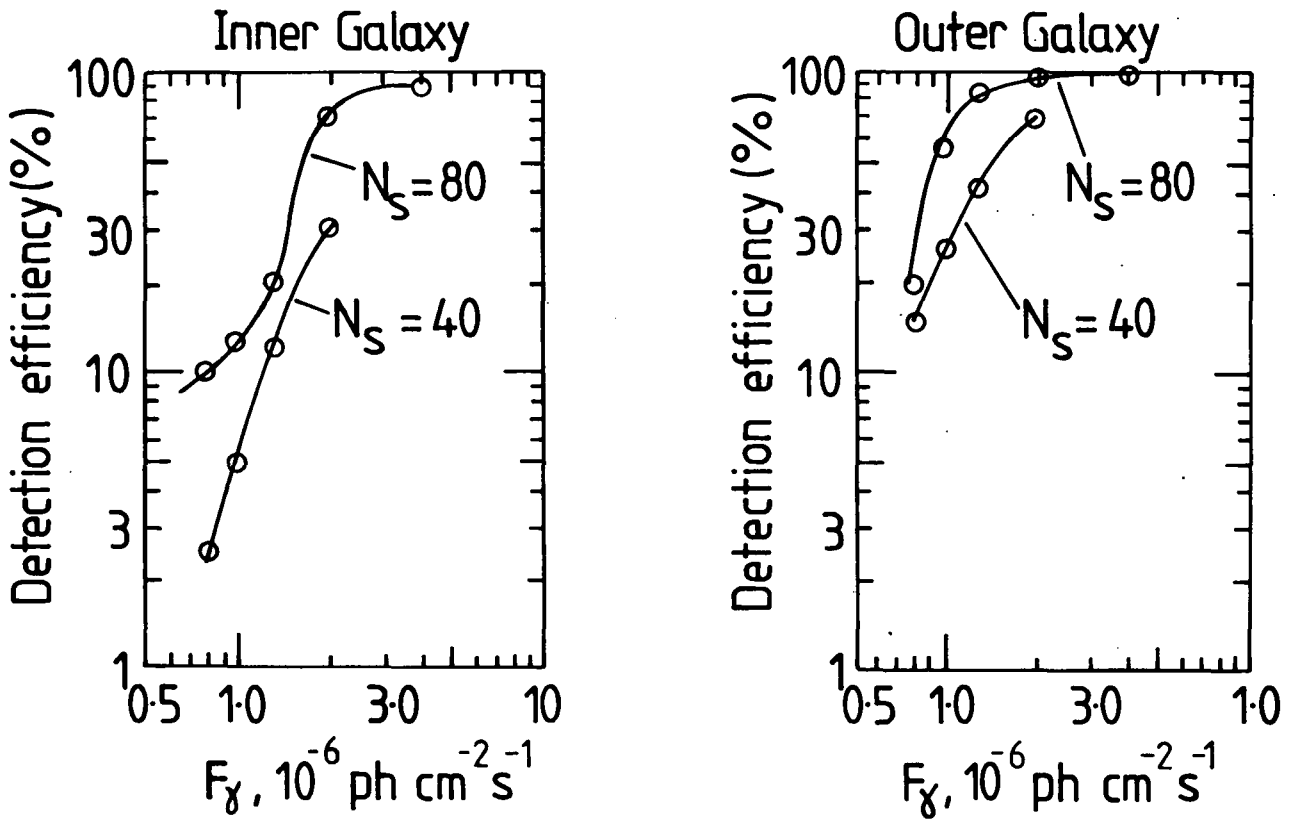

Figure 5.7 Source detection efficiencies derived from Figures 5.3, 5.4 by averaging over the respective longitude ranges for the Inner Galaxy ($270^o < l < 90^o$) and the Outer Galaxy ($90^o < l < 270^o$).

for the two cases N_s = 80, 40 counts/flux unit. The 2CG sources in the inner Galaxy are binned in $\Delta S = 0.2$ flux units to obtain the differential count ($\Delta N/\Delta S$) after interpolating between the discrete flux levels of the integral count. The binned counts are then corrected using the efficiencies of Figure 5.7, making allowance for the small effect of flux enhancement apparent in Figures 5.5 and 5.6. We only correct for the case N_s = 80 counts/flux unit and note that relative to the N_s = 40 counts/flux unit corrections this is a lower limit. However, the former is considered more appropriate for the 2CG sources, the latter serving only as an upper bound to illustrate the trend of the corrections. That is, detection efficiency decreases with reduced exposure. The resultant distributions are rebinned and a power law least squares regression fitted. The corrected distributions, with statistical errors and best fit power laws, are plotted in Figure 5.8. The procedure is repeated for the sources in the outer Galaxy.

Comparison of these distributions shows that the two are intrinsically different in terms of both absolute slope and magnitude at 1.0 flux units. We interpret this as evidence for a population density which varies strongly with Galactocentric distance. It is worth remembering that the corrected source distributions (Figure 5.8) correspond to the true distribution of sources down to 1.0 flux units and the overall Galactic

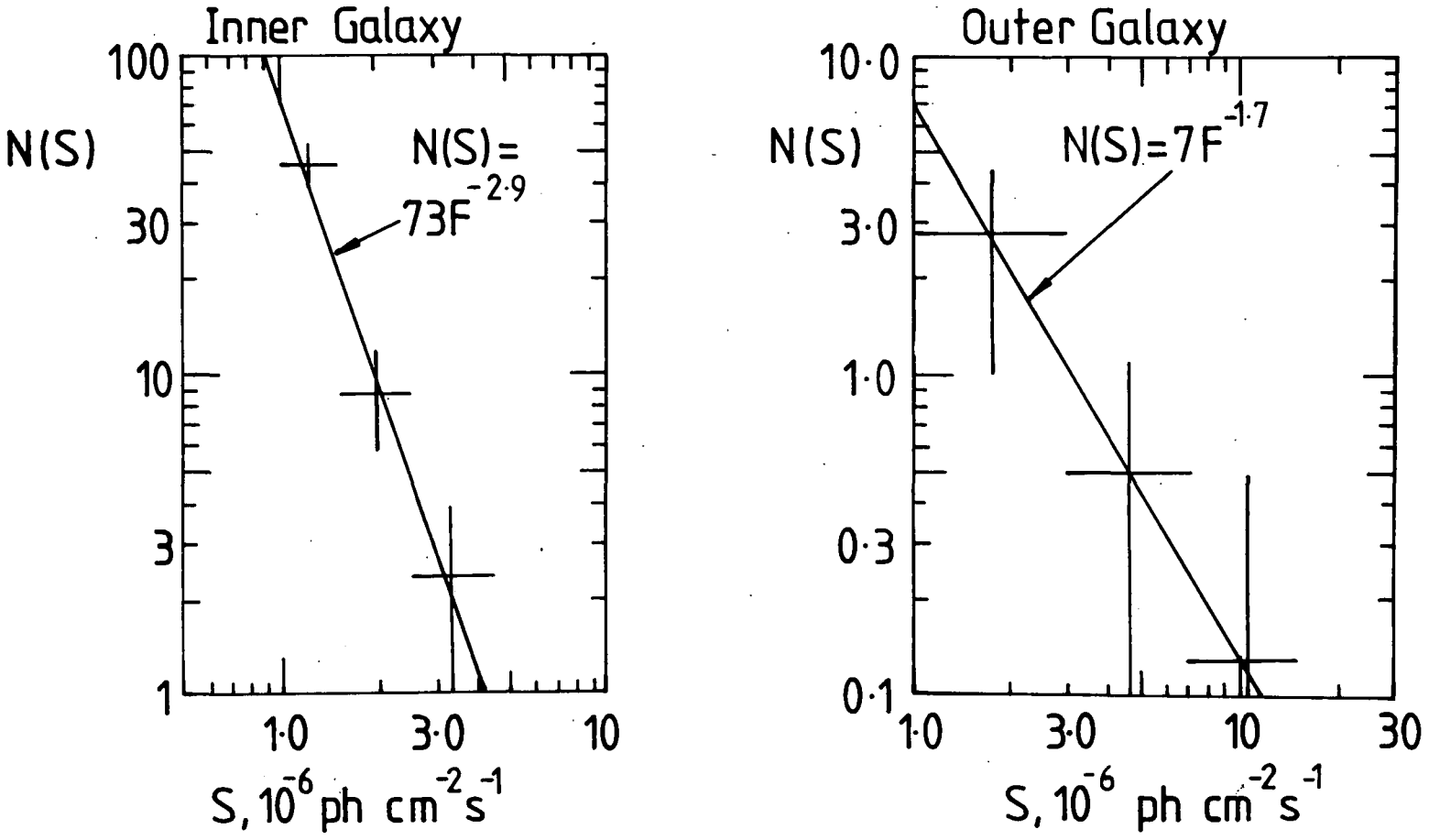

Figure 5.8 Log N - Log S distributions derived from the total 2CG source list ($|b| < 10^{o}$) after applying the appropriate correction factors from Figures 5.5, 5.6, 5.7. Error bars are $\pm 1\sigma$ and the least-squares power law regressions are given in each case.

distribution necessarily extends much fainter. Knowing the minimum source flux level we can therefore estimate the total source contribution.

The minimum source flux is not known but we can make the assumption that the Crab pulsar (2CG 184) is a mono-luminosity source typical of the Galactic population. Its distance ($\simeq$ 2 kpc) and flux (= 3.7 flux units) correspond to a lower flux limit $\simeq$ 0.03 flux units when placed on the far edge of the Galaxy (radius 15 kpc). In the inner Galaxy we assume the power law distribution derived above 1.0 flux units can be extrapolated down to this lower limit. Integrating and including separately the contribution above 1.0 flux units, as derived in Figure 5.8 ($\simeq$ 60 flux units), gives 1973 flux units.

The observed COS B flux for this region is not directly available. However, the gross similarity of COS B and SAS II are sufficient to allow a useful comparison with SAS II. From these data (Fichtel et al., 1978b) we obtain F_γ (> 100 MeV) = 230 $\pm$ 5 flux units ($270° < l < 90°$, $|b| < 4.8°$). The discrepancy between the observed Galactic flux and that expected from sources is serious. However, the assumption of uniform power law dependence is unlikely to be valid. A genuine Galactic source population would have a geometry dependent distribution which would be reflected in the differential count at lower flux levels. In the following section we therefore consider possible source populations, and use the observed distributions above 1.0 flux units

to constrain the total number of Galactic sources.

5.9 Model source populations

Two different source populations are considered. The first assumes an exponential dependence of source concentration with Galactocentric radius. In this model the gamma-ray sources have a distribution similar to that of young active stars, which Montmerle (1979) previously considered as possible candidates for the 2CG sources. The second model assumes a radial dependence following that of supernovae remnants (Kodaira, 1974). Supernovae, and their associated shock fronts, are widely considered to be efficient sources of cosmic rays (up to about 10^{14}eV, e.g. Cesarsky and Lagage 1983). Only two Galactic plane gamma-ray sources (the Crab and Vela pulsars) have been identified with astronomical objects and it is not unreasonable to expect supernovae and their remnants to form a Galactic source population.

For both models we make the assumption of azimuthal symmetry, and a Z dependence $\propto \exp -(Z/Z_o)^2$, where Z is the height above the Galactic plane, and Z_o a variable parameter. The expected integral count can be expressed as

$$N(>S) = \int_1 \int_b \int_o^{r_s} n_o \rho(R) \exp-(Z/Z_o)^2 \, r^2 \, dr \, \cos b \, db \, dl \qquad 5.5$$

The source densities $\rho(R) = \exp-(R/R_o)$ or $F(R)^P$ respectively for the exponential or supernova remnant density relative to the local value. The supernovae

remant density F(R) relative to the local is taken from Kodaira (1974), and p is a dimensionless scaling factor. n_o is an appropriate normalization factor, R the Galactocentric radius and $r_s = (L_\gamma/4\pi S)^{\frac{1}{2}}$ is the line of slight distance from us, with L_γ the intrinsic source luminosity.

We implicitly assume the Galactic gamma-ray sources to have mono-luminosity, as with only two positive identifications, the form of the luminosity function remains open to speculation. From the distances to the Crab and Vela pulsars (2.0 and 0.4 kpc respectively) we estimate L_γ (> 100 MeV) to lie within (0.2 - 1.7) x 10^{39} ph s^{-1} assuming both emit isotropically and have differential gamma-ray spectra of index -2. (The spectral indices measured by COS B are -2.2 and -1.9 for Crab and Vela respectively over the energy range E_γ : 70 - 5000 MeV). We make no allowance for the relative ages of the two pulsars, but adopt a mean luminosity L_γ (> 100 MeV) = 10^{39} ph s^{-1}, and note that variations in the luminosity may make this uncertain by perhaps as much as 50%.

5.10 Model source calculations

The parameters (R_o, Z_o) and (p, Z_o) determine the slope of the Log N - Log S distributions. For each model 5.5 is evaluated numerically over $0° < l < 90°$, $90° < l < 180°$, $|b| < 5°$ and $R_{Gal.} = 15$ kpc, the results being doubled and converted to give the differential count for the inner and outer Galaxy regions. The parameters

of each model are varied and the differential slope α ($N(S) = k\, S^{-\alpha}$) in each case evaluated above 1.0 flux units. The results for $\alpha(R_o, Z_o)$ and $\alpha(p, Z_o)$ are given in Figure 5.9. From these data we seek a unique set of parameters which reproduce the slopes derived from the corrected 2CG distributions : $\alpha = 2.9 \pm 0.32$, 1.72 ± 0.20 for the inner and outer Galaxy regions respectively.

The best fits are found to be:

exponential model:

$$R_o = 0.80^{+\,0.90}_{-\,0.25} \text{ kpc}$$

$$Z_o = 0.14^{+\,2.10}_{-\,0.10} \text{ kpc}$$

supernova remnant model:

$$p = 4.6^{+\,2.9}_{-\,2.3}$$

$$Z_o = 0.13^{+\,6.17}_{-\,0.12} \text{ kpc}$$

The 1σ errors come from the previously determined errors on the source counts. It is seen that both models are only weakly dependent on Z_o, as expected for a thin slab type distribution. For each model, n_o is then chosen to normalize onto the corrected count distribution at 1.0 flux units. It is not possible to find a unique normalization compatible with both inner and outer Galaxy distributions. This may, in part, be due to the low statistics in the outer Galaxy, though it could also suggest a smaller radial variation than implied by the present

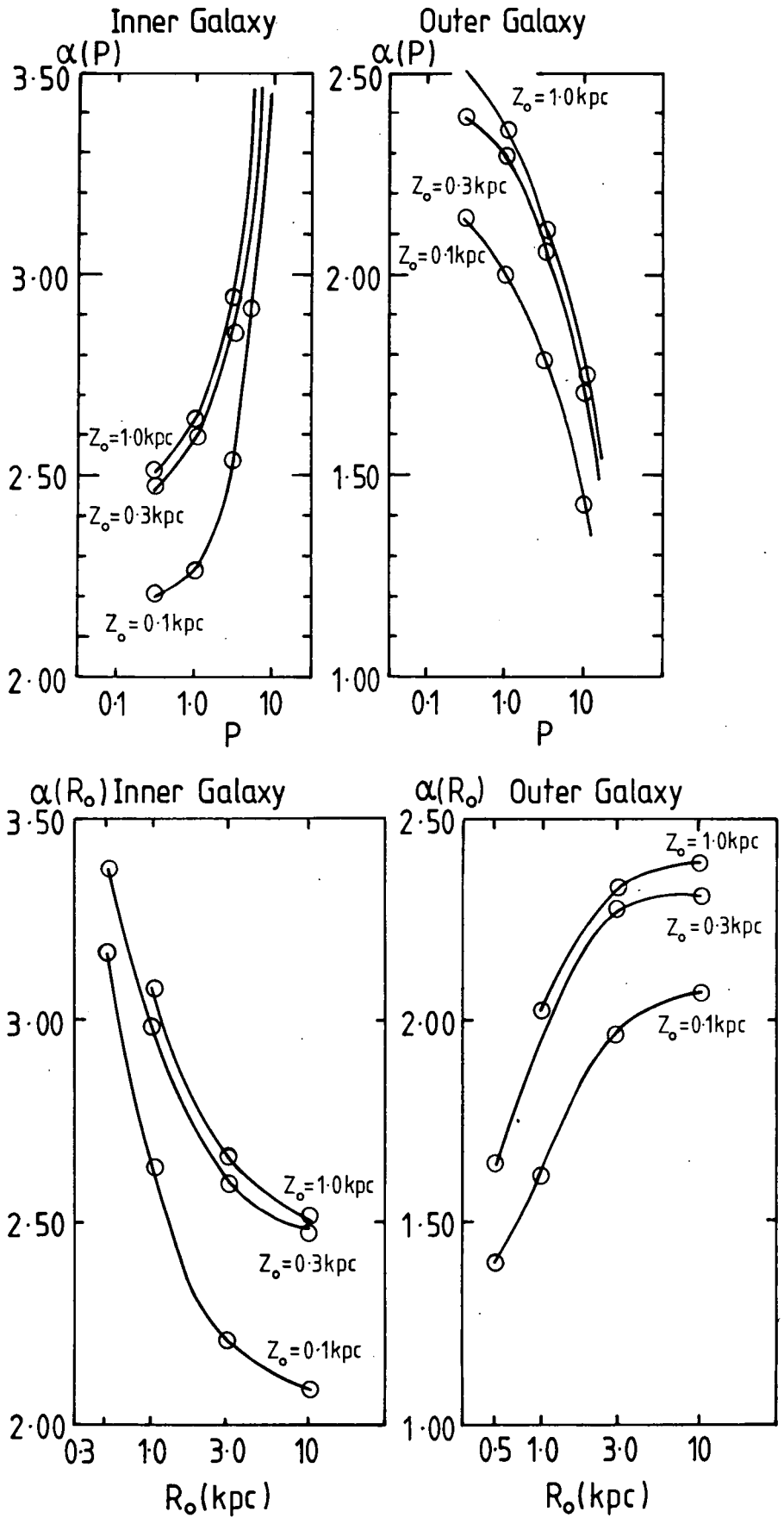

Figure 5.9 Variation of the slope parameter α for model source distributions. Top : $\alpha(p, Z_o)$, supernovae remnant distribution. Bottom : $\alpha(R_o, Z_o)$, exponential distribution.

models. We therefore normalize the models to the data for the inner Galaxy. Both source populations are then integrated over the Galaxy from the minimum flux up to 1.0 flux units. These are combined with the corrected distributions (Figure 5.8) to give the total source count and flux in each case (Table 5.1).

The large upper limits to the expected number and flux, especially for the exponential case, can be understood in terms of the corresponding parameters R_o and p. Small R_o implies rapidly varying Galactocentric density, exponentially increasing continuously towards R = 0. This is an unsatisfactory feature of the model which would be improved by considering a flatter distribution near the Galactic centre. In this respect the supernovae remant model is probably more appropriate in assuming the density decreases smoothly for $R < 5$ kpc.

Nevertheless both models clearly predict an over-abundance in the flux from the Galactic plane, when comparison is made with the SAS II observations. This is unacceptable and we conclude that at least one of the initial assumptions is invalid. It is possible (though unlikely) that discrete sources dominate the Galactic emission in which case the Monte-Carlo model of the diffuse emission is not appropriate. However, the limited angular resolution would require pure source confusion (as with the radio sources) to be considered. In that the total observed flux would then be due to

TABLE 5.1

		Inner Galaxy (l:270°-0°-90°)	Outer Galaxy (l:90°-180°-270°)
Exponential model	Total flux	$4.1^{+430}_{-4.0} \times 10^{-2}$	$5.2^{+120}_{-4.7} \times 10^{-7}$
	Total source count	$4.7^{+150}_{-4.6} \times 10^{5}$	$1.0^{+36}_{-0.9}$
SNR model	Total flux	$4.7^{+16}_{-1.5} \times 10^{-4}$	$9.1^{+140}_{-8.6} \times 10^{-7}$
	Total source count	$4.0^{+21}_{-1.2} \times 10^{3}$	$1.9^{+40}_{-1.8}$
SAS II	Total Flux ($\|b\|<4.8°$)	$(230 \pm 5) \times 10^{-6}$	$(110 \pm 4) \times 10^{-6}$

Table 5.1

Flux (ph $cm^{-2}s^{-1}$) and source count for the two models fitted to the corrected 2CG source list. The SAS II flux is derived from the data of Fichtel et al. (1978b).

an unresolved clumped source distribution, the detection efficiences are likely to be similar to the present case, and the flux overabundance would remain. The alternative, and more likely possibility, is that not all the observed sources are genuine, particularly those at the weakest flux limit. In this case, the corrected numbers would be greatly reduced, decreasing both the slope and absolute number of the differential count. The model predictions are consequently reduced.

We conclude, therefore, that the 2CG catalogue most likely contains several spurious low flux sources. These, like the unidentified sources extracted from the SAS II analysis (Section 4.5), can be explained as upward statistical fluctuations of the structured background. While the present analysis cannot distinguish between genuine and spurious sources, it does suggest that a reduced genuine source population is likely to be more compatible with the total observed Galactic plane flux.

5.11 Derivation of the best genuine source list

As the results of the previous section suggest that the 2CG catalogue is unlikely to be competely genuine, we now endeavour to assess all the evidence on each source to determine a best catalogue of genuine sources. Using these we can then rework the previous analysis to derive an improved estimate of the total Galactic contribution from genuine sources. This can be compared with the total emission.

The 22 2CG sources ($|b| < 10°$) are considered in Table 5.2. We draw on the SAS II cross-correlation analysis (Chapter 4) which is able to offer varying degrees of confirmation for each of these sources. In addition we use the results of Li and Wolfendale (1982) and Arnaud et al. (1982). These workers employ a Monte-Carlo analysis of the expected gamma-ray sky from cosmic ray interactions with HI and H_2 over the range 1 : 65° - 180°. In essence this is similar to the Monte-Carlo model of the sky background in the present analysis (Section 5.2). They find sufficient consistency between peaks in the HI and H_2 distributions (principally H_2) and several of the 2CG sources. These are identified in Table 5.2 as giant molecular clouds.

These objects can be further categorized into two types by comparing the observed flux with that expected assuming a uniform distribution of cosmic rays throughout the Galaxy. Those requiring cosmic ray enhancements close to unity (i.e. irradiated by the ambient cosmic ray flux) are most likely considered to be giant molecular clouds not resolved by the gamma-ray detectors. For several, however, enhancement factors $\geq$ 2 are required, and the giant molecular cloud explanation must be considered less certain. Though we also note that cosmic ray enhancements of the order of 10 may be possible in giant clouds (Dogiel et al. 1983, Houston and Wolfendale, 1984) and that the exclusion of cosmic rays above few 10^8eV is considered unlikely (Skilling and Strong, 1976). Indeed

TABLE 5.2

F_γ,COS B	2CG	SAS II	G.M.C.	Genuine (max)	Genuine (min)
2.4	006			*	*
1.0	013		b	*	
1.9	036	a	b		
1.3	054	a		*	*
1.2	065		b		
1.3	075	a	b		
2.5	078		b		
1.1	095				
1.0	121	a	c	*	
1.0	135	a	c	*	
3.7	184			*	*
4.8	195			*	*
1.0	218			*	*
1.0	235			*	*
13.2	263			*	*
2.7	284	a		*	*
1.6	288		*		
2.1	311	a	d	*	
3.8	333	a	d	*	
2.0	342	a	d	*	
2.6	356			*	
1.8	359			*	*

Table 5.2 The 2CG source list ($|b|<10°$), F_γ, COS B being the source flux ($x10^{-6}$phcm^{-2}s^{-1}) measured by COS B. SAS II indicates those peaks confirmed from an analysis of the SASII data (Table 4.1, Table 4.2) (a) being those peaks detected at reduced significance. (Note non-detection by SAS II does not exclude the possible reality of a source) G.M.C. those sources which as explained in the text can be explained in terms of cosmic ray irradiation of giant molecular clouds. (b) Li & Wolfendale (1982), (c) Arnaud et al. (1982), but both require cosmic ray enhancement > 2 relative to the local value. (d) Riley et al. (1984) based on incomplete data. Genuine (max), (min) are the best estimates of the maximum and minimum number of genuine sources.

the work of Issa and Wolfendale (1981b) suggests that enhancements may be required for nearby clouds. These topics are dealt with more fully in the following chapter in relation to the Orion molecular cloud.

We also utilize the analysis by Riley et al. (1984), who attempt to apply the same criteria to the HI + H_2 and gamma-ray data in the fourth Galactic quadrant. To date CO surveys in this region have been limited in extent (either $|b| < 1°$ or a series of thin latitude slices). This makes any analysis less than complete, as a wide coverage is required for convolution with the gamma-ray point spread function to enable an accurate comparison to be made. Nevertheless, progress can be made and we include these data in Table 5.2.

We derive two discrete source sets; the maximum and minimum samples. The major difference between the two lies in the uncertainty over the fourth quadrant data. Presumably the best estimate is somewhere between these two sets. From our knowledge of the previous analyses of the data in the first and second quadrants, we expect the best estimate to be closer to the minimum.

5.12 Best estimate of the genuine source flux

We follow the methods previously described in correcting both genuine source lists for losses due to confusion, using only the corrections for N_s = 80 counts/flux unit (Figure 5.7). The results and best fit power laws to the differential counts are given

in Figure 5.10. In all but one case the regression fits have a differential slope $\alpha < 2.0$, and the best estimates for both inner and outer Galaxy regions have $\alpha < 2.0$.

For a uniform, two dimensional mono-luminosity source distribution the differential slope $\alpha = 2.0$, which can be considered the limiting case of a uniform thin slab Galactic disk population. If the source density decreases with Galactocentric radius then $\alpha > 2.0$, $\alpha < 2.0$ for the inner and outer Galaxy respectively. The case of $\alpha < 2.0$ in the inner Galaxy requires the source density to decrease with distance from us, at least over the distance corresponding to $F_\gamma > 1.0$ flux units (about 3 kpc for the assumed $L_\gamma = 10^{39}$ph s^{-1}). This requires a physically unacceptable source geometry, and the corrected inner Galaxy distribution with $\alpha < 2.0$ must be rejected as due to small sample behaviour.

Remembering that the minimum sample set of Table 5.2 is considered more plausible we adopt $N(S) = 10\ S^{-2}$ as best describing the genuine source distribution for the inner Galaxy. By necessity we must also have $\alpha = 2.0$ in the outer Galaxy and the flatter distribution derived in Figure 5.10 is rejected as also due to small sample behaviour.

This approach is not without difficulty in that the need to restrict the corrected count distributions effectively limits our estimate of the true source geometry to a uniform, or at most a very slowly varying, Galactocentric

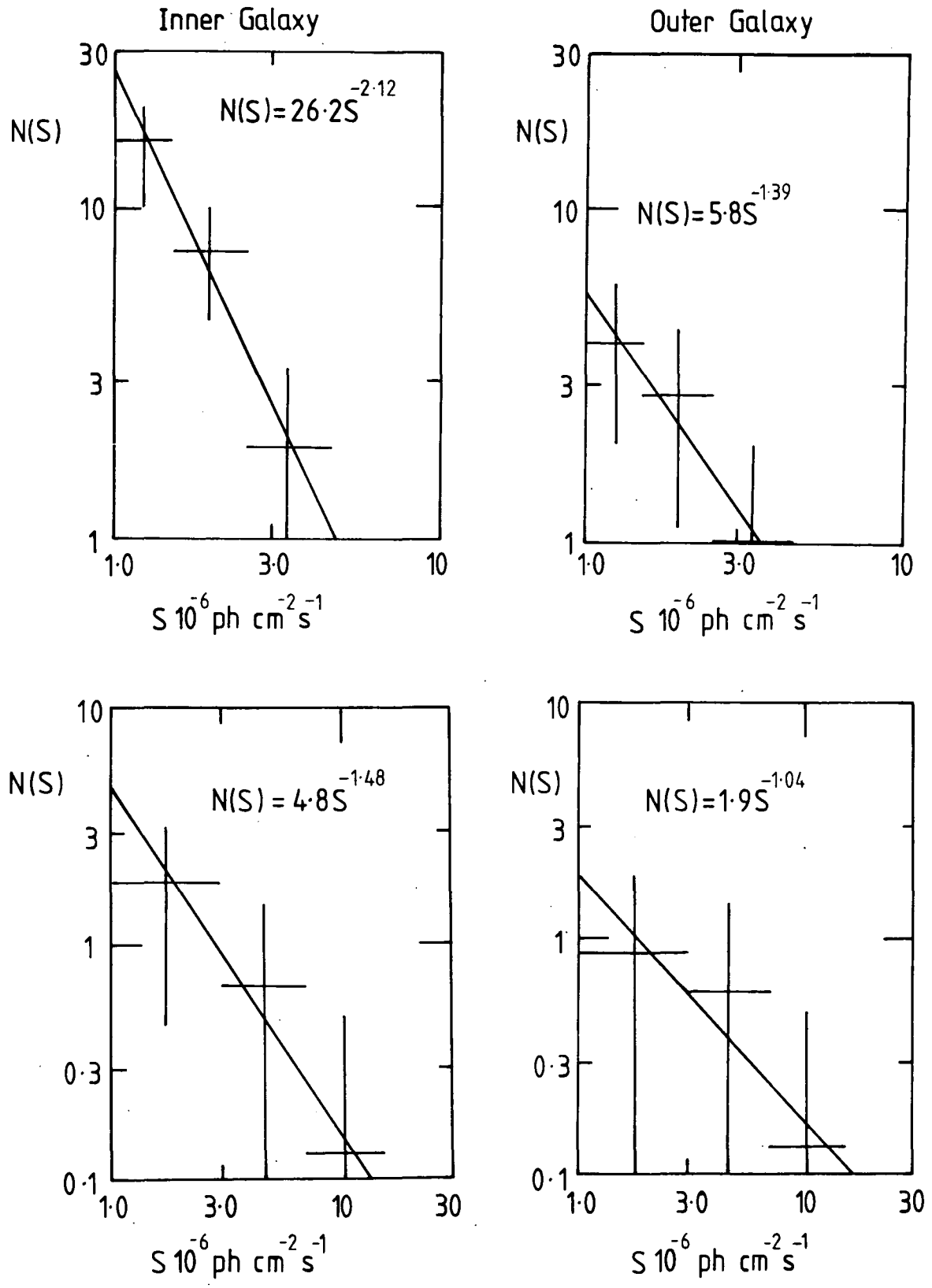

Figure 5.10 Log N - Log S distributions derived from the maximum (top) and minimum (bottom) genuine source lists of Table 5.2, after applying the appropriate correction factors. Error bars are $\pm 1\sigma$ and least squares regression lines are given.

radial density. The true source density may indeed vary, but due to very small numbers locally the nature of the variaiton may not be apparent in the observed count distribution. Nevertheless we proceed.

Rather than make a detailed analysis of the type already performed for the entire 2CG source list, we assume that Z_o = 0.13 kpc and vary p, R_o to obtain $\alpha \simeq 2.0$ for the inner Galaxy. We find p = 0.1 and R = 20 kpc for the supernova remnant and exponential models respectively fit this criterion, giving similar fluxes in both cases. The results in Table 5.3 include the contributions from our minimum estimate of the genuine sources above 1.0 flux units.

5.13 Discussion of the discrete source contribution

It is seen that the expected total source flux is less than the SAS II observations of the Galactic plane. This is encouraging, but the large percentage contributed by sources (23%, 27% for the inner and outer Galaxy respectively) are not consistent with our initial assumption that the total observed flux is dominated by diffuse processes. An improved model should take account of these results iteratively by repeating the Monte-Carlo analysis using a reduced background intensity. We can not consider a reduction of the emissivity in the inner Galaxy, that is the cosmic ray intensity must be at least equal to the local value. However, the situation regarding the absolute density of H_2 is still

TABLE 5.3

		Inner Galaxy (l:270°-0°-90°)	Outer Galaxy (l:90°-180°-270°)	Inner/ Outer
	Total	230	111	2.1
Flux	Sources	52(26)	30(25)	1.7(1.0)
	Diffuse	178(204)	81(86)	2.2(2.4)
Source/ Total		23(11)%	27(23)%	0.9(0.5)
Diffuse/Total		77(89)%	73(77)%	1.1(1.2)

Table 5.3

Best estimates of the gamma-ray flux x 10^{-6}ph $cm^{-2}s^{-1}$ ($>$100 MeV) for $|b| < 5°$. Two values are given for the genuine source flux the former corresponds to the calculations based on the original Monte-Carlo background whereas the latter bracketed values are estimated for the case of a reduced diffuse background.

uncertin (Section 5.4). Indeed, we can view the Monte-Carlo results as indirectly confirming the need for a decreased distribution of target material in the inner Galaxy. Such a situation is consistent with the arguments for including the metallicity gradient in deducing H_2 from CO.

Use of the metallicity gradient clearly lowers the gas column density in the inner Galaxy, and thus the intensity of the structured background. We make an approximate estimate of these effects without re-calculating the detection efficiencies for the reduced background model. This background is likely to be rather similar to that for the outer Galaxy in the present model. Therefore the latter correction factors (Figure 5.7) can be applied to the revised genuine source distribution. As indicated in Table 5.3 we estimate the genuine source fluxes to be further reduced by a factor of 2.

We are now able to percieve a reasonably self-consistent picture of the Galactic gamma-ray emission from the results of Table 5.3. Most of the Galactic emission can be explained as diffuse in origin with sources (observed and unresolved) contributing about 11-23% of the total flux. This is in good agreement with the independent estimate by Harding (1981), who considers the Galactic pulsar population and calculates their total integrated flux to be about 15-20%.

Finally, we note the low source to diffuse flux ratio in Table 5.3. We assume the cosmic rays at these energies (above about 1 GeV) are predominantly Galactic in origin, and both cosmic and gamma-ray sources have similar distributions; for example that of supernovae remnants. The low ratio is then interpreted as evidence for significant diffusion of the cosmic ray particles from their sources. That is, the diffuse emission traces the cosmic rays in the interstellar medium, while discrete gamma-ray sources indicate the initial distribution of cosmic ray sources.

CHAPTER 6

THE ORION MOLECULAR CLOUD COMPLEX

6.1 Giant molecular clouds in the Galaxy

Molecular cloud complexes have become a widely studied phase of the interstellar medium. Observations of cloud dynamics, internal chemistry and their relationship to star formation are important areas of investigation. Scoville and Solomon (1975) made the first Galactic plane survey of Giant Molecular Clouds (GMC) by way of observations of CO. Further observations (e.g. Gordon and Burton 1976; Cohen and Thaddeus 1977; Solomon, Sanders and Scoville 1979; Cohen, Tomasevich and Thaddeus 1979; Kutner and Mead 1981; List, Xiang and Burton 1981, Sanders 1981; Robinson, McCutcheon and Whiteoak 1982; and Solomon, Stark and Sanders 1983) have extended the coverage to include the first, second and fourth Galactic quadrants.

These surveys generally provide undersampled observations in l and b, nevertheless much information has been obtained. There is a wide consensus of opinion on the origin of the CO emission. Specifically it is localized to the regions which typically have H_2 densities $\simeq 10^{2-3}$ cm^{-3}, linear dimensions $\simeq$ 10-50 pc and masses $\simeq 10^{4-6} M_\odot$. The question of cloud masses is dependent on the assumed $CO \rightarrow H_2$ conversion factor and the effect if any, of the Galactic metallicity gradient (Section 5.4). There are important consequences for the inferred mass of H_2 in the inner Galaxy and therefore also for the interpretation

of the Galactic gamma-ray emission. Furthermore, following the discussion in Chapters 4 and 5 it is likely that many molecular clouds may be confused for genuine discrete gamma-ray sources.

To further understand the relevance of giant molecular clouds to gamma-ray astronomy, it is worthwhile to study in detail the gamma-ray emission from specific clouds, which we hope are typical of those observed throughout the Galaxy.

6.2 Cosmic rays and molecular clouds

Previous analyses of the gamma-ray flux from molecular clouds have assumed that the clouds are irradiated by the ambient cosmic ray flux and are inert in the sense of containing no cosmic ray sources (Issa and Wolfendale 1981a,b; Bloemen et al., 1984b). Under these assumptions the analysis of the SAS II data by Issa and Wolfendale concludes that for most local clouds the observed flux is approximately consistent with that expected from knowledge of the local cosmic ray spectrum and cloud masses derived from molecular studies. However, in a few cases (Cas OB6, Carina Nebula) the observed flux is greater than expected by factors of up to 20. It is unlikely that the mass estimates could be consistently and significantly low, thus holding out the possibility of enhancement of the ambient cosmic ray flux in at least some clouds. Houston and Wolfendale (1984b) consider the energy density within a cloud and show that a simple equipartition argument also suggests a cosmic ray enhancement.

Theoretical consideration has been given to the interaction of cosmic rays and molecular clouds by several workers. Skilling and Strong (1976) have studied the energy losses of cosmic rays in a dense cloud and the subsequent exclusion of cosmic rays from the cloud due to scattering by self-generated Alfven waves. They conclude that for typical clouds ($M \simeq 10^5 M_\odot$) cosmic rays above about 10 MeV/nucleon can freely penetrate the cloud, though lower energy particles are increasingly excluded. Similar conclusions are obtained by Cesarsky and Volk (1978). Morfill (1982a,b) further considers the effect on cosmic ray electrons, which because of their higher energy than protons of the same rigidity can be convected and accelerated into the cloud by the proton-generated Alfven waves. Gamma-ray production above 100 MeV can occur from cosmic ray nucleons of a few GeV or electrons of several hundred MeV. While the former are unaffected by this mechanism the latter can be enhanced within a typical cloud thereby enhancing electron bremsstrahlung gamma-ray emission.

Dogiel et al. (1983) consider the possibility of accelerating cosmic rays within collapsing clouds, though this is believed unlikely as the energy losses in typical clouds are considered too great.

Montmerle (1979) suggests that spatially linked supernovae remnants and OB associations may enhance cosmic ray and hence gamma-ray fluxes within molecular clouds.

In this model low energy cosmic rays produced in the stellar wind of OB stars are accelerated by the shock wave of the supernova remnant interacting with the molecular cloud.

Present models are necessarily simplified though they do at least allow the possibility of cosmic ray enhancement within molecular clouds, whether from the ambient cosmic ray flux or from sources therein. Any attempt therefore to use gamma-rays as a probe of the gas in a molecular cloud should allow for this possibility.

6.3 Dust in the interstellar medium

The origin of dust grains and their role in the field of interstellar chemistry is still poorly understood, though their effects on observational astronomy have been extensively studied. The formation and reprocessing of dust grains is intimately linked to processes of molecule formation in the high density regions known as molecular clouds. Dust's most significant function in these regions, the likey sites of star formation, is to re-radiate optical and UV photons as black-body radiation heating the surrounding material ($\sim$30 - 300 K) and making them intense submillimetre sources.

Interstellar extinction, scattering and polarization of starlight are widely used by astronomers to investigate the nature of observed sources and the intervening material of the interstellar medium. It is the cumulative effect of dust grains along the line of sight which is responsible

and extensive work is devoted to comparing the optical data with those expected from models of grain size and composition. Optical astronomy (including infra-red, visible and UV) is effectively restricted from regions of high extinction where recourse to other wavelengths is necessary to probe the physical processes there and beyond.

Extinction varies approximately as $^1/\lambda$, at least over the range of wavelengths corresponding to the B,V passbands (B(4400, 980A^o); V(5500, 890A^o)). The absorption of light is most efficient when the grain size is of the same order as the wavelength of the incident radiation. The characteristics of typical extinction curves (including the "graphite peak" near 2200A^o) strongly suggests the presence of several different types and sizes of dust grains in the interstellar medium.

The increasing absorption of blue light results in the reddening of stellar images obscured by dust. The colour excess or reddening is defined as the difference in colour index between two stars of the same spectral class, one reddened the other observed in normal light. The reduction in apparent magnitude, that is the extinction A_V, is proportional to the colour excess E(B-V) or E(U-B). From a combination of this ratio $A_V/E(B-V)$ and that of gas column density to colour excess $N_H/E(B-V)$ it is possible to derive

N_H directly from A_V towards specific stars.

In the same way that stellar images suffer extinction, extragalactic objects such as galaxies will also be affected by intervening dust in our Galaxy. Assuming that galaxies are uniformly distributed on the sky, variations in the galaxy count from position to position can be used to map out the extinction and hence total gas throughout the Galaxy.

Lilley (1955) used Hubble's (1933) galaxy counts to derive optical extinction values, and hence the optical depth of dust, for a region below the Galactic plane ($b \sim -10^o$ to -20^o) incorporating the dark clouds in Perseus, Orion and Taurus. He compares these values with the optical depths obtained from a survey of HI 21 cm emission, assuming the HI to be optically thin. Although the data are of low quality there is a good correlation between τ_{gas} and τ_{dust} and evidence for residual gas in the absence of dust, i.e. $\tau_{gas} = a\,\tau_{dust} + b$. Lilley considers this as most likely due to a variation in the gas to dust ratio in the regions observed. At that time HI was considered to be the dominant constituent of the interstellar medium, though van de Hulst (1954) had discussed the possibility of H_2 existing in significant quantities. As H_2 is not detected by 21 cm emission it was believed that this additional component of gas would also contribute to the extinction.

With the advent, in the late 1960's, of widespread detections of increasingly complex molecular species by radio-astronomical techniques, the understanding of the interstellar medium has changed substantially. H_2 must be a major constituent of the gas in the interstellar medium and as such must also contribute to extinction through any dust associated with it. Additionally, a small fraction ($\sim$ 4%) of the hydrogen in the interstellar medium is ionized and exists in high density regions, usually associated with areas of recent star formation. It is assumed that HII will also be associated with dust thereby contributing to interstellar extinction. Dust can therefore be used, in theory at least, to estimate the column density of all gas along the line of sight to the observed source.

The relevance to gamma-ray astronomy is apparent when it is remembered that the diffuse component of Galactic gamma-rays are produced by cosmic ray interactions with the gas and radiation of the interstellar medium. For $E_\gamma > 100$ MeV, it is widely believed that p-p collisions are the dominant production mechanism (Section 1.2) and therefore knowledge of the total gas in the Galaxy is essential. In an early analysis of the SAS II data, Puget et al. (1976) use the extinction as measured to nearby stars ($\leqslant$ 2 kpc) to estimate the contribution to the observed flux from cosmic ray interactions in the local interstellar medium. By subtracting off this

expected local irregular longitudinal flux distribution they are better able to analyse the large scale variation in Galactic gamma-ray emission, comparing the unfolded radial distribution with that of other Galactic tracers. They also note one of the limitations of using extinction to estimate gas column density. For regions of high extinction ($E(B-V) \gtrsim 1.5$, $Av \gtrsim 4.5$) the method only gives a lower limit to the total column density. This tends to be a serious problem for the central regions of dense molecular clouds and close to the Galactic plane in the direction of the inner Galaxy.

6.4 The gas-to-dust ratio

Calibration of the ratio $N_H/E(B-V)$ (gas column density to colour excess) for the local interstellar medium requires direct measurements of both gas column densities and extinction. Savage et al. (1977) use UV data from the Copernicus satellite to measure the column density of H_2 towards local stars ($\lesssim$ 500 pc). The technique utilizes the absorption of UV photons by H_2 (transition between J = 0 and J = 1 rotational level of the $\nu'' = 0$ vibrational state), the depth of the absorption features being proportional to the column density of molecular gas. The direct measurement of H_2 by this technique is only possible for the very local region around the Sun because the absorption features rapidly saturate at larger distances, thereby

only being able to give lower limits to N_{H_2}.

Similar results are obtained for N_{HI} (Bohlin et al. 1978) by measuring the spectral region for L_α absorption to obtain N_{HI}. Again this technique can only be applied locally; but it has many advantages over measurements of N_{HI} from 21 cm emission which is dependent on instrumental calibration, the need for optical depth corrections and the effects of Galactic rotation on observed emission velocities.

The combined data for 96 star positions gives a calibration value of

$$N(HI + 2H_2)/E(B-V) = 5.8 \times 10^{21} \text{ at cm}^{-2}\text{mag}^{-1}.$$

This value does not allow for the presence of HII as it is believed that $\simeq$ 4% of the total gas in the local interstellar medium is ionized. This is believed to be less than the systematic error in measuring E(B-V) and is consistent with the accepted electron density $\langle n_e \rangle \simeq 0.03$ cm^{-3} derived from pulsar measurements.

From extensive measurements of extinction curves towards local stars the extinction to colour excess ratio $A_v/E(B-V)$ is estimated to be about 3.1 ± 0.1 (Savage and Mathis, 1979). This is essentially limited to regions within about 2-3 kpc of the Sun and is thus a local value. Its large scale uniformity strongly suggests the size distribution of grains in the interstellar medium is constant, at least over the region observed.

The gas to dust ratio is a combination of both measurements. There are small anomalous regions, notably in the directions of dense molecular clouds, where this ratio varies significantly from the mean value considered appropriate for the general interstellar medium. Measurements of E(B-V) are limited towards specific stars. Extinction, through the use of galaxy counts, can sample much larger areas of the sky thereby leading to estimates of total gas column density along a line of sight.

6.5 The Orion molecular clouds

The Orion complex is an extensive association of gas, dust, HII regions, reflection nebulae, infra-red sources and OB associations, approximately 500 pc from the Sun in the direction $(l, b) \sim (210^{o}, -20^{o})$. It is generally believed that this is a region of ongoing star formation. HI observations (e.g. Lilley, 1955; Menon, 1958; Gordon 1970) reveal emission with a velocity pattern suggestive of an expanding shell. Tucker et al. (1973) made initial observations of the molecular gas (via CO) around Orion B (NGC 2024). These workers discovered intense CO emission which extended over more than 1^{o}.

Since then the Columbia group have pursued a detailed observational program of ^{12}CO and ^{13}CO emission line studies from the Orion-Monoceros region (Kutner et al., 1977; Thaddeus, 1982). From these data it is clear that CO is a good large-scale tracer of the likely star formation sites. The most intense areas of CO emission lie along the leading edges of cone-shaped structure formed by the junction of the two molecular clouds Orion A and Orion B. Interestingly the bulk of the active sources (i.e. HII regions, infra-red sources, OB association) also follow a similar alignment.

Blaauw (1964) studied the four main OB association subgroups in the Orion complex. Their estimated ages decrease from Ia ($\sim 12 \times 10^{6}$yr) to Id ($\sim 2 \times 10^{6}$yr). These subgroups also exhibit a marked spatial alignment

with the oldest Ia lying outside and to the south of the molecular clouds. The others are distributed along the leading edges of the intense CO emission observed in Orion A and B. Kutner et al. (1977) observed a systematic CO velocity gradient in Orion B. This may be suggestive of an overall rotation of the cloud, though Kutner et al. note that the sense of rotation does not correspond with that expected from the Galactic differential rotation in that region. Furthermore the OB associations do not exhibit a similar velocity gradient which might be expected if these were formed in the clouds about 10^{6-7} years ago.

An alternative explanation is that the mechanism responsible for the star formation might have produced the velocity gradient. Kutner et al. (1977) and Thaddeus (1982) believe this model is more likely as the conical shape of the clouds and the distribution of OB associations is indicative of a shock or wind sweeping into the cloud from the direction of the oldest OB association. This picture is further supported by detailed studies of H_2 emission (vibrational transitions) and high resolution kinematic features of ^{12}CO and ^{13}CO emission in the Orion nebula (NGC 1976) (Beckwithet al., 1979; Loren 1979; Beckwith et al. 1983).

The Orion nebula has been widely studied at many wavelengths and in the central region (diameter $\simeq$ 0.1 pc) H_2 densities $\gtrsim 10^6$ cm^{-3} are inferred from observations

of NH_3 emission (Batrla et al., 1983). This is direct evidence of high density clumping within the overall cloud structure, for which mean H_2 densities of 10^{2-3} cm^{-3} are estimated from ^{12}CO and ^{13}CO observations.

Berger (1981) made polarimetry and photometry studies of the Orion nebula and concluded that the reddening $A_V/E(B-V)$ is abnormally large $\simeq$ 5-6. Polarimetry measurements show the mean grain size is larger around the nebula. It is believed that the smaller grains are destroyed by radiation from hot stars in the region, and the extinction E(B-V) is therefore less at shorter wavelengths. This has interesting consequences for the estimates of gas column density based on the galaxy count technique. We return to this topic later (Section 6.11).

Talent and Dufor (1979) studied the Galactic metallicity gradient as determined from observations of local HII regions. They find that the radial gradient (8-14 kpc) in the spiral arms (Orion, Perseus and Sagittarius) is 2-3 times greater than that determined for the overall interstellar medium. The observations in the Orion arm are limited to the Orion nebula and NGC 2467, though Hawley (1978) finds a similar result for the Orion arm based on 6 HII regions. It is not clear whether this metal deficiency is characteristic of all the gas in the Orion arm, and specifically that in the molecular cloud complex, or is relative only to the HII regions.

Clearly,in the former case, making allowance for the effect of the metallicity correction on the conversion factor α (Section 5.4) reduces the mass estimates for the clouds.

The metal abundances in the Orion nebula have been studied in detail by Peimbert (1982). After correcting the Orion measurements for electron temperature variations Peimbert finds the differences between Orion and the Sun are of the same order as the absolute accuracy of the abundance determinations ($\simeq$ 0.2 - 0.5 dex, i.e. a factor of 1.6-3). However the abundances in Orion are consistently lower than measured for the Sun strongly suggesting the difference is genuine. Peimbert estimates the Orion nebula is about 0.2 dex deficient in heavy elements (C,N,O,S,Ne) relative to the Sun. This compares with the metal deficiencies $\simeq$ 0.08 dex and 0.13 dex for the Orion arm determined by Hawley (1978) and Talent and Dufor (1979) respectively.

6.6 The method of analysis

The Orion molecular complex is sufficiently close ($\simeq$ 500 pc) to be fully observed in radio emission (CO and HI) and resolved in the gamma-ray data ($E_\gamma > 100$ MeV). Thus as a local giant molecular cloud it is ideally suited as a test of several basic questions regarding cosmic ray interactions with molecular clouds. Specifically two problems must be addressed. The first concerns the total mass as derived from CO observations by an

appropriate conversion factor $\alpha = 2N_{H_2} / \int T(^{12}CO)dv$. Secondly we must consider the extent to which the cosmic ray flux is enhanced or reduced within the cloud.

We can express the observed gamma-ray intensity I_γ in the following manner:

$$I_\gamma = q/4\pi (N_{HI} + 2N_{H_2}) + I_b \qquad 6.1$$

or

$$(I_\gamma - I_b) - q/4\pi N_{HI} = q/4\pi \left[\alpha W_{CO}\right]^N \qquad 6.2$$

where $q/4\pi$ is the gamma-ray emissivity N_{HI} the atomic hydrogen column density and I_b the isotropic gamma-ray background intensity. W_{CO} is the integrated CO emission, α the $CO \rightarrow H_2$ conversion factor and we introduce a scale factor N to approximate the effect of cosmic ray enhancement or exclusion in the molecular gas.

As it is not feasible to model the precise geometry of regions within the cloud which are likely to affect the ambient cosmic ray flux, we make the reasonable assumption that the denser regions (high W_{CO}) are more likely to be the regions of cosmic ray exclusion, enhancement or production (a simple consequence of the fact that star formation is greater there). Thus 6.2 should in essence contain the necessary parameters to represent the gross relationship between cosmic rays, gas and gamma-rays.

While the potential cosmic ray sources may have a distribution similar to that of the CO in the cloud, the contrast in cosmic ray intensity is likely to be much smaller unless the cosmic rays diffuse away remarkably

slowly. For a cosmic ray of few GeV, the mean free path in the ISM in general is $\lambda \sim 0.1$ pc and the lifetime $\tau \sim 10^7$ yr. Thus the typical linear dimensions of the cosmic ray distribution from a single source is given by $< x^2 > = 2 \lambda c \tau$. On substitution, we find $X_{rms} \simeq 800$ pc, which is much larger than the dimensions of the Orion cloud. λ will be smaller than 0.1 pc in the cloud but X_{rms} will still be at least the linear dimension of the cloud; thus, it seems appropriate to apply the scale factor N to the CO distribution smoothed to the gamma-ray resolution rather than at its original resolution.

By analysing the appropriate data for the Orion complex we endeavour to derive the best fit values for α , N in 6.2, thereby estimating the total mass and the degree to which cosmic rays interact with the cloud.

It is realized that this method of determining the local value of α is susceptible to many uncertainties, not least the statistical accuracy of the gamma-ray data. Clearly another method, circumventing the cosmic ray, gamma-ray link, would be advantageous. Instead of using gamma-rays as a total gas tracer we can use galaxy counts as a measure of total gas and compare this with direct measurements of HI and H_2 (via CO). Thus we write:

$$N_{H_t}(N_G) = N_{HI} + 2N_{H_2} \qquad 6.3$$

or

$$N_{H_t}(N_G) - N_{HI} = \left[\propto W_{CO}\right]^N \qquad 6.4$$

Again we introduce a scaling parameter N. In this case we are allowing for the gas to dust ratio to vary within the cloud as the left-hand side of 6.4 is really a measure of the extinction (i.e. dust) associated with the molecular cloud.

6.7 Description of the data

Gamma-ray data for the Orion region are available both from the SAS II and COS B satellites. We use those collected by COS B because of their superior statistical accuracy. A restricted subset of the COS B database is available (Caravane collaboration, private communication). These data, observed count, estimated background count and exposure factors for $E_\gamma > 100$ MeV, are binned ($\Delta l \times \Delta b = 1^o \times 1^o$) over the region $l : 198^o$ to 222^o and $b : -5^o$ to -25^o. Observed intensities are calculated, from which an isotropic background level $I_b = 5.8 \times 10^{-5}$ ph $cm^{-2}sr^{-1}s^{-1}$ is already subtracted. This background is an average determined from extensive analysis of the complete COS B data (Strong, 1984; Bloemen, private communication). From these data we derive $I_\gamma - I_b$ (see 6.2). Figure 6.1 is a contour map of the gamma-ray intensity ($I_\gamma - I_b$) for the Orion region. As noted previously (Section 4.3), determination of the COS B isotropic background presents many problems

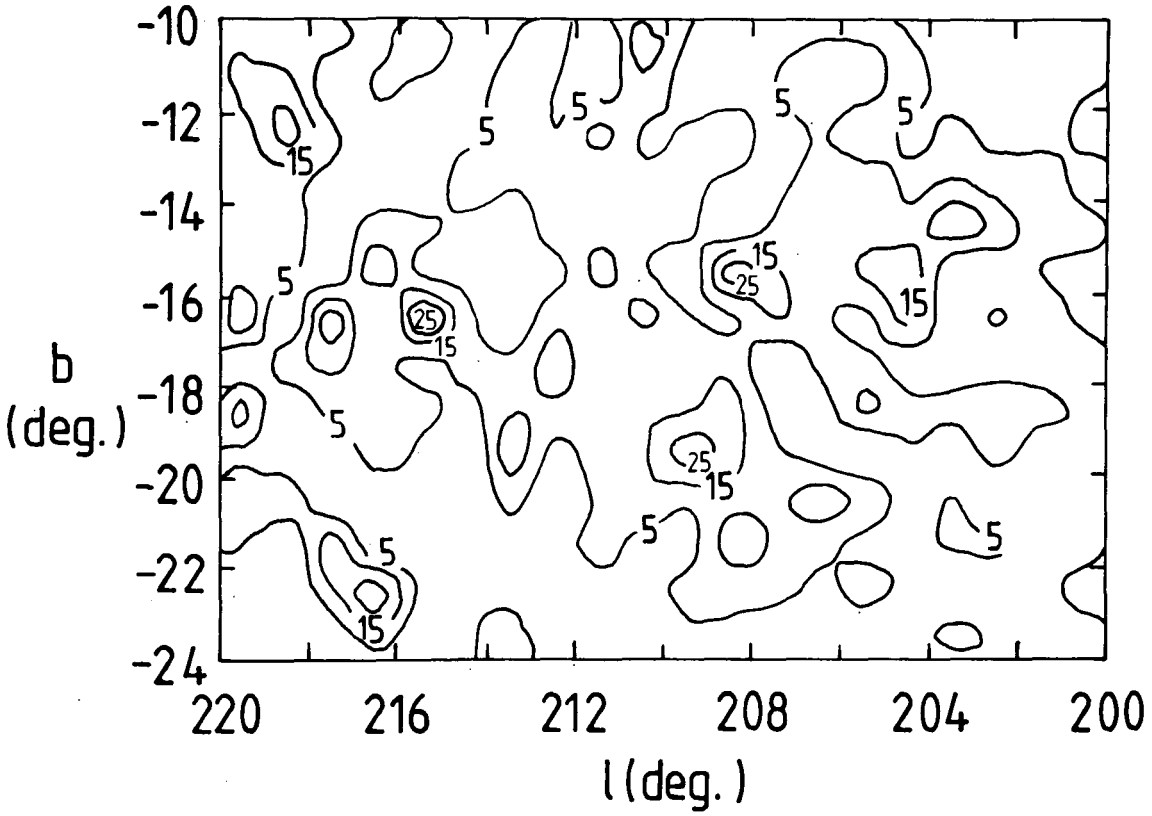

FIGURE 6.1 COS B gamma-ray intensity map for the Orion region. Contours are $I_\gamma(>100\ \text{MeV}) \times 10^{-5}$ ph $cm^{-2}sr^{-1}s^{-1}$, with an isotropic background $I_b = 5.8 \times 10^{-5}$ ph $cm^{-2}sr^{-1}s^{-1}$ subtracted.

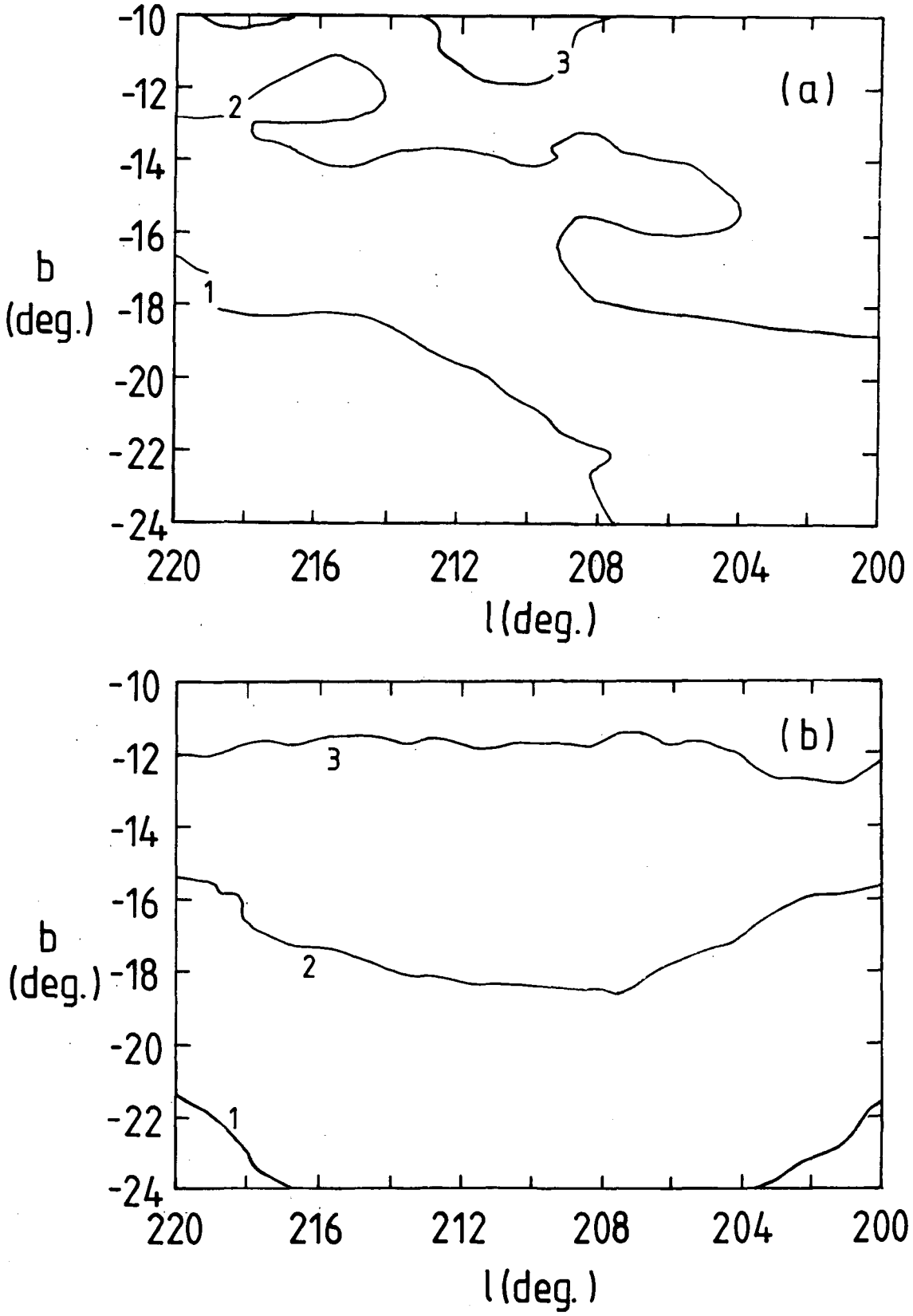

FIGURE 6.2 HI column densities x 10^{21} at cm^{-2},
(a) at original resolution,
(b) smoothed to gamma-ray resolution.

and there is likely to be further uncertainty associated with the present level. We return to this possibility and its effects on the analysis in Section 6.10.

The HI data are taken from the surveys of Weaver and Williams (1973) and Heiles and Habing (1974). We adopt a spin temperature T_s = 125 K to calculate the column densities N_{HI} following the procedure described in Section 5.3. For proper comparison with the gamma-ray data the column densities are smoothed to the COS B resolution ($E_\gamma > 100$ MeV). The column densities before and after smoothing are presented in Figure 6.2. The smoothing procedure has a small effect on N_{HI} as the column density is initially smoothly distributed, rising gradually with increasing latitude. Using these data (Figure 6.2b) it is difficult to distinguish spatially the HI gamma-ray component from the background, that is, treat them both as independent variables (see 6.1). It is preferable to consider the gamma-ray intensity from HI as an additional slowly varying background (see 6.2).

Extensive ^{12}CO coverage of Orion is available from the Columbia group (Kutner et al., 1977, Thaddeus, 1982). Figure 6.3a is a contour map of the high resolution (HPBW = $\frac{1}{8}$°) integrated ^{12}CO emission. For direct comparison with the gamma-ray and HI data, this map is smoothed to the COS B resolution ($E_\gamma > 100$ MeV), Figure 6.3b). The effect of smoothing on the ^{12}CO distribution is

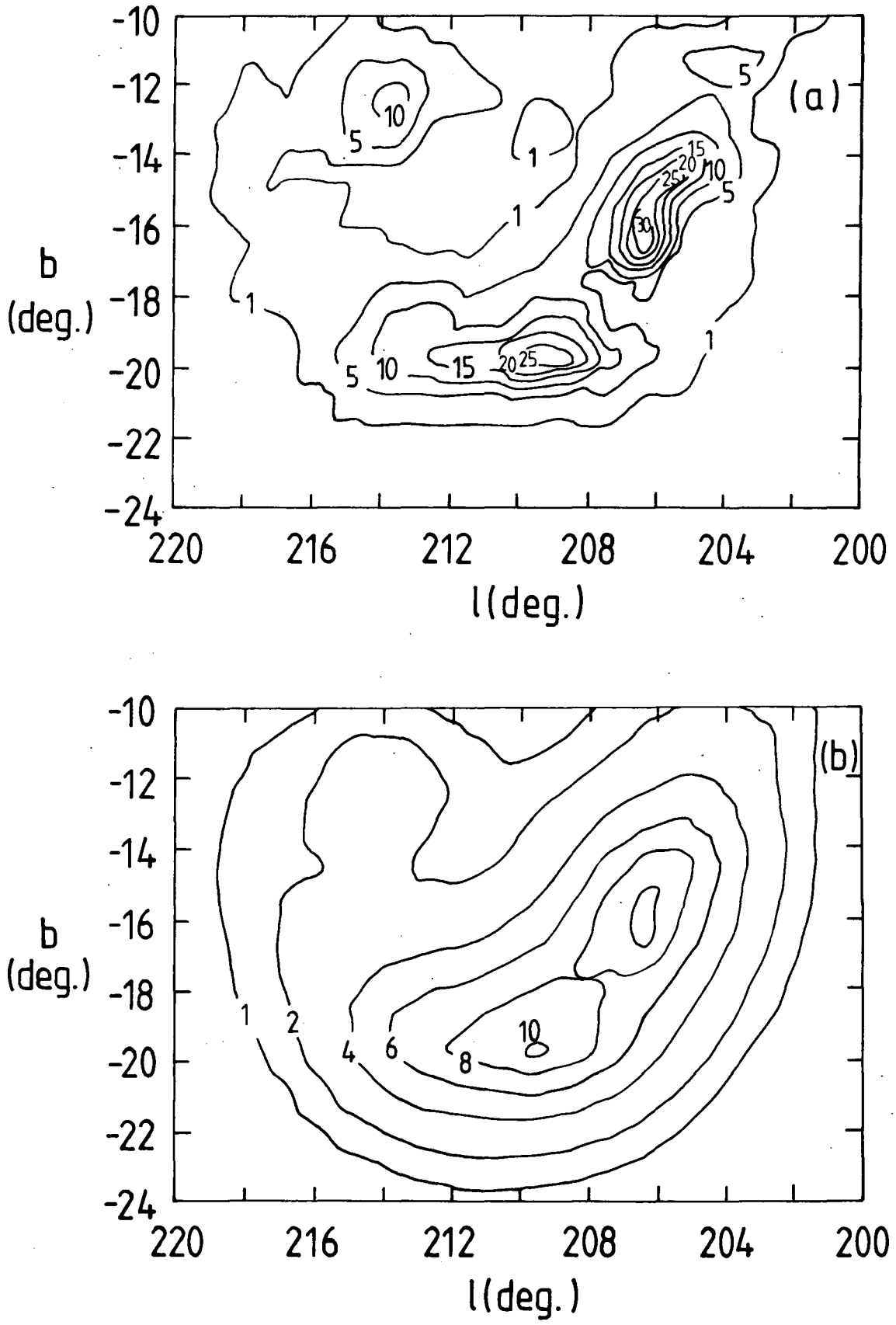

FIGURE 6.3 $\int T(^{12}CO)dv$ in units of K kms^{-1}

(a) at original resolution,

(b) smoothed to gamma-ray resolution.

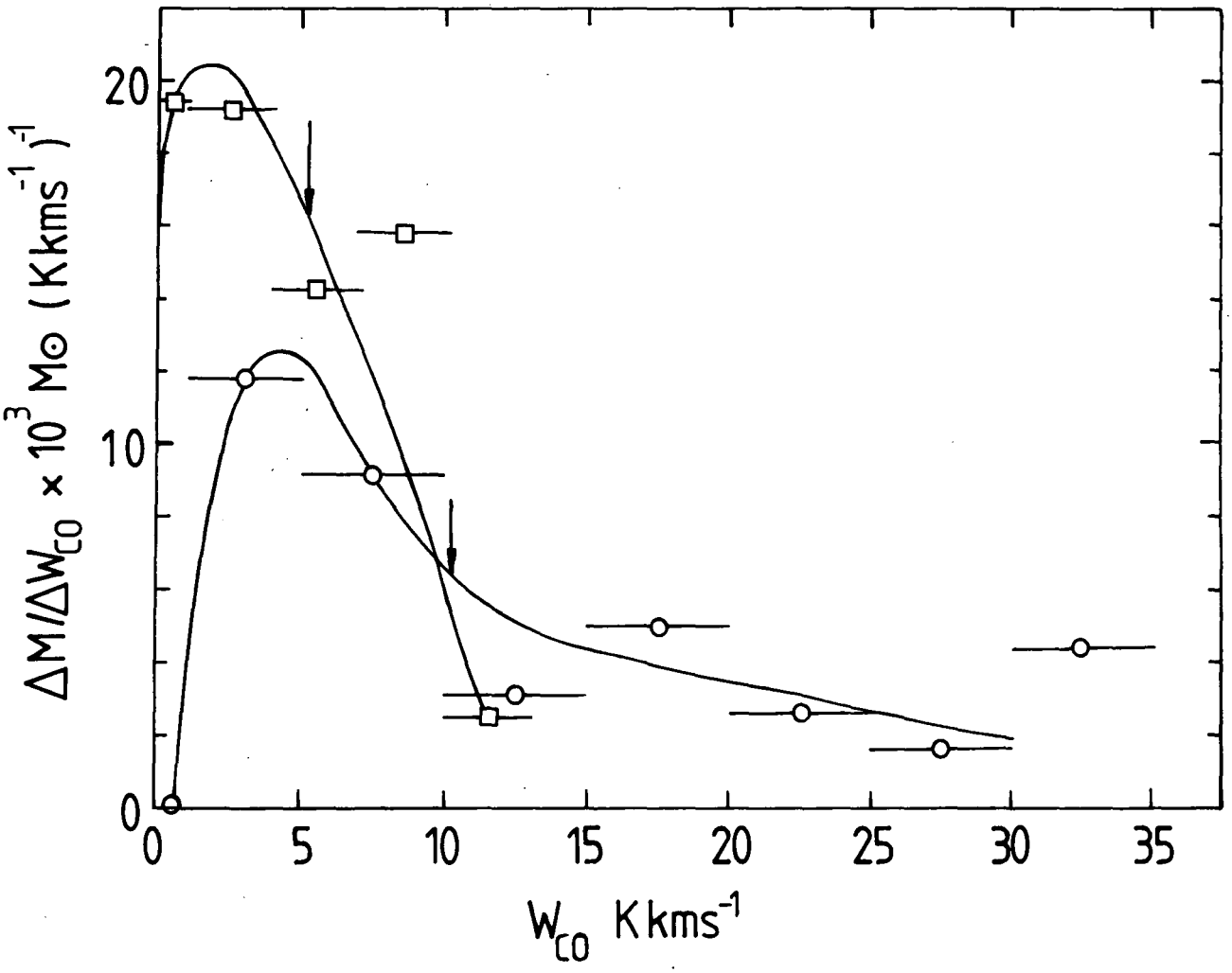

Figure 6.4 Differential mass distributions derived from the high resolution (circles) and smoothed (squares) contour maps of Figure 6.3, assuming $\alpha \doteq 4.0 \times 10^{20}$ at cm^{-2}(Kkms^{-1}). The arrows indicate the median mass contour ($W_{CO} > 1.0$ K kms^{-1}). Curves are drawn as a visual aid to illustrate the general trend.

apparent in Figure 6.4 where we plot the differential mass distributions for both the high resolution and smoothed contour maps of Figure 6.3. Smoothing concentrates a greater fraction of the observed mass below W_{CO} = 5 K kms^{-1}. Additionally, because of the restricted area covered in Figure 6.3, degrading the angular resolution necessarily smooths part of the emission out of the particular region of interest. By considering the total emission within W_{CO} = 1 K kms^{-1} in both contour maps (Figure 6.3) we estimate the reduction to be $\simeq$ 12%. This loss is considered later (Section 6.11) in relation to the determination of α from the gamma-ray and HI data.

The galaxy count data are those of the Lick survey (Shane and Wirtanen, 1967) reduced to 1^o x 1^o bins and corrected for the effect of atmospheric absorption (Strong and Lebrun, 1982). These counts give the mean number of galaxies brighter than $m_V \simeq 18.0$ covering the region dec. $> -20^o$. The conversion from mean galaxy count N_G to total gas column density N_{H_t} used in the present analysis is

$$N_{H_t}(N_G) = 2 \times 10^{21} \log_{10} (N_G^o/N_G) \text{ at cm}^{-2} \qquad 6.5$$

following Strong and Wolfendale (1981), where N_G^o = 75 is the mean galaxy count per square degree in the absence of extinction. This value is not unique, with other workers adopting N_G^o in the range 50-100 giving a systematic

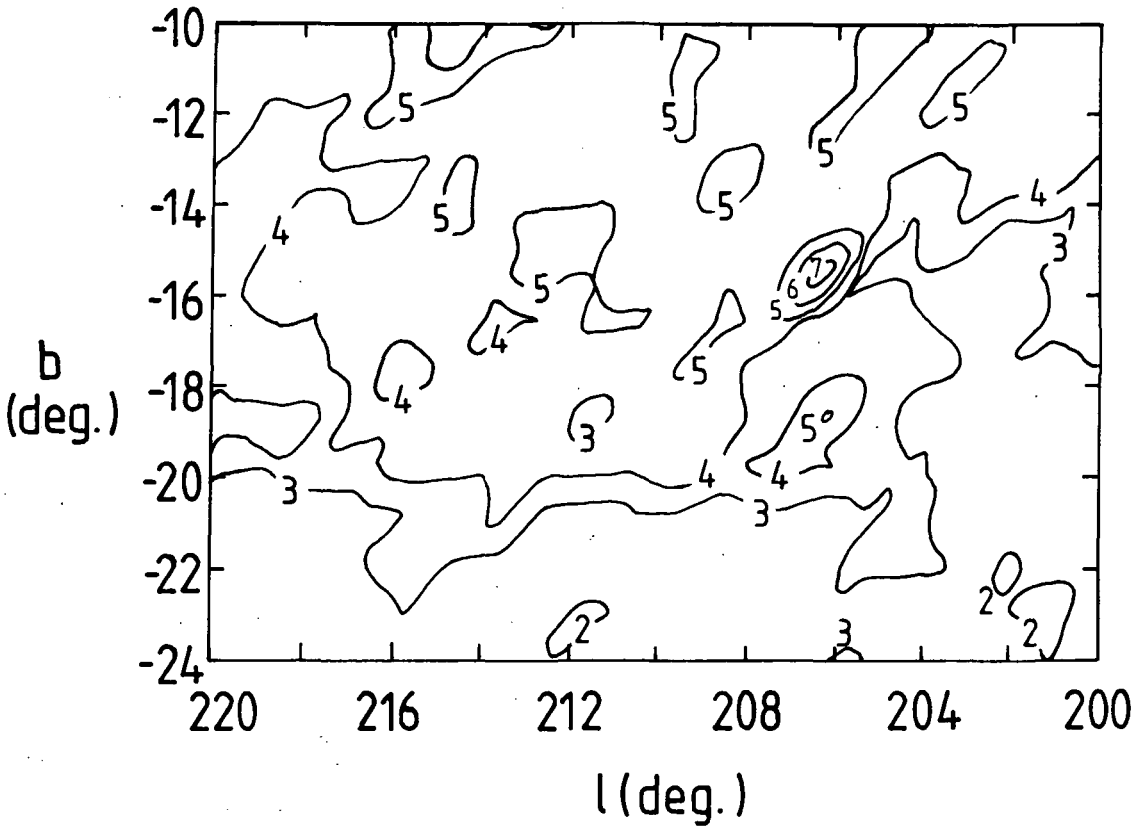

FIGURE 6.5 Total gas column density in units of 10^{21} at cm^{-2} derived from galaxy counts.

shift ($\lesssim$ 10%) in N_{H_t} relative to the present levels.

Over the Orion region many data bins have zero galaxy counts, indicating the presence of saturation where the extinction can only give a lower limit to the total gas column density. It is realized that any method of estimating the total column density in these bins will have a crucial effect on the analysis as it is those bins with $N_G = 0$ which tend to have the most intense CO emission. Figure 6.5 is a map of the total column density derived using 6.5. As described in Section 6.11 minimum values $N_G(min)$ (Table 6.3) are substituted into those bins for which $N_G = 0$.

6.8 The local gamma-ray emissivity

We seek to use 6.2, fitting the gamma-ray HI and CO data to obtain α and N. However it is first necessary to know $q/4\pi$, the local emissivity above 100 MeV, appropriate for the Orion cloud region. Many workers have used both the SAS II and COS B data to derive local emissivities in each energy range. Tables A1 and A2 are summary of these results, outlining the relevant analyses used.

Each technique involves fitting the observed gamma-ray intensities to the total gas column densities under the assumption of a uniform cosmic ray density throughout the region analysed. Gas column densities are derived either from HI and CO emission or from the galaxy count technique. Clearly both are subject to the limitations

of the calibrations $CO \rightarrow H_2$ and $N_G \rightarrow N_{H_t}$. Different calibrations are the major source of variation in the derived emissivities. The analyses are generally restricted to intermediate latitudes ($|b| \geqslant 10^o$) where many of the problems are reduced; CO emission being small away from the Galactic plane and galaxy counts are less affected by saturation, though gas-to-dust variations may still be present. In addition the data give a better representation of the local interstellar medium ($\lesssim$ 1-2 kpc) over which the variation in cosmic ray density is likely to be small.

Nevertheless, cosmic ray density variations are likely to limit the analyses and indeed several workers have approached the problem from the perspective of using the data to trace the local cosmic ray gradient (Section 3.3). Theoretical calculations of the local emissivity are themselves limited by the uncertainty in the local interstellar electron spectrum below a few GeV.

Values for $q/4\pi$ are seen to span a wide range: $(1.7 - 3.0) \times 10^{-26}$ ph $at^{-1}sr^{-1}s^{-1}$. We adopt $q/4\pi = 2.0 \times 10^{-26}$ ph $at^{-1}sr^{-1}s^{-1}$ for the analysis but are mindful that the results are likely to be sensitive to the chosen emissivity; $q/4\pi$ appearing on both sides of 6.2. The dependence of α on $q/4\pi$ is considered in the following section.

6.9 Analysis of the gamma-ray data

In deriving the best fit for α, it is important to restrict analysis to the region of the clouds as measured by W_{CO}. As a lower boundary we select only those bins (I_γ, W_{CO}, N_{HI}) for which $W_{CO} \geq 1.0$ K kms^{-1}. With these data and $q/4\pi = 2.0 \times 10^{-26}$ ph at^{-1}sr^{-1}s^{-1}, we substitute into 6.2 for each test value of N(= 0.5, 0.8, 1.0, 1.5, 2.0, 3.0) and perform a linear least squares regression.

The combined data are transformed to a linear scale in W_{CO} and binned. In Figure 6.6 we plot the excess intensity, $I_\gamma - I_b - q/4\pi\, N_{HI}$, against $q/4\pi\, W_{CO}$. The smooth curves are the least squares lines for each N when transformed to the linear scale. These curves give the expected gamma-ray intensity from gas in the Orion clouds for each value of α and N. Figure 6.7a shows the results obtained for the regression values of α_{20} ($\alpha_{20} = \alpha/10^{20}$ at cm^{-2} (K kms^{-1})$^{-1}$) for each case of N. The χ^2 parameter is used to test the goodness of fit for each N with the results given in Figure 6.7b.

The trend indicated by χ^2 suggests that N > 1.0 with a best fit N = 1.7 ($\alpha_{20} = 2.5 \pm 0.9$) at the 64% significance level. Given the uncertainties involved, N = 1.0 ($\alpha_{20} = 3.7 \pm 0.6$) must also be considered at the 17% significance level. For N = 1.0 we repeat the analysis for a range of emissivities spanning the values given in Table A1 . The least squares values of

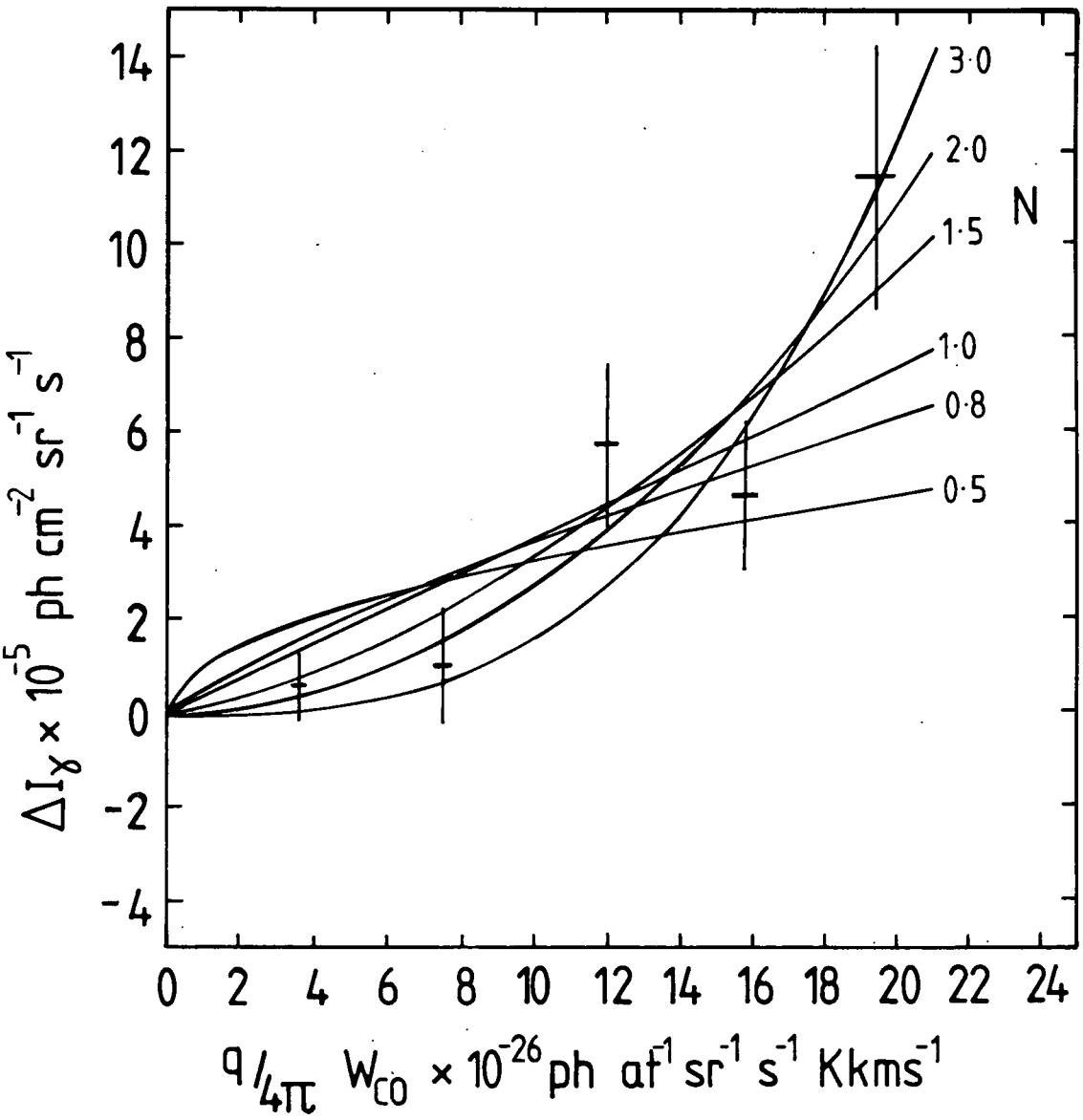

Figure 6.6 Variation of the excess intensity ΔI_γ (> 100 MeV) as a function of $q/4\pi\left[W_{CO}\right]^N$, for the Orion clouds. The binned observations are plotted with standard errors. Smooth curves give the expected gamma-ray intensity for each case of N.

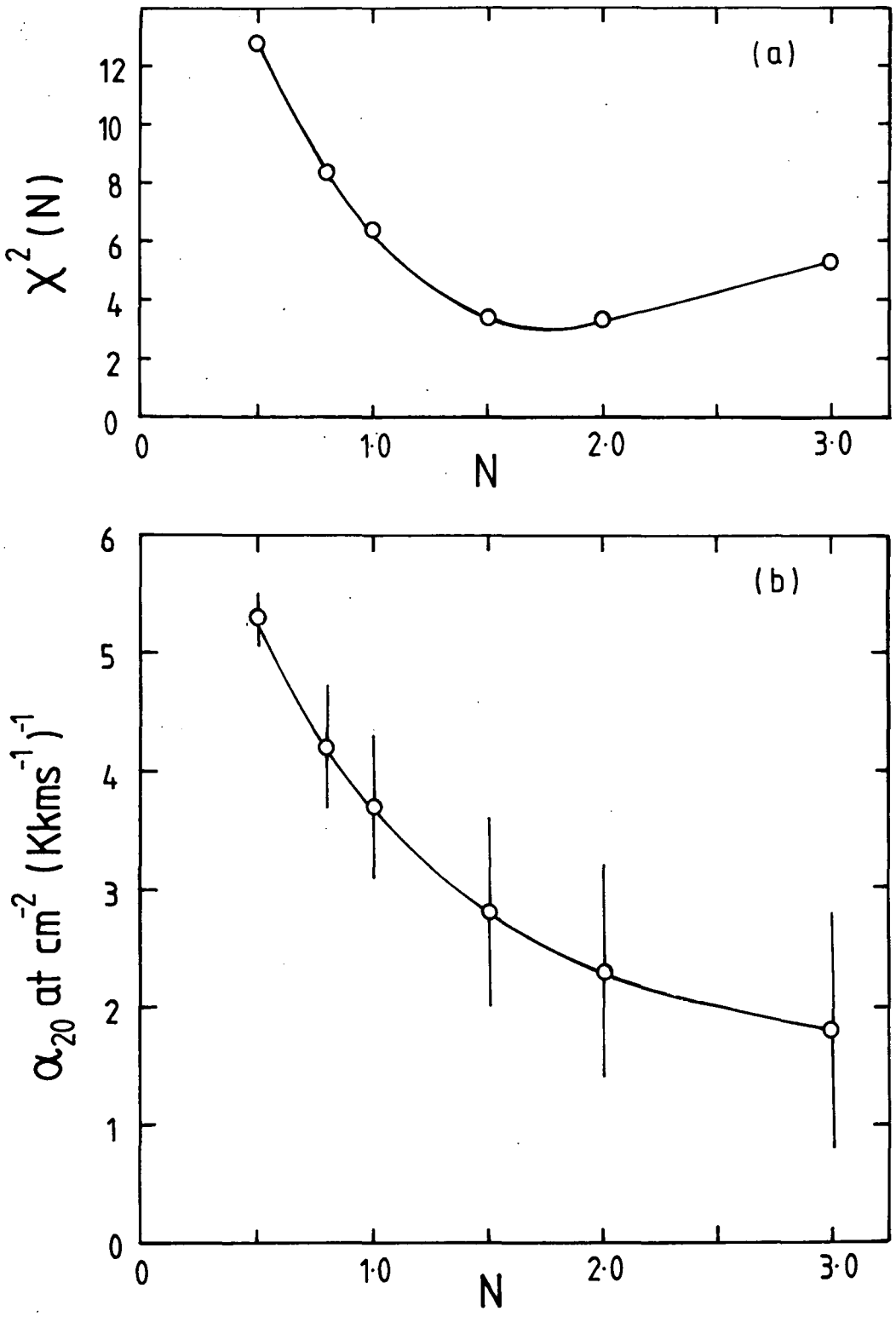

Figure 6.7 (a) Variation of χ^2 as a function of N, (b) α_{20} ($\pm 1\sigma$) as a function of N; from the data of Figure 6.6. $\alpha_{20} = 2N_{H_2}/W_{co}$ in units of 10^{20} at cm^{-2} (K kms^{-1})$^{-1}$.

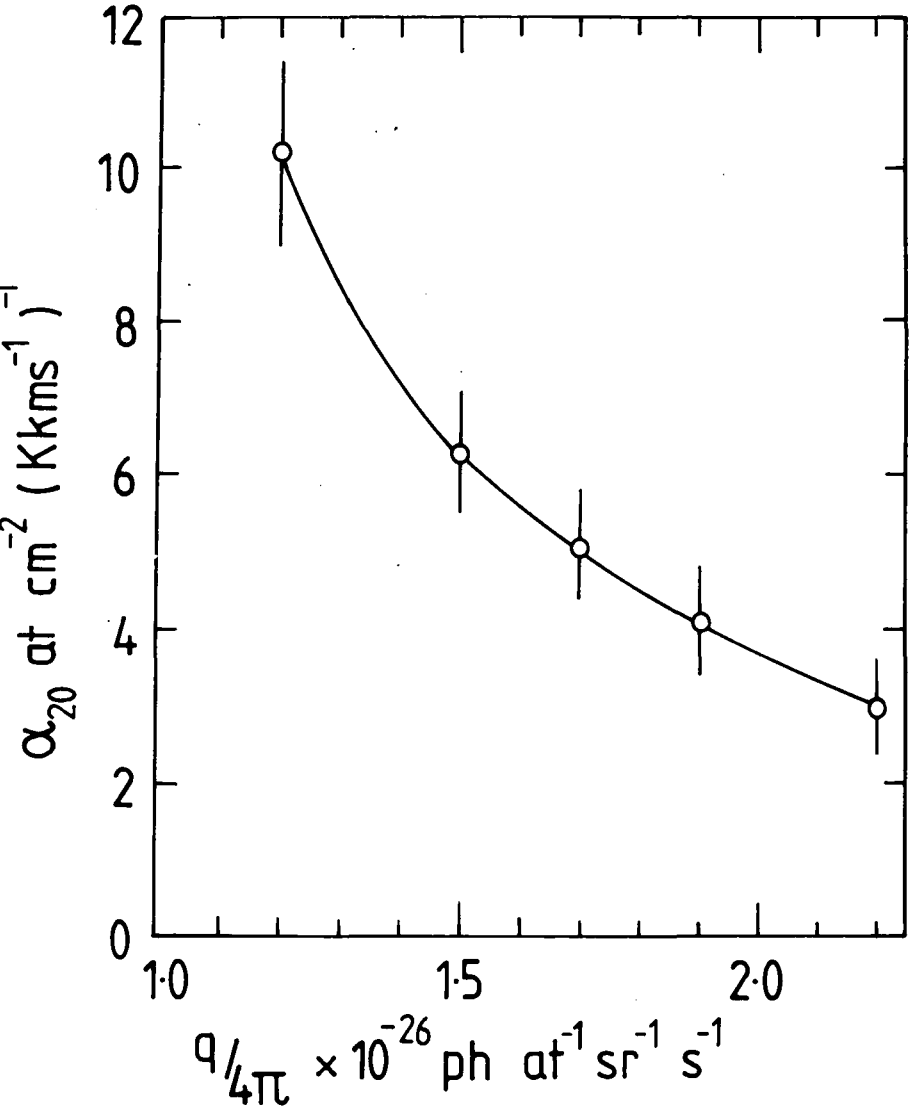

Figure 6.8 α_{20} ($\pm$ 1σ) as a function of $q/4\pi$ for the case N = 1.0.

α_{20} as a function of $q/4\pi$ are plotted in Figure 6.8. We estimate that a $\pm$ 20% uncertainty on $q/4\pi$ = 2.0 x 10^{-26}ph $at^{-1}sr^{-1}s^{-1}$, introduces factors of -35%, +50% variation in α_{20}, ignoring the statistical uncertainty in α_{20}.

Bloemen et al. (1984b) make a similar analysis of the Orion region and derive $\alpha_{20} = 5.2 \pm 2.4$, corresponding to the N = 1.0 case. This value is higher than derived above; however the discrepancy can be attributed to specific differences between the two analyses. Bloemen et al. use an emissivity, $q/4\pi = 1.7 \times 10^{-26}$ ph $at^{-1}sr^{-1}s^{-1}$ derived from a previous analysis of the COS B data (Table A.2). More recent analyses (Table A.2) suggest this is likely to be an underestimate and we note from Figure 6.8 that reducing $q/4\pi$ significantly increases α_{20}. Furthermore Bloemen et al. treat the gamma-ray background term $I_b(6.2)$ as a variable and perform the analysis over the entire Orion region indicated in Figure 6.1 (480 sq. deg.); whereas the present method is restricted to the clouds ($W_{CO} \gtrsim 1$ K kms^{-1}).

As a consistency check we perform the regression analysis over all the data bins (480 sq. deg.), taking N = 1.0, $q/4\pi = 1.7 \times 10^{-26}$ph $at^{-1}sr^{-1}s^{-1}$. We obtain $\alpha_{20} = 5.0 \pm 0.7$, in close agreement with $\alpha_{20} = 5.2$ derived by Bloemen et al. We also reduce the isotropic background to $I_b = 5.1 \times 10^{-5}$ph $cm^{-2}sr^{-1}s^{-1}$ (as obtained by Bloemen et al.) and a similar analysis gives

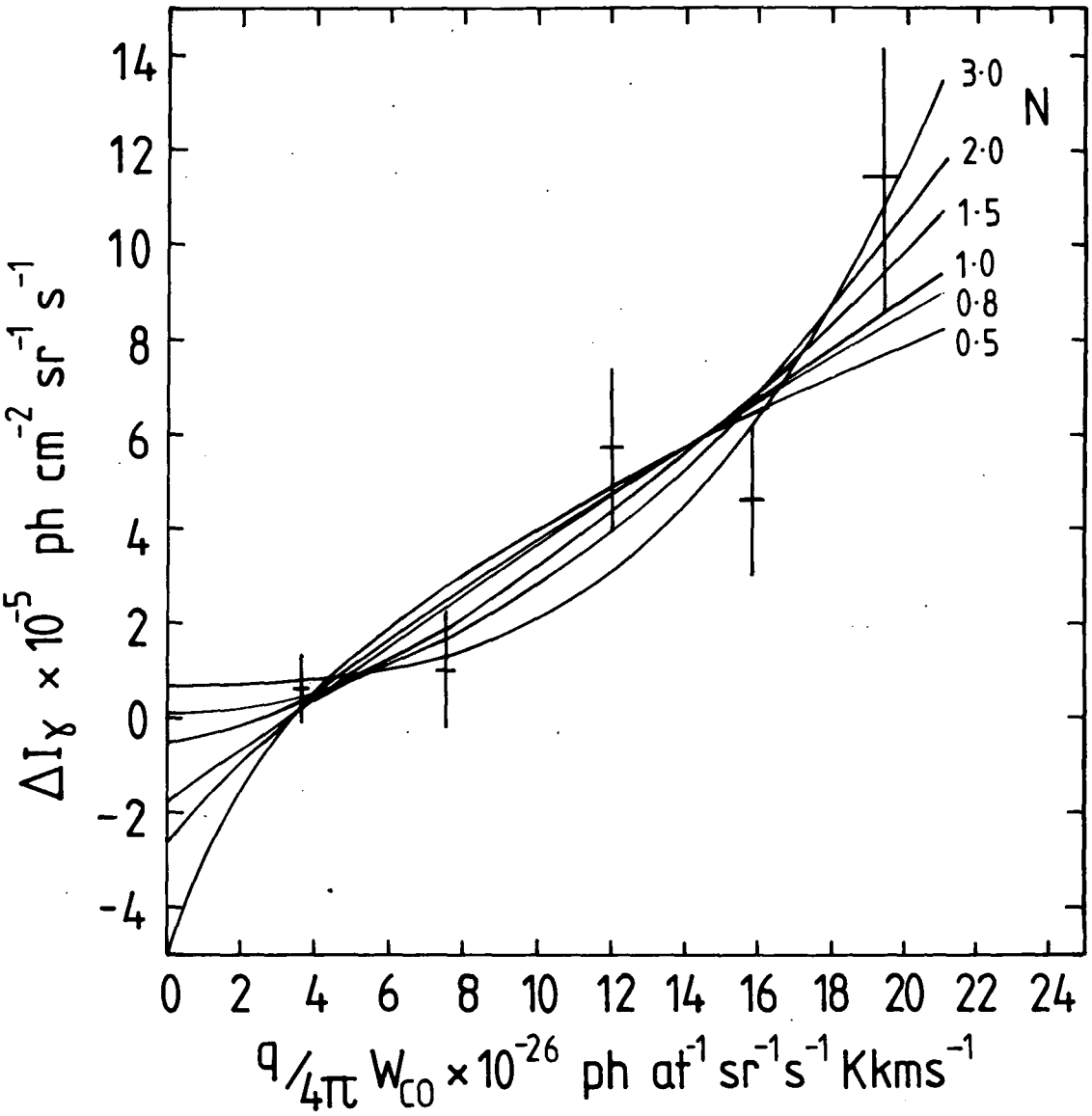

Figure 6.9. Variation of the excess intensity ΔI_γ (> 100 MeV) as a function of $q/4\pi\left[W_{co}\right]^N$, for the Orion clouds. The isotropic background intensity I_b is treated as a variable. The binned observations are plotted with standard errors. Smooth curves give the expected gamma-ray intensity for each case of N.

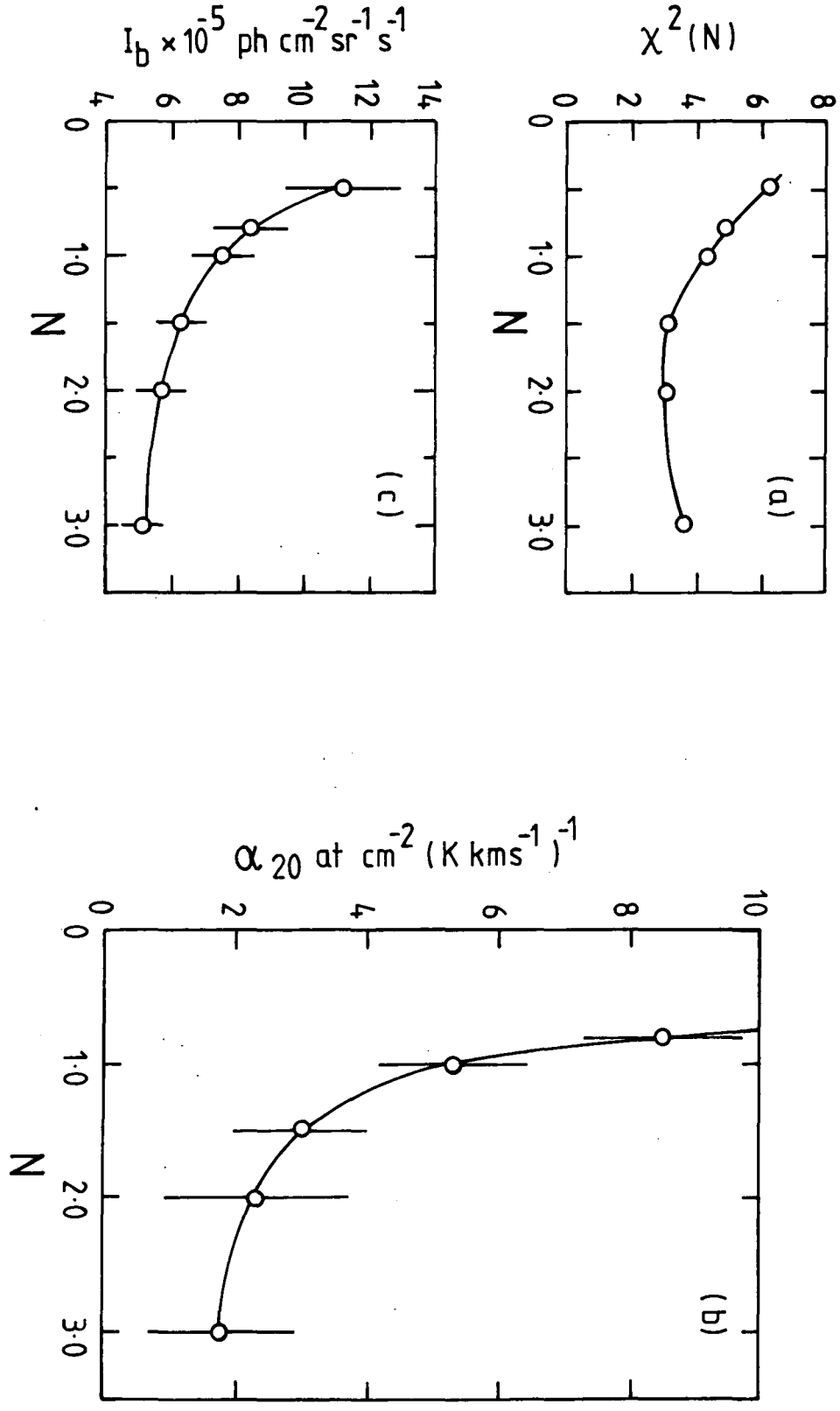

Figure 6.10. The dependence of the parameters χ^2 (a), α_{20} (b) and I_b (c) on N for the data of Figure 6.9. Errors bars are $\pm$ 1σ, $\alpha_{20} = 2N_{H_2}/W_{co}$ in units of 10^{20} at cm^{-2} (K kms^{-1})$^{-1}$.

$\alpha_{20} = 5.9 \pm 0.7$. We conclude there is no significant discrepancy between the present analysis and that of Bloemen et al. Nevertheless it is apparent that the determination of α_{20} is sensitive to the emissivity adopted in the analysis.

It is possible that the gamma-ray background used by us ($I_b = 5.8 \times 10^{-5}$ ph $cm^{-2}sr^{-1}s^{-1}$) is not absolutely determined. We now consider the effect of treating the background as an additional variable. We proceed as before performing linear regressions on the data with $q/4\pi = 2.0 \times 10^{-26}$ ph $at^{-1}sr^{-1}s^{-1}$ and N = (0.5, 0.8, 1.0, 1.5, 2.0, 3.0). The results for each N are presented on a linear W_{CO} scale in Figure 6.9 as smooth curves. χ^2 values are derived and these are plotted in Figure 6.10a along with the best fit values of α_{20}, Figure 6.10b, and the corresponding fitted backgrounds, Figure 6.10c.

The best fit is obtained for N = 2.3 ($\alpha_{20} = 2.0 \pm 1.3$, $I_b = 5.4 \times 10^{-5}$ ph $cm^{-2}sr^{-1}s^{-1}$). N = 1.0 ($\alpha_{20} = 5.3 \pm 1.1$, $I_b = 7.8 \times 10^{-5}$ ph $cm^{-2}sr^{-1}s^{-1}$) also produces a reasonable fit; though the magnitude of the background is large in comparison to the COS B determined level, $I_b = 5.8 \times 10^{-5}$ ph $cm^{-2}sr^{-1}s^{-1}$. However, it is unlikely that the background could be underestimated by $\simeq$ 25% in the COS B analysis.

Thus we consider a further case where the background is reduced to $I_b = 5.1 \times 10^{-5}$ ph $cm^{-2}sr^{-1}s^{-1}$ in accordance

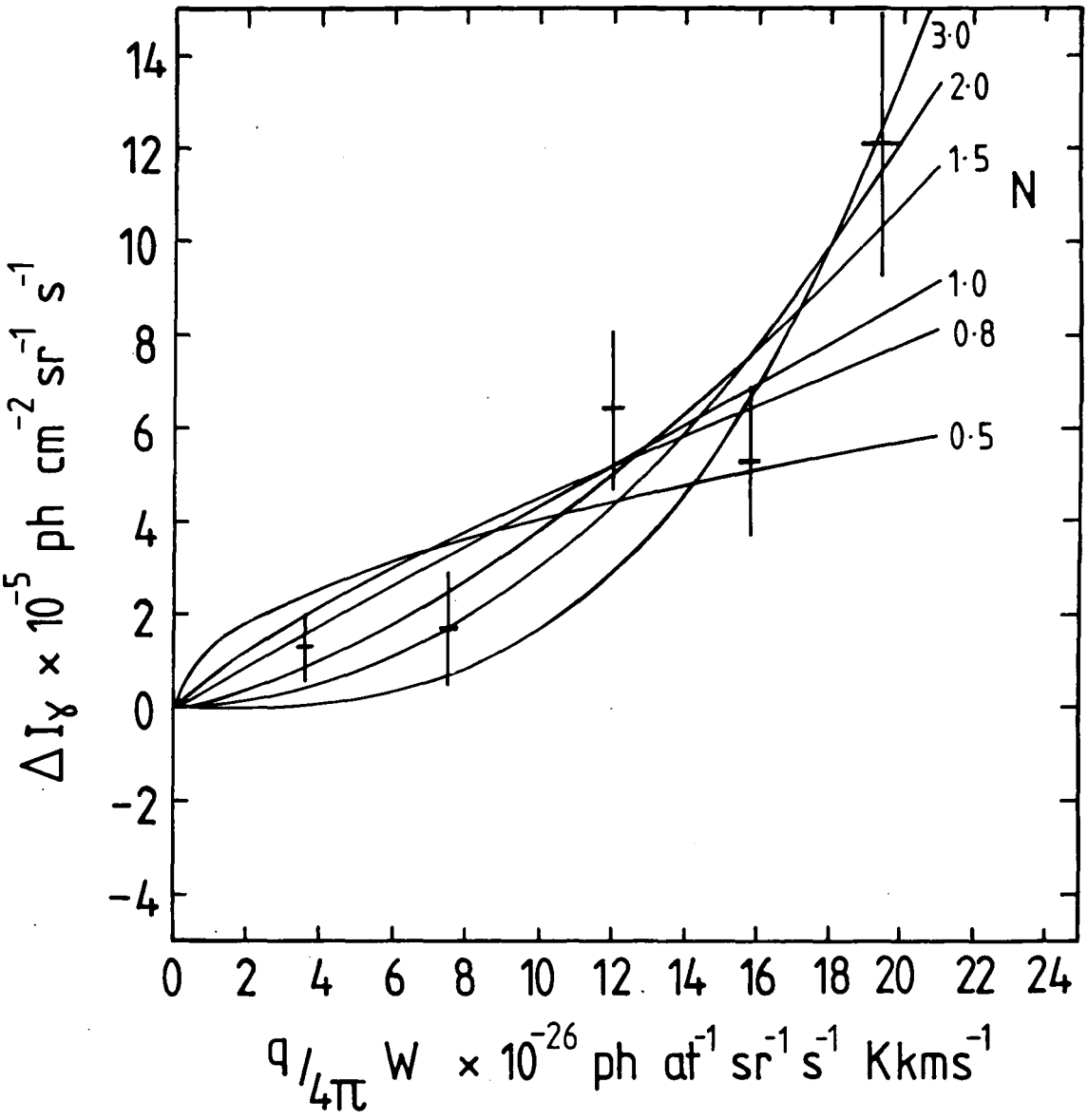

Figure 6.11 Variation of the excess intensity ΔI_γ (>100 MeV) as a function of $q/4\pi\left[W_{co}\right]^N$, for the Orion clouds. A reduced fixed isotropic background intensity is assumed. The binned observations are plotted with standard errors. Smooth curves give the expected gamma-ray intensity for each case of N.

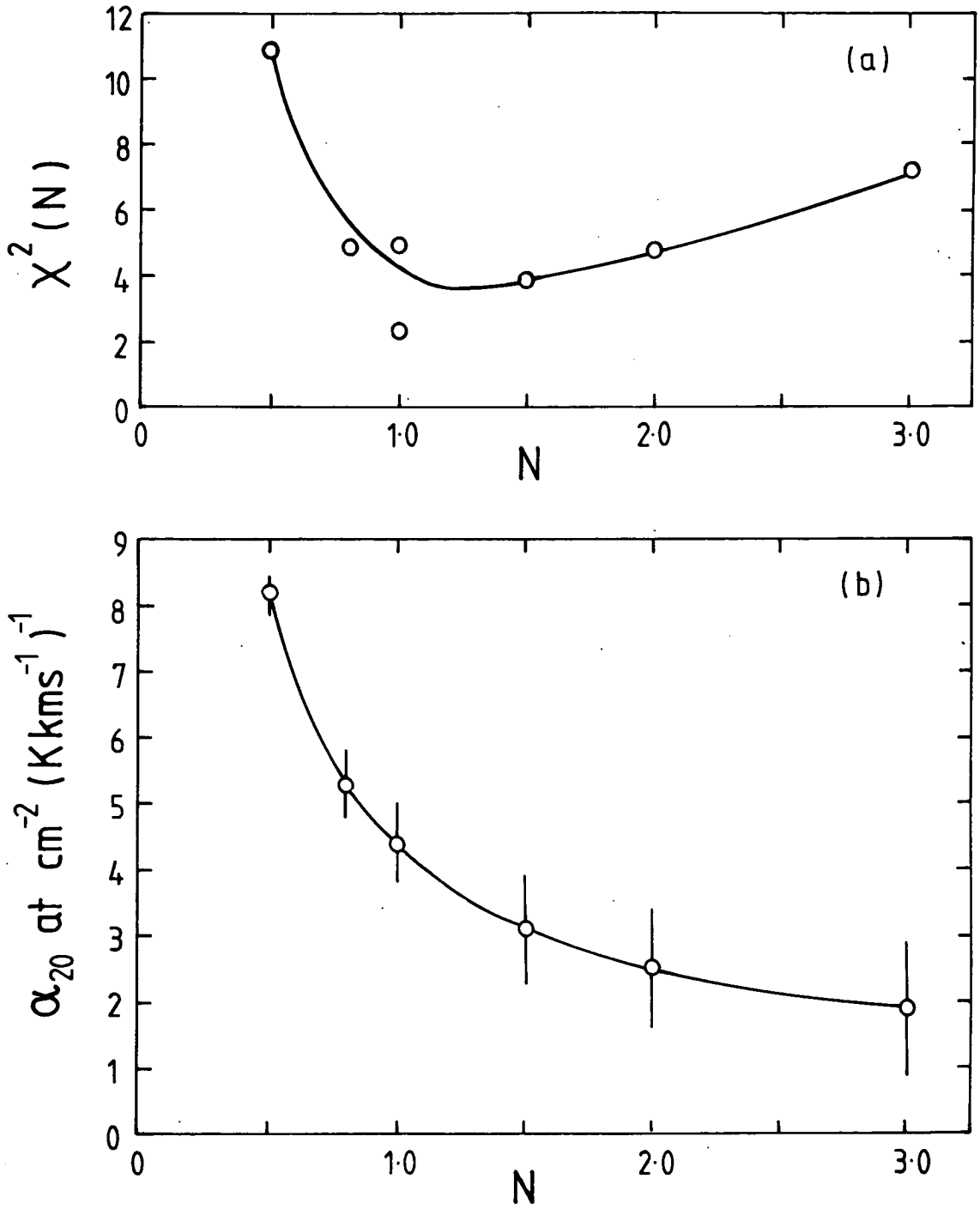

Figure 6.12. The dependence of χ^2 (a) and α_{20} (b) on N for the data of Figure 6.11. Error bars are $\pm 1\sigma$, $\alpha_{20} = 2N_{H_2}/W_{co}$ in units of 10^{20} at cm^{-2} (K kms^{-1})$^{-1}$.

with the fitted value of Bloemen et al. (1984b) and the analysis repreated for $q/4\pi = 2.0 \times 10^{-26}$ ph $at^{-1}sr^{-1}s^{-1}$, N = (0.5, 0.8, 1.0, 1.5, 2.0, 3.0). The regression plots are given in Figure 6.11 χ^2 and α_{20} are plotted in Figure 6.12. For N = 1.0 $\alpha_{20} = 4.4 \pm 0.6$ and the best fit gives N = 1.2, $\alpha_{20} = 3.7 \pm 0.7$.

6.10 Interpretation of the results

The results of the three separate regression sets are summarized in Table 6.1. Taken together they indicate the best case to be $N > 1.0$. Certainly it seems unlikely that $N \ll 1.0$ is consistent with the data. Under the initial assumption of cosmic ray intensity inside the cloud scaling with W_{CO}, $N < 1.0$ is interpreted as increasing cosmic ray exclusion from the denser regions of the cloud. Uniform cosmic ray irradiation of the cloud corresponds to N = 1.0 and $N > 1.0$ indicates cosmic ray production (or enhancement) within the cloud; the enhancement rising towards the denser regions. We conclude that although N = 1.0 ($\alpha_{20} = 3.7 \pm 0.6$) is consistent with the data there is modest evidence favouring $1.0 < N < 2.0$, α_{20} being correspondingly reduced.

Table A3 is a summary of α_{20} values derived by several workers from different methods. Most methods are based on comparison of optical extinction measurements to molecular line observations towards different clouds, though comparisons with gamma-ray data are also now being made. The present value ($\alpha_{20} = 3.7 \pm 0.6$) is generally lower than conventional estimates based on

Gamma-ray analysis	N	Best fit α_{20}	Fit for N=1.0 α_{20}
I_b=5.8x10^{-5} ph cm^{-2}sr^{-1}s^{-1} fixed background	1.7	2.5±0.9 (64%)	3.7±0.6 (17%)
floating background	1.8	2.5±1.2 (57%)	5.3±1.1 (38%)
I_b=5x10^{-5} ph cm^{-2}sr^{-1}s^{-1}	1.2	3.7±0.7 (46%)	4.4±0.6 (35%)
Galaxy count analysis	0.7	2.2±0.1 (15%) (4.0)	1.5±0.1 (1%) (2.7)

Table 6.1 Summary of the results from the gamma-ray analysis (Section 6.10) and the galaxy count analysis (Section 6.12). The best fit (minimum χ^2) values for N and α_{20} ($\pm$ 1σ) are given and also α_{20}($\pm$ 1σ) for the case N = 1.0. $\alpha_{20} = \alpha / 10^{20}$ at cm^{-2} (K kms^{-1})$^{-1}$. Significance levels for each fit are also given. Two values for α_{20} are given for the galaxy count analysis. The bracketed values are corrected for the abnormal reddening in the Orion nebula as described in Section 6.11.

extinction measurements. However, these analyses rely on indirect arguments concerning local thermodynamic equilibrium and virial theorem estimates applied to the clouds. The present analysis concerns a single giant molecular cloud, measuring the mass directly from the gamma-rays produced therein. Taking account of possible cosmic ray density variations limits this technique. Nevertheless in gamma-ray astronomy it is the giant molecular clouds which are believed to be important cosmic ray targets in the Galaxy. Thus the present analysis is considered more appropriate in relation to typical giant molecular clouds.

We recall from Section 6.8 that allowing for the low angular resolution of the gamma-ray data results in the loss of about 12% of the CO emission. This is not a uniform reduction on all the data bins but is more dominant towards the edge of the clouds, that is at low W_{CO} and negligible at high W_{CO}. It is therefore not appropriate to simply increase α_{20} by 12%. We estimate the net reduction in α_{20} to be much less than this and certainly less than the statistical error on α_{20}.

For the present data we directly estimate the H_2 mass in Orion for the case of uniform cosmic ray irradiation ($N = 1.0$, $\alpha_{20} = 3.7$). For the best fit ($N > 1$) the situation is more complicated. We can interpret α_{20} as directly measuring N_{H_2} and these reduced mass

	$N = 1.0$ $\alpha_{20} = 3.7$	$N = 1.7$ $\alpha_{20} = 2.5$	HI	HII
Orion A (51 sq.deg.)	0.74	0.50	0.08	0.12
Orion B (52 sq.deg.)	0.60	0.41	0.05	0.07

Table 6.2 Constituent masses of the gas components in the Orion clouds. The units are $10^5 M_\odot$. The H_2 mass estimates are derived from the high resolution (1^o x 1^o binning) data of Figure 6.3b. Allowing for metallicity effects may reduce the H_2 masses by a factor 1.3 - 1.6, Section 6.10. As explained in Section 6.10, the true H_2 mass estimate may lie between the limits given here.

estimates are also given in Table 6.2. In this case the additional gamma-rays must be produced by the increasing enhancement of the cosmic ray flux towards the denser regions of the cloud (i.e. high W_{CO}). Alternatively the cosmic ray flux may be constant throughout the cloud. The cloud masses are then identical to the N = 1.0 case and N > 1.0 then implies that W_{CO} increasingly underestimates N_{H_2} at large W_{CO}. Intermediate cases of cosmic ray enhancement and W_{CO}/H_2 variation within the clouds will have corresponding H_2 masses between the two limits given in Table 6.2. We also give the estimates of HI and HII mass derived by Houston and Wolfendale (1984b) for the Orion complex.

We can also make allowance for the effect of the metallicity correction on α_{20} (Section 5.4) writing $\alpha_{20} \rightarrow \alpha_{20}/[M]$ where $[M]$ is the metal abundance relative to the solar value. For the Orion nebula $[M] \simeq -0.1$ to -0.2 dex (Section 6.8). If these abundances are typical of the entire cloud then the local estimate of α_{20} is reduced by $\simeq 1.3 - 1.6$.

6.11 Analysis of the galaxy count data

We turn now to the second technique described in Section 6.7. The limitation with this method lies in the galaxy count saturation effect ($N_G = 0$) over the more intense W_{CO} regions of Orion. In an attempt to overcome this problem we use the results of the previous section to estimate the column density N_{H_2} in those

bins for which $N_G = 0$. As a first approximation, we assume that $N = 1.0$, $\alpha_{20} = 3.7$ correctly predicts the H_2 distribution within Orion. Using the CO data at its original resolution (Figure 6.3a) and the N_{HI} data smoothed to the same resolution, we derive the total gas column density $N_{H_t} = \alpha_{20} W_{CO} + N_{HI}$. For those bins with $N_G = 0$ we can then invert 6.5 to derive the equivalent $N_G(\text{min})$.

We restrict the analysis to those bins with $W_{CO} \geqslant 1$ K kms^{-1} and $N_G = 0$. Mean values for $N_G(\text{min})$ are derived for several ranges of W_{CO}. These are given in Table 6.3. It is interesting to note that only two of the bins with $W_{CO} \geqslant 20$ K kms^{-1} also have $N_G = 0$. This is surprising in that we might expect greater extinction in the regions of high W_{CO}. However, these results are consistent with the bulk of the CO emission in these bins being restricted to small regions or knots within the main cloud. Therefore while the extinction towards the CO cores is very high ($N_G = 0$) it is much lower in the surrounding regions ($N_G > 0$) giving a mean non-zero galaxy count. The relative numbers of zero to non-zero galaxy count bins is low for $W_{CO} \geqslant 20$ K kms^{-1} suggesting that the most intense regions of CO emission tend to be more tightly clumped.

We proceed by taking one value of $N_G(\text{min})$ and applying it to estimate N_{H_t} from 6.5 for each bin in the cloud ($W_{CO} \geqslant 1.0$ K kms^{-1}) with $N_G = 0$. We substitute the galaxy

W_{CO} K kms^{-1}	Total no. of bins	No. of bins with $N_G = 0$	N_G(min)
1.0 - 10.0	137	47	1.48
10.0 - 20.0	13	8	0.023
20.0 - 36.0	7	2	0.008

Table 6.3 The distribution of bins in the Orion region as a function of W_{CO} (original resolution). The values of N_G(min) are derived for those bins with zero galaxy counts ($N_G = 0$) as described in Section 6.10.

count, HI and CO data into 6.4 and, for each test value of N(= 0.3, 0.5, 0.8, 1.0, 1.5, 2.0), we perform a linear regression analysis to obtain α_{20}. For each fit we calculate a reduced χ^2 and the procedure is repeated for each of the three values of N_G(min). In all cases the fits are poor, χ^2 increasing with N. For N = 0.3 the best fit is significant at the 3% level. For N < 0.3, the W_{CO} data are increasingly compressed and the scatter converges to thin vertical strips. Determining a best fit for N is thus less than meaningful, nevertheless χ^2 does not show any rising trend down to at least N = 0.1.

Given the wide range in N_G(min) derived in Table 6.3 it is perhaps not surprising that a single value fails to produce a best fit to the data as described by 6.4. Therefore we estimate N_{H_t} using the value of N_G(min) appropriate for the intensity of CO emission in that bin. The data are again substituted into 6.4 and a linear regression performed for each value of N. The data are binned and transformed onto a linear W_{CO} scale. The results of these regressions are plotted as curves in Figure 6.13. χ^2 is plotted in Figure 6.14a and corresponding values of α_{20} in Figure 6.14b. From Figure 6.14a we find the best fit to be N = 0.7 ($\alpha_{20} = 2.2 \pm 0.1$).

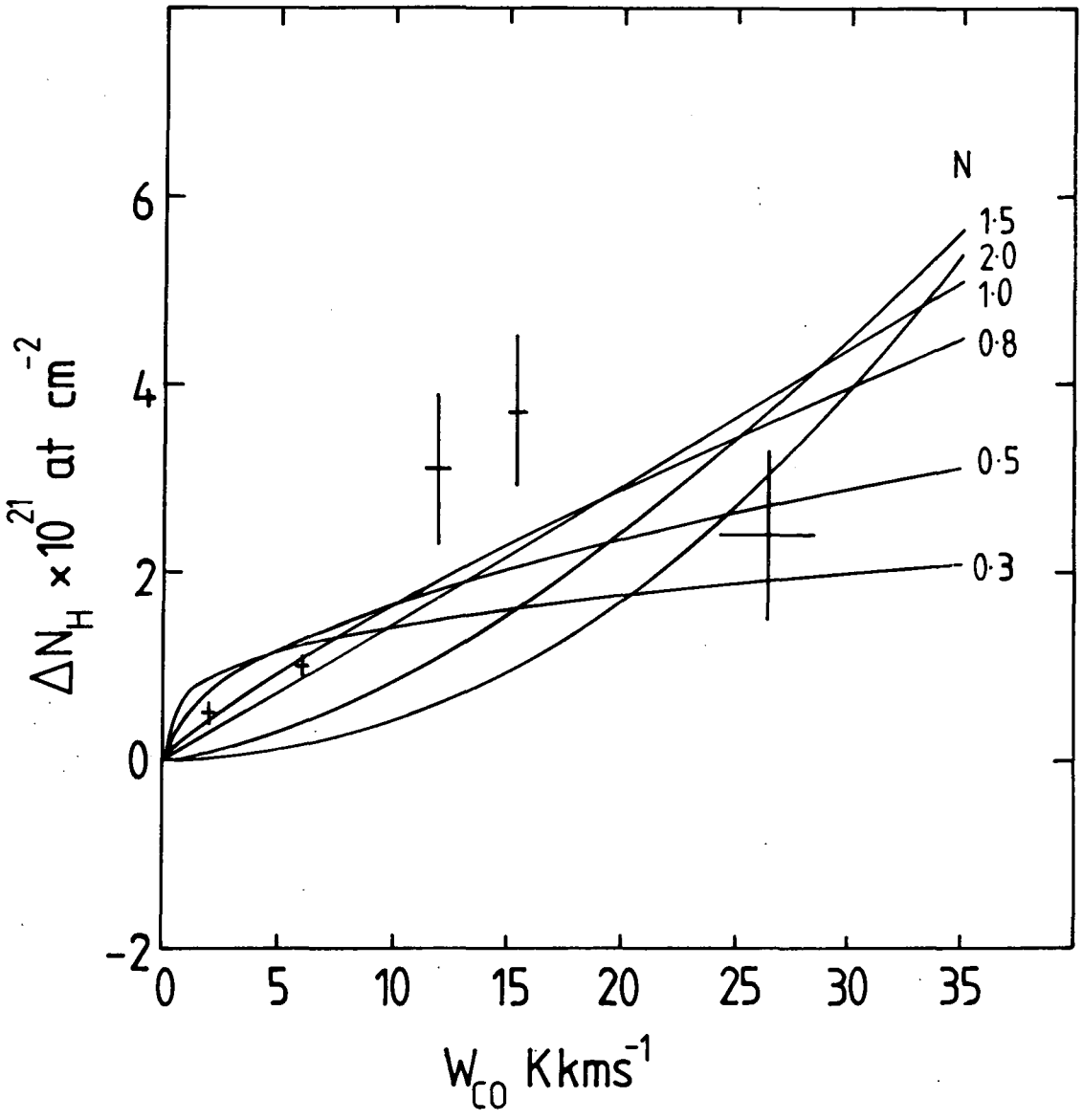

Figure 6.13. Variation of the excess gas column density $\Delta N_H = N_{H_t}(N_G) - N_{HI}$ as a function of W_{co} for the Orion clouds. The binned observations are plotted with standard errors. Smooth curves give the expected excess column density for each case of N.

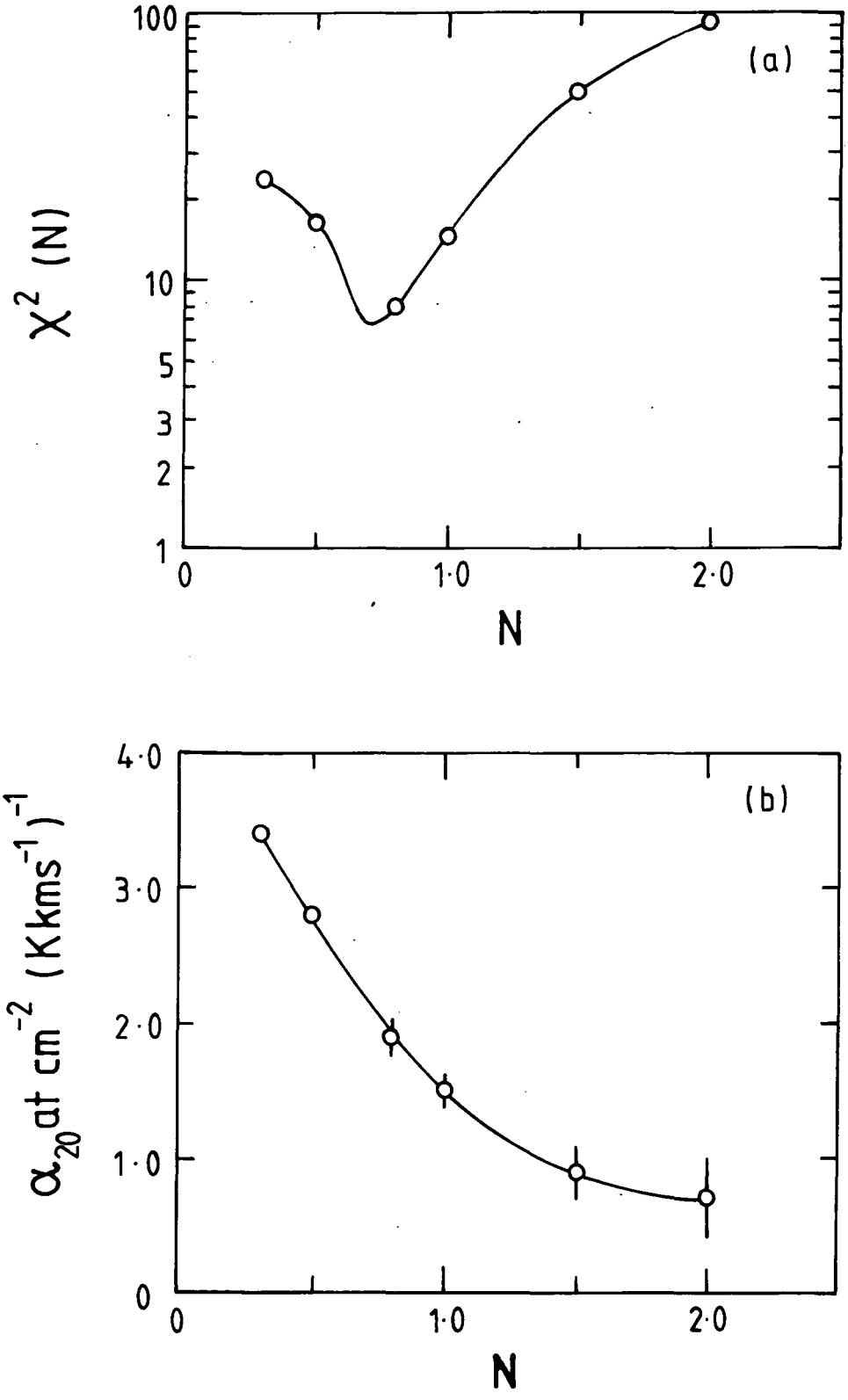

Figure 6.14. Dependence of the parameters χ^2 (a) and α_{20} (b) on N for the data of Figure 6.13. Error bars are $\pm$ 1σ (if larger than symbols), $\alpha_{20} = 2N_{H_2}/W_{co}$ in units of 10^{20} at cm^{-2} $(K\ kms^{-1})^{-1}$.

This result is necessarily heavily dependent on the initial assumptions used to estimate N_{H_t} whenever $N_G \doteq 0$. Although N = 1.0 cannot be excluded it does seem unlikely that N is greater than 1.0. In the galaxy count analysis (Figure 6.13), we are essentially comparing the excess extinction ΔE, not associated with HI; with the total gas (H_2) in Orion as estimated from W_{CO}. The slope of the regression line $\partial \Delta E / \partial W_{CO}$ is therefore the dust to gas ratio, the extinction being due to the dust. For a best fit case of $N < 1.0$, $\partial \Delta E / \partial W_{CO}$ decreases with W_{CO}, that is, the gas to dust ratio increases with W_{CO}. This is consistent with the observations of abnormally large reddening in the Orion nebula region (Section 6.5) and suggests the abnormal reddening may be more widespread within the cloud complex and may vary with position.

We recall from Section 6.5 that the large reddening is interpreted as arising from larger than average dust grains. Thus the low value of α_{20} obtained from the galaxy count analysis can be understood in relation to the reduced colour excess (E(B-V)) towards this region. Therefore to estimate the total gas column density from α_{20} (galaxy counts), we must first correct this value to the mean reddening appropriate for the general interstellar medium. The situation is complicated by the uncertainties of the size spectrum of dust grains throughout Orion and the likelihood that the gas to dust ratio

may vary within this complex. Nevertheless we assume $A_V/E(B-V) \simeq 5.5$. We also assume that α_{20}, determined from extinction measurements (galaxy counts), scales inversly with the reddening. The scaling factor for Orion is then $^{5.5}/3.1 \simeq 1.8$. The best fit α_{20} is increased from 2.2 to ~ 4.0, similarly the fit for N = 1.0 is increased from 1.5 to ~ 2.7.

It is apparent that these corrected values are in better agreement with those obtained from the gamma-ray analysis (Table 6.1). The closeness may in part be fortuitous, but the results are at least consistent with our limited knowledge of the dust particles in the Orion complex.

CHAPTER SEVEN

THE GAMMA-RAY FLUX FROM EXTERNAL GALAXIES

7.1 Introduction

The nature of the isotropic gamma-ray background was discussed in relation to previous analyses of the data in Chapter 3. In this chapter we consider the possibility that unresolved extragalactic sources, specifically radio galaxies and galaxy clusters, might contribute to the extragalactic gamma-ray background. In the present work we endeavour to use radio and X-ray observations to help constrain the possible gamma-ray flux from extragalactic objects. In the context of a simple model we compare the expected gamma-ray fluxes with those derived from an analysis of the SAS II data and estimate the total flux contribution from these extragalactic sources.

The primary difficulty in searching for extragalactic sources relates to the problem of estimating the background signal, which in this case results from cosmic ray interactions throughout the Galaxy. Clearly, the best region to search for extragalactic emission is at high Galactic latitudes where the net flux is significantly reduced. At high latitudes there is only information on the distribution of atomic hydrogen but it is widely believed that there is relatively little molecular hydrogen at these latitudes, a belief confirmed by the CO survey results for the Galactic

plane which indicate that the scale height of CO (and therefore H_2) varies between 60 pc and 80 pc (Cohen et al. 1980; Sanders et al. 1984a). Recent high latitude observations of ^{12}CO (Dewey et al. 1983) cover six small regions with high HI column densities and low galaxy count (i.e. high extinction); and these regions would be expected to have significant column densities of H_2 ($\simeq$ 6 x 10^{20} at cm^{-2}). However, the results place upper limits on the column density $N_{CO} \lesssim 10^{15}$ mol. cm^{-2} implying $N_{H_2} \lesssim 2 \times 10^{20}$ at cm^{-2}. Without an all-sky CO survey, estimates of the total gas in the Galaxy based only on HI emission are necessarily incomplete and another approach is needed.

The standard procedure adopted to overcome the limitation of lack of CO data relies on the use of galaxy counts to estimate the total gas column density along the line of sight. The expected diffuse Galactic gamma-ray flux can therefore be estimated as the product of the gas column density and the mean cosmic ray emissivity; a method similar in approach to that adopted in Chapter 5 to model the expected gamma-ray flux from the Galactic plane. We implicitly assume that discrete Galactic sources make a negligible contribution to the high latitude emission. The use of galaxy counts and their limitations as a tracer of total gas are discussed in detail in Chapter 6.

7.2 Extragalactic background radiation

The question of the relative contribution from each class of extragalactic object to an extragalactic gamma-

ray background is at present not well understood. Indeed the absolute level of this background is still a matter of uncertainty. We can consider the situation at other wavelengths.

In the radio and optical bands the sky brightness is the summed contribution from individual sources, that is, discrete in origin. The microwave background is conventionally interpreted as truly diffuse emission, a relic from the era of recombination, within the framework of a hot big bang cosmology. Ultraviolet measurements have yet to place firm limits on the extragalactic background at these wavelengths; while the recent IRAS satellite observations confirms the existence of an infra-red background along with many extragalactic sources.

The situation at keV X-ray energies is still a matter of controversy. Satellite measurements have established the X-ray background to be $\simeq$ 2.4×10^{-8} erg $cm^{-2}sr^{-1}s^{-1}$ (2-6 keV) with resolved fluxes from normal galaxies, radio galaxies, Seyferts, quasars and galaxy clusters. Table 7.1 is a summary of the relative contributions from extragalactic objects to the diffuse X-ray background at these energies. Not all the diffuse flux can currently be attributed to discrete sources. Murray (1981) suggests that an unresolved high redshift population of strongly evolving quasars may be present. Alternatively, Silk (1973) points out that a truly diffuse component of the X-ray background

TABLE 7.1

Type	$L_x(ergs^{-1})$	(Mpc^{-3})	$df(erg\ cm^{-2}sr^{-1}s^{-1})$
Normal galaxies	2×10^{39}	0.03	0.24×10^{-8}
Radio galaxies	6×10^{41}	3×10^{-5}	0.07×10^{-8}
Seyferts	10^{42}	3×10^{-4}	1.2×10^{-8}
QSO's	3×10^{45}	10^{-8}	0.08×10^{-8}
Clusters	2×10^{44}	10^{-6}	0.8×10^{-8}

Uhuru results on diffuse X-ray background 2-6 keV from review by Kellog (1973).

could originate from thermal bremmstrahlung in a hot inter-cluster gas. Further measurements are required with increased sensitivity and resolution to search for additional sources and small scale anisotropies in the background before this important question can be resolved.

In the gamma-ray region the interpretation of the observations is hampered by low statistics and the poor angular resolution of present detectors. Nevertheless we endeavour to place limits on the flux from likely extragalactic gamma-ray sources and any analysis of the data must necessarily rely on gross statistical properties of individual classes of sources, rather than a complete sample of observed discrete sources.

7.3 Gamma-ray luminosity

We begin by considering normal galaxies and assume our Galaxy to be typical with $L_\gamma(>100\ \text{MeV}) \simeq 1.3 \times 10^{42}$ ph s^{-1} (Strong and Worrall, 1976). Adopting a mean space density for normal galaxies of $\rho = 10^{-2}$ Mpc^{-3} ($H_o = 50$ kms^{-1} Mpc^{-1}, $q_o = \frac{1}{2}$; henceforth used throughout this chapter) and neglecting evolutionary effects, the universal flux F_u is given by

$$F_u = \int_o^{R_H} \frac{L_\gamma}{4\pi r^2} \rho(r)\, dV \qquad 7.1$$

$$F_u = L_\gamma \rho R_H \qquad 7.2$$

where R_H is the Hubble radius. Substitution yields F_u (>100 MeV) $\simeq$ 0.9 x 10^{-6} ph $cm^{-2}s^{-1}$ which is negligible when compared with the observed extragalactic flux F_γ (> 100 MeV) $\simeq (1.4 \pm 0.3) \times 10^{-4}$ ph $cm^{-2}s^{-1}$ from the SAS II experiment (Section 7.11). Of course this is dependent on the use of our Galaxy as a typical normal galaxy. We recall from Section 3.8 that the upper limits to the gamma-ray flux from M31 and the LMC are consistent with the luminosity of our Galaxy if we assume that gamma-luminosity scales as the mass of the parent galaxy. Clearly, if discrete sources are to make a significant contribution to the extragalactic gamma-ray background we must consider (in analogy with the X-ray background) active galaxies, clusters of galaxies and quasars.

Above 100 MeV the dominant production mechanism of the diffuse Galactic gamma-ray emission is proton induced π° decay, with electron processes contributing about 20-30%. A useful estimate of the gamma-ray luminosity, L_γ, from p-p collisions can be derived from the gross properties of the Galactic matter and cosmic ray distribution. L_γ can be expressed as

$$L_\gamma \simeq \tfrac{1}{3} \sigma_{pp} \, n \, c \, \varepsilon_{cr} \, V \qquad 7.3$$

where σ_{pp} is the inelastic cross-section for p-p collisions, n is the mean density of target nucleii, c the velocity of light, ε_{cr} the cosmic ray energy density and V the volume over which the gamma-rays are produced. The factor

of $\frac{1}{3}$ allows for the probability that the collision product is a π° as opposed to $\pi^{\pm}$.

For our Galaxy cosmic rays can be considered to fill a disk of radius 15 kpc with a scale height $\simeq$ 1 kpc. The gas, however, has a maximum scale height $\simeq$ 100 pc with a similar radial extent. The latter disk thickness is more appropriate when considering gamma-ray production; the former for particle trapping. Taking typical values for n $\sim$ 1 at cm^{-3} and $\xi_{cr} \sim 1$ eV cm^{-3} (appropriate for cosmic rays above 1 GeV), then substitution in 7.3 yields L_{γ} ($>$ 100 MeV) $\simeq$ 9.5 x 10^{50} eV s^{-1}. The Galactic gamma-ray spectrum above 100 MeV can well be described by an E_{γ}^{-2} power law, which over the SAS II energy range 100 MeV to 1000 MeV corresponds to a mean photon energy $\simeq$ 2.6 x 10^{8}eV. Thus we find L_{γ} ($>$ 100 MeV) $\simeq$ 3.7 x $10^{42}phs^{-1}$. Making an allowance for a 20% electron contribution we estimate L_{γ}($>$ 100 MeV) $\simeq$ 4.6 x $10^{42}phs^{-1}$ for the diffuse Galactic emission. Strong and Worrall's estimate, derived from the SAS II data, includes a discrete source component. The results of Chapter 5 suggest that at these energies discrete sources contribute about 20% of the Galactic flux. After allowing for this correction we estimate the observed diffuse luminosity to be about (1.0 - 1.1) x $10^{42}phs^{-1}$. Thus our simple model overestimates the diffuse flux by about a factor of 4. To achieve improved agreement would require more detailed

modelling of the cosmic ray and gas distributions throughout the Galaxy. However, the present model is considered sufficient as an order of magnitude estimate.

We could,in principle,use 7.3 to estimate the proton contribution to the gamma-ray flux, though first we require knowledge of the parameters n, $\mathcal{E}_{cr}$ and V. Radio synchrotron data yields information on the interactions of relativistic electrons and magnetic fields within a source region. In radio astronomy such measurements are often used to obtain estimates of the total energy in relativistic electrons. By assuming an appropriate $^{e}/p$ ratio for the observed region the total cosmic ray proton energy can thus be estimated.

7.4 The radio synchrotron minimum energy condition

Many workers have dealt with the minimum energy requirement for a synchrotron source (e.g. Ginzburg and Syrovatskii, 1964; Longair 1981). In this approach the total energy in the source region is expressed as the sum of magnetic field energy and relativistic particle energy as a function of magnetic field. For a power law electron spectrum $N(E) \sim E^{-\gamma}$ and synchrotron spectrum $S_\nu \sim \nu^{-\alpha}$ ($\gamma = 2\alpha + 1$) the minimum energy condition can be expressed as

$$W_{min}(\text{erg}) = 13.34\ V(\text{m}^3)^{3/7} \left[G\eta\ L_\nu\ (\text{WHz}^{-1}) \right]^{4/7} \qquad 7.4$$

where

$$G = \frac{2.34 \times 10^{23}}{(\gamma-2)} \quad \frac{\nu_{min}^{\frac{2-\gamma}{2}} - \nu_{max}^{\frac{2-\gamma}{2}}}{a(\gamma)\ \nu^{\frac{1-\gamma}{2}}} \quad (1.0022)^{\gamma}$$

7.5

and $a(\gamma)$ is a constant dependent on γ such that

γ	1	1.5	2	2.5	3	4	5
$a(\gamma)$	0.283	0.147	0.103	0.0852	0.0742	0.0725	0.0922

It is assumed that cosmic ray protons have an energy spectrum similar to that of electrons and $\mathcal{E}_{total} = \eta\ \mathcal{E}_{electrons}$. The synchrotron power $L_\nu(WHz^{-1})$ is measured at an observed frequency ν(MHz) with a spectral index $\alpha = \frac{\gamma-1}{2}$. Normally ν_{min} and ν_{max}, the limits of the synchrotron spectrum, are taken to be 10 MHz and 100 GHz respectively. For the minimum energy condition it can be shown that W(magnetic field) = $\frac{3}{4}$ W(particles) which is closely associated with the idea of equipartition of energy between magnetic fields and relativistic particles. In our Galaxy the large scale distribution of energy between protons and electrons is such that $\eta \sim 33$, though for the Crab pulsar $\eta \sim 1$, and it is often assumed that η can vary from 1 - 100 in radio galaxies.

Thus by using synchrotron data from known sources we can derive from 7.3, 7.4, 7.5 an estimate of the expected proton induced gamma-ray flux above 100 MeV.

7.5 Estimates of gamma-ray luminosity for nearby galaxies

Before applying this method to known extragalactic radio sources it is first necessary to test its usefulness by applying it to several objects for which firm gamma-ray measurements are available. It is not possible to use our Galaxy in this context because of the large uncertainties involved in deriving the total radio flux from local measurements.

First we consider the nearby galaxy M31, similar in size and structure to our own. Beck and Grave (1981) have made a detailed study of the synchrotron emission from this object and estimate S_ν(408 MHz) $\simeq$ 11.85 Jy, $\alpha \sim 0.75$. Their integrated flux is smaller than previous measurements which were unable to distinguish the additional background contribution from distant radio galaxies. Adopting a distance of 670 kpc and $\eta = 33$ (as for our Galaxy) we find from 7.4 $W_{min}^{(erg)} \sim 2.0 \times 10^{54} R^{9/7}$(kpc). In that M31 is not a spherical source it is inappropriate to adopt a single radius R. However, the equivalent effective radius must be between 10 kpc and 20 kpc yielding $W_{min} \sim 0.4 - 0.9 \times 10^{56}$erg. Adopting $W = 0.6 \times 10^{56}$erg and n = 1 at cm^{-3} we expect F_γ (> 100 MeV) $\simeq 0.7 \times 10^{-6}$ph $cm^{-2}s^{-1}$. For M31 we estimate the observed flux at this energy to be $\simeq 0.3 \times 10^{-6}$ ph $cm^{-2}s^{-1}$ from the SAS II data (Section 3.8). Given the many sources of uncertainty the two values are not inconsistent, though by no means conclusive. We proceed by considering an active radio-

galaxy.

The giant elliptical galaxy M87 lies at a distance of $\simeq$ of 25 Mpc close to the centre of the local Virgo cluster. Allen (1973) summarized the synchrotron data on this object: S_ν (100 MHz) $\simeq$ 1800 Jy, $\alpha \sim 0.8$. For a spherical region, radius R = 20 kpc and η = 100, 7.4 gives $W_{min} \simeq 1.1 \times 10^{59}$erg. Taking n = 1 at cm^{-3} over the source region yields on substitution in 7.3 F_γ (> 100 MeV) $\simeq 10^{-6}$ph $cm^{-2}s^{-1}$. No absolute flux has been measured and an analysis of the SAS II data gives an upper limit F_γ (>100 MeV) $\lesssim 0.3 \times 10^{-6}$ph $cm^{-2}s^{-1}$.

The detection by COS B of a finite flux from NGC 1275 (Strong and Bignami, 1983) suggests we should also consider this object. Allen (1973) gives S_ν(100 MHz) $\simeq$ 130 Jy, $\alpha \sim 0.8$ for NGC 1275, at a distance of 116 Mpc. As for η and R we again adopt the canonical values 100 and 20 kpc respectively, yielding from 7.4 $W_{min} \simeq 1.5 \times 10^{59}$erg. For n = 1 at cm^{-3} we expect L_γ(> 100 MeV) $\simeq 9.4 \times 10^{46}$ ph s^{-1}. This time, the COS B observations have given a detection and they imply L_γ(> 100 MeV) $\simeq 8.6 \times 10^{47}$ ph s^{-1} for this source.

It is also important to remember that these estimates are only for the proton component of gamma-ray emission and it is probable that in many cases electron processes will make a more significant contribution than in our Galaxy. We now consider the extreme case of pure electron source, η = 1. The minimum energy varies as $\eta^{4/7}$ and

is thus reduced by a factor $(0.01)^{4/7} \simeq 0.07$. For an unionized gas the total energy loss rate due to electron bremmstrahlung is given by

$$L_\gamma = 7.26 \times 10^{-16} \; n \; E \; eV \; s^{-1} \qquad 7.6$$

where n is the gas density (at cm^{-3}) and E the total electron energy in eV. For NGC 1275 we find $W_{min} \simeq 1.5 \times 10^{59}$erg for $\eta = 100$ and $W_{min} \simeq 1.1 \times 10^{58}$erg for $\eta = 1$. Substitution into 7.6 with n = 1 at cm^{-3} yields $L_\gamma(> 100 \text{ MeV}) \simeq 1.9 \times 10^{46}$ ph s^{-1}.

For intermediate cases of $1 < \eta < 100$ the total estimated gamma-ray luminosity correspondingly lies between the limits $(1.9 - 9.4) \times 10^{46}$ ph s^{-1}. However the uncertainty attached to the parameters η, n and V, and indeed the possibility of non-equipartition for individual sources, increases the uncertainty on the expected gamma-ray luminosity. Nevertheless,from the limited sample considered, observation and model estimates agree to within an order of magnitude and the technique is applicable to derive a subset of gamma bright extragalactic radio objects.

As an estimate of the uncertainty in the expected fluxes we can assume $V \propto R^3$. The dependence of n on R is not obvious. For our Galaxy n is virtually independent of Galactocentric radius ($4 < R < 10$ kpc) though in other galaxies (e.g. NGC 6946, NGC 4321) n appears to decrease slowly with R (Bhat et al., 1984(b)). For the present

purposes we take $n \propto R^{-1}$ and in conjunction with 7.3 and 7.4 we find $F_\gamma \sim R^{2/7} \eta^{4/7}$. Substituting probable values of R and η for an extragalactic radio source (R = 5-50 kpc, η = 1-100) the variation of F_γ is seen to be small, less than a factor of ten. It is concluded that the minimum energy technique is a useful indicator of gamma-ray activity, at least to within an order of magnitude.

We aim,therefore, to use data on known radio sources to estimate the expected gamma-ray flux for the canonical values of R, η and n. The radio bright objects are expected to be gamma-ray sources and can form the basis for a search of the gamma-ray data for extragalactic sources.

7.6 Activity in galaxy clusters

X-ray properties of rich clusters of galaxies have been extensively studied (e.g. Gursky and Schwartz, 1977; Soltan and Henry, 1983; Abrampoulos and Ku, 1983; Jones and Forman, 1984), and there is now a broad consensus on the interpretation of the accumulated data.

Observations of clusters indicate that the spectra are most likely thermal in nature, the bulk of the emission being genuinely diffuse in origin, although in some cases (e.g. Perseus) there are additional non-thermal components of emission associated with active members of the clusters. In clusters, the thermal emission is believed to originate in an intra-cluster ionized gas with temperature $T \sim 10^{7-8}$K and density $n \simeq 10^{-3} - 10^{-4}$ at cm^{-3} in the

core region (radius $\sim$ 200 - 300 kpc).

The observations in Perseus, Virgo and Coma of a spectral feature at about 6.7 keV is interpreted as iron line emission from the intra-cluster gas (Serlemitsos et al., 1977). This is very strong evidence supporting the thermal nature of the diffuse emission and demonstrates that a significant fraction of the gas has been through a cycle of stellar evolution. The origin of the gas is still uncertain. It may be a remnant from the era of cluster and galaxy formation which is continuously accreting onto the galaxies and being re-expelled. Alternatively it may be due to the expulsion of enriched galactic gas.

For a rich cluster with about 100 normal members we see from Table 7.1 that cluster X-ray luminosity is typically more than three orders of magnitude greater than that of its constituent galaxies. Many workers find a strong correlation of luminosity with cluster morphology (e.g. Gursky et al., 1972; McHardy, 1978; Kowalski, 1982; Abrampoulos and Ku, 1983; Soltan and Henry, 1983). Soltan and Henry find the mean cluster luminosity increases with richness class; L_X(2 - 10 keV) varying from 4.4×10^{44} erg s^{-1} for richness R = 1 to 8.3×10^{44}erg s^{-1} for richness R = 4 and 5. Abrampoulos and Ku find correlations between X-ray luminosity, richness, central galaxy density and velocity dispersion.

Associations between radio sources and rich clusters are also extensively studied (e.g. van den Bergh, 1961; Fomalont and Rogstad, 1966; Riley, 1975). Radio emission from clusters is generally associated with individual radio galaxies but with occasional extended emission as in the Coma cluster (Sastry and Shevgaonkar, 1983). There does not appear to be any correlation between radio luminosity and cluster richness though the radio emission is often associated with giant CD type galaxies in the cluster cores. About 10% - 15% of clusters have one or more radio galaxies as members. Radio galaxies have luminosities $\sim 10^{4-6}$ times those of normal galaxies and their presence in clusters is further indication of violent activity therein.

The evidence from X-ray and radio emission in clusters suggests the presence of copious energy sources. X-ray emission in particular appears to be a wide-spread characteristic. However, its thermal nature does not by itself indicate the presence of relativistic particles necessary for gamma-ray production. The extensive ionized gas in the intra-cluster medium could provide a target for gamma-ray production by relativistic particles diffusing out of active galaxies or being accelerated in situ.

7.7 Gamma-ray emission from rich clusters

Measurements of the cosmic ray flux ($\gtrsim$ 1 GeV) in our Galaxy indicate that the particles traverse about 6 g cm^{-2} of the interstellar medium, that is approximately

$^{1}/10$ of the interaction length. Unless the diffusion coefficient and grammage are markedly different in other galaxies then the cosmic rays will only lose about 10% of their energy in the parent galaxy and the bulk of the cosmic ray flux will diffuse out into the surrounding medium.

For isolated galaxies, like our own, the cosmic rays escape into the intergalactic medium and presumably finish many tens of Mpc away. However, for radio galaxies situated in rich clusters the cosmic rays will diffuse into the cluster cores. These regions are typically 200-300 kpc in radius and X-ray measurements indicate mean gas densities to be $\sim 10^{-3}$ at cm^{-3}. Dennison (1980) suggests that the diffusion of primary protons and the subsequent production of relativistic electrons, through collisions with the intra-cluster medium, can account for the energy requirements of the radio halo observed in the Coma cluster. However, Valtaoja (1984) has shown that the distribution of halo radio emission in Coma is best described by the diffusion of primary electrons.

Although only about 10-15% of clusters are believed to have radio halos this is more likely due to the absence of extensive intra-cluster magnetic fields, rather than low cosmic ray fluxes (Valtaoja, 1984). Thus, assuming relativistic protons are also produced in the radio galaxies, gamma-ray production will necessarily occur both in the radio galaxy and the surrounding medium.

Taking NGC 1275 as a typical cluster radio source we have already estimated $L_\gamma(>100\ \mathrm{MeV}) \simeq 9.4 \times 10^{46}$ ph s^{-1}. If this corresponds to 10% of the cosmic ray energy loss, then the total gamma-ray luminosity is likely to be about 9.4×10^{47} ph s^{-1}. Interestingly this is in close agreement with the luminosity implied by the COS B observations, $\simeq 8.6 \times 10^{47}$ ph s^{-1} above 100 MeV. The gamma-ray emission from the core region will not be uniformly distributed but will depend on the distribution of cosmic rays diffusing from the central source, folded with the gas profile.

We can apply these criteria to the original luminosity estimate for M87 in the Virgo cluster. The net gamma-ray luminosity will then be $L_\gamma = 7.0 \times 10^{47}$ ph s^{-1} above 100 MeV and correspondingly $F_\gamma(>100\ \mathrm{MeV}) \simeq 10^{-5}$ ph cm^{-2} s^{-1}. This is approximately a factor of 30 above the SAS II upper limit for M87 ($\lesssim 0.3 \times 10^{-6}$ ph cm^{-2} s^{-1}), indicating that the parameters ($\eta = 100$, R = 20 kpc) adopted for the present model are too large for this particular object.

7.8 Description of the data

(i) Radio galaxies

The combined data collected by Pooley and Henbest (1974), Riley and Pooley (1975) and Jenkins et al. (1977) constitute a complete sample of 3CR radio sources; S_ν (178 MHz) ≥ 10 Jy, dec $>10°$ and $|b| \geq 10°$. Of the 182 sources 109 have optical identifications and hence distance estimates. It is these which are considered

in the present analysis. In many cases the sources have multiple components corresponding to central hot-spots, double side-lobes and extended tails. We always use the flux measurements from the central region as representative of the source for the purposes of estimating the cosmic ray energy therein. The spectral indices are obtained from a comparison of the flux densities at 5GHz with those at 178 MHz.

McHardy (1979) selects those 4C and 4CT radio sources (S_ν (178 MHz) $\geq$ 2 Jy and dec $> 10°$) lying within 0.9 Mpc of an Abell cluster centre and identified with a galaxy which is almost certainly a member of that cluster. The angular resolution of the 4C survey ($\sim$ 3 arc min at 408 MHz) is such that extended sources are excluded from the catalogue. To eliminate possible distance biasing only those sources definitely or most probably identified with a cluster are accepted. This restricts the sample to 49 sources for which McHardy gives data on the radio power at 408 MHz, the spectral index and the distance.

The range of luminosity of the 158 identified radio sources extends over several orders of magnitude. To analyse the gamma-ray data at all these positions results in the use of many non-independent bins. Additionally the signals from weaker sources are unlikely to be detectable, contributing only to the local background flux in those directions.

For all the radio sources standard values of R = 20 kpc.,

η = 100 and n = 1 at cm^{-3} are adopted. Using 7.3, 7.4, 7.5 the expected flux above 100 MeV is evaluated for each source and only those with F_γ, expected $\geqslant 10^{-10}$ ph $cm^{-2}s^{-1}$ are selected for analysis. These data are further divided into two luminosity classes: those with F_γ, expected $> 10^{-8}$ ph $cm^{-2}s^{-1}$ (15 sources) and those with 10^{-10} ph $cm^{-2}s^{-1} < F_\gamma$, expected $< 10^{-8}$ph $cm^{-2}s^{-1}$ (48 sources). The parameters for both these sets are given in Tables A.4 and A.5.

(ii) Rich clusters

The source of data on galaxy clusters is the Abell catalogue (Abell, 1958) containing 2172 rich clusters. A subset of these (1682 members) is defined as a statistically complete sample for dec > - 27°. Each cluster in the catalogue is assigned to one of 5 richness classes, depending on the number of galaxies in the cluster. The mean distance to each cluster is catalogued in one of 6 intervals, based on the magnitude of the 10th brightest galaxy in the cluster (m_{10}). For an object of unknown redshift, m_{10} is usually taken as an indicator of distance. This is a standard technique developed by Hubble which assumes that on average the 10th brightest members of clusters always have the same intrinsic luminosity. The Hubble diagram ($m_{10} - Z$) is used as the conversion from brightness m_{10} to redshift, and distances are calculated using the standard relation:

TABLE 7.2

Distance Class D	m_{10}	$\overline{Z}$	$\overline{R}$(Mpc)	n(D)
1	13.3 - 14.0	0.027	155	9
2	14.1 - 14.8	0.038	214	2
3	14.9 - 15.6	0.067	359	33
4	15.7 - 16.4	0.090	464	60
5	16.5 - 17.2	0.140	666	657
6	17.3 - 18.0	0.180	808	921
1-4	(15.54)	0.072		104

Richness Class R	No. of galaxies	n(R)
1	50 - 79	1224
2	80 - 129	383
3	130 - 199	68
4	200 - 299	6
5	300 +	1

The distributions in distance and richness classes of Abell's complete cluster sample.

$$D = {}^{c}/H_o q_o^2 (1+z)^2 \left\{ q_o Z + (q_o - 1) \left[(1+2q_o Z)^{\frac{1}{2}} - 1 \right] \right\} \qquad 7.7$$

For the purposes of the present chapter, we assume $q_o = \frac{1}{2}$ and $H_o = 50$ K kms^{-1} Mpc^{-1}. The definitions of Abell's distance and richness classes are given in Table 7.2.

For the present analysis 83 clusters are selected from Abell's complete sample. This restriction is due in part, to the limited coverage of the SAS II data for several sky regions. However, the primary selection is on the distance class criterion with only $D \leqslant 4$ being accepted, effectively limiting the richness to $R \leqslant 2$. The distribution of the clusters finally used is given in Table A.6.

(iii) Galaxy counts

The Lick galaxy counts of Shane and Wirtanen (1967) are used to estimate the total gas column density away from the Galactic plane. These data and their limitations are discussed more fully in Chapter 6. In this chapter we use the same conversion from mean galaxy count N_G to column density N_{H_t}:

$$N_{H_t}(N_G) = 2 \times 10^{21} \log_{10}({}^{N_G^o}/N_G) \text{ at cm}^{-2} \qquad 7.8$$

taking $N_G^o = 75$ as the mean galaxy count per square degree in the absence of extinction.

In their analysis of the gamma-ray flux from the direction of NGC 1275, Strong and Bignami (1983) draw attention to the effect of galaxy clustering leading to an underestimate of the total gas as measured directly by HI. An inspection of the galaxy count data (1° x 1° binning) shows that in many bins containing clusters there is an excess count relative to the surrounding bins. Thus it is important to consider the likely effects of clustering on estimates of the column density obtained using 7.8.

Austen and Peach (1974) give a general luminosity distribution for field galaxies:

$$\log_{10} N(\leqslant m_v) = -8.99 + 0.60\, m_v \qquad 7.9$$

expressed in galaxies per square dgreee in the absence of absorption. The Lick survey is complete to a limiting magnitude $m_v \simeq 18.0$, and from 7.9 we therefore expect about 65 galaxies per square degree in the field. Given the uncertainties associated with defining the low-luminosity tail of the field galaxy distribution this value is in reasonable agreement with $N_G^o = 75$ adopted for the present work.

In the present work attention is restricted to distance classes $D \leqslant 4$ and richness classes $R \leqslant 2$. For this subset of the Abell catalogue we find from Table 7.2 the mean number of galaxies per cluster to be about 75. The Abell radial size criterion for clusters is 3 Mpc, which for a mean redshift $Z = 0.072$ corresponds to an area $\simeq 0.5$ deg^2

on the sky. For this sample the mean cluster richness (75 galaxies over 0.5 deg^2) is therefore significant in relation to the field count ($\simeq$ 65 galaxies over 1 deg^2). However, to allow for the angular resolution of the gamma-ray data, the galaxy counts are averaged over 3 x 3 bins corresponding to an area $\simeq$ 18 deg^2 (Section 7.9). The total field count is then = 1170, to be compared with 75 for the mean cluster. The number of galaxies due to a cluster is thus comparable to the statistical noise level on the background. We expect cluster enhancement on these scales to be small but nevertheless, it is likely to consistently lead to an underestimate of the gas column density towards cluster positions. Thus gamma-ray excess intensities above the Galactic background are likely to be overestimated.

7.9 Derivation of extragalactic intensities and local emissivities

It is not expected that statistically significant fluxes from individual sources can be detected. But by summing together the signals from many positions it is hoped to see a finite excess signal over and above the background from cosmic ray interactions in the Galaxy. The technique used is therefore to compare the gamma-ray intensity at source positions with the total column density of gas in that direction. The latter is taken as a direct measure of the expected intensity from the Galaxy, assuming that the cosmic ray intensity is uniform

along the line of sight. This, of course, is a matter of debate. However even with the existence of a Galactic cosmic ray gradient it is generally believed that the scale height out of the plane is about 1 kpc. The assumption of uniform intensity is therefore reasonable for latitudes well away from the plane, which effectively only sample the local interstellar medium.

For the SAS II data with E_γ > 100 MeV arrays of 3 x 3 bins centred on each cluster position are chosen, and for E_γ: 35 - 100 MeV 5 x 5 bins are adopted; corresponding respectively to 5.5 x 10^{-3}sr and 1.5 x 10^{-2}sr. Because of the limited angular resolution of the gamma-ray data, which smears out the point-like image of a galaxy cluster, the galaxy count data are smoothed to the same resolution. This is done for both energy bands using the point spread functions appropriate for the SAS II detector (Section 4.1). Column densities are then calculated using 7.8.

All the data for $|b| > 9.6°$ are then grouped in 3 x 3 and 5 x 5 arrays; except, of course, for regions with neither gamma-ray exposure or galaxy count coverage. To reduce the large errors associated with individual gamma-ray intensities the data are further grouped into column density bins, and mean values derived by summing over the respective galaxy counts, number of photons and sensitivity. These data are plotted in Figure 7.1 where the weighted least squares linear regressions are indicated by the solid lines. It is interesting to compare

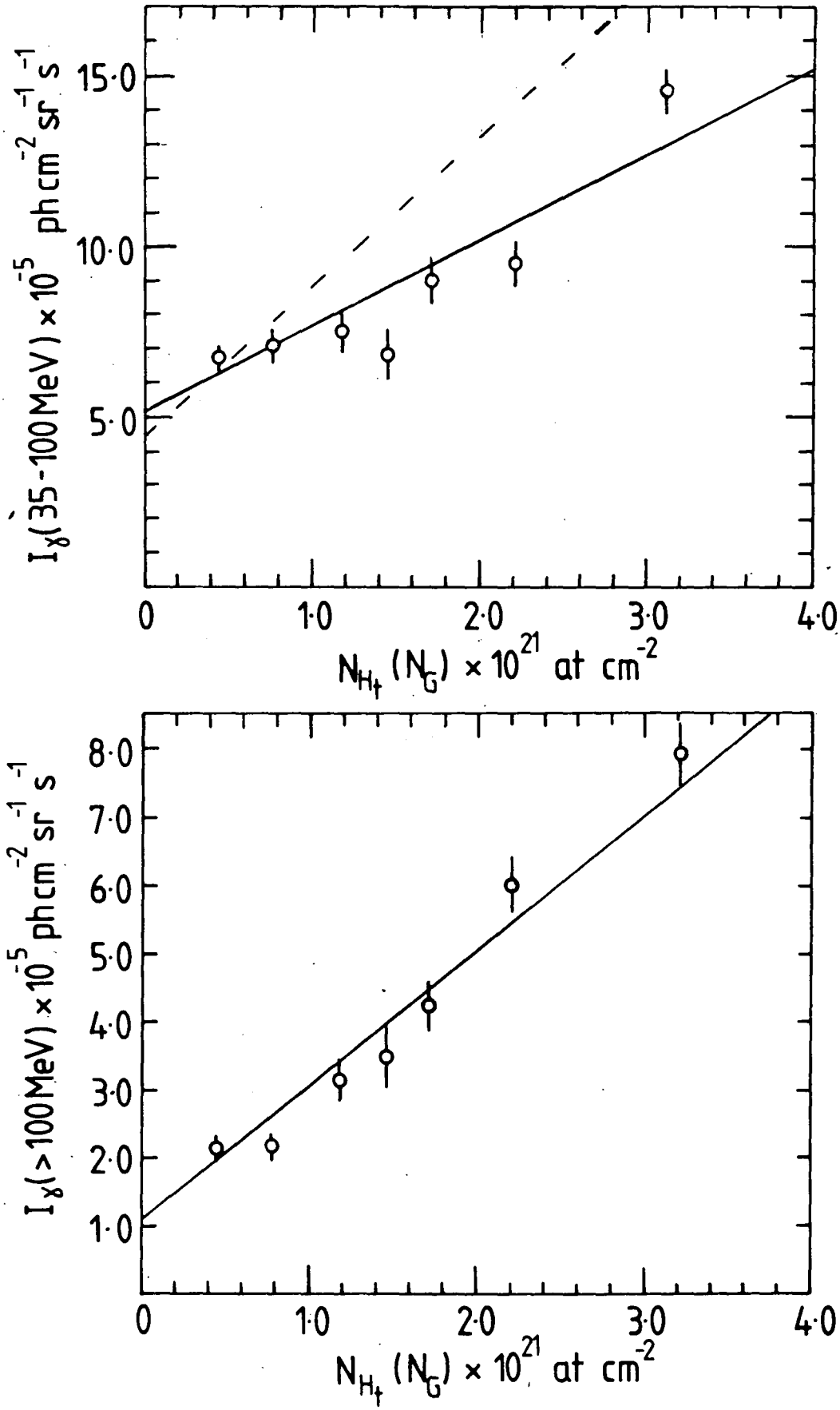

FIGURE 7.1 SAS II intensities $I_\gamma(\pm 1\sigma)$ versus $N_{H_t}(N_G)$ covering those regions $|b| > 9.6°$ with both gamma-ray and galaxy count exposure. The solid lines are the weighted least squares fits to the data.

these results with those obtained in an earlier analysis by Thompson and Fichtel (1982), the broken line, after allowing for the difference in N_G^o in 7.8.

While the data are in excellent agreement for $E_\gamma > 100$ MeV there is a systematic offset between the two lines for E_γ : 35-100 MeV. The discrepancy is due to the use of a single sensitive area ($\simeq 31.4$ cm^2) by the SAS II group for E_γ : 35-100 MeV., whereas we adopt the area factors given in the tabulated SAS II data (40 cm^2 and 30 cm^2 for $|b| < 10°$ and $|b| > 30°$ respectively). The agreement above 100 MeV results from both analyses employing the corresponding energy area factors from the tabulated data (59 cm^2 and 66 cm^2 for $|b| < 10°$ and $|b| > 30°$ respectively). The sensitive area value 31.4 cm^2 is used in an earlier analysis of the SAS II data (Fichtel et al., 1977) and is consistent with a single assumed input gamma-ray spectrum $E_\gamma^{-1.5}$ (Mayer, private communication). However subsequent analyses of both SAS II and COS B data show the observed spectrum to be consistent with E_γ^{-2}, at least in the Galactic plane.

The tabulated data and corresponding area factors used for the present analysis implicitly assume that the high latitude spectrum is steeper than that of the Galactic plane, reflecting the presence of the extragalactic component. To determine the spectral shape of the extragalactic intensity requires an iterative analysis to

derive the appropriate sensitive areas.

For the present analysis it is sufficient to adopt the factors given by Fichtel et al. (1978b) as we are primarily interested in the excess intensity and not its precise spectral shape. The extragalactic intensities are found by extrapolating the regression lines to zero column density giving:

$$I_\gamma(35\text{-}100\ \text{MeV}) = (5.2 \pm 0.7) \times 10^{-5}\ \text{ph cm}^{-2}\text{sr}^{-1}\text{s}^{-1}$$

$$I_\gamma(>100\ \text{MeV}) = (1.1 \pm 0.2) \times 10^{-5}\ \text{ph cm}^{-2}\text{sr}^{-1}\text{s}^{-1}$$

The local emissivities are obtained directly from the slopes of the regression lines:

$$q/4\pi(35\text{-}100\ \text{MeV}) = (2.5 \pm 0.5) \times 10^{-26}\ \text{ph at}^{-1}\text{sr}^{-1}\text{s}^{-1}$$

$$q/4\pi(>100\ \text{MeV}) = (2.0 \pm 0.2) \times 10^{-26}\ \text{ph at}^{-1}\text{sr}^{-1}\text{s}^{-1}$$

7.10 Analysis of the data

Turning now to the question of excess emission from radio galaxies; the intensities from these positions are calculated by summing over 3 x 3 and 5 x 5 bins, centered on the galaxy, for the energy ranges $E_\gamma > 100$ MeV and E_γ : 35 - 100 MeV respectively. The column densities at these positions are also calculated over the same regions of the sky from the galaxy count data convolved to the appropriate SAS II resolution.

The data on the strong radio sources (F_γ, expected $> 10^{-8}$ph cm^{-2}s^{-1}) and the weak sources (10^{-10} ph cm^{-2}s^{-1} $< F_\gamma$, expected $< 10^{-8}$ph cm^{-2}s^{-1}) are treated separately

for each energy range. Each data set is grouped into several column density bins to reduce the statistical uncertainty attached to individual points. The results for both radio source sets (63 sources, E_γ : 35-100 MeV) are presented in Figure 7.2 and those for $E_\gamma > 100$ MeV (60 sources) are presented in Figure 7.3. A slightly reduced coverage in exposure for the SAS II data $E_\gamma > 100$ MeV (due to improved angular resolution) results in three fewer source positions being considered in this energy band.

The excess intensity (over the mean extragalactic background value) from radio galaxies is estimated by fitting a linear least squares line to the points in Figures 7.2 and 7.3. The mean source intensity is given by the height of this intercept relative to that of the background line. Adopting this procedure gives a line non-parallel with that of the background. This is undoubtedly a reflection of the statistical noise associated with each data point and to some extent, the probable range of radio galaxy luminosities. As the present technique is only attempting to look for a mean source excess on a statistical basis it is more appropriate to fit the source points by a weighted least squares line parallel to the mean background. These are indicated in Figures 7.2 and 7.3 by the broken lines. The excess intensities attributable to the radio sources are given in Table 7.3.

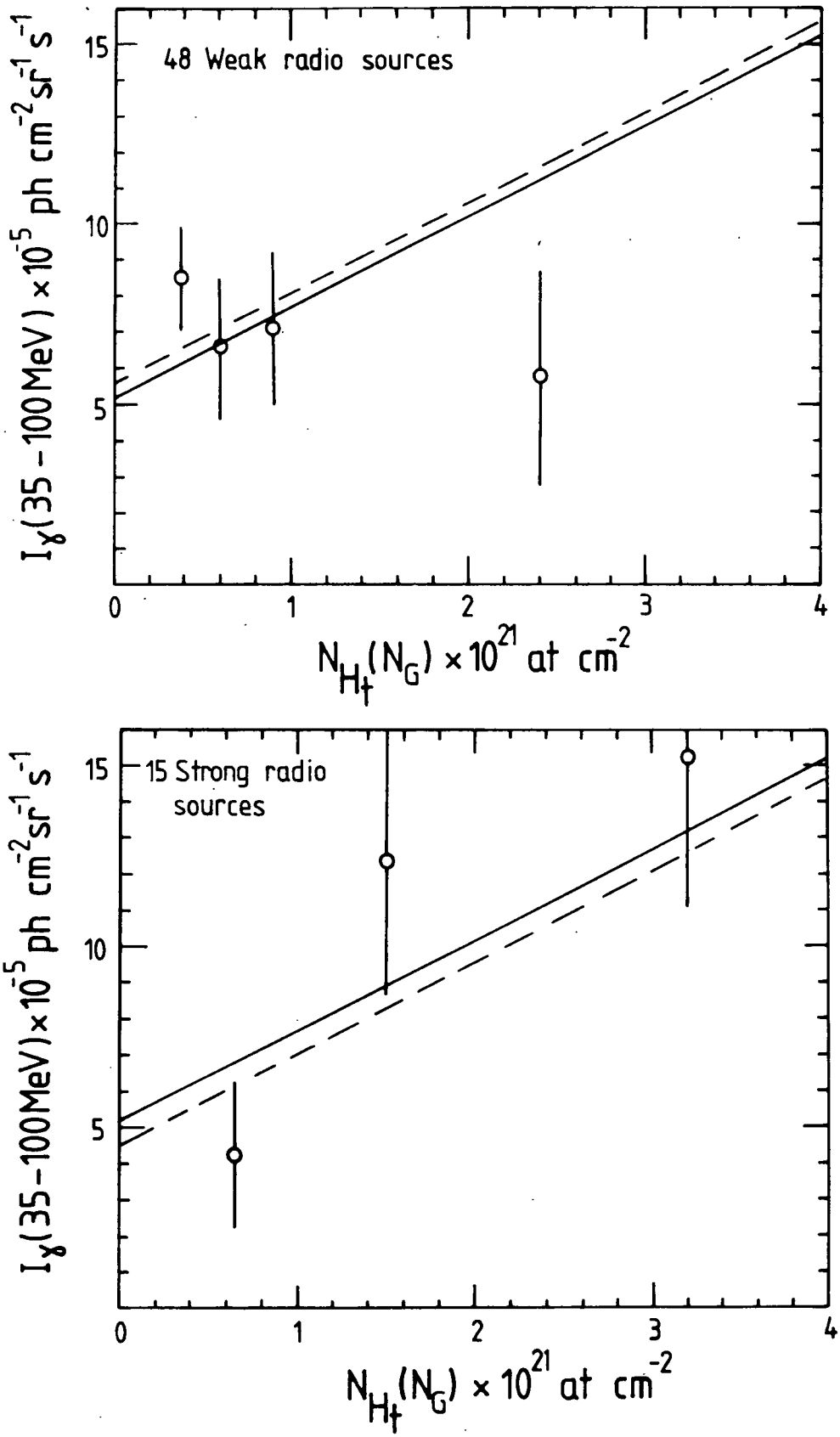

FIGURE 7.2 SAS II intensities I_γ(35-100 MeV)($\pm1\sigma$) versus $N_{Ht}(N_G)$ for the radio source positions. The solid lines are the fits to the mean backgrounds. The excess intensities are given by the broken lines.

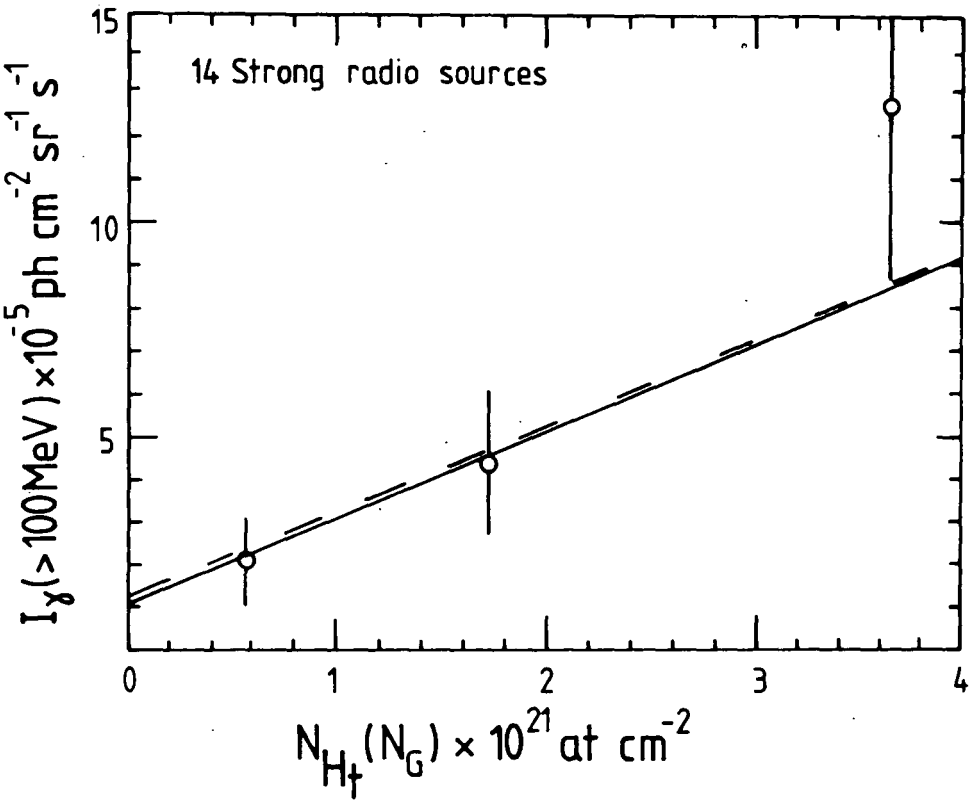

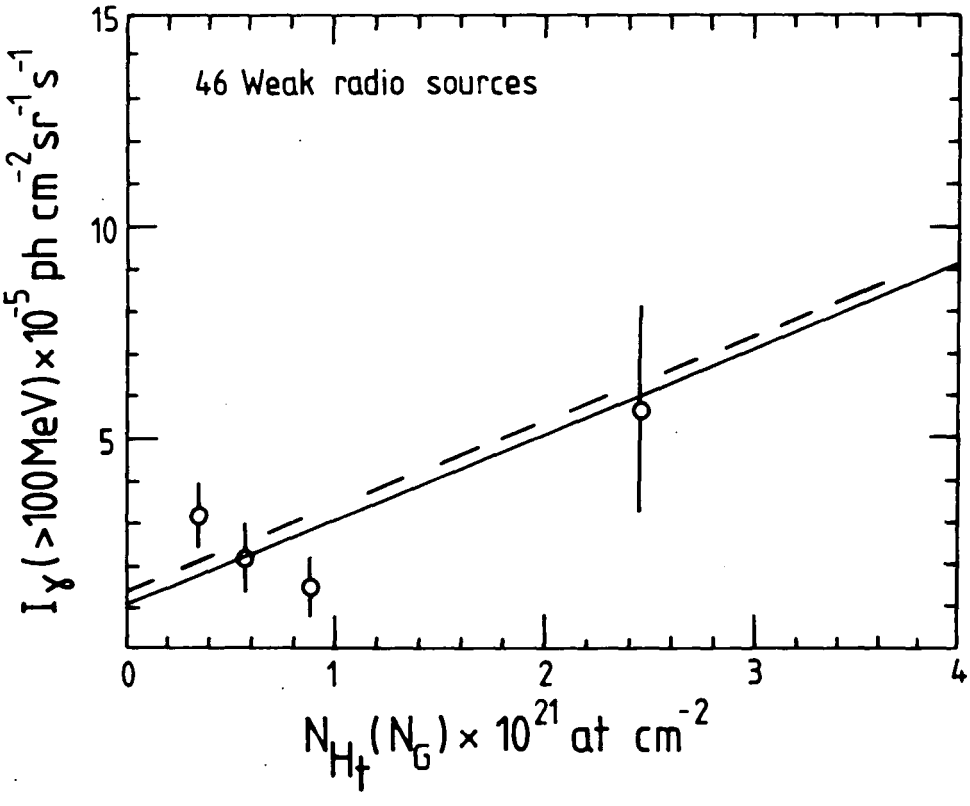

FIGURE 7.3 SAS II Intensities $I_\gamma(>100$ MeV$)(\pm1\sigma)$ versus $N_{H_t}(N_G)$ for the radio source positions. The solid lines are the fits to the mean backgrounds. The excess intensities are given by the broken lines.

The analysis is repeated using the positions of 81 Abell clusters ($E_\gamma > 100$ MeV) and 83 positions (E_γ : 35-100 MeV). The additional positions considered in the lower energy band are due to the increased coverage at this energy. These data are plotted as circles in Figure 7.4.

We also check whether galaxy clustering leads to an underestimate of the column densities and hence a spurious excess intensity. The column densities at the cluster positions are rederived using the bins surrounding those initially used to calculate the intensities and column densities. We take 16 and 24 bins (9.7×10^{-3}sr and 1.5×10^{-2}sr) for $E_\gamma > 100$ MeV and E_γ : 35-100 MeV to calculate the local background column densities. These data are plotted as indicated in Figure 7.4 by the squares.

There is a small systematic horizontal shift of the points to the right. This indicates that over the scales used galaxy clustering effects are on average decreasing the inferred column densities. Excess intensities are derived for the clusters using both the on-source and off-source estimates of N_{H_t}. For the off-source data the intensities are reduced by about 10% and 33% for E_γ : 35 - 100 MeV and $E_\gamma > 100$ MeV respectively. The relative magnitude of the effect reflects the improved angular resolution of the data above 100 MeV. The excess intensities given in Table 7.3 are obtained using the

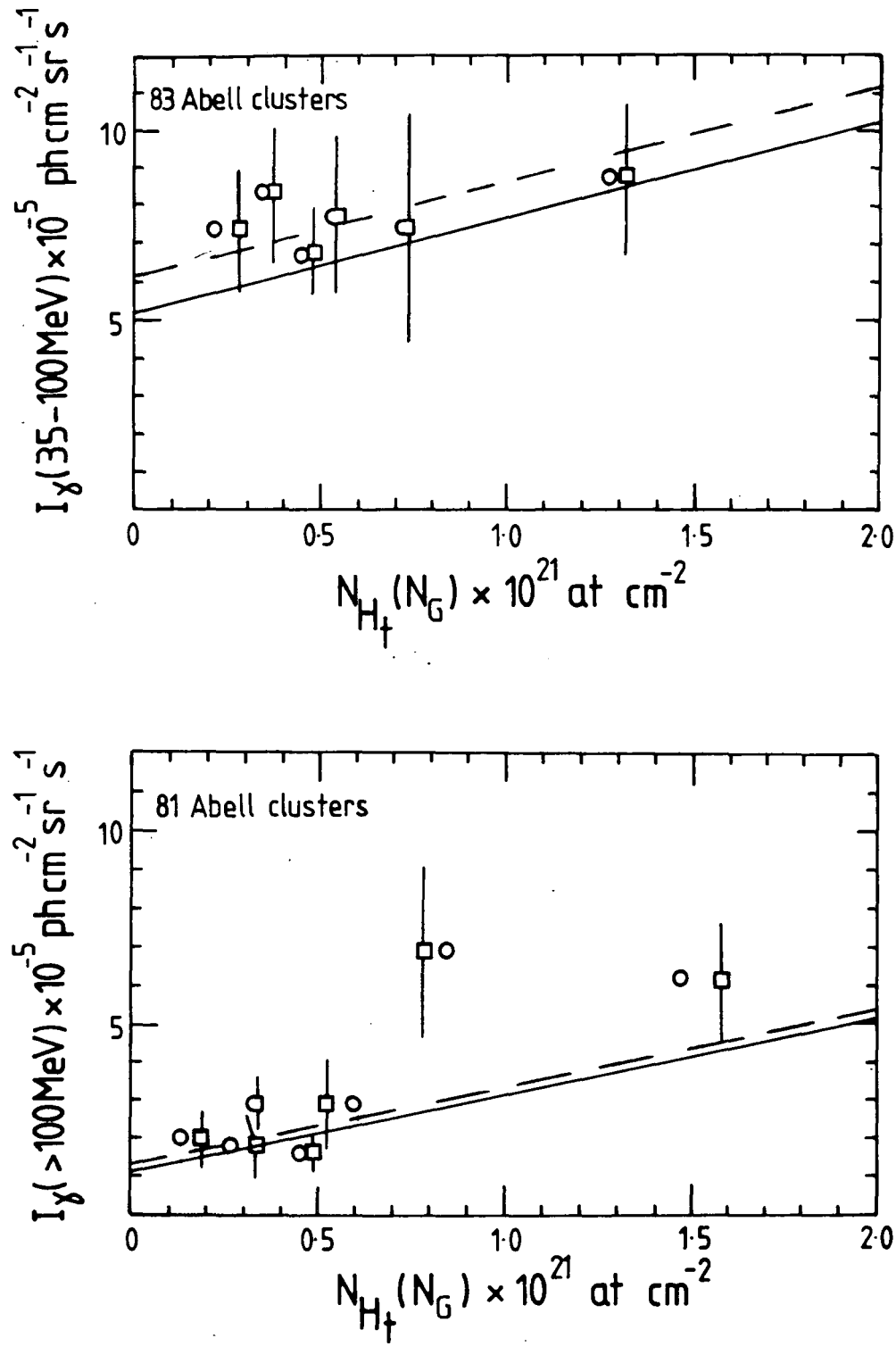

FIGURE 7.4 SAS II intensities $I_\gamma(\pm1\sigma)$ versus $N_{H_t}(N_G)$ for the rich cluster positions. The solid lines are the fits to the mean backgrounds. The circles are the column densities derived at the cluster positions. The squares are the column densities derived from the galaxy count surrounding the cluster positions. The latter are used to derive the excess intensities, given by the broken lines.

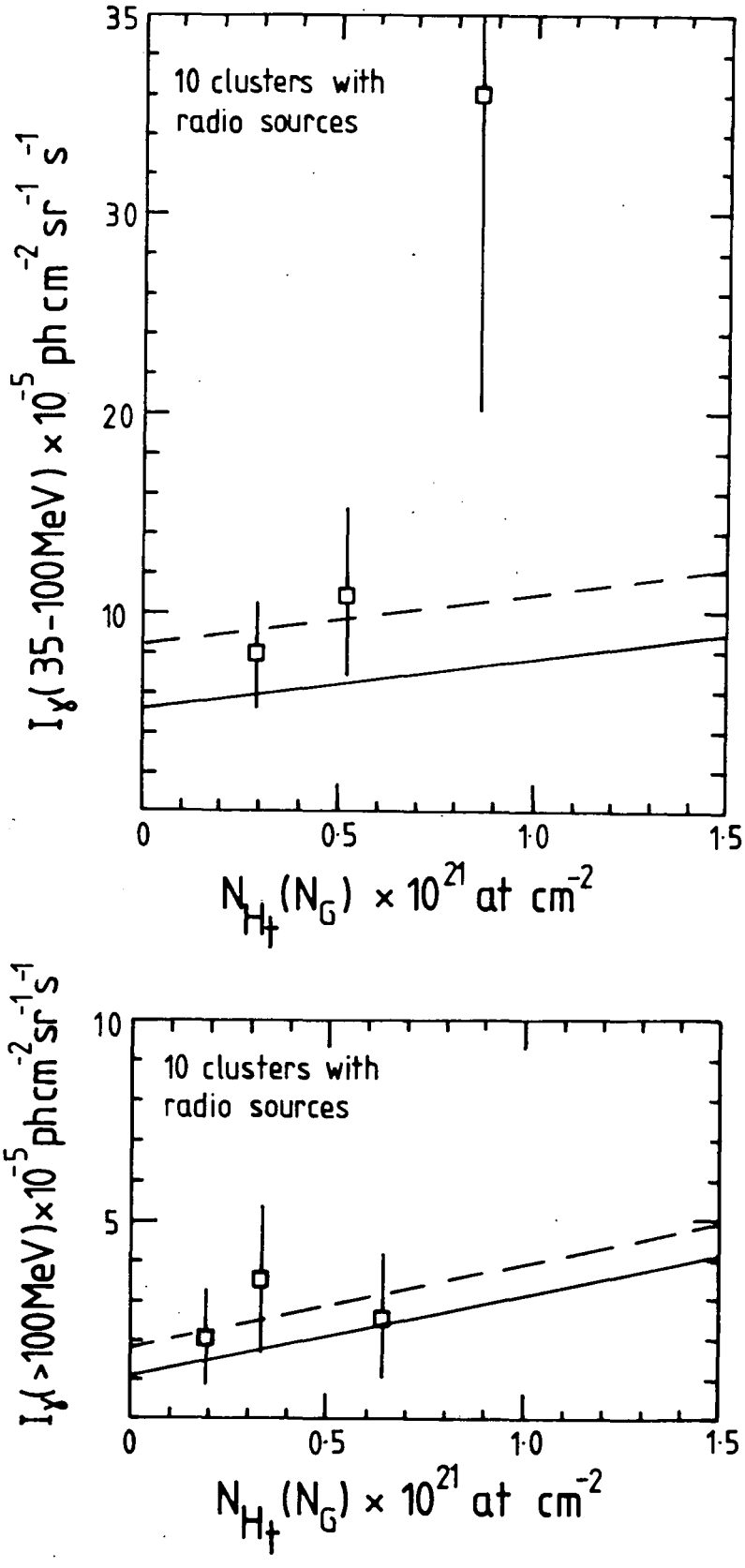

FIGURE 7.5 SAS II intensities $I_\gamma(\pm 1\sigma)$ versus $N_{H_t}(N_G)$ for the clusters with radio sources. The solid lines are the fits to the mean backgrounds. The column densities are estimated from the galaxy count surrounding each cluster position. The excess intensities are given by the broken lines.

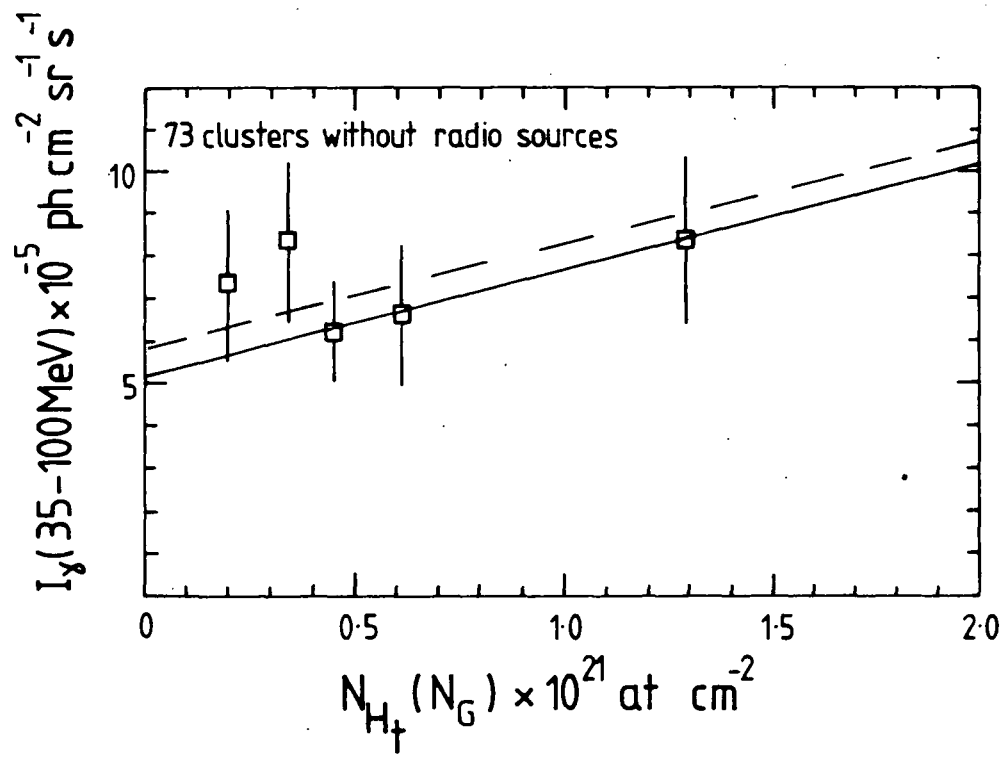

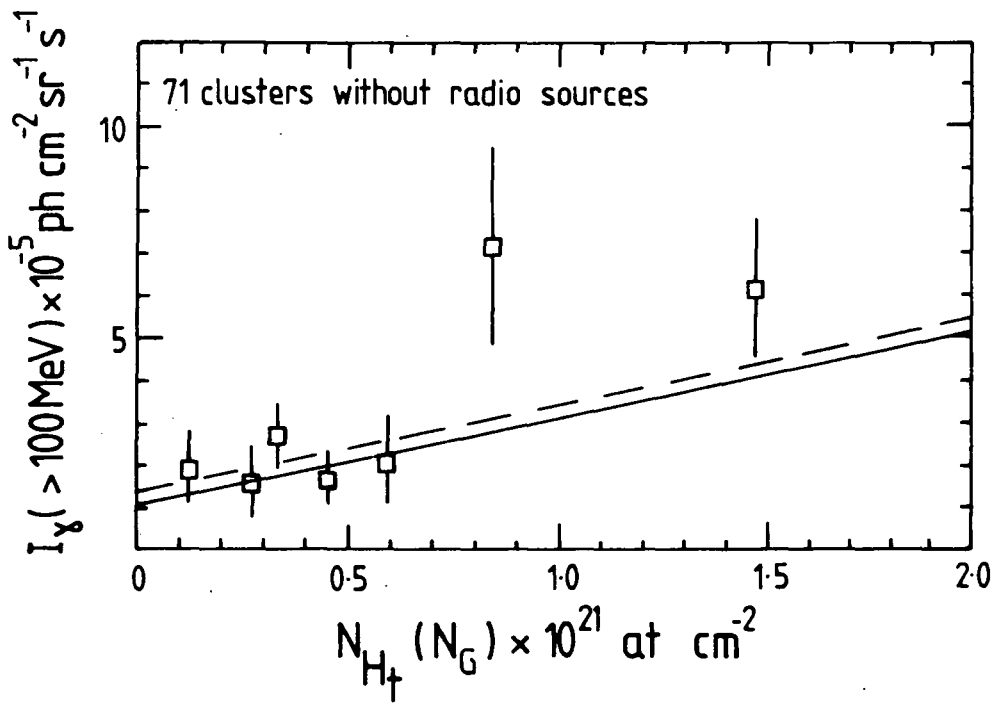

FIGURE 7.6 SAS II intensities $I_\gamma(\pm1\sigma)$ versus $N_{H_t}(N_G)$ for the clusters without radio sources. The solid lines are the fits to the mean backgrounds. The column densities are estimated from the galaxy count surrounding each cluster position. The excess intensities are given by the broken lines.

TABLE 7.3

	$I_\gamma \times 10^{-5}$ ph $cm^{-2}sr^{-1}s^{-1}$	
	E_γ:35-100 MeV	E_γ>100 MeV
15/14 Strong radio sources	-0.7 ± 2.7	0.1 ± 0.8
48/46 Weak radio sources	0.4 ± 1.8	0.3 ± 0.9
83/81 Abell clusters	1.0 ± 0.8	0.3 ± 0.5
10/10 Clusters with radio sources	3.2 ± 3.9	0.8 ± 0.7
73/71 Clusters without radio sources	0.6 ± 0.9	0.3 ± 0.4

The excess intensities ($\pm 1\sigma$) derived for each source type. The numbers preceeding each type refer to the number of objects used in the analysis for E_γ:35-100 MeV and E_γ>100 MeV respectively.

The excess intensities and associated errors derived here differ from those obtained in a previous analysis (Houston et al., 1984b). These differences reflect alternative statistical analyses of the data.

off-source data points, and should therefore be a better estimate of the mean intensity from galaxy clusters.

Of the 48 weak radio sources (Table A.5) 40 are associated with rich clusters. Only 10 of these sources are included in the sample of 83 Abell clusters. This relative abundance ($\simeq$ 12%) is in good agreement with that obtained by McHardy (1979) for the occurrence of 4C sources in Abell clusters ($\simeq$ 10-15%), indicating that the cluster sample used in the present analysis is unbiased. The remaining 30 clusters with weak radio sources consist of clusters beyond distance class D_4 and clusters not belonging to Abell's complete sample. The mean intensity from radio sources in clusters could be considered as similar to that for the weak radio sources alone. However, a better estimate can be made by selecting those 10 clusters which have associated radio sources. These data are plotted in Figures 7.5 and 7.6 and the excess intensities given in Table 7.3.

7.11 Interpretation of the results

From an inspection of Table 7.3 it is clear that the observed excesses have rather poor significances. The statistical errors arise from a combination of the low number of photons detected at the source positions and the errors on the background lines. Nevertheless it is useful to take the excess intensities and derive the mean luminosities for each class of object.

The excess fluxes are calcualted over the solid angles used in the analysis (1.5×10^{-2}sr and 5.5×10^{-3}sr for E_γ : 35-100 MeV and $E_\gamma > 100$ MeV respectively) and are increased by 30% to allow for the loss of signal from a point source smeared out by the poor angular resolution of the detector. Adopting the distances for the radio sources as given in Tables A.4 and A.5 the mean value of $^1/d^2$ is calcualted, and assuming isotropic emission from the sources, the luminosity derived. For the Abell clusters we use the mean distances for each distance class $\leqslant D_4$ given in Table 7.2. We calculate the mean of $^1/d^2$ ($= \sum n_i/D_i{}^2/\sum n_i$) where n_i is the number of clusters in a distance class D_i ($i \leqslant 4$). The mean luminosities for each class are given in Table 7.4.

We can in principle, use the mean luminosities to estimate the contributions to the extragalactic flux from each class. McHardy (1979) determined the density of radio sources to be $\simeq 3 \times 10^{-5}$ Mpc^{-3} and that of radio clusters $\simeq 0.7 \times 10^{-7}$ Mpc^{-3} from his analysis of the 4C survey at 408 MHz. The mean cluster density determined by Bachall and Soneira (1983) is $\simeq 0.73 \times 10^{-6}$ Mpc^{-3}, after allowing for the loss of clusters by Galactic obscuration and enhancement due to the local Virgo super-cluster. By substituting the values from Table 7.4 in 7.2 we estimate the universal flux for each class, Table 7.5. For the weak radio sources the universal fluxes

TABLE 7.4

	Luminosity L_γ ph s^{-1}	
	E_γ: 35–100 MeV	E_γ >100 MeV
Strong radio sources	$< 1.7 \times 10^{47}$	$(0.3 \pm 2.6) \times 10^{46}$
Weak radio sources	$(1.7 \pm 7.5) \times 10^{48}$	$(0.5\ 1.4) \times 10^{48}$
Abell clusters	$(2.7 \pm 2.2) \times 10^{48}$	$(2.7 \pm 4.5) \times 10^{47}$
Clusters with radio sources	$(3.1 \pm 3.8) \times 10^{48}$ $(3.1 \pm 3.8) \times 10^{48}$	$(2.7 \pm 2.4) \times 10^{47}$
Clusters without radio sources	$(1.9 \pm 2.9) \times 10^{48}$	$(3.1 \pm 4.5) \times 10^{47}$

The luminosities derived for each source type from the observed mean intensities in Table 7.3. The upper limit for strong radio sources is 1σ.

TABLE 7.5

	$F_{universal} \times 10^{-4}$ ph cm^{-2} s^{-1}	
	E_γ: 35–100 MeV	$E_\gamma > 100$ MeV
Strong radio sources	< 32.1	0.6 ± 4.9
All Abell clusters	12.4 ± 10.1	1.2 ± 2.1
Clusters with radio sources	1.4 ± 1.7	0.12 ± 0.11
SAS II extragalactic flux	6.5 ± 0.9	1.4 ± 0.3

The net universal fluxes estimated for each source type. The upper limit for strong radio sources is 1σ. The SAS II extragalactic fluxes are derived from our own analysis of the SAS II data.

are found to be more than a factor of 100 above the SAS II observed flux levels. Thus, no useful information is obtained. Also given are the extragalactic fluxes derived from our own analysis of the SAS II data (Section 7.9).

Only for the radio clusters can we usefully compare their net flux with the observed extragalactic background. While they may contribute all of the flux E_γ : 35-100 MeV their contribution is unlikely to be more than about 20% above 100 MeV.

We note that the data are not inconsistent with a significant fraction of the observed extragalactic flux coming from 'discrete' sources. However, further observations are clearly needed, both to improve the statistics and the angular resolution, before more detailed conclusions are drawn. In particular several of the radio cluster sources in Table A6 are expected to have fluxes just below the present detectability threshold. These are prime candidates for future study. Detection of gamma-ray emission above 100 MeV from the cores of radio clusters would be strong evidence for the presence of relativistic protons in these objects.

CHAPTER EIGHT

CONCLUSIONS

8.1 Summary of the present work

In the preceding chapters, several of the problems associated with the interpretation of the current gamma-ray data have been addressed. We began by outlining the links between gamma-ray astronomy and the salient aspects of the origin and propagation of cosmic rays. The information obtained from gamma-ray astronomy is relevant to many facets of the questions posed by cosmic ray physicists. As the clues appear we cautiously begin to perceive the underlying pattern.

The medium energy domain ($E_\gamma \sim$few 10^7eV - few 10^9eV) deals indirectly with the cosmic ray nucleons and electrons having energies of a few 10^8eV - few 10^{10}eV, constituting the bulk of the local cosmic ray energy density. The best method of discriminating between a Galactic or meta-galactic origin for the nucleonic component (energy loss rates for electrons require them to be Galactic) is to compare their density in the Galaxy, particularly towards the inner Galaxy, with the local value. The role of gamma-ray sources is identified as an important limitation in our ability to interpret the Galactic gamma-ray flux and hence the cosmic ray density.

In Chapter 4 an analysis was made of the SAS II data for supportive evidence on the 2CG sources detected

by COS B. It was important to seek independent evidence to asses the true nature of these candidate sources, most of which are unidentified with known astrophysical objects. The existence of the strongest sources : 2CG 263 (Vela), 2CG 195 (Geminga), 2CG 184 (Crab), 2CG 078 and 2CG 359 is unambiguously confirmed. A further 12 sources are confirmed at a lower level of significance. On the basis of the inferior statistical precision of the SAS II data we are unable to positively identify the remaining 5 sources and we note that the SAS II data are not inconsistent with those of COS B, time variability being excluded.

More importantly there is good evidence to suggest that many of the weaker sources are not genuine in the sense of being discrete. Rather, it is likely that they can be explained as unresolved regions of enhanced gamma-ray emission, identified with cosmic ray irradiation of local giant molecular clouds. Very recent analysis of the COS B data supports this conclusion (Bignami, 1984).

Before interpreting the observed Galactic gamma-ray flux allowance must be made for the unresolved discrete sources and the statistical fluctuations and pseudo-sources, which are really elements of the diffuse emission. A Monte-Carlo model of the diffuse gamma-ray emission was constructed in Chapter 5 and used to investigate the detection efficiency of genuine discrete gamma-ray sources. With these data and reasonable models of the discrete

source population limits are derived on the total flux from genuine gamma-ray sources in the Galactic plane. In the content of this model the source flux (>100 MeV) is estimated to contribute $\simeq$ 11-23% of the observed emission from the inner Galaxy ($|b|<5°$) and $\simeq$ 23-27% in the outer Galaxy. These estimates are small, though not negligible. They are subject to many systematic effects, related to the assumptions of the basic model for the diffuse emission. The most probable area of uncertainty, the distribution of H_2 in the inner Galaxy, is also related to the wider problem of deriving the variation in Galactic cosmic ray density from the gamma-ray data.

The nearby Orion molecular complex provides an excellent opportunity to investigate the coupling between cosmic rays and the giant molecular (H_2) clouds. An analysis of the COS B gamma-ray data from this region was performed in Chapter 6. We find no evidence for the exclusion of cosmic rays from the molecular gas. Rather, there is weak evidence favouring a modest enhancement of cosmic rays ($\sim n_H^{0.7}$) throughout the cloud. For the case of uniform cosmic ray irradiation we derive a new calibration for the conversion ratio $\alpha = 2N_{H_2} / \int T(^{12}CO)dv = (3.7 \pm 0.6)$ x 10^{20} at cm^{-2} $(K\ kms^{-1})^{-1}$, lower than conventional estimates based on molecular line studies.

Progress in understanding the extragalactic component

of the gamma-ray flux is still severely limited by the low exposures obtained for the present data. In Chapter 7 the role of extragalactic sources (radio galaxies and rich clusters) was examined. The results are tentative but suggest that the extragalactic flux may be predominantly discrete in nature.

Future gamma-ray observations with increased resolution and exposure will greatly improve our understanding of the gamma-ray emission, both Galactic and extragalactic. In addition a complete CO survey of the Galactic plane will help shed more light on the 2CG sources, particularly in the fourth Galactic quadrant. Detailed studies of more nearby molecular clouds are required to reduce the possible systematic effects present in the analysis of the Orion complex, and to look for further evidence of cosmic ray enhancement or exclusion therin. An extension of the Monte-Carlo technique both to the third and fourth quadrants and to other energy bands will further constrain the discrete source contribution and its energy spectrum.

8.2 The implications for the origin of cosmic rays

We now combine the results of the preceding work in relation to the central question on the origin of the nucleonic component of the cosmic ray flux. The methods of previous workers (Section 3.3) are followed, viz by comparing the unfolded radial gamma-ray emissivity with that expected from cosmic ray interactions with the interstellar medium.

In view of the superior statistical quality of the COS B data over those of SAS II we adopt the radial emissivity unfolded from the COS B data by Mayer-Hasselwander et al. (1982). Attention is restricted to the first Galactic quadrant ($l < 90°$) where coverage of CO emission close to the Galactic plane is extensive.

The observed radial emissivity can be separated into two components, one arising from diffuse processes, the other from discrete sources. Based on the work of Chapter 5 we adopt the supernovae remnant (SNR) distribution of Kodaira (1974) as a reasonable approximation for the gamma-ray source population, with these sources contributing 20% of the inner Galaxy emission. In Figure 8.1 the relative gamma-ray emissivity as a function of Galactocentric radius is plotted, along with the expected source contribution weighted by the SNR distribution.

Also plotted in Figure 8.1 are the radial SNR distribution (Kodaira, 1974), the relative metal abundance $M = [O]/[H]$ (Li et al. 1983) and a possible cosmic ray Galactic density distribution ($\propto \exp - R/6$). The latter is necessarily idealized. Though assuming supernovae are the main sources of Galactic cosmic rays then after allowing for diffusion the cosmic ray distribution will be smoother than that of their sources. For $R > 5$ kpc the exponential cosmic ray variation is likely to be reasonable. From analysis of the local gamma-ray emission several workers find the inferred cosmic ray distribution

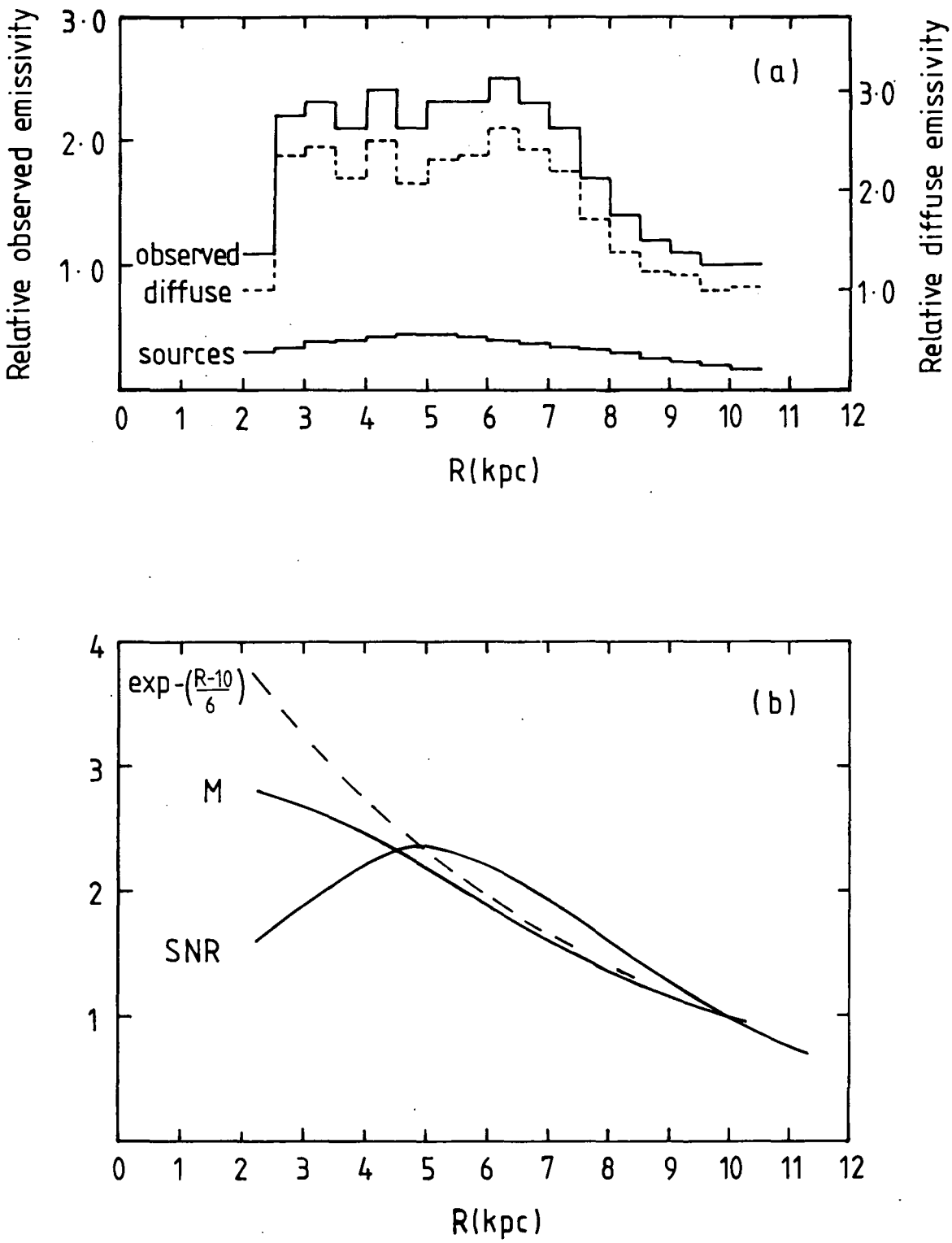

Figure 8.1 (a) The unfolded COS B emissivity $E_\gamma > 100$ MeV. (Mayer-Hasselwander et al., 1982). Local normalization = 2.1 x 10^{-25} ph $cm^{-3}s^{-1}$. The diffuse emissivity is that expected after subtracting a 20% source component. (b) The supernova remnant surface density (Kodaira, 1974) and the metallicity gradient M = $\frac{[O]}{[H]}$ (Li et al., 1983). The exponential represents a possible cosmic ray distribution. All are normalized locally at R = 10 kpc.

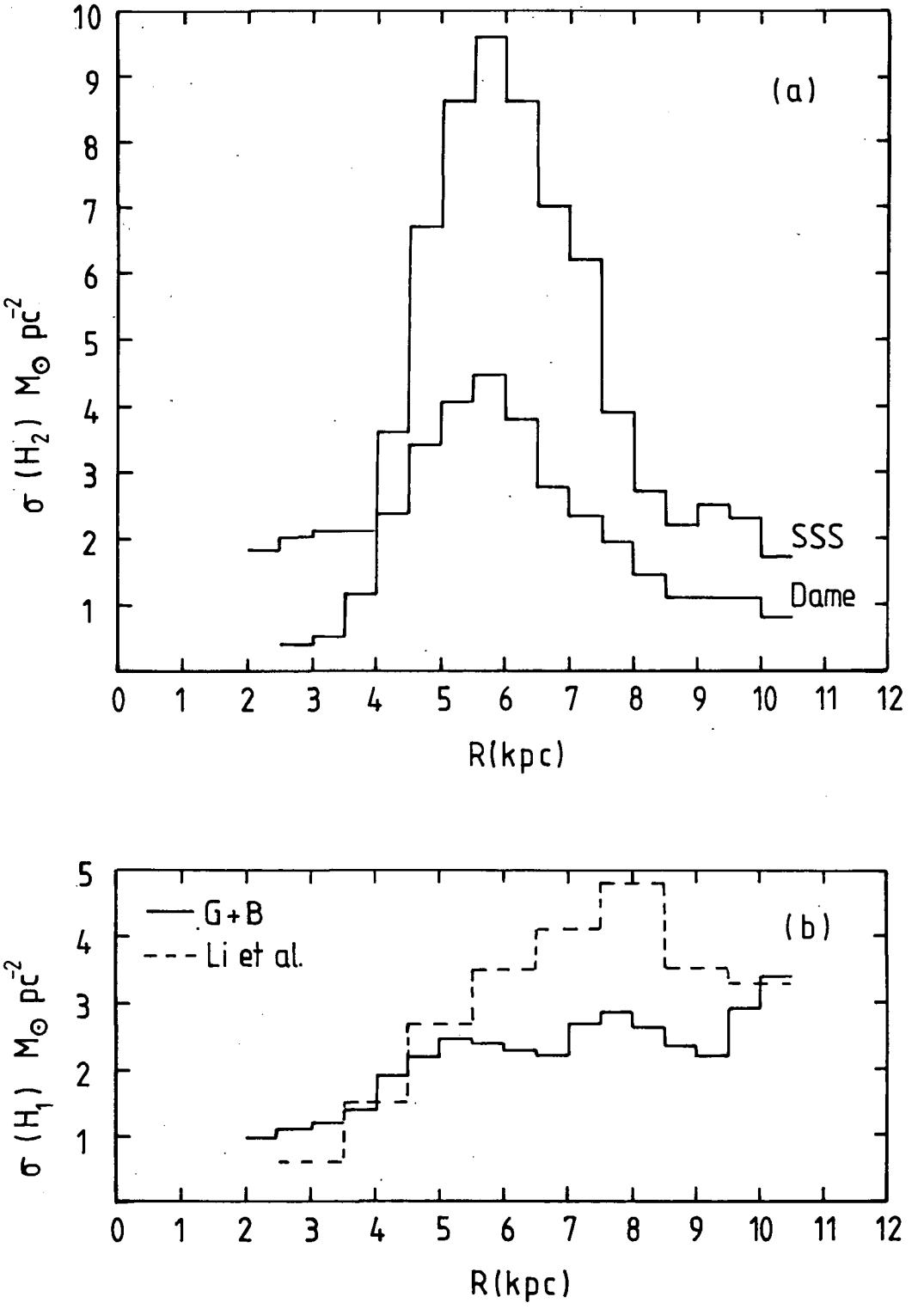

Figure 8.2 (a) The surface densities of H_2 derived from the ^{12}CO surveys by Sanders, Solomon and Scoville (1984a): SSS and Dame (1984). Both are corrected to $\alpha = 3.7 \times 10^{20}$ at cm^{-2} $(K\ kms^{-1})^{-1}$ as described in the text. (b) The surface densities of HI from the data of Gordon and Burton (1976): G + B and Li et al. (1983).

can be approximated by an exponential variation. However for $R < 5$ kpc the situation becomes less certain, especially when we consider the possibility of additional cosmic ray production and diffusion from the region around the Galactic centre.

Radial surface densities of atomic hydrogen, $\sigma(HI)$, have been derived by Gordon and Burton (1976) and Li et al. (1983) for $l < 90^{o}$. These are plotted in Figure 8.2. For 5 kpc $< R <$ 10 kpc the difference between the two distributions reflects the use of different rotation curves for the inner Galaxy and different optical depth corrections. Also plotted in Figure 8.2 are the surface densities of molecular hydrogen, $\sigma(H_2)$, from Sanders, Solomon and Scoville (1984a) (henceforth SSS) and Dame (1984). Both distributions are scaled to our preferred value of $\alpha = 3.7 \times 10^{20}$ at cm^{-2} $(K\ kms^{-1})^{-1}$. The differences in $\sigma(H_2)$ are significant, $\sigma(SSS)/\sigma(Dame) \simeq 2.4$ over 3 kpc $< R <$ 9 kpc. The observed CO intensities of SSS are on average only $\sim$ 30% higher than those of Dame. It is believed that the discrepancy in surface densities arise from differences in the unfolding procedures applied to the repsective data sets (Sanders and Dame, private communication), Dame's data being regarded as unfolded correctly.

We assume Gaussian distributions for the gas normal to the Galactic plane, with $Z_{\frac{1}{2}}(HI) = 130$ pc and $Z_{\frac{1}{2}}(H_2) = 70$ pc locally. For the local gas density this gives

$n(HI + H_2) \simeq 1.1$ at cm^{-3} and 0.8 at cm^{-3} for $\sigma(H_2, SSS)$ and $\sigma(H_2, Dame)$ respectively. For the local gamma-ray emissivity we adopt $q/4\pi(>100\ MeV) = 2.0 \times 10^{-26}$ ph $at^{-1}sr^{-1}s^{-1}$, as estimated in Chapter 6. Thus the local volume emissivities ε_γ (>100 MeV) are

$$\varepsilon_\gamma = 2.0 \times 10^{-25} \text{ ph } cm^{-3}s^{-1} \quad \text{(Dame)}$$

$$\varepsilon_\gamma = 2.8 \times 10^{-25} \text{ ph } cm^{-3}s^{-1} \quad \text{(SSS)}$$

to be compared with the local normalization derived by Mayer-Hasselwander et al. (1982) for the unfolded COS B data:

$$\varepsilon_\gamma = 2.1 \times 10^{-25} \text{ ph } cm^{-3}s^{-1}$$

The gamma-ray emissivity at a distance R from the Galactic centre can be expressed as

$$\varepsilon_\gamma(R) \propto f(R) \left[\sigma(HI; R) + \sigma(H_2; R)/M(R) \right]$$

where f(R) is the ratio of the cosmic ray density relative to the local value times the local gamma-ray emissivity, and the metallicity factor M^{-1} affects the $CO \rightarrow H_2$ conversion (i.e. $N_{H_2} \sim \int Tdv/M$).

Initially we consider the cosmic ray density f(R) to be uniform throughout the Galaxy (corresponding to a metagalactic origin) and the $CO \rightarrow H_2$ conversion to be independent of the metallicity gradient. The diffuse emissivity (Figure 8.1) is compared with that expected using $\sigma(H_2, Dame)$ and both estimates of $\sigma(HI)$, Figure 8.3. For both HI distributions the expected relative emissivities significantly underestimate the observations for $R < 5$ kpc. This may in part be due to the difficulties in unfolding the gas distributions because of velocity

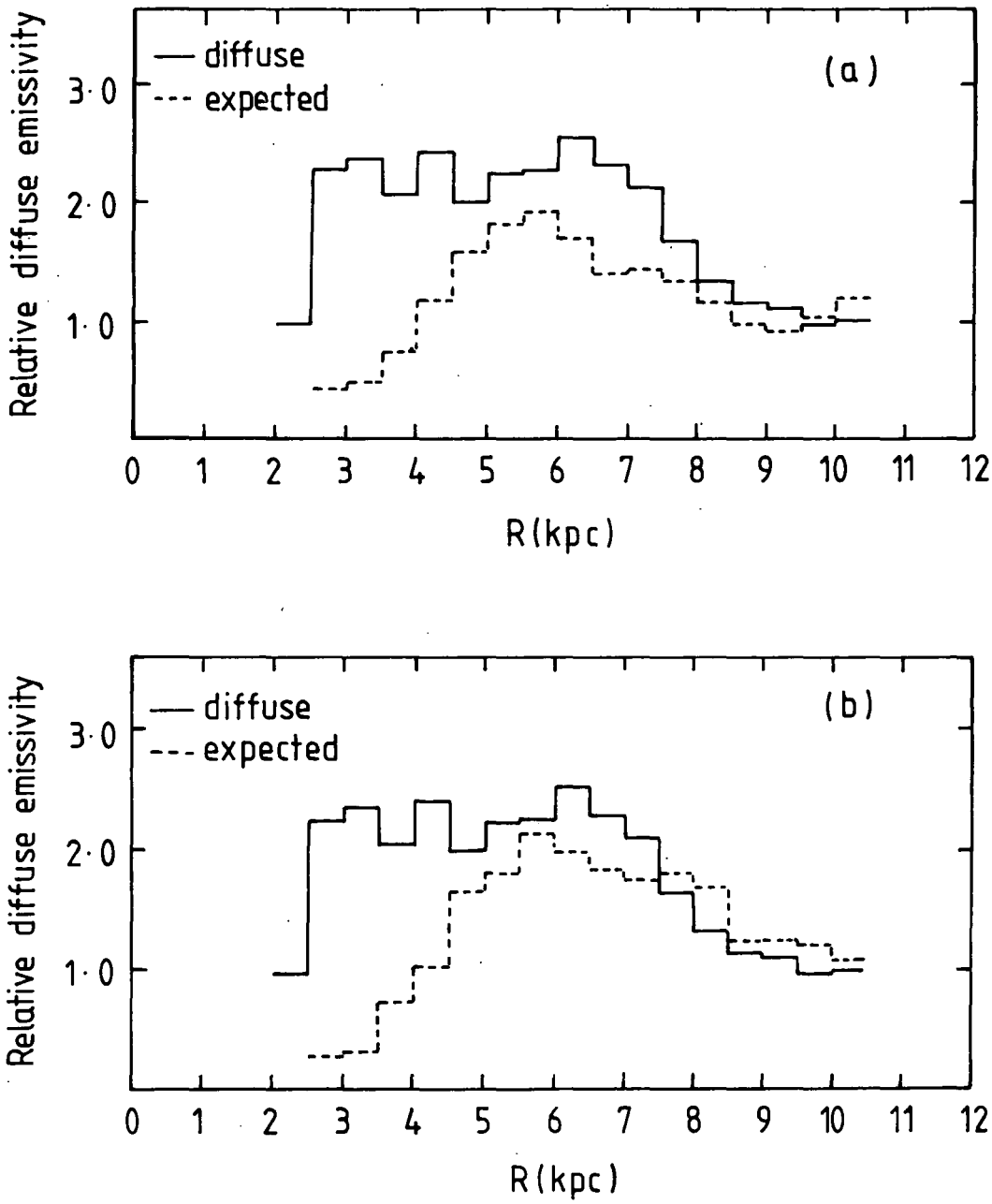

Figure 8.3 The diffuse emissivity of Figure 8.1 compared with that expected from the gas distributions, assuming uniform cosmic ray density and no metallicity effect. (a) σ(HI, Gordon and Burton). (b) σ(HI, Li et al.), both use σ(H_2, Dame).

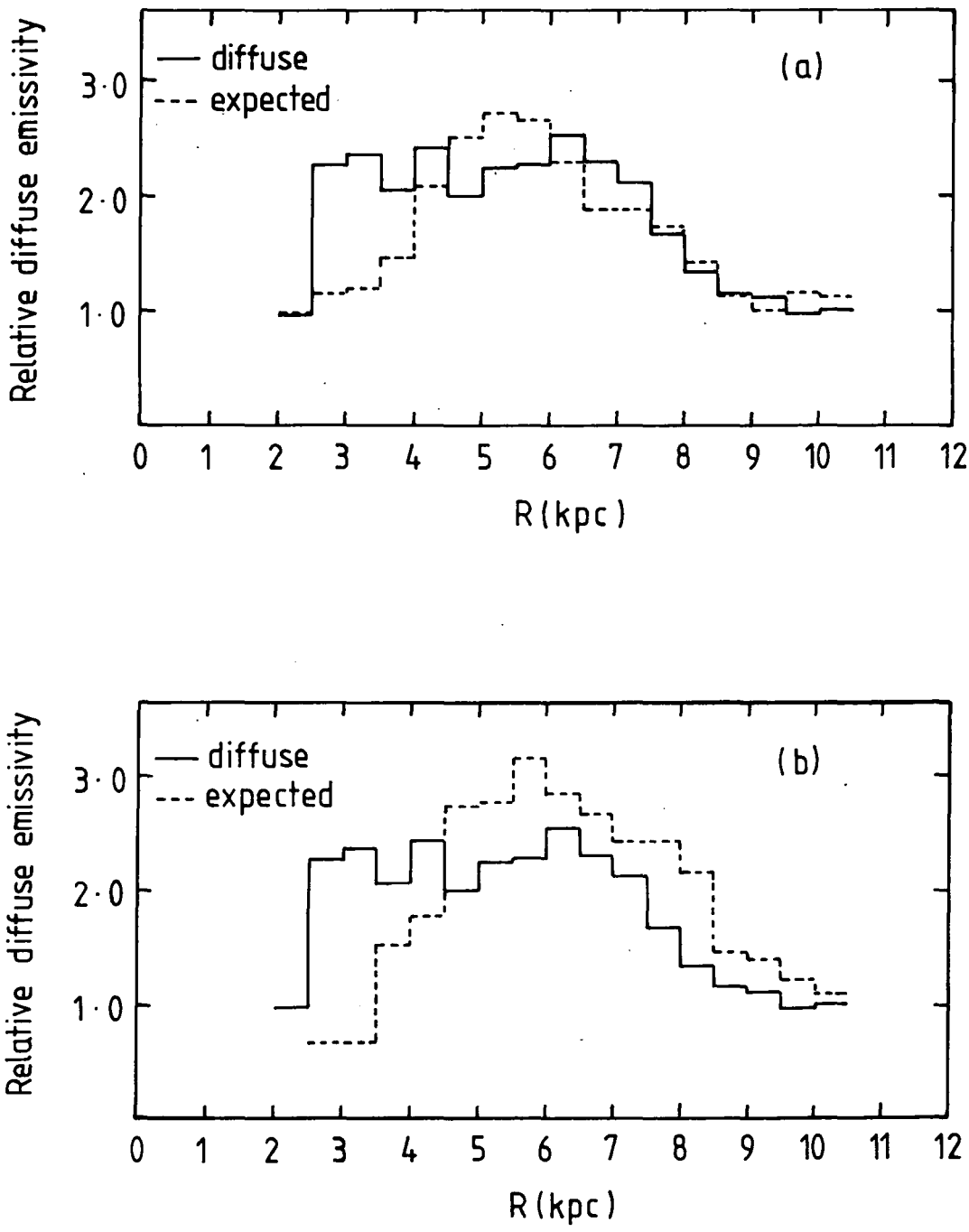

Figure 8.4 The diffuse emissivity of Figure 8.1 compared with that expected from the gas distributions, assuming the cosmic ray density $\propto$ exp $(^{-R}/6)$ and $\sigma(H_2)$ is reduced by the metallicity factor M^{-1}. (a) σ(HI, Gordon and Burton). (b) σ(HI, Li et al.), both use $\sigma(H_2$, Dame).

crowding of the emission profiles and non-circular rotation. For $R > 5$ kpc use of σ(HI, Li et al.) gives the better fit.

Alternatively a Galactic cosmic ray gradient ($\propto \exp - R/6$) is assumed and the metallicity correction applied to $\sigma(H_2)$. For this case the expected diffuse emissivities are compared to the observations in Figure 8.4. Using σ(HI, Gordon & Burton) the agreement is generally good for $R \gtrsim 6$ kpc whereas with σ(HI, Li et al.) the model consistently overestimates the observations for $R \gtrsim 4.5$ kpc. However, for both cases it must be remembered that $f(R) \propto \exp - R/6$ probably overestimates the cosmic ray density for $R < 5$ kpc again leading to reduced emissivities for this region. Use of $\sigma(H_2$, SSS) produces an unacceptable fit with $\mathcal{E}_\gamma$ ($R = 6$ kpc) overestimated by a factor ~ 1.9. Models with only a cosmic ray gradient or a metallicity correction also produce unacceptable fits.

For the region $R \gtrsim 5$ kpc we can be more certain of the unfolded distributions. However, there is still sufficient variation in the estimates of σ(HI) to ensure both the uniform cosmic ray, no metallicity correction model (Figure 8.3b) and the cosmic ray gradient, with metallicity correction model (Figure 8.4a) fit the observations. Other workers consider a gradient likely both in the outer Galaxy and in the local interstellar medium (Section 3.3). The present work indicates that a large scale Galactic cosmic ray gradient can only be

accommodated by allowing for the effect of the metallicity gradient on the CO $\rightarrow H_2$ conversion. Finally we note the constraints placed on the mass of H_2 in the inner Galaxy by the gamma-ray data. For 2.5 kpc $< R <$ 10.5 kpc $M(HI) \simeq (1.5 - 2.1) \times 10^9 M_\odot$, depending on the assumed radial distribution (Figure 8.2). Taking Dame's data on $\sigma(H_2)$ (corrected for our value of $\alpha = 3.7 \times 10^{20}$ at cm^{-2} $(K\ kms^{-1})^{-1}$) $M(H_2)$ $1.2 \times 10^9 M_\odot$ over 2.5 kpc $<$ $R <$ 10.5 kpc. For the preferred combination of cosmic ray gradient and metallicity dependent conversion factor then $M(H_2)$ is reduced to $\simeq 0.8 \times 10^9 M_\odot$ over the same region.

APPENDICES A1 - A6

Source	$q/4\pi \times 10^{-26}$ ph $at^{-1}sr^{-1}s^{-1}$ (35–100 MeV)	(100 MeV)	Comments
Fichtel et al. (1978a)	4.3 ± 1.5	3.0 ± 0.8	$\|b\|>12.8°$, $I_\gamma \propto N_{HI}$
Lebrun and Paul (1980)	3.0 ± 0.2	2.0 ± 0.15	$\|b\|>10°$, $I_\gamma \propto N_{H_t}$ (N_G)
Issa et al. (1981)		2.2 ± 0.3	$\|b\|>10°$, $I_\gamma \propto N_{HI} + 2N_{H_2}$
Thompson and Fichtel (1982)	3.4 ± 0.5	1.8 ± 0.2	$\|b\|>10°$, $I_\gamma \propto N_{H_t}$ (N_G)
Lebrun and Paul (1983)	1.8 ± 0.1 2.4 ± 0.2	2.1 ± 0.1 2.4 ± 0.2	$\|b\|>10°$, $I_\gamma \propto N_{HI}$ $I_\gamma \propto N_{H_t}$ (N_G)
This work (Chapter 7)	2.5 ± 0.5	2.0 ± 0.2	$\|b\|>9.6°$, $I_\gamma \propto N_{H_t}$ (N_G)

TABLE A.1

Local emissivities ($\pm 1\sigma$) derived from the SAS II data. All analyses assume the cosmic ray intensity is constant along the line of sight and compare the gamma-ray intensity I_γ with the total gas column density. Column densities are estimated either directly, N_{HI} $(+2N_{H_2})$, or indirectly from galaxy counts N_{H_t} (N_G).

Source	(70–150 MeV)	(150–300 MeV)	(300–5000 MeV)	(>100 MeV)	
Mayer-Hasselwander et al. (1982)				1.67	$\|b\|<10°$, $I_\gamma \propto N_{HI}$ *
Lebrun et al. (1982)				2.1 ± 0.3	$10°<\|b\|<20°$, $I_\gamma \propto N_{H_t}$ (N_G)
Strong et al. (1982)	1.4	0.53	0.59	(1.8)	$11°<\|b\|<20°$, $I_\gamma \propto N_{H_t}$ (N_G)
Strong (1984)	1.55,1.76	0.93,0.83	0.85,0.55	(2.4)	$10°<\|b\|<20°$ } $I_\gamma \propto N_{HI} + N_{H_2}$
Strong (1984)	1.27,1.48	0.80,0.70	0.75,0.48	(2.1)	$10°<\|b\|<20°$ } $N_{H_2} = N_{H_t}(N_G) - N_{HI}$

TABLE A.2

As Table A.1, but for the COS B data. Strong (1984) derives the emissivities for N_{HI}, $2N_{H_2}$ separately. Two calibrations of the $N_{H_t}(N_G)$ relation are employed. The former (Strong and Lebrun, 1982) resulting in higher emissivities than the latter (Strong, 1984).

Source	α_{20}	Derivation
Gordon and Burton (1976)	4.6	Comparison of optical extinction with CO emission in rotating dust globules.
Blitz (1978)	15.0	Dark cloud derivation.
Solomon, Sanders and Scoville (1979)	12.0	Radiative transfer analysis of inner Galaxy clouds.
Solomon, Scoville and Sanders (1979)	7.2	non-LTE analysis of inner Galaxy clouds.
Blitz and Thaddeus (1980)	7.8	Comparison of extinction in Rosette Nebula with ^{13}CO emission.
Blitz and Shu (1980)	3.6	Comparison of dark cloud extinctions with ^{13}CO emission.
Young and Scoville (1982)	8.0	Comparison of Wco with N_{H_2} derived from extinction (dark clouds) and LTE analysis (GMC cores).
List (1982)	10.0	Comparison of Wco with N_{H_2} for Ophiucus and mean cloud parameters.
Lebrun et al. (1983)	2.0-6.0	Gamma-ray analysis of 1st Galactic quadrant $\|b\| < 5.5°$.
Sanders, Scoville and Solomon (1984)	9.2	Virial theorem analysis of inner Galaxy clouds.
Sanders, Solomon and Scoville (1984a)	7.2	Comparison of dark cloud extinction with ^{13}CO emission.
Bloemen et al. (1984b).	5.2	Gamma-ray analysis of Orion region.
Bhat et al. (1984b)	2.3	Galaxy count analysis towards nearby clouds.
This work	3.7 ± 0.6	Gamma-ray analysis of Orion clouds.

TABLE A.3

Summary of previously adopted conversion factors $\alpha_{20} = 2N_{H_2} / \int Tdv/10^{20}$ at cm^{-2} $(K\ kms^{-1})^{-1}$ and their derivation.

TABLES A.4, A.5

The parameters of the two radio source samples. The weak radio sources (Table A.4) are those for which 10^{-10} ph cm^{-2}s^{-1} $\leq F_\gamma$, expected (>100 MeV) $<$ 10^{-8} ph cm^{-2}s^{-1}. The strong radio sources are those for which F_γ, expected (>100 MeV) $\geq 10^{-8}$ ph cm^{-2}s^{-1} (see Section 7.8). Two measures of the synchrotron flux are used : S_ν the flux at 5GHz (1 Jy = 10^{-26} W Hz^{-1} m^{-2}) or the radiated power P (W Hz^{-1}) at 408 MHz. The spectral index α is obtained from the spectral flux $S_\nu \propto \nu^{-\alpha}$ using additional measurements at 178 MHz (Jenkins et al., 1977). The distances are for the optical counterparts (H_o = 50 kms^{-1} Mpc^{-1}, $q_o = \frac{1}{2}$). The minimum energy W_{min} and the gamma-ray luminosity L_γ (>100 MeV) are derived from the minimum energy requirements for each source (Section 7.4).

Those clusters marked with an asterisk (*) do not meet the requirements for inclusion in Abell's complete statistical sample.

TABLE A4

Source	l^{II}, b^{II}	S_ν(5GHz) Jy	log P(408) W Hz^{-1}	α	r(Mpc)	W_{min} erg	L_γ(>100 MeV) ph s^{-1}	$F_\gamma \times 10^{-8}$ $phcm^{-2}s^{-1}$	Comments
3C123	170.6,-11.7	6.6		1.0	2000	6.2×10^{60}	3.9×10^{48}	0.81	20^m galaxy
3C236	190.1, 54.0	1.48		0.6	550	2.4×10^{59}	1.5×10^{47}	0.41	DE4 galaxy
3C295	97.5, 60.8	3.6		0.9	2070	3.8×10^{60}	2.4×10^{48}	0.46	21^m galaxy
3C346	35.3, 35.8	1.28		0.6	580	2.5×10^{59}	1.6×10^{47}	0.39	16^m galaxy
3C388	74.7, 20.2	0.79		1.0	520	4.2×10^{59}	2.6×10^{47}	0.81	15^m D3 galaxy
3C293	54.6, 76.1	1.7		0.6	260	1.1×10^{59}	6.9×10^{46}	0.84	14.5^m galaxy
3C273	289.9, 64.4		26.55	0.45	733	2.9×10^{59}	1.8×10^{47}	0.28	quasar
3C218	242.9, 25.1		26.14	0.82	349	2.0×10^{59}	1.3×10^{47}	0.85	CD2 galaxy in cluster A780 (Hydra A)
4C10. 35A	317.8, 72.8		26.07	0.69	690	1.6×10^{59}	1.0×10^{47}	0.18	A1684
4C10. 43.1A	17.1, 48.1		26.02	0.65	774	1.5×10^{59}	9.4×10^{46}	0.13	A2091
4C12.76	70.1,-31.8		26.39	1.1	774	3.8×10^{59}	2.4×10^{47}	0.33	A2396*
4C13. 17A	164.2,-38.9		25.17	0.64	340	4.9×10^{58}	3.1×10^{46}	0.22	A401
4C15. 39E	258.6, 73.8		26.06	0.7	690	1.6×10^{59}	1.0×10^{47}	0.18	A1462
4C15.53	28.8, 44.5		24.80	0.44	203	2.9×10^{58}	1.8×10^{46}	0.36	A2147
4C17.66	29.9, 44.0		24.87	0.60	182	3.2×10^{58}	2.0×10^{46}	0.51	A2151
4C17.89	76.1,-34.6		25.64	1.90	512	4.4×10^{59}	2.8×10^{47}	0.87	A2433*
4C18. 41F	24.7, 56.6		25.43	0.73	410	7.3×10^{58}	4.6×10^{46}	0.23	A2036*
4C21. 13	169.6,-24.6		26.13	0.49	747	1.7×10^{59}	1.1×10^{47}	0.16	A468*

Source	l^{II}, b^{II}	S_ν(5GHz) Jy	log P(408) W Hz^{-1}	α	r(Mpc)	W_{min} erg	L_γ(>100 MeV) ph s^{-1}	$E_\gamma \times 10^{-8}$ ph $cm^{-2}s^{-1}$		Comments
4C21.44A	28.9, 60.2		25.68	1.4	690	2.3×10^{59}	1.4×10^{47}	0.25	A2009	
4C25.36	216.2, 75.6		24.11	0.75	512	1.3×10^{58}	8.1×10^{45}	0.03	A1380	
4C26.35A	213.5, 78.1		26.37	0.66	690	2.4×10^{59}	1.5×10^{47}	0.26	A1425	
4C26.42	33.8, 77.2		25.69	0.7	340	1.0×10^{59}	6.3×10^{46}	0.45	A1795	
4C27.50	99.7,-31.3		26.20	0.35	590	1.8×10^{59}	1.1×10^{47}	0.27	A2584*	
4C27.53A	102.8,-32.4		24.80	1.1	328	4.7×10^{58}	2.9×19^{46}	0.23	A2622*	
4C29.41B	201.5, 69.0		25.55	0.56	266	7.8×10^{58}	4.9×10^{46}	0.52	A1213	
4C32.52A	54.8, 36.6		24.98	0.75	340	4.1×10^{58}	2.6×10^{46}	0.18	A2241*	
4C34.45	57.6, 35.0		25.36	0.75	420	6.8×10^{58}	4.3×10^{46}	0.20	A2249*	
4C35.06A	150.6,-19.9		25.13	0.84	258	5.4×10^{58}	3.4×10^{46}	0.42	A407*	
4C35.16A	182.2, 18.3		25.31	1.05	310	8.7×10^{58}	5.4×10^{46}	0.47	A568*	
4C37.48	60.8, 41.8		26.43	0.8	804	2.9×10^{59}	1.8×10^{47}	0.23	A2214*	
4C38.29B	67.2, 67.5		25.83	2.0	690	6.5×10^{59}	4.1×10^{47}	0.71	A1914	
4C39.29	182.6, 55.9		25.15	0.75	690	5.1×10^{58}	3.2×10^{46}	0.06		
4C39.49.1	64.0, 35.6		25.56	0.95	335	1.1×10^{59}	6.9×10^{46}	0.53	A2250	
4C41.23	217.7,-40.7		25.80	0.75	387	1.2×10^{59}	7.5×10^{46}	0.42	A490	
4C41.24	136.0, 75.5		26.27	0.75	774	2.2×10^{59}	1.4×10^{47}	0.19	A1562	
4C41.26	92.6, 73.5		26.68	0.75	1604	3.8×10^{59}	2.4×10^{47}	0.08	A1763	
4C46.23	153.3, 66.6		26.33	0.75	750	2.4×10^{47}	1.5×10^{47}	0.22	A1361	
4C50.33	147.6, 64.1		25.48	0.75	747	7.9×10^{58}	4.9×10^{46}	0.07		
4C51.29.1	139.8, 63.8		25.47	0.74	340	7.7×10^{58}	4.8×10^{46}	0.35	A1452*	
4C57.37B	82.0, 40.8		25.88	0.69	549	1.3×10^{59}	8.1×10^{46}	0.22	A2220*	
4C55.29A	96.1, 56.2		25.97	0.76	633	1.5×10^{59}	9.4×10^{46}	0.24	A1940	
4C58.23C	135.3, 57.9		26.61	0.82	633	3.7×10^{59}	2.3×10^{47}	0.48	A1446	

Source	l^{II}, b^{II}	S_ν(5GHz) Jy	log P(408) W Hz^{-1}	α	r(Mpc)	W_{min} erg	L_γ(>100 MeV) ph s^{-1}	$F_\gamma \times 10^{-8}$ ph $cm^{-2}s^{-1}$		Comments
4C64.20.1A	94.0, 34.9		25.12	1.1	295	7.2×10^{58}	4.5×10^{46}	0.43	A2255	
4C66.07A	149.4, 33.0		25.98	1.1	660	2.2×10^{59}	1.4×10^{47}	0.27	A629	
4C67.21D	125.7, 49.9		26.36	0.87	690	2.8×10^{59}	1.8×10^{47}	0.31	A1559	
4C68.21	99.2, 28.0		26.03	0.57	633	1.5×10^{59}	9.4×10^{46}	0.19		
4C69.10	145.5, 26.1		24.53	0.75	451	2.3×10^{58}	1.4×10^{46}	0.06	A564*	
4C74.20.1	109.9, 38.7		24.79	0.75	690	3.2×10^{58}	2.0×10^{46}	0.04	A2105	

TABLE A5

Source	l^{II}, b^{II}	S_ν(5GHz) Jy	log P(408) W Hz^{-1}	α	r(Mpc)	W_{min} erg	L_γ(>100 MeV) ph s^{-1}	$F_\gamma \times 10^{-8}$ ph $cm^{-2} s^{-1}$	Comments
3C305	103.2, 49.1	0.57		1.0	240	1.3×10^{59}	8.1×10^{46}	1.2	peculiar galaxy
3C433	74.5,-17.7	3.9		0.8	570	6.5×10^{59}	4.1×10^{47}	1.0	
3C430	99.7, 8.0	0.38		1.3	320	3.3×10^{59}	2.1×10^{47}	1.7	15^m elliptical galaxy
3C31	126.8,-30.3	0.14		1.4	100	7.2×10^{58}	4.5×10^{46}	3.7	NGC 383 DE3 galaxy
3C98	179.9,-31.1	2.9		0.8	180	1.6×10^{59}	1.0×10^{47}	2.5	ED3 galaxy
3C264	235.7, 73.0	0.4		1.3	120	1.0×10^{59}	6.3×10^{46}	3.7	NGC 3862 DE1 galaxy in A1367 (Coma)
3C272.1	278.2, 74.5	0.35		1.2	17	8.5×10^{57}	5.3×10^{45}	15.0	M84 E2 galaxy in Virgo
3C449	95.5,-15.9	0.05		1.6	110	7.7×10^{58}	4.8×10^{46}	3.3	
3C111	161.7,-8.8	3.3		0.9	290	3.2×10^{59}	2.0×10^{47}	2.0	19^m N galaxy
3C405.0	76.2, 5.8		27.62	0.77	316	1.3×10^{60}	8.1×10^{47}	7.0	Cygnus A
3C384	63.4,18.0		26.39	1.0	398	3.4×10^{59}	2.1×10^{47}	1.1	Hercules A
4C12.76	74.1,-34.4		25.77	2.21	747	1.2×10^{60}	7.5×10^{47}	1.1	
4C26.64	103.5,-33.1		25.90	0.74	171	1.4×10^{59}	8.8×10^{46}	2.4	
4C39.45	62.9, 43.7		25.93	1.34	177	2.9×10^{59}	1.8×10^{47}	4.8	
4C41.07	150.4,-13.4		25.58	0.71	100	8.7×10^{58}	5.4×10^{46}	4.6	

TABLE A.6

The parameters of the Abell cluster sample used in the present analysis (l^{II}, b^{II}) are the Galactic coordinates of the cluster centres. The distance and richness classes are defined by Abell (1958) (see Table 7.2).

TABLE A6

Abell No.	l^{II} b^{II}	Distance class	Richness class
21	114.8, -34.7	4	1
260	137.2, -29.0	4	1
399	164.6, -40.5	3	1
400	170.2, -45.9	1	1
415	194.2, -59.9	4	1
426	150.4, -14.4	0	2
449	133.7, 16.2	4	1
496	209.6, -37.5	3	1
526	194.3, -22.8	4	1
539	195.7, -18.7	2	1
574	219.4, -37.0	3	2
592	210.2, 15.6	3	1
754	239.3, 24.8	3	2
787	137.9, 36.2	4	2
957	243.0, 42.9	4	1
978	250.0, 40.4	3	1
1020	232.7, 52.3	4	1
1035	179.4, 58.5	3	2
1126	227.5, 61.0	4	1
1185	203.0, 67.8	2	1
1187	175.6, 65.9	3	1
1213	201.5, 69.0	2	1
1216	263.8, 51.1	4	1
1228	186.9, 69.4	1	1
1238	260.0, 56.4	4	1
1254	132.4, 44.5	3	1
1364	270.8, 56.8	4	1
1365	194.5, 74.9	4	1
1367	234.8, 73.0	1	2
1377	140.6, 59.1	3	1
1382	129.9, 44.8	4	1
1399	274.9, 56.4	4	2
1436	136.9, 59.5	3	1
1468	139.5, 64.2	4	1
1474	261.0, 74.2	4	1
1496	131.9, 57.2	4	1

Abell No.	l^{II}	b^{II}	Distance class	Richness class
1541	284.6,	70.9	4	1
1644	304.9,	45.3	4	1
1651	306.7,	58.6	4	1
1656	58.2,	88.0	1	2
1691	105.2,	77.2	3	1
1749	88.0,	76.8	4	1
1767	112.5,	57.0	4	1
1773	331.1,	62.3	3	1
1775	31.9,	78.7	4	2
1793	59.1,	76.6	4	1
1795	33.8,	77.2	4	2
1809	339.5,	63.6	4	1
1831	40.1,	75.0	3	1
1837	329.3,	48.1	4	1
1904	89.7,	62.3	3	2
1913	12.5,	65.6	4	1
1927	34.9,	67.7	4	1
1983	19.0,	60.1	3	1
1991	22.8,	60.5	3	1
1999	91.9,	54.8	4	1
2005	41.8,	61.8	4	2
2022	43.3,	60.7	3	1
2028	8.4,	51.9	4	1
2029	5.5,	50.6	4	2
2063	12.9,	49.7	3	1
2065	42.9,	56.6	3	2
2067	48.7,	56.8	4	1
2089	43.9,	54.4	4	1
2092	49.4,	54.6	4	1
2107	34.4,	51.5	4	1
2124	57.7,	52.3	3	1
2142	44.2,	48.7	4	1
2147	28.8,	44.5	1	1
2175	49.3,	44.4	4	1
2197	64.8,	43.8	1	1
2199	61.9	43.7	1	2
2255	94.0,	34.9	3	2
2256	111.1,	31.7	3	2
2312	99.0,	24.9	4	1

Abell No.	l^{II}, b^{II}	Distance class	Richness class
2315	100.8, 25.6	4	1
2319	75.7, 13.6	3	1
2328	28.8, -34.6	4	2
2382	38.9, -47.9	4	1
2384	33.5, -49.4	4	1
2399	67.4, -35.3	3	1
2410	48.0, -47.6	4	1
2634	103.5, -34.1	1	1

REFERENCES

Abell, G.O., 1958, Astrophys. J. Suppl., 3, 211.

Abrampoulous, F., and Ku, W.H.M., 1983, Astrophys. J., 271, 446.

Allen, C.W., 1973, "Astrophysical Quantities", Athlone Press.

Arnaud, K., Li, T.P., Riley, P.A., Wolfendale, A.W., Dame T., Brock, J.E., and Thaddeus, P., 1982, Mon. Not. R. astr. Soc., 201, 745.

Austen, T.B., and Peach, J.V., 1974, Mon. Not. R. astr. Soc., 168, 591.

Ayre, C.A., Bhat, P.N., Owens, A., Summers, W.M., and Thompson, M.G., 1981, Phil. Trans. R. Soc. Lond., A301, 687.

Bachall, N.A., and Soneira, R.M., 1983, Astrophys. J., 270, 20.

Bartla, N.A., Wilson, T.L., Bastein, P., and Ruf, K., 1983, Astron. Astrophys., 128, 279.

Beck, R., and Grave, R., 1982, Astron. Astrophys., 105, 192.

Beckwith, S., Persson, S.E., and Neugebauer, G., Astrophys. J., 1979, 227, 436.

Beckwith, S., Evans, N.J., Gatley, I., Gull, G., and Russel, R.W., 1983, Astrophys. J., 264, 152.

Berger, M., Gehrz, R.D., and Hackwell, J.A., 1981, Astrophys. J., 248, 963.

Bertsch, D.L., and Kniffen, D.A., 1983, Astrophys. J., 270, 305.

Bhat, P.N., Gupta, S.K., Ramana Murthy, P.V., Sreekantan, B.V., Tonwar, S.C., and Viswanath, P.R., 1980a, Astron. Astrophys., 81, L3.

Bhat, C.L., Sparu, M., and Kaul, C., 1980b, Nature, 288, 136.

Bhat, C.L., Mayer, C.J., and Wolfendale, A.W., 1984a, Astron. Astrophys. (in the press).

Bhat, C.L., Issa, M.R., Houston, B.P., Mayer, C.J., and Wolfendale, A.W., 1984b, Nature (submitted).

Bhat, C.L., et al., 1984c (in preparation).

Bhat, C.L., Sapru, M.L., and Razdan, H., 1984d (in preparation).

Bignami, G,F., Fichtel, C.E., Kniffen, D.A., and Thompson, D.J., 1975, Astrophys. J., 199, 54.

Bignami, G.F., Bennett, K., Buccheri, R., Caraveo, P.A., Hermsen, W., Kanbach, G., Lichti, G.G., Masnou, J.L., Mayer-Hasselwander, H.A., Paul, J.A., Sacco, B., Scarsi, L., Swannenburg, B.N., and Wills, R.D., 1981, Astron. Astrophys., 93, 71.

Bignami, G.F., and Hermsen, W., 1983, Ann. Rev. Astron. Astrophys., 211, 67.

Bignami, G.F., Caraveo, P.A., and Lamb, R.C., 1983, Astrophys. J., 272, L13.

Bignami, G.F., 1984 (preprint).

Bignami, G.F., Caraveo, P.A., and Paul, J.A., 1984, Nature, 310, 464.

Blaauw, A., 1964, Ann. Rev. Astron. Astrophys., 2, 213.

Black, J.H., and Fazio, G.G., 1973, Astrophys. J., 185, L7.

Blitz, L., 1978, Ph.D. Thesis, Columbia University.

Blitz, L., and Shu, F.H., 1980, Astrophys. J., 238, 148.

Blitz, L., and Thaddeus, P., 1980, Astrophys. J., 241, 676.

Bloemen, J.B.G.M., Blitz, L., and Hermsen, W., 1984a, Astrophys. J., 279 , 136.

Bloemen, J.B.G.M., et al., 1984b, Astron. Astrophys. (submitted).

Bloemen, J.B.G.M., Caraveo, P.A., Hermsen, W., Lebrun, F., Maddalena, R.J., Strong, A.W., and Thaddeus, P., 1984c, Astron. Astrophys., 139, 37.

Bohlin, R.C., Savage, B.D., and Drake, J.F., 1978, Astrophys. J., 224, 132.

Bothe, W., and Kolhorster, W., 1929, Zeitschrift fur Physik, 56, 751.

Buccheri, R., Bennett, K., Bignami, G.F., Bloemen, J.B.G.M., Caraveo, P.A., Hermsen, W., Kanbach, G., Masnou, J.L., Mayer-Hasselwander, H.A., Özel, M.E., Paul, J.A., Sacco, B., Scarsi, L., Strong, A.W., Boriakoff, V., and Manchester, R.N., 1983, Astron. Astrophys., 128, 245.

Buffington, A., Schindler, S.M., and Pennypacker, C.R., 1981, Astrophys. J., 248, 1179.

Caraveo, P.A., and Paul, J.A., 1979, Astron. Astrophys., 75, 340.

Caraveo, P.A., Bennett, K., Bignami, G.F., Hermsen, W., Kanbach, G., Lebrun, F., Masnou, J.L., Mayer-Hasselwander, H.A., Paul, J.A., Sacco, B., Scarsi, L., Strong, A.W., Swannenburg, B.N., and Wills, R.D., 1980, Astron. Astrophys., 91, L3.

Caraveo, P.A., Bignami, G.F., Vigroux, L., and Paul, J.A., 1984, Astrophys. J., 276, L45.

Cesarsky, C.J., and Volk, H.J., 1978, Astron. Astrophys., 70, 367.

Cesarsky, C.J., and Lagage, P.O., 1983, Astron. Astrophys., 125, 249.

Cline, T.L., and Desai, U.D., 1976, Astrophys. Space Sci., 42, 117.

Cohen, R.S., and Thaddeus, P., 1977, Astrophys. J., 217, L155.

Cohen, R.S., Tomasevitch, G.R., and Thaddeus, P., 1979, IAU Symp. 84, "The Large Scale Structure of the Galaxy", ed. W.B. Burton, Dordrecht : Reidel, p.53.

Cohen, R.S., Cong, H., Dame, T.M., and Thaddeus, P., 1980, Astrophys. J., 239, L59.

Colgate, S.A., 1968, Can. J. Phys., 46, 5476.

Dame, T.M., 1984, Ph.D. Thesis, Columbia University.

Danaher, S., Fegan,, D.J., Porter, N.A., and Weekes, T.C., 1981, Nature, 289, 568.

Dean, A.J., and Ramsden, D., 1981, Phil. Trans. R. Soc. Lond., A301, 577.

Dennison, B., 1980, Astrophys. J., 239 , L93.

Dewey, R.J., Uson, J.M., Weisberg, J.M., Wilkinson, D.T., and Stark, A.A., 1983, Astron. J., 88, 1832.

Dickey, J.M., 1983, Astrophys. J., 273, L71.

Dickman, R.L., 1978, Astrophys. J. Suppl., 37, 407.

Dodds, D., Strong, A.W., and Wolfendale, A.W., 1975, Mon. Not. R. astr. Soc., 171, 569.

Dogiel, V.A., Kiraly, P., Freedman, I., and Wolfendale, A.W., 1983, Proc. 18th ICRC, Bangalore, 2, 292.

Dowthwaite, J.C., Gibson, A.I., Harrison, A.B., Kirkman, I.W., Lotts, A.P., Macrae, J.H., Orford, K.J., Turver, K.E., and Walmsley, M., 1983, Astron. Astrophys., 126, 1.

Dowthwaite, J.C., Harrison, A.B., Kirkman, I.W., Macrae, J.H., Orford, K.J., Turver, K.E., and Walmsley, M., 1984, Astron. Astrophys., 136, L14.

Erikson, R.A., Fickle, R.K., and Lamb, R.C., 1976, Astrophys. J., 210, 539.

Felten, J.E., and Morrison, P., 1963, Phys. Rev. Lett., 10, 453.

Fichtel, C.E., Hartman, R.C., Kniffen, D.A., Thompson, D.J., and Bignami, G.F., 1975, Astrophys. J., 198, 163.

Fichtel, C.E., Kniffen, D.A., Thompson, D.J., Bignami, G.F., and Cheung, C.Y., 1976, Astrophys. J., 208, 211.

Fichtel, C.E., Hartman, R.C., Kniffen, D.A., and Thompson, D.J., 1977, Astrophys. J., 217, L9.

Fichtel, C.E., Simpson, G.A., and Thompson, D.J., 1978a, Astrophys. J., 222, 833.

Fichtel, C.E., Hartman, R.C., Kniffen, D.A., Thompson, D.J., Ogelman, H.B., Tumer, T., and Ozel, M.E., 1978b, NASA Tech. Memo. 79650.

Fichtel, C.E., and Kniffen, D.A., 1984, Astron. Astrophys., 134, 13.

Fomalont, E.B., and Rogstad, D.H., 1966, Astrophys. J., 146, 528.

Galper, A.M., Kirillov-Ugryumov, V.G., Kurochkin, A.V., Leikov, P.V., Luchkov, B.I., Yurkin, Uy. L., Fomin, V.P., Nespor, Yu. I., Stepanian, A.A., and Vladimirsky, B.M., 1977, Proc. 15th ICRC, Plovdiv, 1, 131.

Ginzburg, V.L., 1968, Astrophys. Space Sci., 1, 1.

Ginzburg, V.L., and Syrovatskii, S.I., 1964, "The Origin of Cosmic Rays", Pergamon Press.

Gordon, C.P., 1970, A.J., 75, 914.

Gordon, M.A., and Burton, W.B., 1976, Astrophys. J., 208, 346.

Grindlay, J.E., Helmken, H.F., Hanbury-Brown, R., Davis, J., and Allen, L.R., 1975, Astrophys. J., 201, 82.

Grindlay, J.E., Helmken, H.F., and Weekes, T.C., 1976, Astrophys. J., 209, 592.

Gursky, H., and Schwartz, D.A., 1977, Ann. Rev. Astron. Astrophys., 15, 541.

Gursky, H., Solinger, A., Kellog, E., Murray, S., Tananbaum,H., Giacconi, R., and Cavaliere, A., 1972, Astrophys. J., 173, L99.

Harding, A.K., 1981, Astrophys. J., 247, 639.

Hartman, R.C., Kniffen, D.A., Thompson, D.J., Fichtel, C.E., Ogelman, H.B., Tumer, T., and Ozel, M.E., 1979, Astrophys. J., 230, 597.

Haslam, C.G.T., Kearsey, S., Osborne, J.L., Phillips, S., and Stoffel, H., 1981, Nature, 289, 470.

Hawley, S.A., 1978, Astrophys. J., 224, 417.

Hayakawa, S., 1952, Prog. Theor. Phys., 8, 571.

Heiles, C., and Habing, H.J., 1974, Astron. Astrophys. Suppl., 14, 1.

Helmken, H.F., Fazio, G.G., O'Mongain, E., and Weekes, T.C., 1973, Astrophys. J., 184, 245.

Hermsen, W., 1980, Ph.D. Thesis, University of Leiden.

Hermsen, W., 1983, Space Sci. Rev., 36, 61.

Hess, V.F., 1912, Physk. Zeitchr., 13, 1804.

Houston, B.P., and Wolfendale, A.W., 1984a, J. Phys. G., 10, 1587.

Houston, B.P., and Wolfendale, A.W., 1984b, J. Phys. G. (in the press).

Hubble, E.P., 1933, Mt. W. Contr., 21, 139.

Hurley, K., 1983, Adv. Space Res., 3, 163.

Hutchinson, G.E., 1952, Phil. Mag., 43, 847.

Issa, M.R., and Wolfendale, A.W., 1981a, J. Phys. G., 7, L187.

Issa, M.R., and Wolfendale, A.W., 1981b, Nature, 292, 430.

Issa, M.R., Riley, P.A., Strong, A.W., and Wolfendale, A.W., 1981, J. Phys. G., 7, 973.

Jenkins, C.J., Pooley, G.C., and Riley, J.M., 1977, Mem. R. astr. Soc., 84, 61.

Jennings, M.C., 1982, Astrophys. J., 258, 110.

Johnson, W.N., and Hames, R.C., 1973, Astrophys. J., 250, 389.

Jones, C., and Forman, W., 1984, Astrophys. J., 276, 38.

Kellog, E.M., 1973, IAU Symp. 55, "X- and Gamma Ray Astronomy", eds. Bradt, H., and Giacconi, R., Dordrecht : Reidel, p.

Kinzer, R.L., Share, G.H., and Seeman, N., 1974, J. Geophys. Res., 79, 4567.

Kiraly, P., Szabelski, J., Wdowczyk, J., and Wolfendale, A.W., 1981, Nature, 293, 120.

Klebsadel, R., Evans, W.D., Larcos, J.G., Strong, I.B., Cline, T.L., Desai, U.D., Teegarden, B.J., Barat, C., Hurley, K., Niel, M., Vedrenne, G., Esttulin, I.V., Kuznetsov, A.V., and Zenchenko, V.M., 1982, Astrophys. J., 259, L51.

Kniffen, D.A., Hartman, R.C., Thompson, D.J., Bignami, G.F., Fichtel, C.E., Ogelman, H., and Tumer, T., 1974, Nature, 251, 397.

Kniffen, D.A., Fichtel, C.E., and Thompson, D.J., 1977, Astrophys. J., 215, 765.

Kodaira, K., 1974, Publ. Astron. Soc. Japan, 26, 255.

Kowalski, M.P., 1982, Ph.D. Thesis, Northwestern University.

Kraushaar, W.L., Clark,e G.E., Garmire, G.P., Helmken, H., Higbie, P., and Agogino, M., 1965, Astrophys. J., 141, 845.

Kraushaar, W.L., Clarke, G.E., Garmire, G.P., Borken, R., Higbie, P., Leong, V., and Thorsos, T., 1972, Astrophys. J., 177, 341.

Kutner, M., Tucker, K.D., Chin, G., and Thaddeus, P., 1977, Astrophys. J., 215, 521.

Kutner, M., and Mead, K., 1981, Astrophys. J., 249, L15.

Lamb, R.C., Fichtel, C.E., Hartman, R.C., Kniffen, D.A., and Thompson, D.J., 1977, Astrophys. J., 212, L63.

Lamb, R.C., 1978, Nature, 272, 429.

Lamb, R.C., Godfrey, C.P., Wheaton, W.A., and Tumer, T., 1982, Nature, 296, 543.

Lebrun, F., and Paul, J.A., 1980 (preprint).

Lebrun, F., Bignami, G.F., Buccheri, R., Caraveo, P.A., Hermsen, W., Kanbach, G., Mayer-Hasselwander, H.A., Paul, J.A., Strong, A.W., and Wills, R.D., 1982, Astron. Astrophys., 107, 390.

Lebrun, F., Bennett, K., Bignami, G.F., Bloemen, J.B.G.M., Buccheri, R., Caraveo, P.A., Gottwald, M., Hermsen, W., Kanbach, G., Mayer-Hasselwander, H.A., Montmerle, T., Paul, J.A., Sacco, B., Strong, A.W., Wills, R.D., Dame, T., Cohen, R.S., and Thaddeus, P., 1983, Astrophys. J., 274, 231.

Lebrun, F., and Paul, J.A., 1983, Astrophys. J., 266, 276.

Lebrun, F., and Huang, Y.L., 1984, Astrophys. J., 281, 634.

Leventhal, M., MacCallum, C.J., and Watts, A., 1977, Astrophys. J., 216, 491.

Leventhal, M., MacCallum, C.J., and Stang, P.D., 1978, Astrophys. J., 225, L19.

Li, T.P., and Wolfendale, A.W., 1981, Astron. Astrophys., 103, 19.

Li, T.P., Riley, P.A., and Wolfendale, A.W., 1982, J. Phys. G., 8, 1141.

Li, T.P., and Wolfendale, A.W., 1982, Astron. Astrophys., 116, 95.

Li, T.P., Riley, P.A., and Wolfendale, A.W., 1983, Mon. Not. R. astr. Soc., 203, 87.

Lilley, A.E., 1955, Astrophys. J., 121, 559.

Ling, J.C., Mahoney, W.A., Willett, J.B., and Jacobson, A.S., 1979, Astrophys. J., 231, 896.

List, H.S., Xiang, D., and Burton, W.B., 1981, Astrophys. J., 249, 532.

List, H.S., 1982, Astrophys. J., 262, 198.

Lloyd-Evans, J., Coy, R.M., Lambert, A., Lapikens, J., Patel, M., Reid, R.J.O., and Watson, A.A., 1983, Nature, 305, 784.

Longair, M.S., 1981, "High Energy Astrophysics", Cambridge University Press.

Loren, R.B., 1979, Astrophys. J., 234, L207.

Matteson, J.L., 1982, AIP Proc. No. 83, "The Galactic Centre", eds. G.R. Riegler, and R.D. Blandford, p.109.

Mayer-Hasselwander, H.A., Bennett, K., Bignami, G.F., Buccheri, R., D'Amico, N., Hermsen, W., Kanbach, G., Lebrun, F., Lichti, G.G., Masnou, J.L., Paul, J.A., Pinkau, K., Scarsi, L., Swannenburg, B.N., Wills, R.D., 1980, Ann. N.Y. Acad. Sci., 336, 211.

Mayer-Hasselwander, H.A., Bennett, K., Bignami, G.F., Buccheri, R., D'Amico, N., Hermsen, W., Kanbach, G., Lebrun, F., Lichti, G.G., Masnou, J.L., Paul, J.A., Pinkau, K., Scarsi, S., Swannenburg, B.N., and Wills, R.D., 1982, Astron. Astrophys., 105, 164.

Meegan, C.A., and Fishman, G.J., 1979, Astrophys. J., 234, L123.

Menon, T.K., 1958, Astrophys. J., 127, 28.

McHardy, I., 1978, Mon. Not. R. astr. Soc., 184, 783.

McHardy, I., 1979, Mon. Not. R. astr. Soc., 188, 495.

Millikan, R.A., and Cameron, G.H., 1926, Phys. Rev., 27, 645.

Montmerle, T., 1979, Astrophys. J., 231, 95.

Morello, C., and Navarra, G., 1983, Proc. 18th ICRC, Bangalore, 1, 127.

Morfill, G.E., 1982a, Mon. Not. R. astr. Soc., 198, 583.

Morfill, G.E., 1982b, Astrophys. J., 262, 749.

Morrison, P., 1958, Nuovo Cim., 7, 858.

Mukanov, J.B., and Fishman, G.J., 1979, Astrophys. J., 234, L123.

Murdoch, H.S., Crawford, D.F., and Jauncey, D.L., 1973, Astrophys. J., 183, 1.

Murray, S.S., 1981, "X-ray Astronomy with the Einstein Satellite", ed. R. Giacconi, p.281.

Omnes, R., 1969, Phys. Rev. Lett., 23, 38.

Pagel, B.E.J., and Edmunds, M.G., 1981, Ann. Rev. Astron. Astrophys., 19, 77.

Paul, J.A., Bennett, K., Bignami, G.F., Buccheri, R., Caraveo, P.A., Hermsen, W., Kanbach, G., Mayer-Hasselwander, H.A., Scarsi, L., Swannenburg, B.N., and Wills, R.D., 1978, Astron. Astrophys., 63, L31.

Peimbert, M., 1982, Ann. N.Y. Acad. Sci., 395, 24.

Pollock, A.M.T., Bignami, G.F., Hermsen, W., Kanbach, G., Lichti, G.G., Masnou, J.L., Swannenburg, B.N., and Wills, R.D., 1981,. Astron. Astrophys., 94, 116.

Pooley, G.G., and Henbest, S.N., 1984, Mon. Not. R. astr. Soc., 169, 477.

Protheroe, R.J., 1983, "Composition and Origin of Cosmic Rays", ed. M.M. Shapiro, Dordrecht:Reidel, p. 351

Protheroe, R.J., Clay, R.W., and Gerhardy, P.R., 1984, Astrophys. J., 280, L47.

Puget, J.L., and Stecker, F.W., 1974, Astrophys. J., 191, 323.

Puget, J.L., Ryter, C., Serra, G., and Bignami, G.F., 1976, Astron. Astrophys., 50, 247.

Ramaty, R., and Lingenfelter, R.E., 1981, Phil. Trans. R. Soc. Lond., A301, 671.

Rana, N.C., Sadzinska, M., Wdowczyk, J., and Wolfendale, A.W., 1984, Astron. Astrophys. (in the press).

Riegler, G.R., Ling, J.C., Mahoney, W.A., Wheaton, W.A., Willett, J.B., Jacobson, A.S., and Prince, T.A., 1981, Astrophys. J., 248, L13.

Riley, J.M., 1975, Mon. Not. R. astr. Soc., 170, 53.

Riley, J.M., and Pooley, G.G., 1975, Mon. Not. R. astr. Soc., 180, 105.

Riley, P.A., Wolfendale, A.W., Chun-xian, Xu., Manchester, R.N., Robinson, B.J., and Whiteoak, J.B., 1984, Mon. Not. R. astr. Soc., 206, 423.

Riley, P.A., and Wolfendale, A.W., 1984, J. Phys. G., 10, 1149.

Robinson, B.J., McCutcheon, W.H., and Whiteoak, J.B., 1982, Internat. J. Infrared Millimetre Waves, 3, 63.

Said, S.S., Wolfendale, A.W., Giler, M., and Wdowczyk, J., 1982, J. Phys. G., 8, 383.

Samorski, M., and Stamm, W., 1983a, Astrophys. J., 268, L17.

Samorski, M., and Stamm, W., 1984b, Proc. 18th ICRC, Bangalore, 1, 135.

Sanders, D.B., 1981, Ph.D. Thesis, State University of New York at Stonybrook.

Sanders, D.B., Solomon, P.M., and Scoville, N.Z., 1984a, Astrophys. J., 276, 182.

Sanders, D.B., Scoville, N.Z., and Solomon, P.M., 1984b, Astrophys. J. (in the press).

Sastry, Ch.V., and Shevgaonkar, R.K., 1983, J. Astrophys. Astr., 4, 47.

Savage, B.D., Bohlin, R.C., Drake, J.F., and Budich, W., 1977, Astrophys. J., 216, 291.

Savage, B.D., and Mathis, J.S., 1979, Ann. Rev. Astron. Astrophys., 17, 73.

Schonfelder, V., Grasser, U., and Penninsfeld, F.P., 1980, Astrophys. J., 240, 350.

Scoville, N.Z., and Solomon, P.M., 1975, Astrophys. J., 199, L105.

Serlemitsos, P.J., Smith, B.W., Boldt, E.A., Holt, S.S., and Swank, J.H., 1977, Astrophys. J., 211, L63.

Shane, D.C., and Wirtanen, C.A., 1967, Publs. Lick Obs., 22, 1.

Share, G.H., Kinzer, R.L., and Seeman, N., 1974, Astrophys. J., 187, 511.

Silk, J., 1973, Ann. Rev. Astron. Astrophys., 11, 269.

Skilling, J., and Strong, A.W., 1976, Astron. Astrophys., 53, 253.

Solomon, P.M., Sanders, D.B., and Scoville, N.Z., 1979, IAU Symp. 84, "The Large Scale Structure of the Galaxy", ed. W.B. Burton, Dordrecht:Reidel, p.35.

Solomon, P.M., Scoville, N.Z., and Sanders, D.B., 1979, Astrophys. J., 232, L89.

Solomon, P.M., Stark, A.A., and Sanders, D.B., 1983, Astrophys. J., 267, L29.

Soltan, A., and Henry, J.P., 1983, Astrophys. J., 271, 442.

Stecker, F.W., 1969, Astrophys. J., 157, 507.

Stecker, F.W., 1975, "Origin of Cosmic Rays", eds. J.L. Osborne and A.W. Wolfendale, Dordrecht:Reidel, p.267.

Stecker, F.W., 1983, IAU Symp. 104, "Early Evolution of the Universe and Its Present Structure", eds. G.O. Abell and G. Chincarini, Dordrecht:Reidel, p.437.

Stecker, F.W., and Wolfendale, A.W., 1984, Nature, 309, 37.

Strickman, M.S., Kurfess, J.D., and Johnson, W.N., 1982, Astrophys. J., 253, L23.

Strong, A.W., and Worrall, D.M., 1976, J. Phys., A9, 823.

Strong, A.W., and Wolfendale, A.W., 1981, Phil. Trans. R. Soc. Lond., A301, 541.

Strong, A.W., Bignami, G.F., Bloemen, J.B.G.M., Buccheri, R., Caraveo, P.A., Hermsen, W., Kanbach, G., Lebrun, F., Mayer-Hasselwander, H.A., Paul, J.A., and Wills, R.D., 1982, Astron. Astrophys., 115, 404.

Strong, A.W., and Lebrun, F., 1982, Astron. Astrophys., 105, 159.

Strong, A.W., and Bignami, G.F., 1983, Astrophys. J., 274, 549.

Strong, A.W., 1984, Astron. Astrophys. (in the press).

Sturrock, P.A., and Baker, K.B., 1979, Astrophys. J., 234, 612.

Swannenburg, B.N., Bennett, K., Bignami, G.F., Buccheri, R., Caraveo, P.A., Hermsen, W., Kanbach, G., Lichti, G.G., Masnou, J.L., Mayer-Hasselwander, H.A., Paul, J.A., Sacco, B., Scarsi, L., and Wills, R.D., 1981, Astron. Astrophys., 243, L69.

Talent, D.L., and Dufor, R.J., 1979, Astrophys. J., 233, 888.

Thaddeus, P., 1982, Ann. N.Y. Acad. Sci., 895, 9..

Thompson, D.J., Fichtel, C.E., Kniffen, D.A., and Ogelman, H.B., 1975, Astrophys. J., 200, L79.

Thompson, D.J., and Fichtel, C.E., 1982, Astron. Astrophys., 109, 352.

Thompson, D.J., Bertsch, D.L., Hartman, R.C., and Hunter, S.D., 1983, Astron. Astrophys., 127, 220.

Trombka, J.I., Dyer, C.S., Evans, L.G., Bielefeld, M.J., Seltzer, S.M., and Metzger, A.E., 1977, Astrophys. J., 212, 925.

Tucker, K.D., Kutner, M., and Thaddeus, P., 1973, Astrophys. J., 186, L13.

Valtaoja, E., 1984, Astron. Astrophys., 135, 141.

van den Bergh, S., 1961, Astrophys. J., 134, 970.

van den Hulst, H.C., Muller, C.A., and Oort, J.H., 1954, B.A.N., 12, 117.

Verter, F., 1981, Phys. Rep., 81, 293.

Vladimirsky, B.M., Stepanian, A.A., and Fomin, V.P., 1973, Proc. 13th ICRC, Denver, 1, 456.

Wdowczyk, J., and Wolfendale, A.W., 1983, Nature, 305, 609.

Wdowczyk, J., and Wolfendale, A.W., 1984, J. Phys. G., 10, 1453.

Weaver, H., and Williams, D.R.W., 1973, Astrophys. J., 236, 448.

Weekes, T.C., and Helmken, H.F., 1977, Proc. 12th ESLAB Symp., Frascati, Italy (ESA SP-124, p.39).

Wolfendale, A.W., 1981, IAU SYmp. 94, "Origin of Cosmic Rays", eds. G. Setti, G. Spada, and A.W. Wolfendale, Dordrecht:Reidel, p.309.

Worrall, D.M., 1977, Ph.D. Thesis, University of Durham.

Worrall, D.M.,, and Strong, A.W., 1977, Astron. Astrophys., 57, 229.

Yoshimori, M., Watanake, H., Okudeira, K., Hirasima, Y., and Murakami, H., 1979, Aust. J. Phys., 32, 375.

Young, J.S., and Scoville, N.Z., 1982, Astrophys. J., 258, 467.

ACKNOWLEDGEMENTS

The University of Durham is thanked for the provision of a Research Studentship during the first year of this work. The Department of Education for Northern Ireland is thanked for the provision of a Postgraduate Studentship for the subsequent period.

I am indebted to my Supervisor, Professor A.W. Wolfendale, F.R.S., for the opportunity to commence this work. His constant support and enthusiasm are gratefully acknowledged.

I wish to thank the members of Durham Physics Department, in particular Drs. C.L. Bhat, C.J. Mayer and P.A. Riley for advice, encouragement and many helpful discussions.

I also wish to thank Dr. W. Hermsen, University of Leiden, for useful criticism; and Dr. E.C.M. Young, University of Hong Kong, for his helpful collaboration.

The Caravane Collaboration (via Mr. J.B.G.M. Bloemen) are thanked for the provision of COS B gamma-ray data.

The facilities of the Physics Department and Computer Unit, University of Durham, are acknowledged.

I must also express my thanks to Ms. M.A. Chipchase for her dedicated work in typing this Thesis, and Mrs. P.A. Russell for skilfully drawing the diagrams.